

# **AstroParticles**

J. A. Aguilar

2024-01-31

# Table of contents

<b>Preface</b>	<b>3</b>
Why Python? . . . . .	3
Disclaimer and Acknowledgments . . . . .	3
<b>1 Basic Concepts and Notations</b>	<b>4</b>
1.1 The Computational Framework . . . . .	4
1.1.1 Natural Units . . . . .	4
1.1.2 Larmor Radius and Rigidity . . . . .	6
1.1.3 Superposition model . . . . .	7
1.1.4 Cross sections, number density, lifetime, and interaction lengths . . . . .	7
1.2 Coordinates and Time . . . . .	8
1.2.1 Milky Way . . . . .	9
1.2.2 Local Group . . . . .	10
1.2.3 Virgo Supercluster . . . . .	10
1.2.4 Time scales and time standards . . . . .	11
1.2.5 Time representations: JD and MJD . . . . .	11
1.2.6 Time in experiments . . . . .	12
1.2.7 Coordinate System . . . . .	13
1.3 Special Relativity . . . . .	17
1.3.1 Introduction . . . . .	17
1.3.2 Lorentz Transformations . . . . .	18
1.3.3 Consequences of Lorentz transformations . . . . .	19
1.4 Relativistic kinematics . . . . .	20
1.4.1 Four-vectors . . . . .	20
1.4.2 Transformation to the Center-of-Momentum Frame (COM) . . . . .	20
1.4.3 Fixed-target experiment . . . . .	21
1.4.4 Collider experiment . . . . .	22
1.4.5 Two-body decay in COM . . . . .	23
1.5 Cosmology . . . . .	24
1.5.1 Red-shift . . . . .	24
1.5.2 Relativistic Redshift . . . . .	24
1.5.3 Hubble expansion . . . . .	26
1.6 Cosmological principle . . . . .	27
1.6.1 Friedmann–Lemaître–Robertson–Walker . . . . .	28
1.6.2 Friedman Equations . . . . .	29

1.6.3	Cosmological Constants . . . . .	30
1.6.4	The Cosmological Constant . . . . .	31
1.6.5	Evolution of the Cosmological Constants . . . . .	31
1.6.6	Observational results . . . . .	32
1.6.7	Cosmic Microwave Background . . . . .	32
1.6.8	Before Planck . . . . .	34
1.6.9	After Planck . . . . .	34
1.6.10	Cosmography . . . . .	34
<b>2</b>	<b>Cosmic Rays</b>	<b>40</b>
2.1	What are Cosmic Rays? An historic perspective . . . . .	40
2.2	The Cosmic Ray Spectrum . . . . .	43
2.2.1	Cosmic Ray as function of... . . . . .	46
2.2.2	Primary Cosmic Rays . . . . .	47
2.2.3	Galactic Cosmic Ray Composition . . . . .	50
2.2.4	Electrons . . . . .	50
2.2.5	Antimatter . . . . .	53
2.3	Galactic Cosmic Rays . . . . .	54
2.3.1	Propagation of Cosmic Rays . . . . .	54
2.3.2	Acceleration of Galactic Cosmic Rays . . . . .	69
2.3.3	Sources of Galactic Cosmic Rays . . . . .	82
2.4	Extra-Galactic Cosmic Rays: The Knee and Beyond . . . . .	84
2.4.1	The Knee . . . . .	84
	References . . . . .	92
<b>3</b>	<b>Cosmic Rays in the Atmosphere</b>	<b>93</b>
3.1	Interactions of CR particles in the atmosphere . . . . .	93
3.1.1	Introduction . . . . .	93
3.1.2	The Atmosphere . . . . .	94
3.1.3	Energy Losses in the Atmosphere . . . . .	96
3.1.4	Electromagnetic Shower . . . . .	98
3.1.5	Hadronic Showers . . . . .	100
3.2	Muons and Neutrinos . . . . .	104
3.2.1	Muons and Neutrinos Productions . . . . .	105
3.2.2	Muon Fluxes . . . . .	106
3.2.3	Muon Bundles . . . . .	111
3.2.4	Neutrinos Fluxes . . . . .	113
3.2.5	Fluxes and Kinematics . . . . .	115
3.2.6	Prompt Fluxes . . . . .	117
3.3	Particles Underground . . . . .	118
3.3.1	Muon Interactions . . . . .	118
3.3.2	Muon Energy losses . . . . .	119
3.3.3	Muon Range . . . . .	121

3.3.4	Neutrino Interactions . . . . .	122
3.3.5	Neutrino cross-sections at GeV energies . . . . .	123
3.3.6	Neutrino cross-sections at TeV energies . . . . .	126
3.3.7	High energy Cross-Sections . . . . .	127
3.3.8	Neutrino signatures in a neutrino detector . . . . .	129
3.3.9	Event rate in an underground experiment. . . . .	129
3.3.10	Neutrino Oscillations . . . . .	130
3.3.11	The PMNS Matrix . . . . .	131
3.3.12	The 2-flavor mixing case . . . . .	131
3.3.13	General case . . . . .	135
3.3.14	About symmetries. . . . .	137
3.3.15	Mass hierarchy . . . . .	137
3.3.16	Solar Neutrinos . . . . .	139
3.3.17	Atmospheric Neutrinos . . . . .	140
3.3.18	Reactor Neutrinos . . . . .	141
3.3.19	Neutrino oscillations in matter. . . . .	141
3.3.20	Tutorial III: Calculate the probabilities of $\nu_e \rightarrow \nu_x$ as function of L/E .	141
3.4	What else? . . . . .	143
<b>4</b>	<b>Multimessenger Astronomy</b>	<b>144</b>
4.1	The Beam Dump . . . . .	144
4.2	Gamma-ray Astronomy . . . . .	144
4.2.1	Spectral Energy Distribution . . . . .	145
4.2.2	Gamma-ray production mechanism . . . . .	146
4.2.3	Leptonic models . . . . .	146
4.2.4	Single-electron in uniform magnetic field . . . . .	149
4.2.5	Tutorial I. Working with SED . . . . .	156
4.2.6	Inverse Compton scattering. . . . .	157
4.2.7	Tutorial II Working with SED . . . . .	159
4.2.8	Hadronic models . . . . .	161
4.2.9	Pion bump in SNR with Molecular Cloud . . . . .	163
4.2.10	Galactic gamma-ray diffuse emission . . . . .	164
4.2.11	Extragalactic Background Light . . . . .	165
4.2.12	Gamma-ray Detection . . . . .	166
4.2.13	Cherenkov emission . . . . .	167
4.2.14	Tutorial II: Plot of the Cherenkov angle as funcion of the spectral index.	168
4.2.15	Number of photons . . . . .	169
4.2.16	Atmospheric extintion. . . . .	171
4.3	Gamma-rays, Cosmic-Rays and Neutrinos . . . . .	172
4.3.1	Introduction . . . . .	172
4.3.2	p-p interactions . . . . .	172
4.3.3	p-gamma interations . . . . .	173
4.3.4	The Waxman-Bahcall neutrino flux . . . . .	173

4.3.5	The neutrino and gamma connection . . . . .	175
4.3.6	Tutorial II: Calculation of astrophysical neutrino oscillations . . . . .	177
4.3.7	Gamma-ray neutrino relation . . . . .	178
4.3.8	Neutrino Astronomy . . . . .	179
4.3.9	Diffuse flux of Astrophysical Neutrinos . . . . .	179
4.3.10	The Search for Point Sources . . . . .	180
4.3.11	The Olbers' Paradox . . . . .	180
4.3.12	Tutorial III: Calculate the value of $\xi$ . . . . .	183
<b>5</b>	<b>Dark Matter</b>	<b>188</b>
5.1	Existance of Dark Matter . . . . .	188
5.1.1	1. The mass-to-light ratios . . . . .	188
5.1.2	2. The rotational curves of Galaxies . . . . .	190
5.1.3	3. Gravitational lensing . . . . .	190
5.1.4	4. Cosmic Microwave Background . . . . .	191
5.1.5	5. Big Bang nucleusintesis (BBN) . . . . .	192
5.2	Dark matter? . . . . .	194
5.2.1	Modified Newtonian Dynamics (MoND) . . . . .	194
5.2.2	The Bullet Cluster . . . . .	194
5.3	Dark Matter Candidates . . . . .	195
5.3.1	Introduction . . . . .	195
5.3.2	The Boltzman equation . . . . .	195
5.3.3	Thermal freeze-out and the WIMP "miracle" . . . . .	196
5.3.4	Direct detection . . . . .	197
5.3.5	Indirect detection . . . . .	197
5.3.6	Targets for indirect detection . . . . .	198
5.3.7	Capturing of DM in local celestial bodies . . . . .	199
5.4	Bibliography . . . . .	200
<b>References</b>		<b>201</b>

# Preface

This is a book on astroparticle physics created from markdown and executable code in `python`.

## Why Python?

Although certainly is not a requirement to understand the physics processes involved in astroparticle phenomena, it is beneficial to resolve numerically some of the proposed problems in order to better assimilate the concepts discussed during this course. The `python` programming language is used as a tool for constructing these numerical solutions. The advantage is that there exist complete mathematical libraries (`numpy/scipy`) for `python`, astronomical and analysis toolboxes (`astropy/healpy`), as well as powerful graphical visualization frameworks (`matplotlib`), which make it possible to easily construct problem solvers in a matter of minutes along with its graphical output. The idea is also to familiarize with what has become one of the most popular analysis tools in the high-energy physics as well as in the astronomy communities. A long this week we will use the following `python` modules related with astroparticle physics:

- `astropy`
- `healpy`
- `gammapy`
- `crdb`

References will be added

## Disclaimer and Acknowledgments

These notes are far from original work. I limited myself to read the literature on the subject, assimilate and also re-elaborate concepts into what I hope is a coherent story, useful to give a feeling of how wonderful our Universe and Nature are. There is an endless list of people that inspired these notes and many references. Particularly, I acknowledge: T. K. Gaisser, F. Halzen, K. Hanson, A. Kappes, C. de los Heros, S. Gabici, T. Montaruli, and a long etc.

# 1 Basic Concepts and Notations

## 1.1 The Computational Framework

In this part we are going to review the concepts that we will use in the rest of the course. It will also serve to set up the conventions, units, etc.

### 1.1.1 Natural Units

In high energy physics and astro-particle physics it is very common to use the natural units where  $\hbar = c = 1$ . The correspondence between natural units and physical units can be established by use of

$$\hbar = 6.58 \times 10^{-16} \text{ GeV} \cdot \text{ns} = 1 \Rightarrow 1 \text{ GeV} = 1.52 \times 10^{15} \text{ ns}^{-1}$$

$$c = 30.0 \text{ cm/ns} = 1 \Rightarrow 30 \text{ cm} = 1 \text{ ns}$$

In these units there is then only one fundamental dimension:

- Energy and momentum, usually expressed in GeV
- Time and space are  $\text{GeV}^{-1}$

#### Tutorial I: Working with Units

Along these notes you are going to find different tutorials in python dealing with will help to develop your programing skills in and solve some numerical problems. In this case we are going to see an easy way to work with different units which is using the module `units` that exist for example in `astropy`:

```

import astropy.units as u
from astropy import constants as const
from IPython.display import display, Markdown

M_Earth = 5.97E24 * u.kg
M_Sun = 1.99E30 * u.kg
M_MW = 1E12 * M_Sun
#By adding the quantity u.kg you can print directly the mass in Kg
display(Markdown (f"Mass Earth is: {M_Earth}" %M_Earth))

```

Mass Earth is: 5.97e+24 kg

Note that the variables defined above already have their units attached to them, so when you make a print or similar statement it will provide as well the units as a string.

```

R_Earth = 6.371E6 * u.m # meters
R_Sun = 6.955E8 * u.m # meters
AU = 1.496E11 * u.m # meters

```

With the radius we can calculate the mean density of Earth and Sun. We will show that units are preserved along calculations:

```

import numpy as np
vol_sphere = lambda r: 4*np.pi/3*r**3
rho_Sun = M_Sun / vol_sphere(R_Sun)
rho_Earth = M_Earth / vol_sphere(R_Earth)

#A unit can be changed calling the .to(u.unit) method
display(Markdown (rf"\rho_{\oplus} = {rho_Earth.to(u.g/u.cm**3):.2f}"))
display(Markdown (rf"\rho_{\odot} = {rho_Sun:.2f}"))

```

$$\rho_{\oplus} = 5.51 \text{ g / cm}^3$$

$$\rho_{\odot} = 1412.12 \text{ kg / m}^3$$

We can use this module to make different transformations of units, for example from light years to meters:

```

ly = 1 * u.lyr

display(Markdown (f"Number of seconds for light to travel from Sun to Earth: {1./const.c.to(u.s)}"))
display(Markdown (f"Meters in a light year: {ly.to(u.m):.2e}"))

```

Number of seconds for light to travel from Sun to Earth: 4.99e+02 s / AU  
Meters in a light year: 9.46e+15 m

Assuming that the Galaxy is roughly a disk 50 kpc in diameter and 500 pc thick we can now calculate its density:

```
V_Gal = np.pi * (25000*u.pc)**2 * 500*u.pc

display(Markdown (f"Volume of the Milky Way is approximately: {V_Gal.to(u.m**3):.2e}"))
M_Gal = 1E12 * M_Sun
rho_Gal = M_Gal / V_Gal
display(Markdown (f"Average density of Milky Way is {rho_Gal.to(u.g/u.cm**3):.2e}"))
```

Volume of the Milky Way is approximately: 2.88e+61 m<sup>3</sup>  
 Average density of Milky Way is 6.90e-23 g / cm<sup>3</sup>

### 1.1.2 Larmor Radius and Rigidity

Larmor radius, or gyroradius,  $r_L$ , is the radius of the orbit of a charged particle moving in a uniform, perpendicular magnetic field, obtained by simply equating the Lorentz force with the centripetal force/

It is defined as:

$$qvB = \frac{mv^2}{r_L} \rightarrow r_L = \frac{p}{ZeB}$$

where  $p$  has replaced  $mv$  in the classical limit. However, this also holds for the relativistic generalization by considering  $p$  to be the relativistic 3-momentum. There are several adaptations of this formula, tuned to units natural to various scenarios. One such is

$$r_L \simeq 1 \text{ kpc} \left( \frac{p}{10^{18} \text{ eV} \cdot c} \right) \left( \frac{1}{Z} \right) \left( \frac{\mu\text{G}}{B} \right)$$

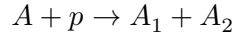
In cosmic ray physics, one often sees references in the literature to the **rigidity** of a particle, defined as:

$$R \equiv r_L B c = \frac{pc}{Ze}$$

note that the rigidity,  $R$  has units of Volts.

### 1.1.3 Superposition model

Another concept that we will use frequently in cosmic-ray physics is the *superpositoin model*. In the superposition model, a nucleus with mass  $A$  and energy  $E(A)$  is considered as  $A$  independent nucleons with energy  $E_0$ . In a spallation process the energy per nucleon is approximately consnserved therefore:



$$\begin{aligned} E(A) &= AE_0, \\ E(A_1) &= A_1 E_0, \\ E(A_2) &= A_2 E_0 \end{aligned}$$

### 1.1.4 Cross sections, number density, lifetime, and interaction lengths

The **cross-section** of a reaction is a very important parameter. It can be considered as the effective area for a collision between a target and a projectile. The cross-section of an interaction depends on interaction force, the energy of the particle, etc...

Cross-section is typically measured in surface,  $\text{cm}^2$  or “barns”:

$$1\text{barn} = 10^{-24}\text{cm}^2$$

The unit barn comes from the expression “big as a barn” as in the past physisits saw with surprise that interactions were more frequent than expected, and they thought the nucleus was in fact bigger than they thought... big as a barn.

If a flux of *projectile* particles are crossing a volume of *target* particles with cross section  $\sigma_N$  then the disappearance of flux will be proportional to the initial number, the length travelled and number of target particles:

$$dI = -In\sigma_N dx$$

where  $n$  is the **number density**, ie, the number of particles per volume unit:

$$n = \frac{N}{V}$$

note that the number density is related with the mass density as:

$$n = \frac{N_A}{M} \rho_m = \frac{\rho_m}{m_N}$$

where  $N_A$  is the avogadro number,  $M$  is the total mass of a mol and  $m_N$  is the mass of is the mass of a single particles N making up the volume. Solving the equation above we have:

$$I = I_0 e^{-\frac{x}{n\sigma_N}}$$

where we can define:

$$\lambda = \frac{1}{n\sigma_N}$$

as the **interaction length**. Likewise if projectile particles are travelling at speed  $v$ , the length travelled can be expressed as  $dx = vdt$  giving a similar expression with a time constant:

$$\tau = \frac{1}{nv\sigma_N}$$

Known as the **lifetime**. If several processes are taking place, we need to replace  $n\sigma_N$  as  $\sum n_i\sigma_i$ , which gives:

$$\frac{1}{\tau_{total}} = \frac{1}{\tau_1} + \frac{1}{\tau_2} + \dots + \frac{1}{\tau_n}$$

## 1.2 Coordinates and Time

In this section we are going to review a bit the geography around our Galaxy as well as the different systems in which we can reference to objects in the sky (coordinate systems) or events (time standards).

### 1.2.1 Milky Way

The Sun is **7.6-8.7 kpc** from the Galactic Center where there appears to be a supermassive black hole of **1 million solar masses** ( $M_{\odot} = 1.99 \times 10^{30}$  Kg) which coincides with a radio source known as **Sagittarius A\***.

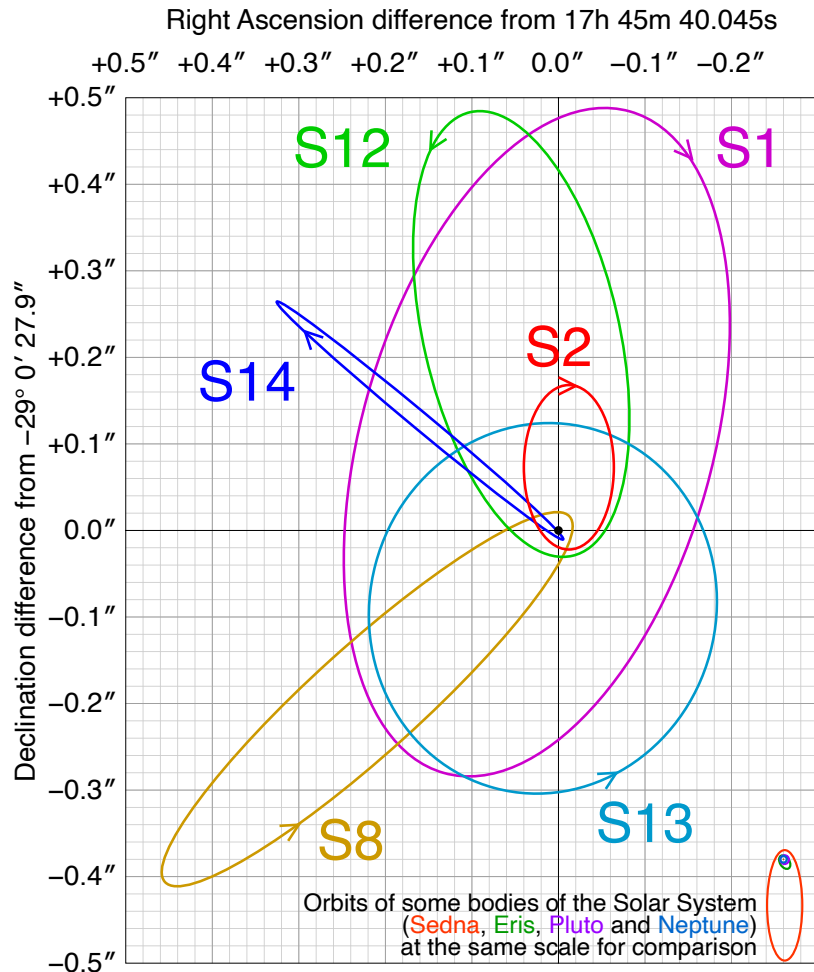


Figure 1.1: Source: Wikipedia

The trajectories of stars around Str A\* can be used to estimate the mass of the black hole. It is the up to now, best prove of the existence of a black hole. Although it is a galaxy with a black hole in their center, the Milky Way is not considered to have an Active Galactic Nuclei due to the low mass of the black hole. If we assume the Milky Way to have a cylindrical shape it will have a radius of **30 kpc** and thickness of **300 pc**. Its mass is estimated to be  $5.8 \times 10^{11} M_{\odot}$ .

### 1.2.2 Local Group

The Milky Way is surrounded by 54 known satellite galaxies (most of them dwarf galaxies) in a group known as the **Local Group** (A dwarf galaxy has  $\sim$  billion stars compared to our Milky Way's 200-400 billion stars). The most notable are the Large Magellanic Cloud (50 kpc) and the Small Magellanic Cloud (60 kpc). The LMC mass is  $10^{10} M_{\odot}$ . Next nearest full-fledged galaxy is Andromeda or M31 ( $1.5 \times 10^{12} M_{\odot}$ ) at a distance of approximately **780 kpc**. The group contains also other galaxies MW, M31, M33 (Triangulum Galaxy) and it has volume of diameter of about **3 Mpc**.

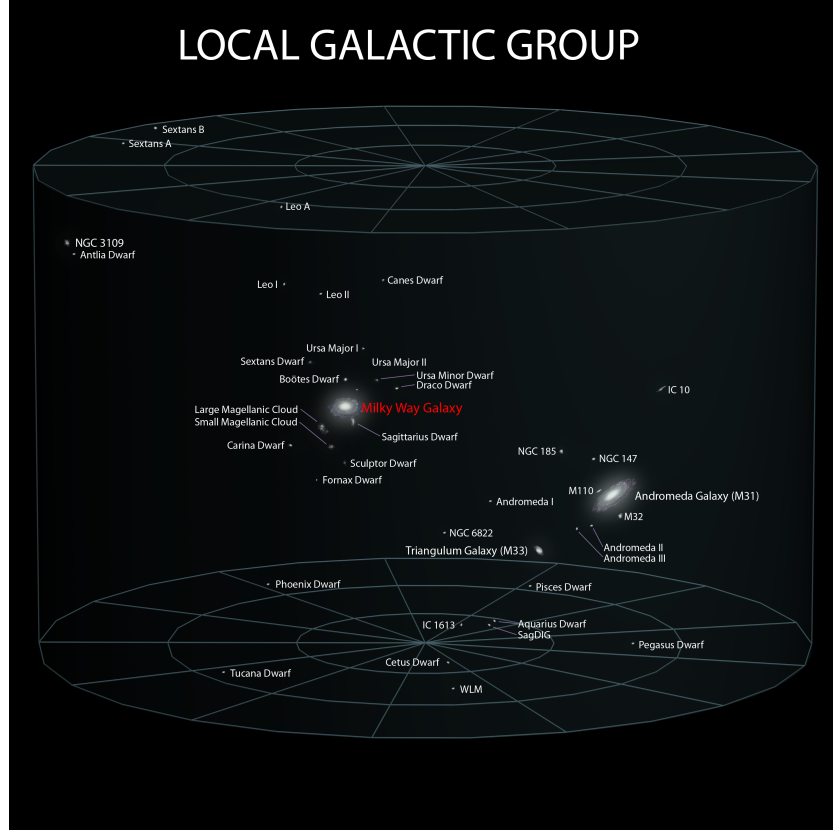


Figure 1.2: Source: Wikipedia

### 1.2.3 Virgo Supercluster

The Local Group is itself contained within the *Virgo Supercluster* or *Local Supercluster* (LC) of galaxies extending out to about 33 Mpc. It has a total mass of  $10^{15} M_{\odot}$ .

#### 1.2.4 Time scales and time standards

There are several time standards or ways to specify time. A time standard can affect the rate (ie, how long is a day) or reference or point in time, or both. Some standards are:

- **Mean solar time** There are two solar times, the apparent one (also called true one) which depends on latitude and the year and the Mean solar time which the time of *mean sun*, the difference between the two is called the **equation of time**. The length of the mean solar day is slowly increasing due to the tidal acceleration of the Moon by the Earth and the corresponding slowing of Earth's rotation by the Moon.
- **Universal Time (UT0, UT1)** Is a time scale based on the mean solar day, defined to be as uniform as possible despite variations in Earth's rotation
- **International Atomic Time** Is the primary international time standard from which other time standards, including UTC, are calculated. TAI is kept by the BIPM (International Bureau of Weights and Measures), and is based on the combined input of many atomic clocks around the world.
- **Coordinated Universal Time (UTC)** is an atomic time scale designed to approximate Universal Time. UTC differs from TAI by an integral number of seconds. UTC is kept within 0.9 second of UT1 by the introduction of one-second steps to UTC. The difference with UT1 is known as DUT1.

#### 1.2.5 Time representations: JD and MJD

These are not technically standards (or scales), they are just representations (formats) of the aforementioned standards typically used in Astronomy:

- **Julian Date** Is the count of days elapsed since Greenwich mean noon on 1 January 4713 B.C., Julian proleptic calendar. Note that this day count conforms with the astronomical convention starting the day at noon, in contrast with the civil practice where the day starts with midnight (in popular use the belief is widespread that the day ends with midnight, but this is not the proper scientific use).
- **Modified Julian Date** Is defined as  $MJD = JD - 2400000.5$ . The half day is subtracted so that the day starts at midnight in conformance with civil time reckoning. There is a good reason for this modification and it has to do with how much precision one can represent in a double (IEEE 754) variable. Julian dates can be expressed in UT, TAI, TDT, etc. and so for precise applications the timescale should be specified, e.g. MJD 49135.3824 TAI.

### 1.2.6 Time in experiments

Practically speaking, in experiments time comes from one or more of the following sources:

- **Atomic clocks (Cs, Rb)** -They use the microwave signal that electrons in atoms emit when they change energy levels. These have very good short term performance but a Rb clock left by itself will wander by several ns per day. Cs clocks are perhaps better by a factor of 100x.
- **GPS** - The GPS gives precision timing too. The system consists of the space segment of O(30) satellites each equipped with Caesium atomic clocks and each constantly getting corrections from the central control facility. GPS broadcasts navigation and time messages synchronized to this ultraprecise time from which the user segment can extract time and space coordinates accurate to O(10) ns and meters, respectively. GPS time is based on the 86400 second day. It indirectly accounts for leap years. There are *no* leap seconds in GPS time.

#### Tutorial II: Using Time Standards in Astropy

Time conversions and coordinate conversions are best left to well-tested libraries. SLALIB is a famous set of Fortran libraries that do several transformation. For python I will use **Astropy**. The [Astropy Project](#) is a community effort to develop a single core package for Astronomy in Python and foster interoperability between Python astronomy packages. Is included by default in the Anaconda distribution.

```
from astropy.time import Time
import datetime
i = datetime.datetime.now()
print(f"Today's date and time: {i.isoformat()}")
times = ['1999-01-01T00:00:00.123456789', i.isoformat()]
t = Time(times, format='isot', scale='utc')
print(f"Today's julian date (UTC) is {t[1].jd:.2f}")
print(f"Today's modified julian date (UTC) is {t[1].mjd:.2f}")

dt = t[1] - t[0]
print(f"The time difference in mjd is {dt.value:.2f}")
print(f"The time difference in seconds is {dt.sec:.2f}")
```

Today's date and time: 2024-10-03T11:39:42.389962

Today's julian date (UTC) is 2460586.99

Today's modified julian date (UTC) is 60586.49

The time difference in mjd is 9407.49

The time difference in seconds is 812806787.27

## 1.2.7 Coordinate System

Coordinate systems are used to map objects position in the sky. They can divided into local coordinates and celestial coordinate systems:

### 1.2.7.1 Local coordinates

These are those that depend on from where on Earth you observe, ie they have the observer's local position as reference. For example the horizontal coordinate system is expressed in terms of **altitude** (or elevation or zenith) angle and **azimuth**. These coordinates are not useful to unequivocally identify the position of an object in the sky since celestials object local coordinates change with time.

### 1.2.7.2 Celestial coordinate systems

Those systems are independent of the observer's local position. Two of the mostly used coordinates systems in astroparticle are:

- **Equatorial coordinates:** It's defined by an origin at the center of the Earth, a fundamental plane consisting of the projection of the Earth's equator onto the celestial sphere. Coordinates are give by **right ascension** and **declination**.

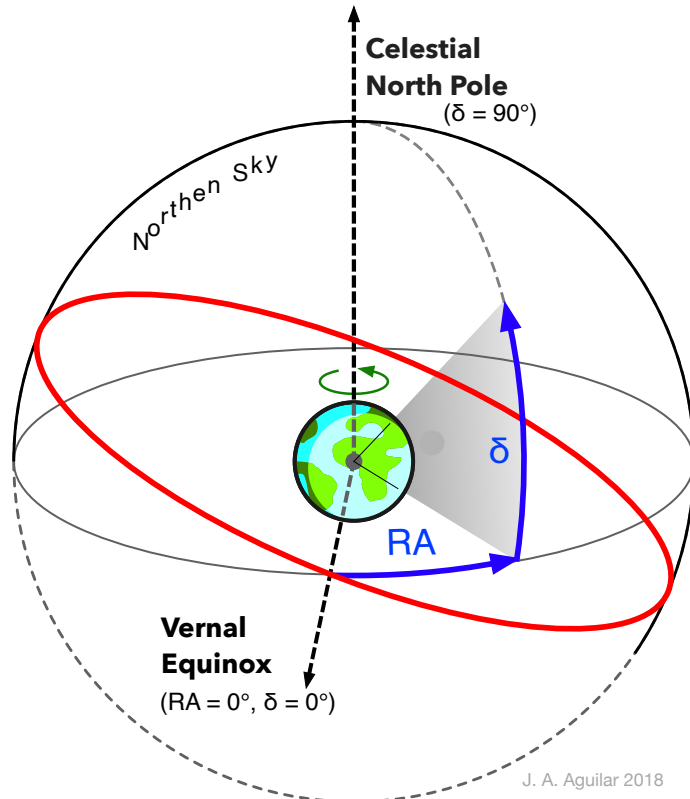


Figure 1.3: Equatorial coordinate system

- **Galactic coordinates:** The **galactic longitude**,  $\ell$  is the angular distance Eastward (counterclockwise looking down on the Galaxy from the GNP) from the Galactic Center and the **galactic latitude**,  $b$ , is the angular distance outside of the plane of the Galaxy, positive up, negative down. Note that having a large galactic latitude is neither a necessary nor a sufficient condition for an object being extragalactic. This is how to get the image of the Galactic plane on the celestial sphere.

### Tutorial III: Coordinate Transformations

Let's do some "representation" of the galactic plane. We generate some random points using numpy following a 2-dimensional gaussian in the  $\ell$ :  $-\pi, +\pi$  and  $b$ :  $-\pi/2, +\pi/2$  space. Now we are going to use `matplotlib` to make plots, for that we are going to call the magic command `%matplotlib inline` to make the plots appear inside the notebook:

```
%matplotlib inline
import matplotlib.pyplot as plt
plt.rcParams['font.family'] = "STIXGeneral"

#We call random.multivariate_normal to generate random normal points at 0
import numpy as np
#Lets use the inline figure format as svg
%config InlineBackend.figure_format = 'svg'

disk = np.random.multivariate_normal(mean=[0,0], cov=np.diag([1,0.001]), size=5000)
#disk is a list of pairs [l, b] in radians
print(disk[0:10])
f = plt.figure(figsize=(7,5))
ax = plt.subplot(111, projection='aitoff')
#There are several projections: Aitoff, Hammer, Lambert, MollWeide
ax.set_title("Galactic\n Coordinates")
ax.grid(True)
ll = disk[:,0]
bb = disk[:,1]
#ax.set_axis_bgcolor("black")
#ax.tick_params(axis='x', colors='white')
ax.plot(ll, bb, 'o', markersize=2, alpha=0.3)
plt.show()
```

```
[[ -1.36726093e+00  2.46061233e-03]
 [ 5.26590348e-01 -2.35016968e-02]
 [-1.27918990e+00 -8.87673509e-03]
 [-9.95746000e-01 -1.13125889e-02]
 [-2.14040946e+00  7.11257714e-03]
 [-2.46932820e+00  4.41397056e-03]
 [-3.92373303e-02  4.19132152e-03]
 [ 1.32063929e+00  1.43130027e-03]
 [ 1.11585689e+00  6.76867543e-03]
 [-9.53669597e-02 -8.80443866e-02]]
```

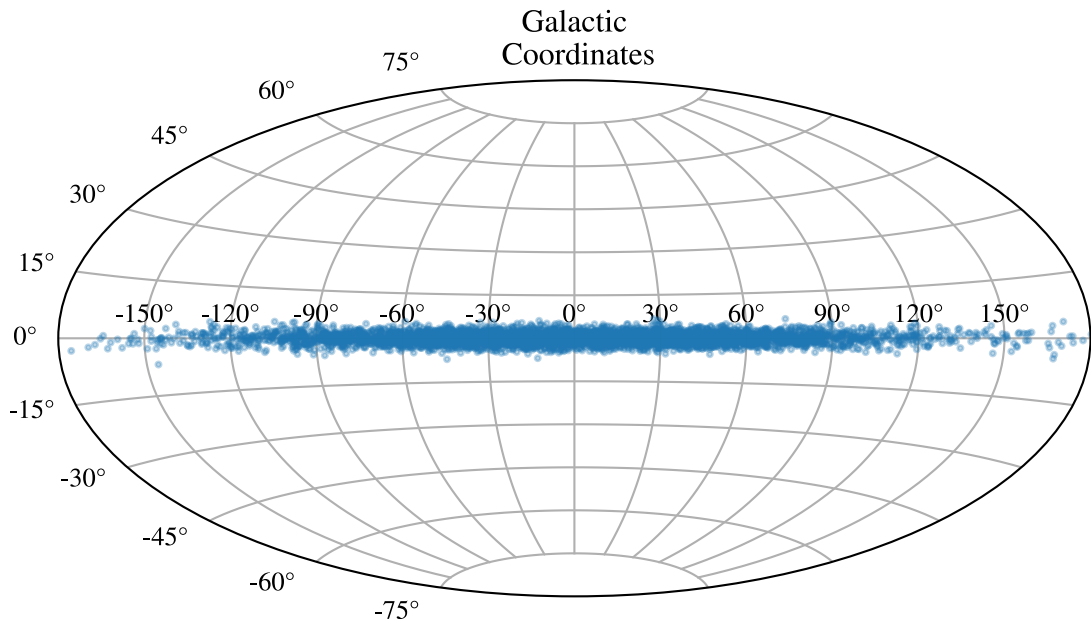


Figure 1.4: Galaxy in Galactic Coordinates

Now let's plot it in equatorial coordinates (right ascension, declination).

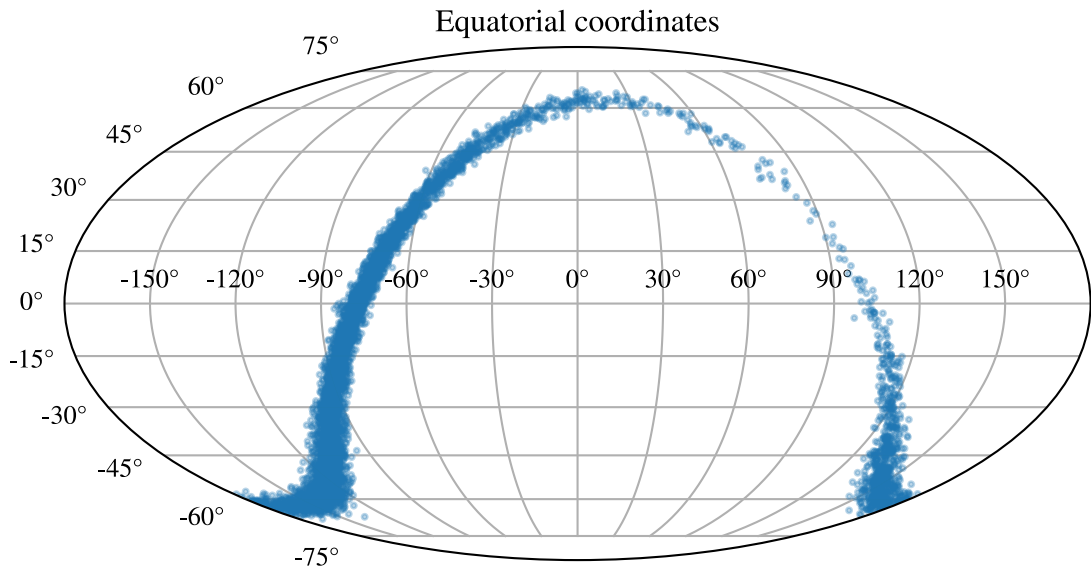
```
from astropy import units as u
from astropy.coordinates import SkyCoord

c_gal = SkyCoord(l=ll*u.radian, b=bb*u.radian, frame='galactic')
c_gal_icrs = c_gal.icrs
```

Because `matplotlib` needs the coordinates in radians and between  $-\pi$  and  $\pi$ , not 0 and  $2\pi$ , we have to convert them.

```
ra_rad = c_gal_icrs.ra.wrap_at(180 * u.deg).radian
dec_rad = c_gal_icrs.dec.radian

plt.figure(figsize=(7,5))
ax = plt.subplot(111, projection="mollweide")
ax.set_title("Equatorial coordinates")
plt.grid(True)
ax.plot(ra_rad, dec_rad, 'o', markersize=2, alpha=0.3)
plt.show()
#NOTE: Normally right ascension is plotted from right (0 deg.) to left (360 deg.)
```



## 1.3 Special Relativity

### 1.3.1 Introduction

Why is it important?

$$\gamma = \sqrt{\frac{1}{1 - \beta^2}}, \beta = \frac{v}{c}$$

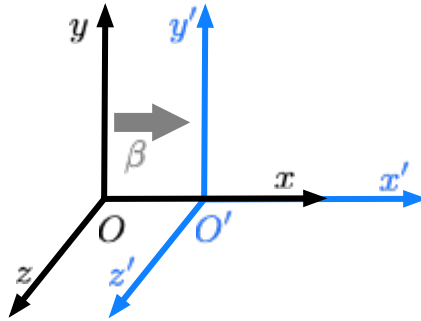
- Jets emitted by supermassive black holes have:  $\gamma \approx 30 \rightarrow \beta = 0.9984$
- Electrons spiraling in B-field lines of pulsars have:  $\gamma \sim 10^7$
- Lorentz factors of protons of  $10^{20}$  eV:  $\gamma = \frac{E}{m_p c^2} = \frac{10^{20}}{1 \times 10^9} = 10^{11}$

Two principles:

1. *The Principle of Relativity* – The laws by which the states of physical systems undergo change are not affected, whether these changes of state be referred to the one or the other of two systems in uniform translatory motion relative to each other
2. *The Principle of Invariant Light Speed* – “... light is always propagated in empty space with a definite velocity [speed]  $c$  which is independent of the state of motion of the emitting body.”

### 1.3.2 Lorentz Transformations

As a simple case, consider a reference frame  $O$  and an observer in another frame  $O'$  moving at constant speed  $\beta$  along the  $x$  axis:



A Lorentz transformation or *boost* is the transformation from one inertial reference frame to another. In general it is a  $(4 \times 4)$  matrix which encapsulates the system of equations describing the transformation (in natural units).

$$\begin{aligned} t' &= \gamma(t - \beta x) \\ x' &= \gamma(x - \beta t) \\ y' &= y \\ z' &= z \end{aligned}$$

The matrix form of this transformation is

$$x'^\mu = \Lambda^\mu{}_\nu x^\nu, \quad \Lambda^\mu{}_\nu = \begin{pmatrix} \gamma & -\beta\gamma & 0 & 0 \\ -\beta\gamma & \gamma & 0 & 0 \\ 0 & 0 & 1 & 0 \\ 0 & 0 & 0 & 1 \end{pmatrix}$$

This is just a particular case of a Lorentz transformation (there is nothing special on the x-axis) and a variable invariant under a Lorentz transformation is called *Lorentz invariant or scalar*.

The line element  $\Delta s^2$  is a Lorentz invariant:

$$\Delta s^2 = \Delta t^2 - \Delta x^2 - \Delta y^2 - \Delta z^2$$

This can be rewritten as the inner product of a 4-vector  $x^\mu$ :

$$\Delta s^2 = x^2 \equiv x^\mu x_\mu = g_{\mu\nu} x^\mu x^\nu$$

where *metric tensor*  $g_{\mu\nu}$  is:

$$g_{00} = +1, g_{11} = g_{22} = g_{33} = -1, g_{\mu\nu} = 0, \text{ for } \mu \neq \nu$$

is called the **Minkowski space**.

### 1.3.3 Consequences of Lorentz transformations

Lorentz transformation have the following (some of them really bizarre) consequences:

- **Relativity of simultaneity.**  $\Delta t' = 0$  in  $O'$  doesn't imply  $\Delta t = 0$  in  $O$ :

$$\Delta t' = \gamma(\Delta t - \beta \Delta x)$$

- **Time dilatation.** If  $\Delta x = 0$  i.e. the ticks of one clock:

$$\Delta t' = \gamma \Delta t$$

- **Length contraction.** For events satisfying  $\Delta t' = 0$ :

$$\Delta x' = \frac{\Delta x}{\gamma}$$

- **Equivalence of mass and energy.**

In 1905, Einstein gave his first derivation of the mass-energy equivalence by studing, in different reference frames, the energy balance of a body emitting electromagnetic radiation. You can replace *body* with a *cat* and check a quick proof of the mass energy equivalence in this video:

<https://www.youtube.com/watch?v=hW7DW9NIO9M>

Figure 1.5: Source: Minute Physics

## 1.4 Relativistic kinematics

### 1.4.1 Four-vectors

We saw that position vectors in Minkowski space become 4-vectors with zeroth component.  $x^0 = t$ , identified with time. Likewise momentum 4-vector has  $p^0 = E$ :

$$\mathbf{P} = (E, \vec{p})$$

$$\mathbf{X} = (t, \vec{x})$$

We saw that the inner product in Minkowski space is invariant under Lorentz transformations. In this case, the Lorentz invariant is:

$$s = p_\mu p^\mu = m_0^2 = E^2 - \vec{p} \cdot \vec{p} \rightarrow E^2 = \vec{p} \cdot \vec{p} + m_0^2$$

which is the *relativistic energy-momentum relationship*.

$$E = m = \gamma m_0$$

One can derive the expresions for relativistic 3-momentum and kinetic energy:

$$|\vec{p}| = \beta E$$

$$E_{kin} \equiv E - m_0 = (\gamma - 1)m_0$$

### 1.4.2 Transformation to the Center-of-Momentum Frame (COM)

As a concrete example of how 4-vectors aid real calculations, let's take the classic case of a transformation to the center-of-momentum frame (COM), that is, a coordinate frame where the total three-momentum  $\vec{p} = 0$ . In this case the invariant square of a system is equal to the total COM energy square or:

$$\sqrt{s} = E_{COM}$$

In the case of a two-particle system with particles A and B with energies ( $E_A$ ) and ( $E_B$ ), and 3-momenta ( $\vec{p}_A$ ) and ( $\vec{p}_B$ ):

$$\begin{aligned}
2s = p^2 &= (E_A + E_B)^2 - (\vec{p}_A + \vec{p}_B)^2 \\
&= m_A^2 + m_B^2 + 2E_A E_B - 2(\vec{p}_A \cdot \vec{p}_B) \\
&= m_A^2 + m_B^2 + 2E_A E_B(1 - \beta_A \beta_B \cos \theta) \\
&= E_{COM}^2
\end{aligned}$$

where we used the fact that:

$$\vec{p}_A \cdot \vec{p}_B = |\vec{p}_A| |\vec{p}_B| \cos \theta$$

and

$$|\vec{p}| = E\beta$$

The energy available for new particle creation is  $\epsilon = E_{COM} - m_B - m_A$ . If  $E_A \gg m_A$  and  $E_B \gg m_B$  then:

$$\epsilon^2 \approx 2(E_A E_B - \vec{p}_A \vec{p}_B).$$

#### 1.4.3 Fixed-target experiment

If the target particle B is at rest in the laboratory system (as is the case in accelerator fixed-target experiments or UHE cosmic rays striking nucleons in the atmosphere, or ...) then ( $E_B = m_B$ ) and ( $\vec{p}_B = 0$ ). In this case,

$$E_{COM}^2 = m_A^2 + m_B^2 + 2E_A m_B.$$

which in the ultra-relativistic limit where energies are much higher than the masses ( $E \gg m$ ) simplifies to

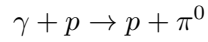
$$\epsilon = E_{COM} \simeq \sqrt{2m_B E_A}.$$

Equivalently, the threshold energy of the beam particle A needed to produce a particle of mass ( $m_*$ ) at rest in the boosted frame is:

$$E_{A,\text{thresh}} = \frac{m_*^2}{2m_B}.$$

 Example 1: Pion production

Considering the photoproduction of pion on a target proton at rest mass:



$$\begin{aligned}\sqrt{s} &= \sqrt{m_p^2 + 2E_\gamma m_p} \geq m_p + m_{\pi^0} \\ m_p^2 + 2E_\gamma m_p &\geq m_p^2 + m_{\pi^0}^2 + 2m_p^2 m_{\pi^0}^2 \\ E_\gamma &\geq m_{\pi^0} + \frac{m_{\pi^0}^2}{2m_p} \approx 145 \text{ MeV}\end{aligned}$$

#### 1.4.4 Collider experiment

In the case of a collider experiment where beam particles A and B are counter-circulating in an accelerator and collide head-on, then

$$\vec{p}_A \cdot \vec{p}_B = -|\vec{p}_A||\vec{p}_B|$$

and the equation of the 3-momenta  $\vec{p}_A$  becomes

$$s = E_{COM}^2 = m_A^2 + m_B^2 + 2(E_A E_B + |\vec{p}_A||\vec{p}_B|) \rightarrow \epsilon^2 \simeq 4E_A E_B,$$

in the relativistic limit where mass can be ignored. This in turn has the consequence that in a collider experiment the energy available in the COM to produce new particles rises linearly with beam energy when  $E_A = E_B$ .

Nevertheless, it is still the case that the COM energies probed by astroparticles exceeds the LHC's reach by a factor of 10!

 Example 2: UHECR protons

Consider an UHECR proton at  $E_p = 10^{10}$  GeV interacting with a proton ( $m_p = 1$  GeV) at rest in the atmosphere, what is the energy in the COM frame?

$$E_{COM} = \sqrt{2m_p^2 + 2E_p m_p} \simeq 142 \text{ TeV}$$

### 1.4.5 Two-body decay in COM

The COM is also useful to estimate the energy of two particles from the decay of a particle with mass  $M$ . If a particle A decays into  $m_1$  and  $m_2$ , we have that in the COM the particle A has  $\vec{p}_A = \vec{p}_{COM} = 0$ . Then the invariant is given by:

$$s = M^2 = (E_1 + E_2)^2 - (\vec{p}_1 + \vec{p}_2)^2$$

where  $\vec{p}_1 = -\vec{p}_2$ . The energies in the COM are given by:

$$M^2 = (E_1 + E_2)^2 \rightarrow M = E_1 + E_2$$

$$E_1^2 = p_1^2 + m_1^2 \quad \text{and} \quad E_2^2 = p_2^2 + m_2^2$$

since  $|\vec{p}_1| = |\vec{p}_2|$  we can make the subtraction:

$$E_1^2 - E_2^2 = m_1^2 - m_2^2 \rightarrow E_2^2 = E_1^2 - m_1^2 + m_2^2$$

sustituting  $E_2^2$  in  $M^2 = E_1^2 + E_2^2 + 2E_1E_2$  and using  $E_2 = M - E_1$  we have:

$$M^2 = E_1^2 + E_1^2 - m_1^2 + m_2^2 + 2E_1(M - E_1)$$

$$M^2 = 2E_1^2 - m_1^2 + m_2^2 - 2E_1^2 + 2E_1M$$

$$E_1 = \frac{1}{2M}(M^2 + m_1^2 - m_2^2)$$

likewise we can prove:

$$E_2 = \frac{1}{2M}(M^2 + m_2^2 - m_1^2)$$

and the momentum:

$$|\vec{p}_1|^2 = E_1^2 - m_1^2 = \frac{1}{4M^2}(M^4 - 2M^2(m_1^2 + m_2^2) + (m_1^2 + m_2^2)^2) = |\vec{p}_2|^2$$

Energies and momentums are fixed, the only unknowns are the angles.

## 1.5 Cosmology

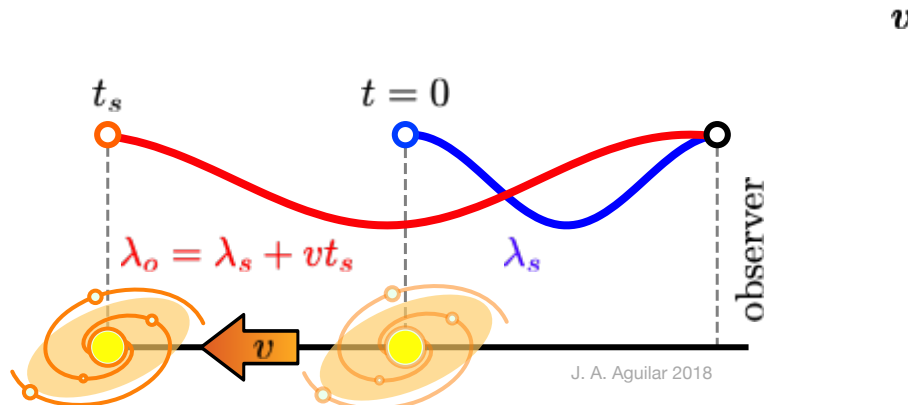
### 1.5.1 Red-shift

Red-shift is the shift (towards red) in the electromagnetic spectrum and is defined as:

$$z = \frac{\lambda_{obs} - \lambda_{emit}}{\lambda_{emit}}$$

If a source of the light is moving away from an observer, then redshift ( $z > 0$ ) occurs; if the source moves towards the observer, then blueshift ( $z < 0$ ) occurs. This is true for all electromagnetic waves and is explained by the Doppler effect. Consequently, this type of redshift is called the *Doppler redshift*.

### 1.5.2 Relativistic Redshift



The wavefront moves with velocity  $c$ , but at the same time the source moves away with velocity  $v$ . After a time  $t_s$  the source has receded  $vt$ . The crest of the wave emission is at  $\lambda + vt_s = ct_s$ . The period in the reference system of the source is given by:

$$t_s = \frac{\lambda}{c-v} = \frac{c}{(c-v)f_s} = \frac{1}{(1-\beta)f_s}.$$

Remember that when a reference  $O_s$  was moving at speed  $\beta$  from another reference  $O_o$ , the time relation was:

$$\Delta t_s = \gamma(\Delta t_o - \beta\Delta x_o).$$

Since  $\Delta x_o = 0$  (we are just measuring when the crest of the waves arrive), then the time observed  $t_o$  in the reference system O is given:

$$t_o = \frac{t_s}{\gamma}.$$

The corresponding observed frequency is

$$f_o = \frac{1}{t_o} = \gamma(1 - \beta)f_s = \sqrt{\frac{1 - \beta}{1 + \beta}} f_s.$$

The ratio

$$\frac{f_s}{f_o} = \sqrt{\frac{1 + \beta}{1 - \beta}},$$

is called the *Doppler factor* of the source relative to the observer.

The corresponding wavelengths are related by

$$\frac{\lambda_o}{\lambda_s} = \frac{f_s}{f_o} = \sqrt{\frac{1 + \beta}{1 - \beta}},$$

and the resulting redshift

$$z = \frac{\lambda_o - \lambda_s}{\lambda_s} = \frac{f_s - f_o}{f_o},$$

can be written as

$$z = \sqrt{\frac{1 + \beta}{1 - \beta}} - 1.$$

When interpreted as a relativistic Doppler shift from object receding at velocity  $\beta$ , this is:

$$\lambda_o = \sqrt{\frac{1 + \beta}{1 - \beta}} \lambda_s \simeq (1 + \beta) \lambda_s$$

In the non-relativistic limit (when  $v \ll c$ ) this redshift can be approximated by  $z \simeq \beta = \frac{v}{c}$  corresponding to the classical Doppler effect.

### 1.5.3 Hubble expansion

When plotting their redshift (ie speed) as function of distance (measured with the techniques we saw, parallax, etc.) in 1929 Hubble found a correlation between redshift and radial distance from Earth:

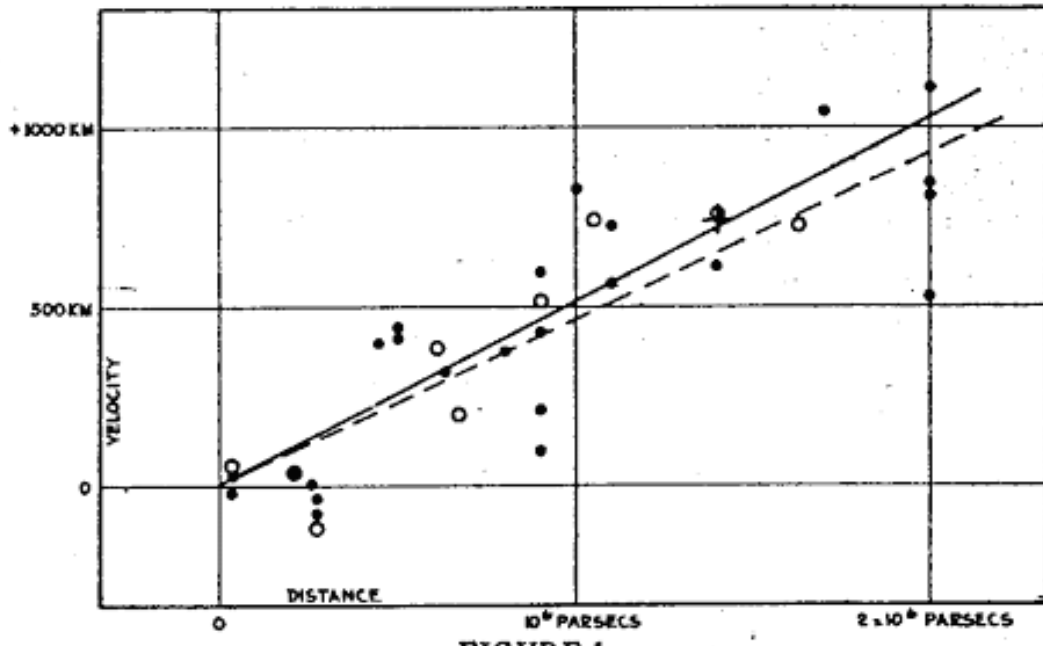


FIGURE 1

$$v = H_0 r, \quad H_0 = 72 \text{ km/s/Mpc}$$

Note that  $H_0$  has only units of  $\text{time}^{-1}$  we explicitly write the other dimensions to better understand its meaning.

But Doppler redshift does not depend on distance! So this is not a doppler redshift but a **Cosmological redshift**. In this case the redshift is not due to relative velocities, the photons instead increase in wavelength and redshift because the spacetime through which they are traveling is expanding.

But we said that for mildly relativistic objects (and galaxies are moving at mildly relativistic speeds) we can approximate  $z \approx \beta$  so we *can use z to estimate distances!*:

$$r \simeq \frac{c}{H_0} z \simeq 4000 \text{ Mpc} \cdot z$$

For small  $v$  over distance  $r$  the **velocity is proportional to the distance**. Note that however this only holds only for *small redshifts!*

For larger redshifts other relations with the distance need to be invoked.

#### 1.5.3.1 Age of the Universe (first approximation)

If we assume that the rate of expansion (ie  $H$ ) is essentially constant (it is not!) the age of the Universe can be estimated by this relation:

$$\frac{dr}{dt} = H_0 r \rightarrow \int \frac{1}{r} dr = \int H_0 dt$$

$$\ln r = H_0 t \rightarrow r = e^{H_0 t}$$

where Universe increases by a factor  $e$  every  $t_{\text{Hubble}} = \frac{1}{H_0} = 14 \times 10^9 \text{ yr}$  which is the **Hubble time**.

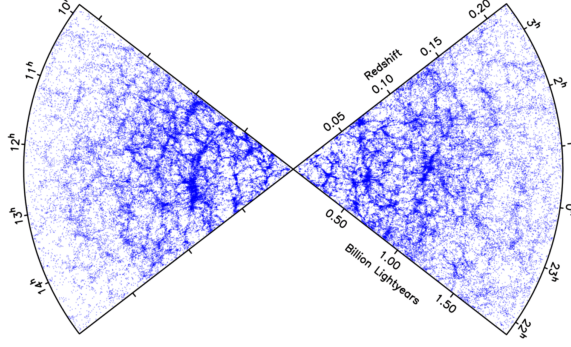
#### 1.5.3.2 Are we expanding?

[Brooklyn is not expanding!](#) *Annie Hall*

## 1.6 Cosmological principle

The *cosmological principle* is the notion that the distribution of matter in the Universe is **homogeneous** and **isotropic** when viewed on a large enough scale.

- **Homogeneity** states that the distribution of matter is even in each epoch.
- **Isotropy** states that there are no preferred directions in the distribution of matter in space.



The [End of Greatness](#) is an observational scale discovered at roughly 100 Mpc where the lumpiness seen in the large-scale structure of the universe is homogenized and isotropized, this together with the isotropy of the CMB reinforced the idea of the [Cosmological Principle](#).

However, in 2013 a new structure **3 Gpc** wide has been discovered, the [Hercules–Corona Borealis Great Wall](#), which puts doubt on the validity of the cosmological principle.

### 1.6.1 Friedmann–Lemaître–Robertson–Walker

Despite seeing all galaxies receding, we are not at the center of the Universe. The common interpretation of the expansion is that we are living in a Universe that can be thought of lying on the surface of a balloon. Distances between objects (points on the balloon) on this manifold are expressed as:

$$r(t) = R(t)r_0$$

where  $R(t)$  is a scale factor, depending on the time, and  $r_0$  is a *comoving coordinate* without time dependence or current distance if we assume  $R(0) = 1$ , but sometimes it's better to explicitly use a *normalized* scale factor as  $a(t) = R(t)/R(0)$

So we are looking for a Universe that is isotropic, homogeneous and it is expanding. The metric that describes such a Universe is given by the **Friedmann–Lemaître–Robertson–Walker** metric:

$$\begin{aligned} ds^2 &= dt^2 - R(t)^2 d\Sigma(k)^2 \\ &= dt^2 - a^2(t)R_0^2 \left[ \frac{dr^2}{1 - kr^2} + r^2(d\theta^2 + \sin^2\theta d\phi^2) \right] \end{aligned}$$

where  $d\Sigma(k)$  refers to the spatial 3-dimensional metric depending on the curvature parameter  $k$  which takes the discrete values +1, 0, -1, corresponding to a closed, open or spatially flat geometry, and we used the normalized form of the scale factor  $a(t) = R(t)/R_0$ .

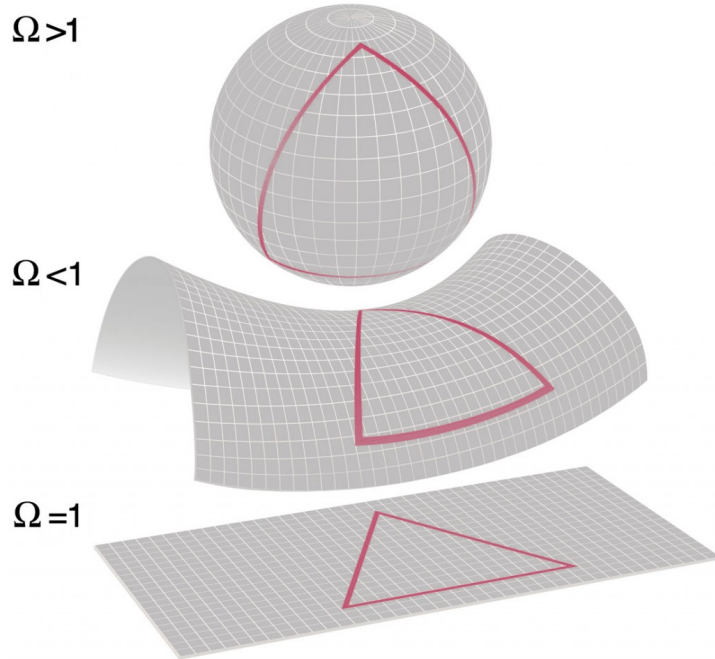


Figure 1.6: Source: quantum-bits.org

The evolution of the scale parameter as in the case of wavelength (see Exercises):

$$a(t) = \frac{1}{1+z}.$$

### 1.6.2 Friedman Equations

The dynamics's of the FLRW metric is governed by the Einstein's equations. Einstein's original field equations are:

$$R_{\mu\nu} - \frac{1}{2}Rg_{\mu\nu} = 8\pi GT_{\mu\nu}.$$

In Newtonian gravity, the source is mass. In special relativity, is a more general concept called the energy-momentum tensor, which may be modeled as a perfect fluid for which:

$$T_{\mu\nu} = (\rho + p)U_\mu U_\nu + pg_{\mu\nu},$$

where  $U_\mu$  is the fluid four-velocity in co-moving coordinates,  $\rho$  is an energy density and  $p$  is the isotropic pressure. The FLRW metric solution to the Einstein equations can be reduced to the two **Friedmann equations**:

$$H^2 \equiv \left(\frac{\dot{a}}{a}\right)^2 = \frac{8\pi G}{3}\rho - \frac{kc^2}{a^2 R_0^2},$$

and

$$\frac{\ddot{a}}{a} = -\frac{4\pi G}{3}(\rho + 3p).$$

### 1.6.3 Cosmological Constants

Given the Friedmann equations we can calculate for any value of  $H$  the critical density such as the geometry is flat ( $k = 0$ ):

$$\rho_{crit} = \frac{3H^2}{8\pi G}$$

It is convenient to measure the total energy density in terms of critical density by introducing the density parameters:

$$\Omega \equiv \frac{\rho}{\rho_{crit}} = \left(\frac{8\pi G}{3H^2}\right) \rho$$

In general the energy density will have contributions of distinct components so we can define:

$$\Omega_i \equiv \frac{\rho_i}{\rho_{crit}} = \left(\frac{8\pi G}{3H^2}\right) \rho_i$$

where  $i$  stands for the different components of the energy density as we will see later: matter (or dust), radiation, cosmological density, curvature density.

For the special case of  $a(t_0) = 1$ , ie, today, we have the formula:

$$H_0^2 \Omega_0 = \frac{8\pi G}{3} \rho_0$$

### 1.6.4 The Cosmological Constant

Einstein was interested in finding  $\dot{a} = 0$  (ie static) solutions. This can be achieved if  $k = +1$  and  $\rho$  is appropriately tuned. But  $\ddot{a}$  will not vanish in this case. Einstein therefore modified his equations to:

$$R_{\mu\nu} - \frac{1}{2}Rg_{\mu\nu} = 8\pi GT_{\mu\nu} + \Lambda g_{\mu\nu},$$

where the  $\lambda$  term is put in the rhs of the equation as it is interpreted as an effective energy-momentum tensor for the vacuum. With this modification the Friedmann equations become:

$$\begin{aligned} H^2 &= \left(\frac{\dot{a}}{a}\right)^2 = \frac{8\pi G}{3}\rho + \frac{\Lambda}{3} - \frac{kc^2}{a^2 R_0^2} \\ \frac{\ddot{a}}{a} &= -\frac{4\pi G}{3}(\rho + 3p) + \frac{\Lambda}{3} \end{aligned}$$

The discovery by Hubble that the Universe is expanding eliminated the empirical need for a static world. However, we believe that  $\Lambda$  is actually nonzero, so Einstein was right after all. Assuming that cosmological constant is due to the vacuum energy, most quantum field theories predict a  $\Lambda$  that is 120 orders of magnitude larger than the observational values! this is so-called **cosmological constant problem**.

### 1.6.5 Evolution of the Cosmological Constants

In general the energy density will have contributions of distinct components which will evolve differently with the Universe expansion:

- Massive particles with negligible velocities are known in cosmology as *dust* or simply *matter*. Their density scales as the number density times their rest mass. Their number density scales as the inverse of the volume while the rest mass is constant:  $\rho_M \propto a^{-3}$
- Relativistic particles are known as *radiation* (although it is not only photons) and their energy density is the number density times the particle energy, the latter is proportional to  $a^{-1}$  (as they redshift with expansion) and so:  $\rho_r \propto a^{-4}$
- Vacuum energy does not change as universe expand so we can define a  $\rho_\Lambda \equiv \frac{\Lambda}{8\pi G} \propto a^0$
- It is useful to pretend that  $-ka^{-2}R_0^{-2}$  represents an effective *curvature energy density* defining  $\rho_k \equiv -(3k/8\pi G R_0^2)a^{-2}$ .

Given this evolution it is possible to write:

$$H^2(t) = H_0^2[\Omega_M^0(1+z)^3 + \Omega_r^0(1+z)^4 + \Omega_k^0(1+z)^2 + \Omega_\Lambda^0]$$

### 1.6.6 Observational results

- There are good reasons to believe that the energy density of radiation is much less than matter, as photon contribute only to  $\Omega_r \sim 5 \times 10^{-5}$  mostly in the CMB. Therefore it is useful to parametrize the universe today as  $\Omega_k = 1 - \Omega_M - \Omega_\Lambda$ .
- **Direct measures of the Hubble constant.** The most reliable result on the Hubble constant comes from the [Hubble Space Telescope Key Project](#). They use the Cepheids to obtain distances to 31 galaxies (They also use Type Ia Supernovae). A recent study with over 600 Cepheids yielded the number  $H_0 = 73.8 \pm 2.4 \text{ km s}^{-1} \text{ Mpc}^{-1}$ . The indirect measurement from *Planck* Collaboration gives somehow a lower value (this discrepancy as well as the cosmic distance-ladder method are under investigation).
- **Supernovae.** Two major studies, the Supernova Cosmology Project and the High- $z$  Supernova Search Team, found evidence for an accelerating Universe. When combined with the CMB data indicating flatness (ie  $\Omega_k = 0 \rightarrow \Omega_M + \Omega_\Lambda = 1$ ), the best-fit values were  $\Omega_M \approx 0.3$  and  $\Omega_\Lambda \approx 0.7$ )
- **Cosmic Microwave Background.** See next section.

### 1.6.7 Cosmic Microwave Background

The cosmic microwave background (CMB) is electromagnetic radiation that remains from the time when photons decoupled from matter shortly after the recombination of electrons and protons into neutral hydrogen atoms. Once photons decoupled from matter, they traveled freely through the universe without interacting with matter. For an observer today this CMB is observed as a distribution of temperatures (from black body radiation) at on a two-dimensional sphere. This temperature distribution, however, was shown to have anisotropies. If we denote  $\Delta T(\theta, \phi)$  the temperature difference measured in the direction  $(\sin \theta \cos \theta, \sin \theta \sin \theta, \cos \theta)$  with respect to  $T_0 = 2.725 \text{ K}$ , the average temperature we can decompose these anisotropies over the bases of spherical harmonics, the so called  $Y_{\ell m}(\theta, \phi)$ , the same way as we can decompose a function in a curved space over sines and cosines by the Fourier transform:

$$\frac{\Delta T}{T} = \sum_{\ell m} a_{\ell m} Y_{\ell m}(\theta, \phi)$$

This decomposition tell us the amount of anisotropy at a given the multipole moment  $\ell$  or angular scale  $\theta = \frac{180^\circ}{\ell}$

$$C_\ell = \langle |a_{\ell m}|^2 \rangle$$

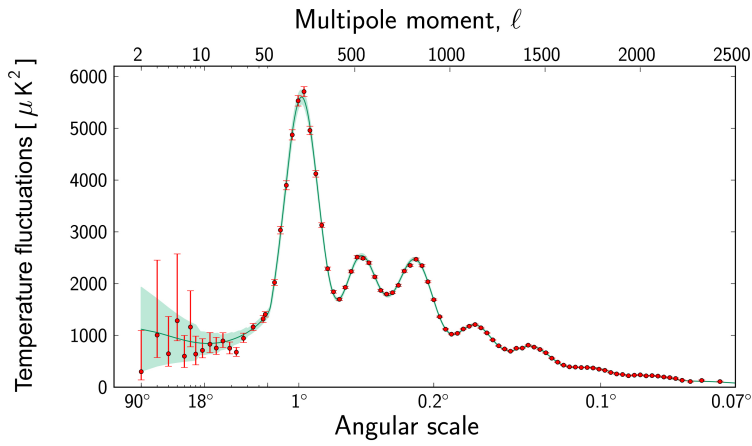


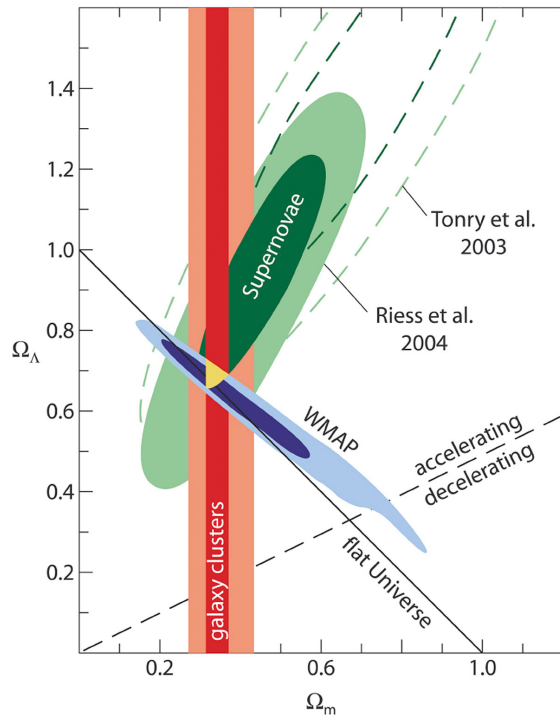
Figure 1.7: Source: ESA

The power spectrum of the CMB represents the anisotropies of the CMB as a function of the angular scale. The typical spectrum features a plateau at large angular scales (small  $\ell$ ) followed by some oscillatory features (aka acoustic peaks or *Doppler peak*). These peaks represent the oscillation of photon-baryon fluid around the decoupling. The first peak at  $\ell \sim 200$  probes the spatial geometry, while the relative heights probe the baryon density. The position of the first peak constrains the spatial geometry in a way consistent with a flat Universe ( $\Omega_k \sim 0$ )

Build your own Universe

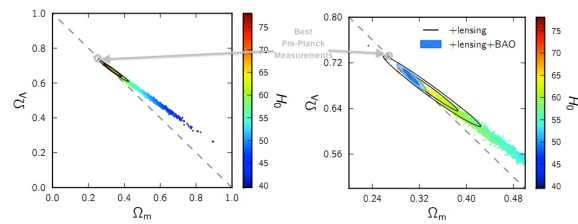
You can build your own Universe [here](#)

### 1.6.8 Before Planck



### 1.6.9 After Planck

Planck showed that the amount of dark energy in the Universe is appreciably less than we had previously thought, while the amount of dark-and-normal matter is appreciably greater than we thought.



### 1.6.10 Cosmography

Using the Hubble equation we are going to derive some quantities related to the measurement of the Universe.

### 1.6.10.1 Age of the Universe

We have shown the evolution of the Hubble expansion as a function of the redshift using the closure parameters. We know that

$$H(z) = \frac{\dot{a}}{a} = -\left(\frac{dz/dt}{(1+z)}\right) \rightarrow dt = -\frac{dz}{(1+z)H(z)}$$

And so the age of the universe can be calculated as (where  $z = 0$  corresponds to today  $t_0$ ):

$$\int_0^{t_0} dt = t_0 = \frac{1}{H_0} \int_0^{\infty} \frac{dz}{E(z)}$$

where we defined the following function:

$$E(z) \equiv \sqrt{\Omega_M(1+z)^4 + \Omega_r(1+z)^5 + \Omega_k(1+z)^3 + \Omega_{\Lambda}(1+z)}.$$

Assuming a flat Universe  $\Omega_k = 0$  and ignoring the radiation  $\Omega_r \ll \Omega_M$  the integral gets simplified to:

$$H_0 t_0 = \frac{1}{3\sqrt{1-\Omega_M}} \ln \left( \frac{1+\sqrt{1-\Omega_M}}{1-\sqrt{1-\Omega_M}} \right)$$

where we used  $1 = \Omega_{\Lambda} + \Omega_M$ .

For  $\Omega_M = 0.70$  and  $\Omega_{\Lambda} = (1 - \Omega_M) = 0.30$  one finds  $H_0 t_0 = 0.964$  so that  $t_0 \approx \frac{0.96}{H_0} = 13.5$  Gyr. Which is similar to the assumption we did with a constant  $H_0$ .

### 1.6.10.2 Comoving distance (Line of Sight)

The comoving distance between two nearby objects in the Universe is the distance between them which remains constant with epoch if the two objects are moving with the *Hubble flow*. That an object follows the *Hubble flow* if there is no peculiar velocities, ie, the only reason the 2 objects separate is due to the expansion of the Universe and not because they have relative velocities among them. The comoving distance has the expansion factored out and therefore remains constant with epoch. You can think of it as the distance measured with a ruler that also expands with the Universe. Using the same argument as above with the age of the Universe we can multiplying by the speed of light we can derive:

$$D_c(z) = \int_t^{t_0} c dt = \frac{c}{H_0} \int_0^z \frac{dz'}{E(z')}.$$

This is the comoving distance along the *line of sight*. Ie, is the comoving distance from a galaxy at redshift  $z$  from us. If we want to estimate, let's say, the distance between 2 galaxies at the same redshift but separated in angle  $\Delta\theta$ , then the distance is given by  $D_M\Delta\theta$  where  $D_M$  is the *transverse comoving distance*. For a flat Universe  $D_M = D_c$  but if the curvature is not zero, the relationship depends on the trigonometric functions  $\sinh$  (for a closed Universe) and  $\sin$  (for an open Universe) to account for the curvature of spacetime.

### 1.6.10.3 Luminosity distances

The luminosity distance defined in cosmology is defined as the distace in which an object with intrinsic luminosity  $L$  is observed with flux  $f$ , ie:

$$f = \frac{L}{4\pi d_L^2}.$$

This in terms of bolometric values, however sometimes we only observe a given bandwidth in frequency, ie, we have to replace  $f \rightarrow f(\nu_o)$  and  $L \rightarrow L(\nu_e)$  where  $\nu_o$  and  $\nu_e$  are the observed and emitted frequencies. Since the luminosity is defined as energy delivered over interval of time, we can approximate it as:

$$\begin{aligned} L(\nu_e) &= \frac{Nh\nu_e}{\Delta t_e}, \\ L(\nu_o) &= \frac{Nh\nu_o}{\Delta t_o}, \end{aligned}$$

being  $N$  the number of photos. However the photons emitted are redshifted and photons observed at  $\nu_o$  were emitted at  $(1+z)\nu_e$ . The time intervals are also related by the expansion of the Universe as:

$$\frac{\Delta t_e}{\Delta t_o} = \frac{1}{(1+z)}.$$

So we have that the emitted luminosity and the observed luminosity are related as:

$$L(\nu_o) = \frac{L(\nu_e)}{(1+z)^2}.$$

The observed luminosity is smaller than the emitted luminosity. On the other hand the relation between the observed flux and observed luminosity is the same as in a non-expanding Universe. ie:

$$f(\nu_o) = \frac{L(\nu_o)}{4\pi D_c^2},$$

where  $D_c$  is the co-moving distance. Putting everything together we have that:

$$f(\nu_o) = \frac{1}{(1+z)^2} \frac{L(\nu_e)}{4\pi D_c^2} = \frac{L(\nu_e)}{4\pi D_L^2},$$

so we have the relation between the luminosity distance and the co-moving distance as:

$$D_L = D_c(1+z).$$

#### Tutorial IV: Age of the Universe

In the about the age of the Universe we calculated an analytical solution for a given condition. Now we are going to use `python` to numerically solve the look-back time for any given set of cosmological parameters. For that we are going to rewrite the lookback formula in terms of the scale factor  $a$  since we have the redshift scale relation:

$$(1+z) = \frac{1}{a}$$

we can prove that:

$$\frac{dz}{1+z} = -\frac{da}{a}$$

Therefore the equation above that relates  $dt$  with redshift we can rewrite it at:

$$dt = \frac{da}{H(a)a}$$

with

$$H^2(a) = H_0^2[\Omega_M^0 a^{-3} + \Omega_r^0 a^{-4} + \Omega_k^0 a^{-2} + \Omega_\Lambda^0]$$

We need to numerically integrate the right hand side of the equation. However, for some parameters this integration is circular, reaching a  $a_{max}$  then the  $H^2(a_{max}) = 0$

```

#We take the current value of H0 from the astropy package

from astropy.cosmology import Planck13
H0 = Planck13.H(0).value

#We define the friedman equation ignoring the radiation component omega_r <<
def friedman(a, omega_M, omega_lambda):
    omega_k = 1 - omega_M - omega_lambda
    H2 = H0**2 * (omega_M * a**-3 + omega_k * a**-2 + omega_lambda)
    return H2

import scipy.integrate as integrate

#This is a simple integration, it does not take into account a possible Big Crunch
"""
def calculate_times(omega_m, omega_lambda):
    t0 = integrate.quad(lambda x: 1/x * 1/np.sqrt(friedman(x,omega_m, omega_lambda)), 0, 1)
    times = []
    scales = np.arange(0.1, 2, 0.01)
    for a in scales:
        time = integrate.quad(lambda x: 1/x * 1/np.sqrt(friedman(x,omega_m, omega_lambda)))
        times.append(H0*(time - t0))

    return np.array(times), np.array(scales)
"""

#This integration takes into account a Big Crunch
def calculate_times(omega_m, omega_lambda):
    #Lets check if there is a maximal, ie, if H^2(a) = 0
    astep = 0.001
    amax = 3
    scales = np.arange(0.1, amax, astep)

    f = friedman(scales, omega_m, omega_lambda)
    ia, = np.where(np.diff(np.sign(f)))

    if len(ia) != 0:
        amax = scales[ia[0]]

    tmax = integrate.quad(lambda x: 1/x * 1/np.sqrt(friedman(x,omega_m, omega_lambda)), 0,
    #time today a = 1
    t0 = integrate.quad(lambda x: 1/x * 1/np.sqrt(friedman(x,omega_m, omega_lambda)), 0, 1)

    #Empty x,y for the plots
    times = []
    scale = []                                41
    for a in scales:
        if a < amax: #If a < amax we do the typical integral 0 -> a
            time = integrate.quad(lambda x: 1/x * 1/np.sqrt(friedman(x,omega_m, omega_lambda)))
            times.append(H0*(time - t0)) #We calibrate at -t0 to place all curves together
            scale.append(a)

        if a >= amax and 2*amax - a > 0: #If a > amax we are out the domain we integrate b
            time = 2*tmax - integrate.quad(lambda x: 1/x * 1/np.sqrt(friedman(x,omega_m, omega_lambda)))
            times.append(H0*(time - t0))
            scale.append(amax)

```

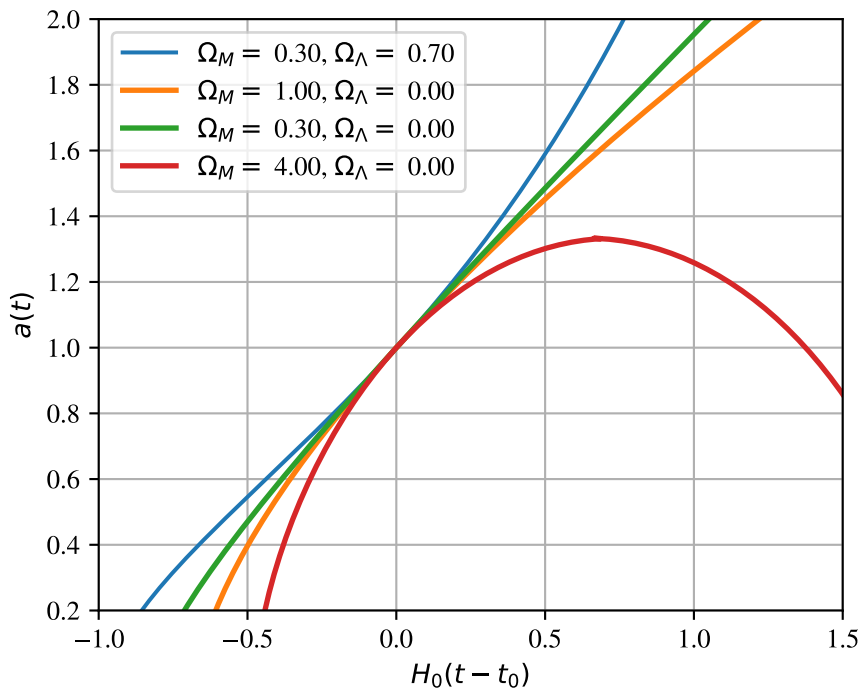


Figure 1.8: Age of the Universe

## References

- Grupen, Claus. n.d. *Astro Particle Physics*.
- Kachelriess, M. 2008. “Lecture Notes on High Energy Cosmic Rays.” <https://arxiv.org/abs/0801.4376>.
- Kampert, Karl-Heinz, and Peter Tinyakov. 2014. “Cosmic Rays from the Ankle to the Cutoff.” *Comptes Rendus. Physique* 15 (4): 318–28. <https://doi.org/10.1016/j.crhy.2014.04.006>.
- Melia, Fulvio. 2009. *High-Energy Astrophysics*. Vol. 14. Princeton University Press. <http://www.jstor.org/stable/j.ctv21r3q4z>.
- Workman, R. L., and Others. 2022. “Review of Particle Physics.” *PTEP* 2022: 083C01. <https://doi.org/10.1093/ptep/ptac097>.

## 2 Cosmic Rays

### 2.1 What are Cosmic Rays? An historic perspective

To explain cosmic rays, we need to go back about 100 years to the year 1912 when Victor Hess concluded a series of balloon flights equipped with an electroscope. He measured how ionization in the atmosphere increased as he moved away from the Earth's surface. The origin of this ionization had to be some type of radiation, and since it increased with altitude, the origin couldn't be terrestrial. In other words, there existed, and still exists, radiation coming from outer space. For this milestone, Victor Hess is known as the discoverer of cosmic rays. However, it would be unfair to attribute the merit solely to Hess, as many physicists before him had already paved the way that would culminate in his famous balloon flights: Theodor Wulf, Karl Bergwitz, and Domenico Pacini, among others, laid the foundations for one of the branches of particle physics that would dominate the field for the next 40 years until the advent of the first particle accelerators in the early 1950s.

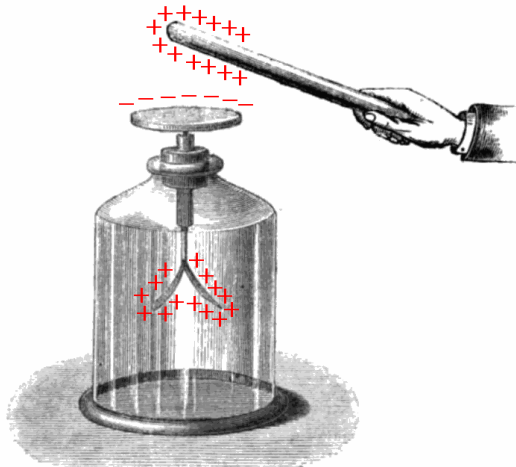


Figure 2.1: Electroscope charged by induction. Source: Sylvanus P. Thompson (1881) Elementary Lessons in Electricity and Magnetism, MacMillan, New York, p.16, fig. 12

From the beginning, cosmic rays were mysterious: What was their origin? What were these ionizing rays? During the 1920s, Bruno Rossi and Robert Millikan engaged in a lively debate

on the nature of cosmic rays. Millikan proposed that cosmic rays were “ultra”-gamma rays, photons of very high energy created in the fusion of hydrogen in space. Rossi’s measurements, showing an East-West asymmetry in the intensity of cosmic rays, suggested instead that cosmic rays must be charged particles, disproving Millikan’s theories. There is a famous anecdote in which Rossi, during the introductory talk at a conference in Rome, said: > Clearly, Millikan is resentful because a young man like me has shattered his beloved theory, so much so that from that moment on, he refuses to acknowledge my existence” A hundred years later, we know that Rossi was indeed correct. The majority, 90%, of cosmic rays are protons and other heavy nuclei. The ratio of nuclei faithfully follows the atomic abundance found in our Solar System, indicating that the origin of these particles is stellar. There are some exceptions; for example, lithium, beryllium, and boron are nuclei that we can find among cosmic rays in a proportion greater than in our environment. These nuclei are actually produced by the fragmentation of heavier ones, such as carbon, during their journey through space. Thus, the abundance ratio between carbon and boron provides information about how long carbon has been traveling through space.

The spectrum, or the number of particles per unit area and time as a function of energy, has also been measured in great detail over the last 30 years thanks to the work of numerous experiments. The cosmic ray spectrum is remarkable in both its variation and energy range. The number of particles, or flux, covers 32 orders of magnitude, so we find that the least energetic particles reach Earth at a rate of one particle per square meter every second. On the other hand, the most energetic ones arrive at a rate of one particle per square kilometer per year. This is why physicists have had to develop various experimental techniques to measure the spectrum of cosmic rays in its entirety: from particle detectors sent into space on satellites or attached to the International Space Station, to experiments deployed on large surfaces of the Earth to detect the most energetic cosmic rays, such as the Pierre Auger Observatory covering an area of about 3000 km<sup>2</sup> on the high plateau of the Pampa Amarilla in Malargüe, Argentina.

But what makes cosmic rays truly fascinating is the amount of energy these particles can reach, far superior to what can be achieved today with the most powerful accelerator built by humans with the Large Hadron Collider (LHC) at the European Organization for Nuclear Research (CERN) in Geneva. The LHC is an underground ring with a length of 27 km located on the Franco-Swiss border near Geneva, Switzerland, using powerful magnets to accelerate protons to 99.99% of the speed of light. Despite the impressiveness of this experiment, if we were to accelerate particles to the energies of cosmic rays with the same technology, we would need an accelerator the size of the orbit of Mercury. The speed of cosmic rays is so high that the effects of space-time relativity are considerable. For example, although the radius of our Galaxy is about 100,000 light-years, due to the temporal contraction of special relativity, the most energetic cosmic rays would experience they will experience the journey in just 10 seconds. When cosmic rays reach Earth, they encounter 10 kilometers of atmosphere which, along with the Earth’s magnetic field, fortunately acts as a shield and protects us from radiation. However, when cosmic rays collide with atoms in the atmosphere, they trigger a shower of new particles. This shower is known as secondary cosmic rays, and in it, we can

find a diverse array of new particles. This is why, for many years, the physics of cosmic rays was the only way for particle physicists to discover and study new particles. Thus, following in Hess's footsteps, during the 1940s, many physicists moved from the laboratory to hot air balloons equipped with bubble chambers (a primitive version of a particle detector) to study this myriad of new particles. Among the new particles discovered were, for example, the first particle of antimatter: the positron, a positively charged electron, as well as the muon, with properties similar to the electron but with greater mass.

But what is the origin of cosmic rays? Which sources in the Universe are capable of accelerating particles to such energies? That is the question that, despite 100 years since Victor Hess's discovery, physicists have not been able to fully answer. The main reason is, however, easy to understand. Cosmic rays, being charged particles, are deflected by magnetic fields during their journey through the Universe. Both the Milky Way and intergalactic space are immersed in magnetic fields, so when cosmic rays reach Earth, their direction has little or nothing to do with the original direction, making it impossible to do *astronomy*. However, despite this disadvantage, we can deduce some things about their origin based on, for example, their energy. We know that low-energy cosmic rays must come from our own Galaxy because the magnetic fields of the Milky Way would confine them until they eventually interact with Earth. On the other end of the spectrum, extremely high-energy cosmic rays (UHECRs) must come from outside our own Galaxy since they are so energetic that the magnetic fields of their respective galaxies would not be able to retain them. The exact turning point in energy between these two origins is uncertain. So far, we have been unable to undoubtivously observe a cosmic-ray source. One of the main candidates for the source of galactic cosmic rays are supernova remnants. At the end of a star's life cycle, it can explode, releasing a large amount of mass and energy. What remains behind can be a neutron star surrounded by all the remnants left from the original star; this is what is called a supernova remnant. It is more challenging to conceive a cosmic accelerator capable of accelerating particles up to the energy equivalent of a soccer ball kicked at 50 km/h, which corresponds to the energies of UHECRs. Here the list of candidates is considerably reduced because there are fewer objects in the Universe with the magnetic field and size sufficient to act as a large particle accelerator. The candidates are active galactic nuclei and gamma-ray bursts. Active galactic nuclei are the nuclei of galaxies with a supermassive black hole at their center. These nuclei show beams of particles in opposite directions that could function as large accelerators. On the other hand, gamma-ray bursts are the most violent events known in the Universe, and their origin and nature would warrant another chapter of this book. Lasting from a few seconds to a few minutes, these events can illuminate the entire sky by releasing their energy mainly in the form of very high-energy photons. But if cosmic rays never point to their source, how can we ever be sure that active galactic nuclei or gamma-ray bursts are the true sources of cosmic rays? To answer this puzzle, we need what has been dubbed as *multi-messenger astronomy*. Thanks to particle physics, we know that under the conditions in which, for example, a proton is accelerated to high energies, reactions with the surrounding matter can occur. These interactions would produce other particles such as very high-energy photons and neutrinos. Neutrinos are especially interesting because they are not only neutral and therefore travel in a straight line without being deflected by magnetic

fields, but they are also weakly interacting particles, so unlike photons, they can traverse dense regions of the Universe without being absorbed. Future multi messenger experiments will be able to solve the mystery of cosmic rays.

## 2.2 The Cosmic Ray Spectrum

Cosmic rays mostly protons accelerated at sites within the Galaxy.

- As they are charged they are deviated in galactic and inter-galactic  $\vec{B}$  and solar and terrestrial magnetic fields. Directionality only possible for  $E \geq 10^{19}$  eV.
- But interactions with CMB at  $E \sim 10^{19}$  limit horizon tens or hundreds of Mpc.
- One century after discovery, origins of cosmic rays, in particular UHECR, remain **unknown**

```
import crdb
import matplotlib.pyplot as plt
plt.rcParams['font.family'] = "STIXGeneral"
plt.rcParams.update({'axes.labelsize': 20})
plt.rcParams.update({'legend.fontsize': 20})
plt.rcParams.update({'figure.figsize': [8, 6]})
plt.rcParams['xtick.labelsize'] = 18
plt.rcParams['ytick.labelsize'] = 18
plt.rcParams['xtick.major.width'] = 1.5
plt.rcParams['xtick.minor.width'] = 1
plt.rcParams['xtick.major.pad'] = 8
plt.rcParams['xtick.direction'] = 'in'
plt.rcParams['ytick.major.size'] = 10
plt.rcParams['ytick.minor.size'] = 5
plt.rcParams['ytick.major.width'] = 1.5
plt.rcParams['ytick.minor.width'] = 1
plt.rcParams['ytick.major.pad'] = 8
plt.rcParams['ytick.direction'] = 'in'
plt.rcParams['legend.frameon'] = False
plt.rcParams['lines.linewidth'] = 1.5
plt.rcParams['axes.linewidth'] = 1.5

import numpy as np

from crdb.experimental import convert_energy
```

```

fig, ax = plt.subplots(1,1, figsize=(5, 7))
elements = ("H", "He", "C", "N", "O", "Si", "Fe")
elements += ("1H-bar", "e-+e+", "AllParticles")

tabs = []
for energy_type in ("EKN", "ETOT"):
    for elem in elements:
        tab = crdb.query(
            elem,
            energy_type=energy_type,
            energy_convert_level=1,
        )
        if energy_type == "EKN":
            tab = convert_energy(tab, "EK")
        tabs.append(tab)
tab = np.concatenate(tabs).view(np.recarray)

#Lets ignore data without systematic errors
mask = (tab.err_sys[:, 0] > 0) & (tab.err_sta[:, 0] / tab.value < 0.5)
tab = tab[mask]
ax.set_xlim(1e-2, 5e11)
for elem in elements:
    ma = tab.quantity == elem

    t = tab[ma]
    if len(t) == 0:
        continue
    sta = np.transpose(t.err_st)
    color = "k" if elem == "AllParticles" else None
    ax.errorbar(t.e, t.value, sta, fmt=". ", color=color)
ax.loglog()
ax.set_ylabel(r"$E_k$ d$J/d$E_k$ [1/(m$^2$ s sr)]")
ax.set_xlabel(r"$E_k$ [GeV]")
ax.grid()

m = 1
km = 1e3 * m
s = 1
sr = 1
hour = 60**2 * s
day = 24 * hour
month = 30 * day

```

```
year = 356 * day
century = 100 * year

for flux_ref in (
    "1/m^2/s/sr",
    "1/m^2/day/sr",
    "1/m^2/year/sr",
    "1/km^2/day/sr",
    "1/km^2/century/sr",
):
    v = eval(flux_ref.replace("^2", "**2"))
    label = flux_ref.replace("^2", "$^2$")
    ax.axhline(y=v, color="0.4", lw = 2)
    ax.text(
        10**11,
        v * 1.1,
        label,
        va="bottom",
        ha="right",
        color="0.4",
        zorder=0,
    )
```

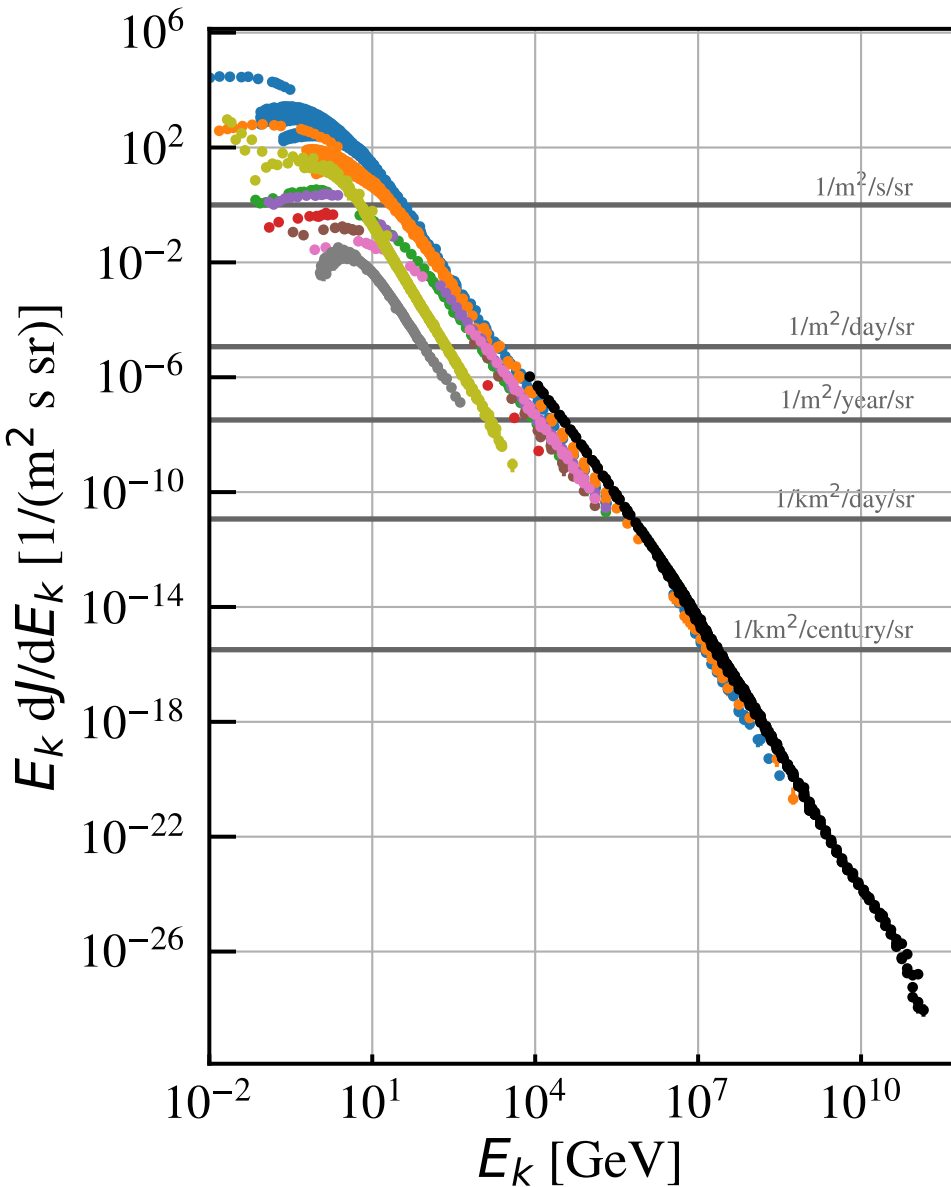


Figure 2.2: All particle cosmic ray spectrum

### 2.2.1 Cosmic Ray as function of...

There are four different ways to describe the spectra of the cosmic ray radiation:

- By **particles per unit rigidity**. Propagation and deflection on magnetic fields depends on the rigidity.

- By **particles per energy-per-nucleon**. Fragmentation of nuclei propagating through the interstellar gas depends on energy per nucleon, since that quantity is approximately conserved when a nucleus breaks up on interaction with the gas.
- By **nucleons per energy-per-nucleon**. Production of secondary cosmic rays in the atmosphere depends on the intensity of nucleons per energy-per-nucleon, approximately independently of whether the incident nucleons are free protons or bound in nuclei.
- By **particles per energy-per-nucleus**. Air shower experiments that use the atmosphere as a calorimeter generally measure a quantity that is related to total energy per particle.

For  $E > 100$  TeV the difference between the kinetic energy and the total energy is negligible and fluxes are often presented as **particle per energy-per-nucleus**.

For  $E < 100$  TeV the difference is important and it is common to present **nucleons per kinetic energy-per-nucleon**. This is the usual way of presenting the spectrum for nuclei with different masses: the conversion in energy per nucleus is not trivial.

### 2.2.2 Primary Cosmic Rays

The energy spectrum of primary nucleons from GeV to  $\sim 100$  TeV is given by:

$$I(E) \approx 1.8 \times 10^4 \left( \frac{E}{1 \text{ GeV}} \right)^{-2.7} \frac{\text{nucleons}}{\text{m}^2 \text{ s sr GeV}}$$

Where  $\alpha \equiv 1 + \gamma = 2.7$  is the differential spectral index and  $\gamma$  the integral spectral index. The composition of the bulk of cosmic rays are: 80% protons, 15% He, and the rest are heavier nuclei: C, O, Fe and other ionized nuclei and electrons (2%)

```
elements = {
    "H": 0,
    "He": -2,
    "C": -4,
    "O": -6,
    "Ne": -8,
    "Mg": -10,
    "Si": -12,
    "S": -14,
    "Ar": -16,
    "Ca": -18,
    "Fe": -21,
}
xlim = 1e-2, 1e6
```

```

tabs = []
for elem in elements:
    tabs.append(crdb.query(elem, energy_type="EKN"))

tab = np.concatenate(tabs).view(np.recarray)
# use our energy range
tab = tab[(xlim[0] < tab.e) & (tab.e < xlim[1])]
# we don't want upper limits
tab = tab[~tab.is_upper_limit]
# statistical errors less than 100 %
tab = tab[np.mean(tab.err_sta, axis=1) / tab.value < 1]
# skip balloon data
mask = crdb.experiment_masks(tab)["Balloon"]
tab = tab[~mask]

fig, ax = plt.subplots(1,1,figsize=(6, 9))
masks = crdb.experiment_masks(tab)
for exp in sorted(masks):
    t = tab[masks[exp]]
    first = True
    color = None
    marker = None
    for elem, fexp in elements.items():
        f = 10**fexp
        t2 = t[t.quantity == elem]
        if len(t2) == 0:
            continue
        sta = np.transpose(t2.err_sta)
        l = ax.errorbar(t2.e, t2.value*f, sta*f, fmt=".", color=color, label = exp if first else None)
        first = False
        color = l.get_children()[0].get_color()

    for elem, fexp in elements.items():
        t = tab[tab.quantity == elem]
        ymean = np.exp(np.mean(np.log(t[t.e < xlim[0] * 100].value))) * 10**fexp
        s = f"\{elem}\n$\times 10^{{{fexp}}}$" if fexp != 0 else f"\{elem}"
        ax.text(2e-3, ymean, s, va="center", ha="center")

ax.grid(color="0.9")
ax.set_xlim(xlim[0]/30, xlim[1])
ax.loglog()
ax.legend()

```

```

    fontsize="xx-small", frameon=False, loc="upper left", ncol=2, bbox_to_anchor=(1, 1)
)
#ax.legend()

```

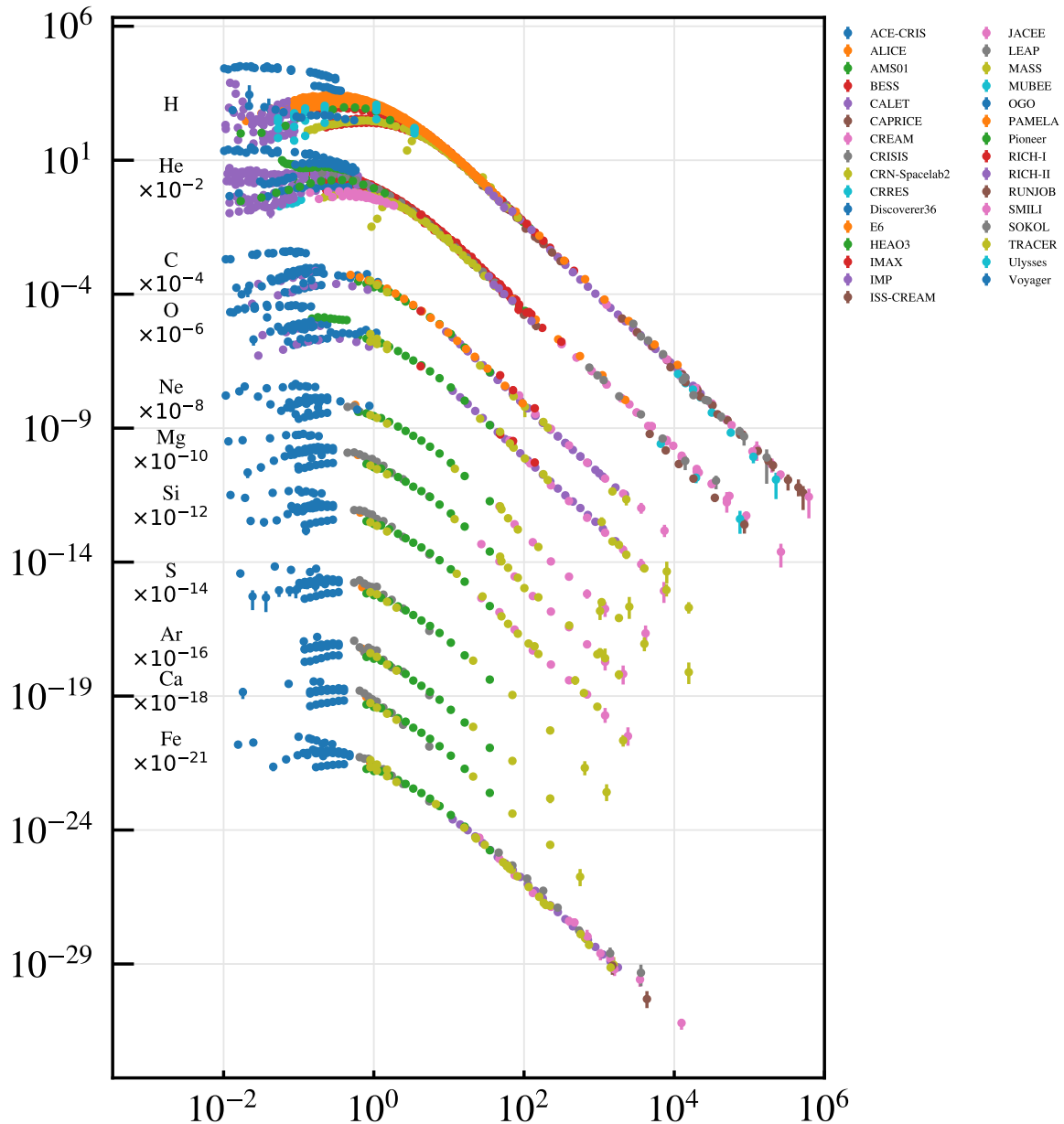


Figure 2.3: Cosmic Ray spectrum per element

### 2.2.3 Galactic Cosmic Ray Composition

- The chemical composition of cosmic rays is similar to the abundances of the elements in the Sun indicating an **stellar origin of cosmic rays**.
- However there are some differences: Li, Be, B are secondary nuclei produced in the spallation of heavier elements (C and O). Also Mn, V, and Sc come from the fragmentation of Fe. These are usually referred as **secondary cosmic rays**.
- The see-saw effect is due to the fact that nuclei with odd Z and/or A have weaker bounds and are less frequent products of thermonuclear reactions.

By measuring the primary-to-secondary ratio we can infer the propagation and diffusion processes of CR.

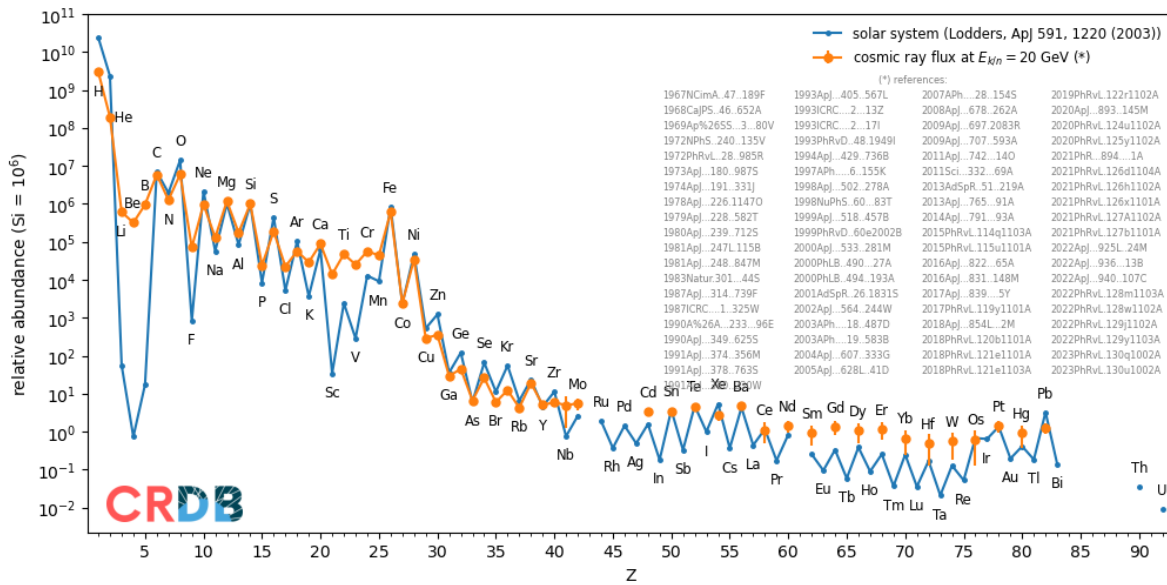


Figure 2.4: Cosmic ray composition. Source: CRDB

### 2.2.4 Electrons

The spectrum of electrons is expected to steepen because the radiative energy loss in the Galaxy. Electrons will lose energy primarily due to **synchrotron radiation** and inverse Compton scattering

```
tab = crdb.query("e-+e+", energy_type="EK")

xlim = 1, 1e4
tab = tab[(xlim[0] < tab.e) & (tab.e < xlim[1])]
```

```

exclude_exp = ("Balloon", "LEE")
fig, ax = plt.subplots(1, 1, figsize=(6, 4))
for i, (exp, mask) in enumerate(crdb.experiment_masks(tab).items()):
    t = tab[mask]
    f = t.e**3 #We plot Flux*E**3
    sta = np.transpose(t.err_st)
    if exp in exclude_exp: # Let's exclude balloon experiments
        continue
    ax.errorbar(
        t.e, t.value*f, sta*f, fmt=". ", label=exp
    )

ax.set_xlim(*xlim)
ax.set_ylim(1, 8e2)
ax.set_xlabel(r"E_k [GeV]")
ax.set_ylabel(r"E_k^3 dJ/dE_k [GeV^2 / (m^2 s sr)]")
ax.legend(fontsize="xx-small", ncol=3, frameon=False, bbox_to_anchor=(1, 1))
ax.loglog()
ax.grid(color="0.9")
ax.loglog()
ax.legend(
    fontsize="xx-small", frameon=False, loc="upper left", ncol=2, bbox_to_anchor=(1, 1)
)

```

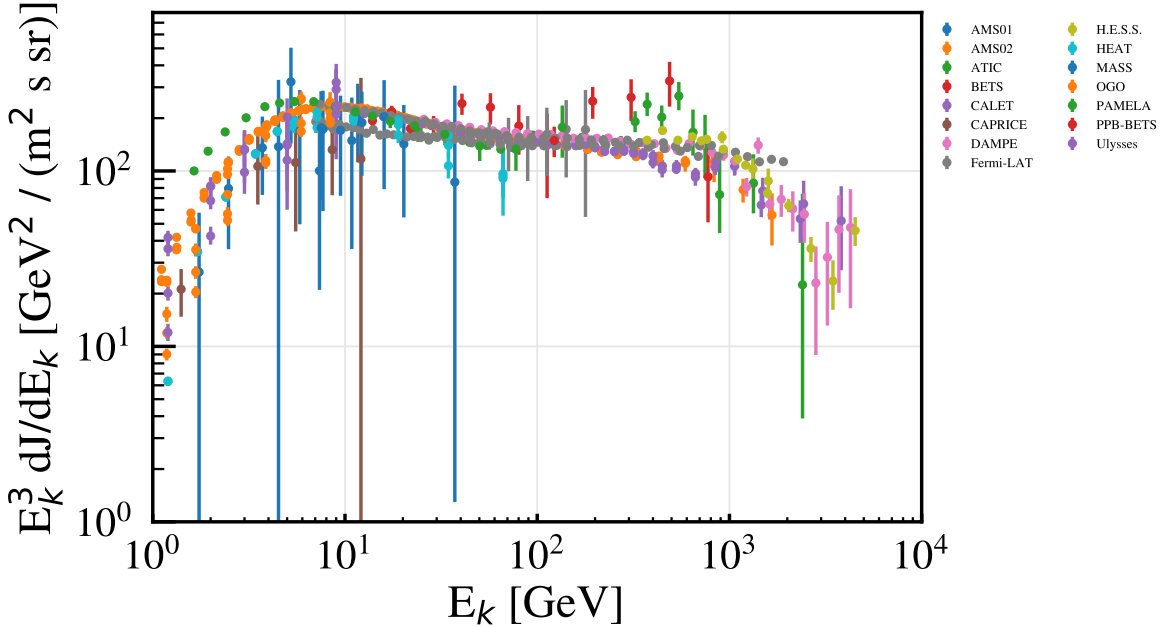


Figure 2.5: Spectrum of  $e^- + e^+$  cosmic rays

The plot above shows the  $(e^- + e^+)$  spectrum, only PAMELA data refers only to  $e^-$ . As can be seen there are several features worth noting:

- For  $E \leq 20$  GeV the spectra is dominated by solar modulations and somehow follows the same spectral index as the proton spectrum, although with factor 0.01 in the normalization, which means that electrons contribute only 1% to the overall CR spectrum.
- At about 5 GeV there is a change in the spectrum. Sometimes identified as the energy when electrons start to loose energy, and therefore the spectrum becomes steeper.
- For  $E > 50$  GeV spectra is well fitted with a power law of  $\sim 3.1$  for  $e^-$  and  $\sim 2.7$  for  $e^+$ . Since  $e^-$  dominate over  $e^+$  the overall spectrum  $(e^- + e^+)$  also follows a spectral index of  $\sim 3$ . Electron spectrum is much steeper than the proton one.
- The sum spectrum  $(e^- + e^+)$  has a sharp break at  $E \simeq 1$  TeV, however this is dominated by the  $e^-$  with an estimate of a ratio of  $3 - 4$  in  $e^-/e^+$ . This cutoff has been confirmed by DAMPE making it the first direct observation of this cutoff.
- There is an excess measured by ATIC at  $\sim 700$  GeV. The existence of that feature has, however, never been confirmed by other experiments (Fermi, DAMPE, HESS).

**! Important**

Given the diffusion loss length of electrons is about 300 pc and confinement time in the Galaxy about  $100 = yrs$  it is assumed that the electron spectrum above few TeV is

dominated by nearby and young cosmic ray sources.

### i Question

Assuming the electron flux is only 1% of the protons. Is it the Earth positive charged-up?

#### 2.2.5 Antimatter

- As antimatter is rare in the Universe today, all antimatter we observe are by-product of particle interactions such as Cosmic Rays interacting with the interstellar gas.
- The PAMELA and AMS-02 satellite experiments measured the positron to electron ratio to increase above 10 GeV instead of the expected decrease at higher energy.

```
fig, ax = plt.subplots(1,1, figsize=(6,5))

tab = crdb.query("e+/e-+e+", energy_type="EK")

xlim = 0.8, 1e3
tab = tab[(xlim[0] < tab.e) & (tab.e < xlim[1])]

experiments = ("AMS01", "AMS02", "PAMELA")
for i, (exp, mask) in enumerate(crdb.experiment_masks(tab).items()):
    t = tab[mask]
    sta = np.transpose(t.err_st)
    if exp in experiments:
        ax.errorbar(t.e, t.value, sta, fmt=". ", label=exp)

ax.set_xlim(*xlim)
ax.set_ylim(0, 0.3)
ax.grid(color="0.4")
ax.set_xlabel(r"$E_k$ [GeV]")
ax.set_ylabel(r"$\frac{e^+}{e^-+e^+}$")
ax.legend(
    ncol=1,
    loc="upper left",
)
ax.semilogx()
```

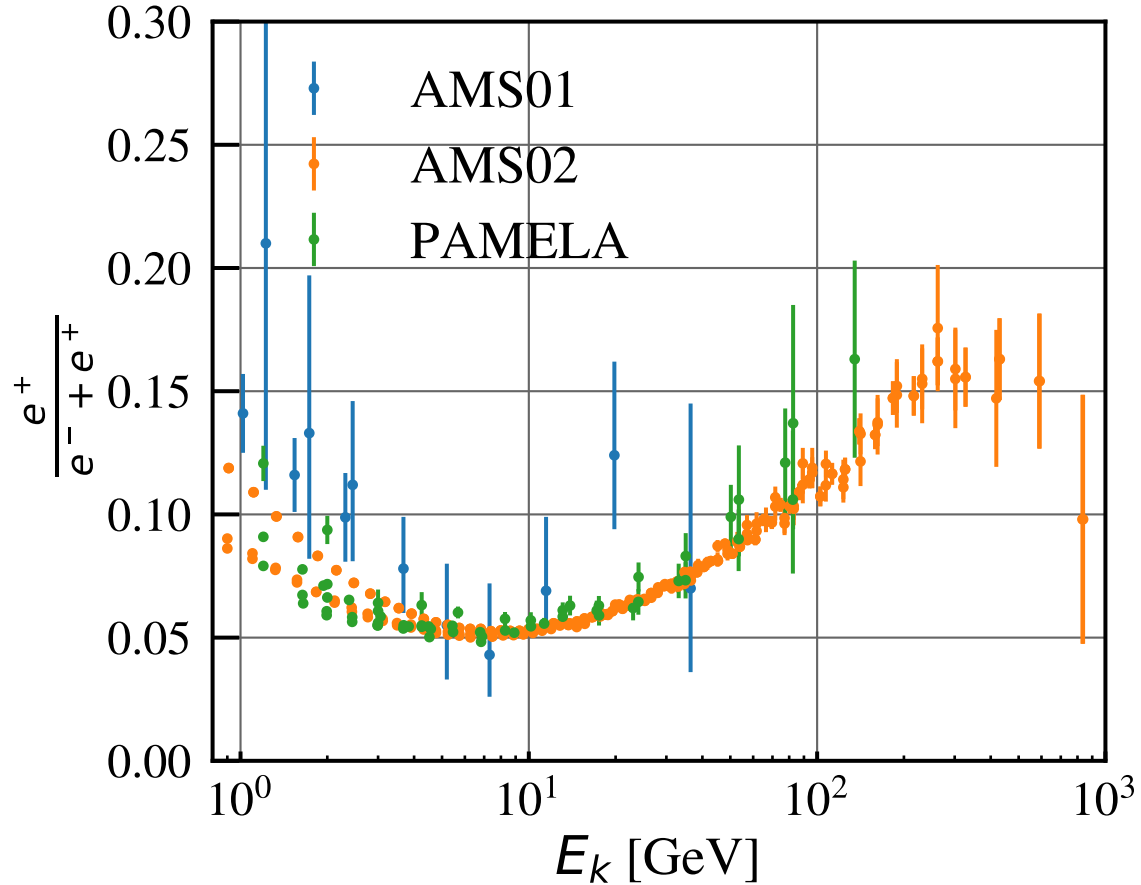


Figure 2.6: Positron excess

This excess might hint to contributions from individual nearby sources (supernova remnants or pulsars) emerging above a background suppressed at high energy by synchrotron losses.

## 2.3 Galactic Cosmic Rays

### 2.3.1 Propagation of Cosmic Rays

One trivial argument to discriminate between a Galactic or extra-Galactic origin of the origin of cosmic rays is to check whether or not the larmor radius,  $r_L$ , of cosmic ray particles is of the order of the size of the Galaxy. As we showed, we can express the larmor radius as:

$$r_L \simeq 1 \text{ kpc} \left( \frac{E}{10^{18} \text{ eV}} \right) \left( \frac{1}{Z} \right) \left( \frac{\mu\text{G}}{B} \right)$$

and so the maximum energy to contain cosmic rays in the Galaxy is:

$$E < 10^{18} \text{ eV} \left( \frac{h}{1 \text{ kpc}} \right) \left( \frac{\mu\text{G}}{B} \right)$$

There are many uncertainties in these numbers but we can assume that the size of the Galactic halo is  $h \sim 1 - 10$  kpc, and the magnetic field in the halo is about  $B \sim 0.1 - 10 \mu\text{G}$ . Putting this number gives maximum energy of  $E_{max} \sim 10^{17} - 10^{20}$  eV. Given this result we can assume that lower energy cosmic rays come from own Galaxy, otherwise they would have escaped.

### 2.3.1.1 Cosmic-ray Interactions

Since the bulk of cosmic-ray particles are expected come from the Galaxy we can now evaluate where and how they will interact during their travel. There are two chiefly process in which a cosmic-ray particle can interact:

- **Coulomb collisions:** They occur when a particle interacts with another particle via electric fields.
  - The Coulomb cross-section for a 1 GeV particle is  $10^{-30} \text{ cm}^2$ .
  - For 1 GeV cosmic-ray propating in the ISM ( $n \sim 1 \text{ cm}^{-3}$ ) the mean Coulomb interacion length rate is  $1/n\sigma \sim 324100 \text{ Mpc}$  which is much larger than the Galaxy size. Therefore **coulomb collisions can be neglected**.
- **Spallations processes:** It occurs when C, N, O, Fe nuclei impact on intestellar hydrogen. The large nuclei is broken up into smaller nuclei. A clear indication of a spallation comes precisely from the composition comparison with stellar matter.

```
sigma = 1e-30 #in cm2
n = 1 # in cm-3
l = 1./(n*sigma) * 3.241e-25 # in Mpc
print (f"The interaction length for Coulomb collisions is {l:.2} Mpc")
```

The interaction length for Coulomb collisions is  $3.2 \times 10^5 \text{ Mpc}$

### 2.3.1.2 The Interstellar Medium (ISM)

Given the low density of the Galactic halo it is clear that the spallation processes must occur in the Galactic Disk. The Galactic Disk is mostly populated by the Interstellar Medium or ISM. It is mostly composed by Hydrogen in 3 different phases:

- Molecular Gas. This phase is the more clumpsy as they gathered in molecular clouds that can reach densities of  $10^6 \text{ cm}^{-3}$  which is still very low for our atmosphere standards (14 lower). It is composed of hydrogen in molecular form,  $\text{H}_2$ , CO. Sometimes called stars nurseries they are stars forming regions.
- Atomic Gas. Made up of neutral atomic Hydrogen (HI in astronomical nomenclature). The maps tracing the HI that is organized in a spiral pattern, like  $\text{H}_2$ , and also its structure is quite complex, with overdensities and holes.
- Ionized Gas. Is ionized Hydrogen or HII.

The overall density of the ISM is  $\sim 0.1 - 1 \text{ cm}^{-3}$ . The interstellar gas is not a static gas, but rather is subject to a turbulent motion.

### 2.3.1.3 The Leaky Box Model

The *Leaky Box model* is a very simple model used to describe cosmic-ray confinement. In this simplified phenomenological picture CRs are assumed to be accelerated in the galactic plane and to propagate freely within a cylindrical box of size  $H$  and radius  $R$  (see Figure 2.7) and reflected at the boundaries; the loss of particles is parametrized assuming the existence of a non-zero probability of escape for each encounter with the boundary (Poisson process).

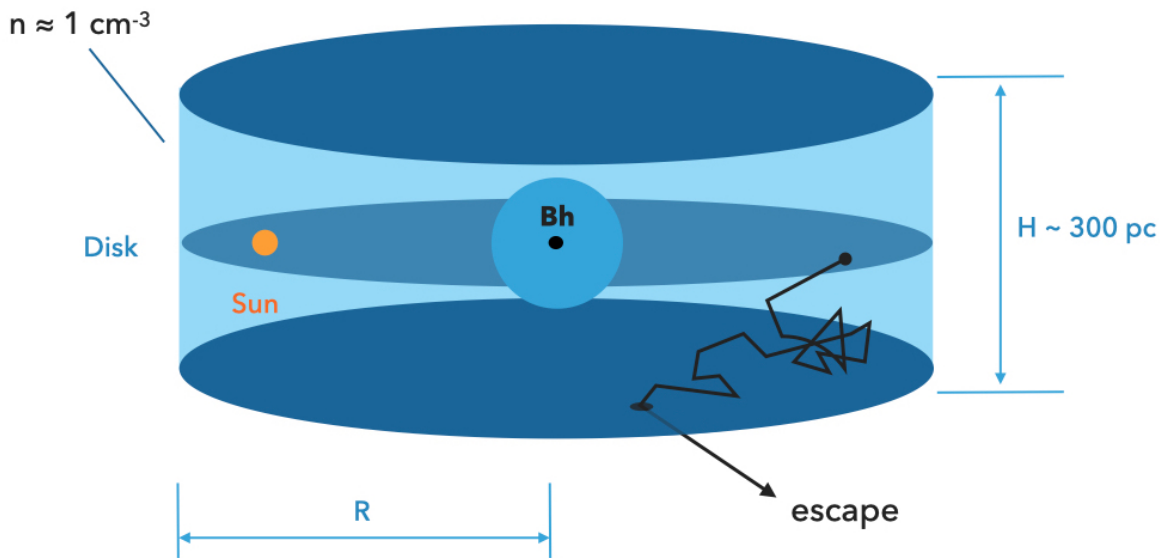


Figure 2.7: Representation of the *leaky box* model of the Galaxy

#### 2.3.1.4 Primary-to-Secondary Ratios

Since we know the partial cross-section of spallation processes we can use the secondary-to-primary abundance ratios to infer the gas column density traversed by the average cosmic ray.

Let us perform a simply estimate of the *Boron-to-Carbon ratio*. Boron is chiefly produced by Carbon and Oxygen with approximately conserved kinetic energy per nucleon (see *Superposition principle*), so we can relate the *Boron source production rate*,  $Q_B(E)$  to the differential density of Carbon by this equation:

$$Q_B(E) \simeq n_{ISM} \beta c \sigma_{f,B} N_C$$

where,  $n_{ISM}$  denotes the average interstellar gas number density and  $N_C$  is the Carbon density and  $\beta c$  is the Carbon velocity and  $\sigma_{f,B}$  is the spallation or fragementation cross-section of Carbon into Boron.

The Boron disappears by escaping the galaxy in Poisson process or lossing its energy. The disappearance of Boron can be written using a lifetime  $\tau$  as:

$$D_B = \frac{N_B}{\tau}$$

assuming the amount of Boron in the Galaxy is constant per unit time,  $\dot{N}_B = 0$ , then the production of Boron has to be equal to the disappearance rate, in other words:

$$\dot{N}_B = 0 = Q_B - D_B$$

We can write:

$$\frac{N_B}{N_C} \simeq n_H \beta c \sigma_{\rightarrow B} \tau$$

##### 2.3.1.4.1 Boron-to-Carbon Ratio

The plot below represents the latest measurements from PAMELA and AMS satellites of the Boron-to-Carbon ratio. The decrease in energy of the Boron-to-Carbon ratio suggests that high energy CR spend less time than the low energy ones in the Galaxy before escaping.

```

tab = crdb.query("B/C", energy_type="EKN")

# select only entries with systematic uncertainties
mask = tab.err_sys[:, 1] > 0
tab = tab[mask]

fig, ax = plt.subplots(1, 1, figsize=(6,5))

from matplotlib import pyplot as plt
# Let's plot AMS02 only
for i, (exp, mask) in enumerate(crdb.experiment_masks(tab).items()):
    t = tab[mask]
    sta = np.transpose(t.err_st)
    ax.errorbar(t.e, t.value, sta, fmt=". ", label=exp)

ax.legend(ncol=2, frameon=False)
ax.grid()
ax.set_xlabel("$E_{\mathrm{kin}} / \mathrm{A} / \mathrm{GeV}$")
ax.set_ylabel("B/C")
ax.loglog()

```

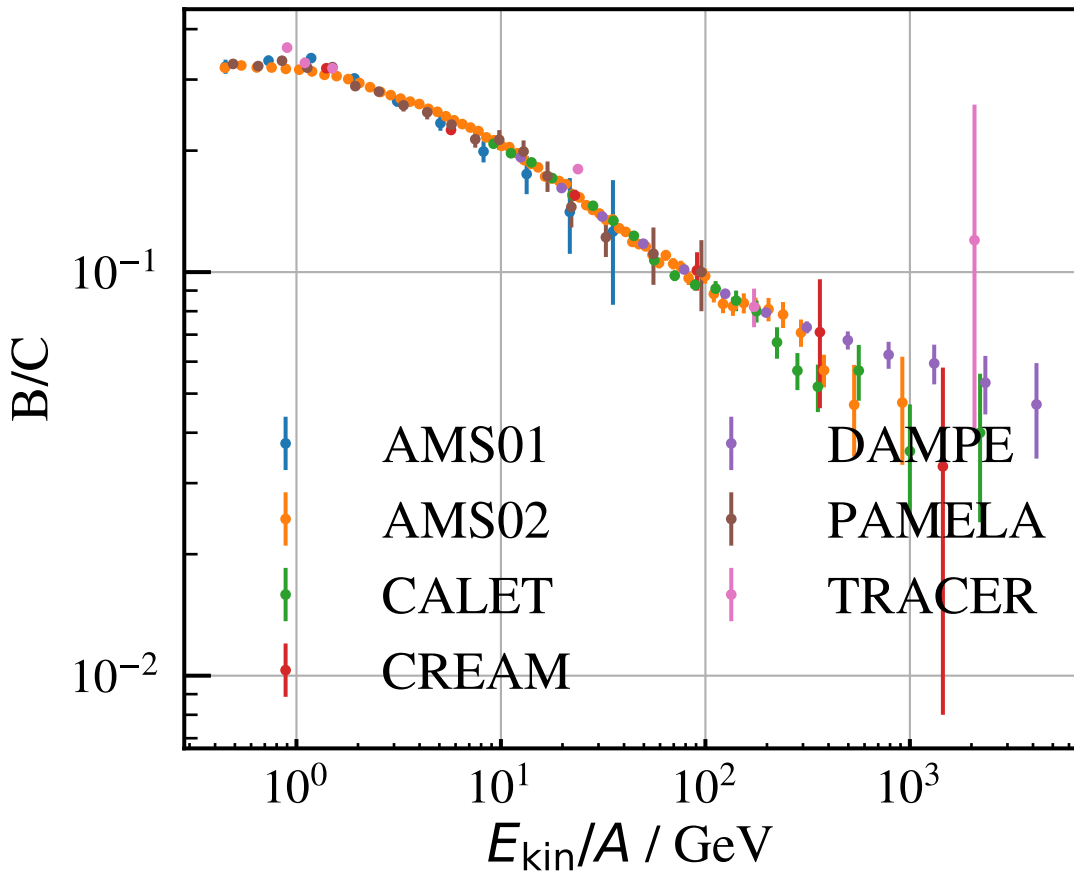


Figure 2.8: B/C ratio

**Tutorial I: Fit the B/C spectrum of AMS-02 data**

We are going to retrieve the data and fit it. We are going to use python to download the data

```

tab = crdb.query("B/C", energy_type="EKN")

# select only entries with systematic uncertainties
mask = tab.err_sys[:, 1] > 0
tab = tab[mask]

fig, ax = plt.subplots(1, 1, figsize=(6,4))

from matplotlib import pyplot as plt
# Let's plot AMS02 only
for i, (exp, mask) in enumerate(crdb.experiment_masks(tab).items()):
    if exp == "AMS02":
        t = tab[mask]
        sta = np.transpose(t.err_st)
        ax.errorbar(t.e, t.value, sta, fmt=". ", label=exp)
#Let's use a simple linear model in log-log
def model(x, a, b):
    return a + b * x

from scipy.optimize import curve_fit
#We only fit in the linear part, ie when E > 10 GeV and we ignore statistical errors.
mask = t.e > 10
popt, pcov = curve_fit(model, np.log10(t.e[mask]), np.log10(t.value[mask]))

ax.plot(t.e[mask], np.power(10, model(np.log10(t.e[mask])), popt[0], popt[1])), linewidth=2

ax.legend(ncol=2, frameon=False)
ax.grid()
ax.set_xlabel("$E_{\mathrm{kin}} / \mathrm{GeV}$")
ax.set_ylabel("B/C")
ax.loglog()

print(f"The values are \u03b1 = {10**popt[0]:.2} and \u03b2 = {popt[1]:.2}")

```

The values are  $\alpha = 0.44$  and  $\beta = -0.34$

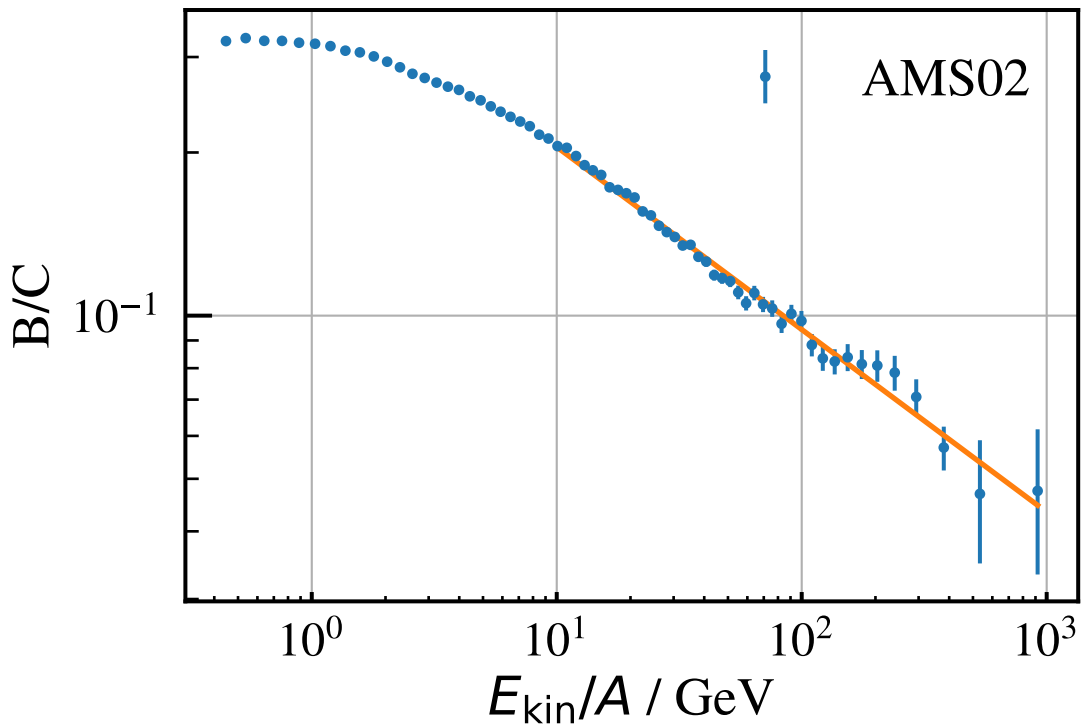


Figure 2.9: Boron to Carbon ratio

Above about 10 GeV/nucleon the **experimental data** can be fitted to a test function, therefore the Boron-to-Carbon ratio can be expressed as:

$$\frac{N_B}{N_C} = n_H \beta c \sigma_{f,B} \tau = 0.4 \left( \frac{E}{\text{GeV}} \right)^{-0.3}$$

For energies above 10 GeV/nucleon we can approximate  $\beta \sim 1$ , which leads, using the values of the cross-section, to a life time gas density of:

$$n_H \tau \simeq 10^{14} \left( \frac{E}{\text{GeV}} \right)^{-0.3} \text{ s cm}^{-3}$$

#### 2.3.1.4.2 Boron Lifetime

But what is this Boron lifetime? The lifetime  $\tau$  for Boron includes the **catastrophic loss** time due to the partial fragmentation of Boron,  $\tau_{f,B}$  and the **escape probability** from the Galactic confinement volume,  $T_{esc}$ . The fragmentation cross section is  $\sigma_{f,B} \approx 250$  mbarn so we find that:

$$n_H \tau_{f,B} = \frac{n_H}{n_H \beta c \sigma_{f,B}} \simeq 1.33 \times 10^{14} \text{ s cm}^{-3}$$

which is a good match with the loss time bound at  $\sim 1$  GeV but is larger at higher energies and does not depend on energy. For example at 1 TeV it is an order of magnitude larger:

$$n_H \tau(1 \text{ TeV}) \simeq 10^{14} 1000^{-0.3} \sim 1.3 \times 10^{13} \text{ s cm}^{-3}$$

#### 2.3.1.4.3 Boron Escape

It could be that Boron escape the leaky box, but that time will be  $\tau_{esc} = \frac{H}{c}$  which will be roughly:

$$\tau_{esc} = \frac{300 \text{ pc}}{c} \simeq 3 \times 10^{10} \text{ s}$$

which is too small compared to the effective lifetime found. This seems to indicate that CR do not travel in straight lines. Let's assume that the overall process is a combination of both the boron fragmentation and another process with a lifetime  $T$ . By summing the inverse of these processes (being exponential processes):

$$\tau^{-1} = n_H \beta c \sigma_{f,B} + T^{-1}$$

and solving for  $T$  we have that:

$$n_H T = \frac{n_H}{\frac{1}{\tau} - \frac{1}{\tau_{f,B}}} \simeq \frac{10^{14} \text{ s cm}^{-3}}{\left(\frac{E}{\text{GeV}}\right)^{-0.3} - 0.7} \simeq 10^{14} \left(\frac{E}{\text{GeV}}\right)^{-0.55} \text{ s cm}^{-3}$$

There no other physical loss process for Boron, so  $T$  really must be the escape of the galactic confinement (leaky box). But if the box has a size  $H$ ,  $T_{esc}$  will be  $H/c$  which is the time required by CR generated in the Galactic plane to escape the box of height  $H$ ! However we know that  $T \gg H/c$ . So there must be something else confining the CR in the galaxy... what could it be?

### 2.3.1.5 Dynamics of Charge Particles in Magnetic Fields.

Before solving the problem what process in the Galaxy is confining the cosmic-rays, let's review a bit the dynamics of charge particles in magnetic fields.

Let's assume the simplest case of a test particle or mass  $m_0$  and charge  $Ze$  and lorentz factor  $\gamma$  in an uniform static magnetic field,  $\mathbf{B}$ .

$$\frac{d}{dt}(\gamma m_0 \mathbf{v}) = Ze(\mathbf{v} \times \mathbf{B})$$

knowing the expression of  $\gamma$  we derive this:

$$m_0 \frac{d}{dt}(\gamma \mathbf{v}) = m_0 \gamma \frac{d\mathbf{v}}{dt} + m_0 \gamma^3 \mathbf{v} \frac{\mathbf{v} \cdot \mathbf{a}}{c^2}$$

In a magnetic field the acceleration is always perpendicular to  $\mathbf{v}$  so  $\mathbf{v} \cdot \mathbf{a} = 0$  resulting in:

$$m_0 \gamma \frac{d\mathbf{v}}{dt} = Ze(\mathbf{v} \times \mathbf{B})$$

This equation tell us that there is no change in the  $v_{||}$  the parallel component of the velocity and the acceleration is only perpendicular to the magnetic field direction,  $v_{\perp}$ . Beacuse  $\mathbf{B}$  is constant this results in a spiral motion around the magnetic field. Now we are going to test what happens if the magnetic field is not uniform.

**Tutorial II: Motion of a charge particle in a slowly changing magnetic field**

```

from mpl_toolkits.mplot3d import Axes3D

q = 1.0
m = 10.0
dt = 1e-3
t0 = 0
t1 = 10
t2 = 20

t = np.linspace(t0, t2, int((t2 - t0)/dt))
n = len(t)

r = np.zeros((n,3))
v = np.zeros((n,3))

#Initial conditions

r[0] = [0.0, 0.0, 0.0]
v[0] = [2.0, 0.0, 3.0]

#B = array([0.0, 0.0, 5.0])

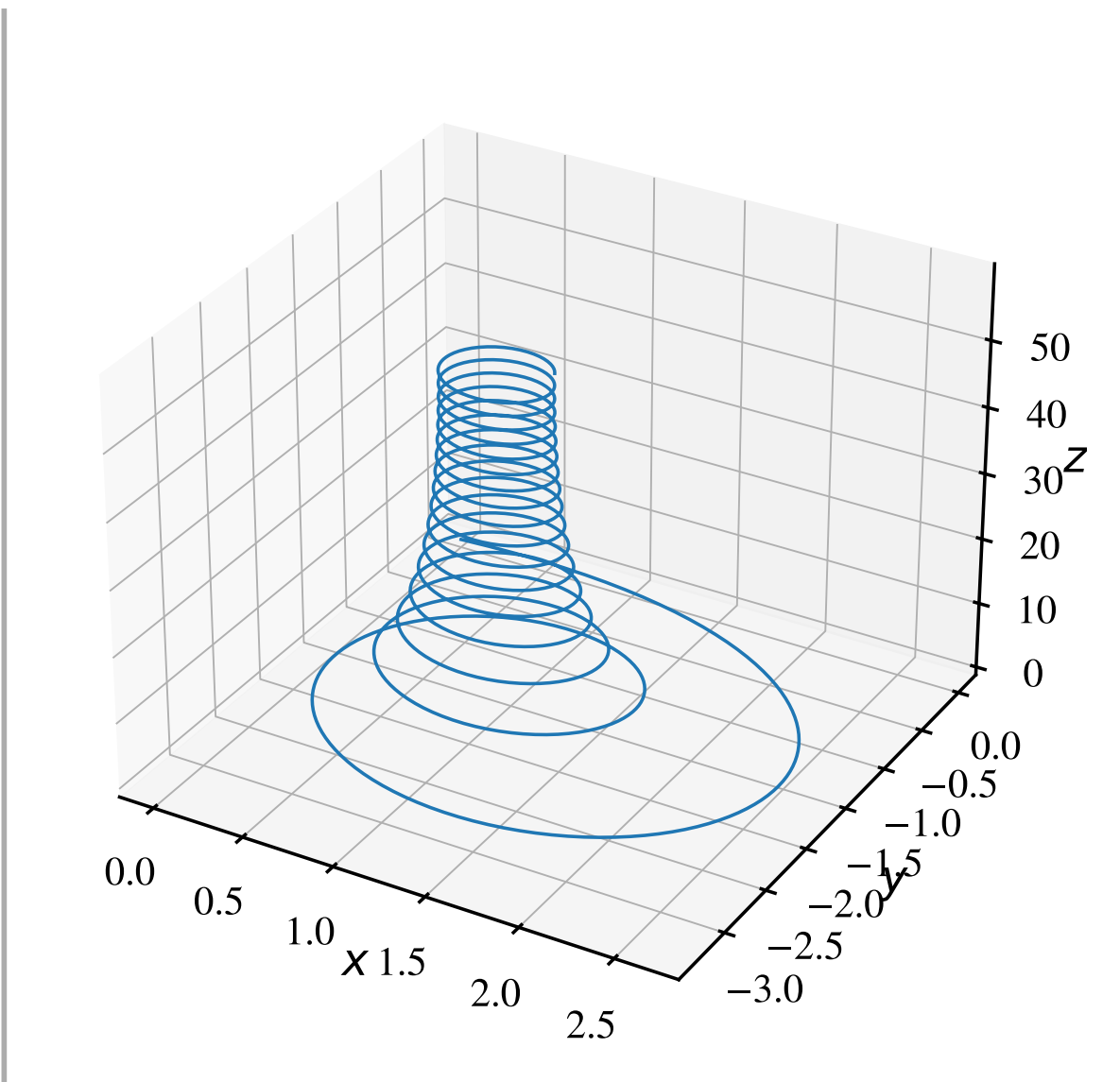
B = np.zeros((n,3))
B[0] = np.array([0.0, 0.0, 4.0])
dB = np.array([0.0, 0.0, 5e-3])
for i in range(n-1):
    a = q/m* np.cross(v[i],B[i])
    v[i+1] = v[i] + a*dt
    r[i+1] = r[i] + v[i+1]*dt
    B[i+1] = B[i] + dB

fig = plt.figure(figsize=(8,8))

ax = fig.add_subplot(111, projection='3d')
ax.plot(r[:,0], r[:,1], r[:,2])

ax.set_xlabel("$x$")
ax.set_ylabel("$y$")
ax.set_zlabel("$z$")
plt.show()

```



#### 2.3.1.6 Scattering in Plasma

The picture above holds while the gyroradius is larger or smaller than the variation of the magnetic field. In the first case when  $R_g \ll (\Delta B)$  the charge particle will follow the substructure of the magnetic field. In the second case  $R_g \gg (\Delta B)$  the magnetic field irregularities are transparent to the particle. However when  $R_g \approx (\Delta B)$  then the particle *sees* the magnetic irregularities. In this case the particle will scatter almost inelastically in these irregularities. The picture of a test-particle moving in a magnetic field is a simplistic one. In reality cosmic ray particles propagate in collisionless, high-conductive, magnetized plasma consisting mainly

of protons and electrons and very often the energy density of cosmic ray particles is comparable to that of the background medium. As a consequence of that, the electromagnetic field in the system is severely influenced by the cosmic ray particles and the description is more complex than the motion of a test charged particle in a fixed electromagnetic field. This will generate irregularities in the magnetic field. The **irregularities in the Galactic magnetic field** are responsible for the **diffusive propagation** of cosmic rays.

### 2.3.1.7 Diffusion of Cosmic Rays

The results above leads to think that CR experience diffusion in the galaxy. The equation that we used to relate the Boron production rate by the Carbon spallation process can be seen as a diffuse equation.

In diffusion the continuity equation states that the variation of the density  $N$  in time is given by its transfer of flux in area plus the source contribution:

$$\frac{\partial N}{\partial t} = -\nabla \cdot \mathbf{J} + Q$$

where  $Q$  is intensity of any local source of this quantity and  $\mathbf{J}$  is the flux.

**Fick's first law:** the diffusion flux is proportional to the negative of the concentration gradient in an isotropic medium:

$$\begin{aligned}\mathbf{J} &= -D\nabla N \\ J_i &= -D \frac{\partial N}{\partial x_i}\end{aligned}$$

where the proporcionality constant,  $D$ , is called diffusion coefficient. Which leads to the diffusion equation of:

$$\frac{\partial N}{\partial t} = D\Delta N + Q$$

where  $\Delta$  (or  $\nabla^2$ ) is the Laplace operator.

In the Leaky Box model the diffusion equation, ignoring other effects, can be written as:

$$\frac{\partial N_i}{\partial t} = D\Delta N_i = -\frac{N_i}{T_{esp}}$$

We made use of the fact that the escape probability is constant per unit time (Poisson process) and so the distribution in time can be writen as:

$$N_i(t) = n_0 e^{-\frac{t}{T_{esc}}}$$

In the absent of collisions and other energy changing processes, the distribution of cosmic ray path lengths can also be written as:

$$N_i(z) = n_0 e^{-\frac{z}{H}}$$

with  $z$  the travel distance in the z-axis and  $H$  the height of the box. Using both expressions of the cosmic ray distribution (in time and in space), together with the diffusion formula above give us equation:

$$T_{esp} = \frac{H^2}{D}$$

However we found from the B/C ratio that  $T_{esc} \propto E^{-\delta}$  with  $\delta = 0.55$ , therefore the diffusion coefficient is:

$$D(E) \propto E^\delta \sim E^{0.55}$$

Note that physically  $D = D(z)$  ie, diffusion will depend on distance to the disc, however in the leaky-box model we assumed that  $D$  is independent of that, which it is only an approximation.

### 2.3.1.8 The State-of-Art of Diffusion

The leaky box model is a very simplistic approximation but more realistic diffusion models, such as the numerical integration of the transport equation in the [GALPROP](#) code (Strong and Moskalenko 1998), lead to results for the major stable cosmic-ray nuclei, which are equivalent to the Leaky-Box predictions at high energy. However sophisticated models of transport should include effects such as:

1. Diffusion coefficient non spatially constant.
2. Anisotropic diffusion (Parallel vs Perpendicular)
3. Effect of self-generation waves induced by CR.
4. Damping of waves and its effects in CR propagation
5. Cascading of modes in wavenumber space

Each of these effects might change the predicted spectra and CR anisotropies in significant ways.

### 2.3.1.9 Transport Equation on Primary Cosmic Rays

The general simplified transport/dissusion equation that relate the abundances of CR elements can be given by:

$$\frac{\partial N_i(E)}{\partial t} = \frac{N_i(E)}{T_{esc}(E)} = Q_i(E) - \left( \beta c n_H \sigma_i + \frac{1}{\gamma \tau_i} \right) N_i(E) + \beta c n_H \sum_{k \geq i} \sigma_{k \rightarrow i} N_k(E)$$

where now  $Q_i(E)$  is the **local production rate by a CR accelerator**, the middle part represents the **losses due to interactions** with cross-section  $\sigma_i$  and **decays for unstable nuclei** with lifetime  $\tau_i$ . The last term is the **feed-down production** due to spallation processes of heavier CR. We can simplify this equation depending if we are dealing with Primary or Secondary CR:

- Primaries → neglect spallation feed-down.
- Secondaries → neglect production by sources:  $Q_s = 0$

For example, let's assume now a primary CR,  $P$ , where feed-down spallation is not taking place (ie, they are not product of heavier CR) and no decay (most nuclei are stable, one exception is  $^{10}\text{Be}$  which is unstable and  $\beta$ -decay), the equation can be written as:

$$\frac{N_P(E)}{T_{esc}(E)} = Q_P(E) - \frac{\beta c \rho_H N_P(E)}{\lambda_P(E)} \rightarrow N_P(E) = \frac{Q_P(E)}{\frac{1}{T_{esc}(E)} + \frac{\beta c \rho_H}{\lambda_P(E)}}$$

where we wrote  $n_H = \rho_H/m$  and  $\lambda_P$  is the mean free path in  $\text{g/cm}^2$ .

While  $T_{esc}$  is the same for all nuclei with same rigidity,  $\lambda_i$  is different and depends on the mass of the nucleus. The equation suggests that at low energies the spectra for different nuclei will be different (eg for Fe interaction dominates over escape) and will be parallel at high energy if accelerated on the same source. For proton with interaction lengths  $\lambda_{proton} \gg \lambda_{esc}$  at all energies so the transport equation gets simplified to:

$$N_p(E) = Q_p(E) \cdot T_{esc}(E)$$

ie, we observe at Earth a proton density of  $N_p(E) \propto E^{-(\gamma+1)} \sim E^{-2.7}$ , and  $T_{esc}(E)$  goes with the inverse of the diffusion coefficient  $D(E)$ , ie  $T_{esc}(E) \propto E^{-\delta}$ , then at the production site the spectrum must follow  $Q_p(E) \propto E^{-\alpha}$  with:

$$\alpha = (\gamma + 1) - \delta \approx 2.1$$

### 2.3.2 Acceleration of Galactic Cosmic Rays

Three questions:

- What is the source of power?
- What is the actual mechanism?
- Can it reproduce the spectral index found? ### Energy density of galactic cosmic-rays

In cosmic ray physics we call spectrum to the flux per steradian, so the relationship between them is:

$$\Phi(E) = \int_{\Omega} d\Omega I(E) = 4\pi I(E)$$

For all-hemispheres. So we can relate the number density of CR with the spectrum by:

$$n(E) = \frac{4\pi}{v} I(E)$$

since the flux is just the number density times the velocity.

And so **kinetic energy density** of CR,  $\rho_{CR}$  is therefore the integral of the **energy density spectrum**,  $E \cdot n(E)$ :

$$\rho_{CR} = \int E n(E) dE = 4\pi \int \frac{E}{v} I(E) dE$$

assuming for the Galactic CR (and that  $v = c$  for relativistic particles):

$$I(E) \approx 1.8 \times 10^4 \left( \frac{E}{1 \text{ GeV}} \right)^{-2.7} \frac{\text{nucleons}}{\text{m}^2 \text{ s sr GeV}}$$

we can calculate the energy density for cosmic-rays from above the solar modulations up the *knee*, which is given by:

$$\rho_{CR} = \frac{4\pi}{c} \frac{1.8}{1 - 1.7} \left[ \left( \frac{E_{max}}{1 \text{ GeV}} \right)^{1-1.7} - \left( \frac{E_{min}}{1 \text{ GeV}} \right)^{1-1.7} \right] \approx 1 \text{ ev cm}^{-3}$$

```

import scipy.constants as cte
from astropy.constants import pc

cspeed = cte.value("speed of light in vacuum") * 1e2 # in cm/s

emin = 1. #GeV
emax = 1e5 # 100 TeV
rho = 4 * np.pi /cspeed * 1.8 / (1 - 1.7) * (np.power(emax,1-1.7) - np.power(emin,1-1.7)) *

print(r"The energy density is $\rho_{CR} \approx %.2f$ $\mathrm{ev/cm}^3 $" %rho)

```

The energy density is  $\rho_{CR} \approx 1.08 \text{ ev/cm}^3$

This energy density is comparable with the energy density of the CMB  $\rho_{CMB} \approx 0.25 \text{ eV/cm}^3$

### 2.3.2.1 Required Power for Galactic Cosmic Rays

If we assume this value to be the constant value over the galaxy, the power required (called *luminosity* in astrophysics) to supply all the galactic CR and balance the escape processes is:

$$\mathcal{L}_{CR} = \frac{V_D \rho_{CR}}{\tau_{esc}} \sim 4 \times 10^{40} \text{ erg s}^{-1}$$

where  $V_D$  is the volume of the galactic disk

$$V_D = \pi R^2 d \sim \pi (15 \text{ kpc})^2 (300 \text{ pc}) \sim 6 \times 10^{66} \text{ cm}^3.$$

```

R = 15000 * pc.to("cm").value # radius in Cm
h = 300 * pc.to("cm").value
Vd = np.pi * R **2 * h
print(r"Galactic Volume is %.1e $\mathrm{cm}^{-3}$" %Vd)
evtoerg = cte.value("electron volt-joule relationship") * 1e7
tesc = 1e14 # s cm^3 at 1 GeV
tesc = tesc/0.1 # s
power = (Vd * rho) * evtoerg / tesc
print(f"Power L ~ {power:.2e} erg /s")

```

Galactic Volume is  $6.2 \times 10^{66} \text{ cm}^{-3}$   
Power L ~  $1.08 \times 10^{40} \text{ erg /s}$

It was emphasized long ago (Ginzburg & Syrovatskii 1964) that supernovae might account for this power. For example a type II supernova gives an average power output of:

$$\mathcal{L}_{SN} \sim 3 \times 10^{42} \text{ erg s}^{-1}$$

Therefore if SN transmit a few percent of the energy into CR it is enough to account for the total energy in the cosmic ray beam. That was called the **SNR paradigm**

### ! Power Required for $> 100 \text{ TeV}$

The derivation above was considered using the CR flux with an integral spectral index of  $\gamma = \alpha - 1 = 1.7$  which describes well the CR up to the *knee* (See Section 2.4.1). This is the bulk of cosmic ray density. The power required for the high energy part will be significantly less due to the steeply falling primary cosmic ray spectrum. For example assuming an integral index of  $\gamma = 1.6$  for  $E < 1000 \text{ TeV}$  and  $\gamma = 2$  for higher energy we get:

$$\begin{aligned} &\sim 2 \times 10^{39} \text{ erg/s for } E > 100 \text{ TeV} \\ &\sim 2 \times 10^{38} \text{ erg/s for } E > 1 \text{ PeV} \\ &\sim 2 \times 10^{37} \text{ erg/s for } E > 10 \text{ PeV} \end{aligned}$$

which are considerably less than the total power required for all the cosmic-rays. This power might be available from a few very energetic sources.

#### 2.3.2.2 Fermi Acceleration

Fermi studied how it is possible to transfer macroscopic kinetic energy of moving magnetized plasma to individual particles. He considered an iterative process in which for each *encounter* a particle gains energy which is proportional to the energy.

Let's write the increase in energy as  $\Delta E = \xi E$  after  $n$  encounters then:

$$E_n = E_0(1 + \xi)^n$$

where  $E_0$  is the injection energy in the *acceleration region*. If the probability of escaping this *acceleration region* is  $P_{esc}$  per *encounter*, after  $n$  the remaining probability is  $(1 - P_{esc})^n$ . To reach a given energy  $E$  we need:

$$n = \log \left( \frac{E_n}{E_0} \right) / \log(1 + \xi)$$

after each interaction there is a fraction  $(1 - P_{esc})$  that remain and the rest escapes the accelerator. If  $N_0$  particles entered the “encounter” in the first place, after  $n$  interaction those remaining are:

$$N(\geq E_n) = N_0(1 - P_{esc})^n$$

These particles will always eventually escape since  $P_{esc}$  is not 0, but for any given number of cycles,  $n$ , we can be sure that those remaining particles (whenever they escape) will have more energy than those that escaped at the cycle  $n$ . We can rewrite:

$$\log\left(\frac{N}{N_0}\right) = n(1 - P_{esc})$$

equalling  $n$  with the equation above we have:

$$\frac{\log(N/N_0)}{\log(E_n/E_0)} = \frac{\log(1 - P_{esc})}{\log(1 + \xi)}$$

For any given energy then we have:

$$N(\geq E) = N_0 \left(\frac{E}{E_0}\right)^{-\gamma}$$

where we defined

$$\gamma = \log\left(\frac{1}{1 - P_{esc}}\right) \frac{1}{\log(1 + \xi)} \approx \frac{P_{esc}}{\xi} = \frac{1}{\xi} \cdot \frac{T_{cycle}}{T_{esc}}$$

where  $T_{cycle}$  is the characteristic time of acceleration cycle, and  $T_{esc}$  is the characteristic time to escape the acceleration region.

Note that  $N(\geq E)$  is the integral spectrum, the differential spectrum is given by:

$$n(E) \propto E^{-1-\gamma}$$

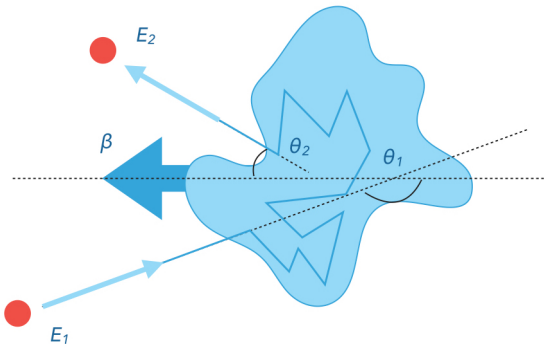
### 2.3.2.2.1 Fermi Mechanism

A mechanism working for a time  $t$  will produce a maximum energy:

$$E \leq E_0(1 + \xi)^{t/T_{cycle}}$$

Two characteristic features are apparent from this equation:

- High energy particles take longer to accelerate
- If a given kind of Fermi accelerator has a limited lifetime this will be characterized by a maximum energy per particle that can produce. In the general mechanism we can imagine a particle encountering something moving at a speed  $\beta$ . This “something” can be for example a magnetic cloud.



In this general approach, the particle might enter at different angles and exit at different angles. Let's assume  $O'$  to be the reference system where the magnetic cloud is in the rest frame. A particle with energy  $E_1$  in the lab reference system will have total energy in this reference system given by the boost transformation with  $\beta$  being the speed of the plasma flow (cloud:

$$E'_1 = \gamma E_1 (1 - \beta \cos \theta_1)$$

Before leaving the gas cloud the particle has an energy  $E'_2$ . If we transform this back to the lab reference system we get:

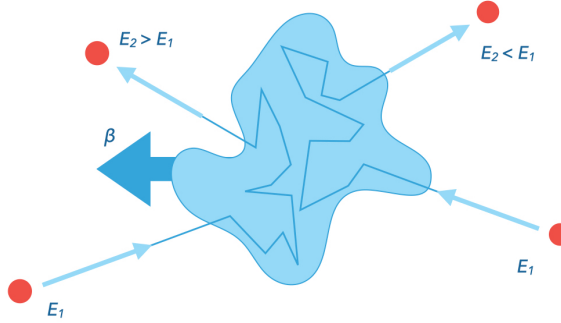
$$E_2 = \gamma E'_2 (1 + \beta \cos \theta'_2)$$

As the particle suffers from collisionless scatterings inside the cloud the energy in the moving frame just before it escapes is  $E'_2 = E'_1$  and so we can calculate the increment in energy  $\Delta E = E_2 - E_1$  as:

$$\xi = \frac{\Delta E}{E_1} = \frac{1 - \beta \cos \theta_1 + \beta \cos \theta'_2 - \beta^2 \cos \theta_1 \cos \theta'_2}{1 - \beta^2} - 1$$

### 2.3.2.2.2 Fermi 2nd Order Acceleration.

In the **second order** (first chronologically) Fermi considered *encounters* with moving clouds of plasma.



- The scattered angle is uniform so the average value is  $\langle \cos \theta'_2 \rangle = 0$ .
- The probability of collision at angle  $\theta$  with the cloud of speed  $V$  is proportional to the relative velocity between the cloud and the particle  $c$  if we assume it relativistic (factor  $1/2$  is there to have a proper normalization):

$$\frac{dn}{d \cos \theta_1} = \frac{1}{2} \frac{c - V \cos \theta_1}{c} = \frac{1 - \beta \cos \theta_1}{2}, \text{ for } -1 \leq \cos \theta_1 \leq 1$$

and so:

$$\langle \cos \theta_1 \rangle = \frac{\int \cos \theta_1 \cdot \frac{dn}{d \cos \theta_1} d \cos \theta_1}{\int \frac{dn}{d \cos \theta_1} d \cos \theta_1} = -\frac{\beta}{3}$$

Particles can gain or lose energy depending on the angles, but on average the gain is

$$\xi = \frac{1 + \frac{1}{3}\beta^2}{1 - \beta^2} \sim \frac{4}{3}\beta^2$$

! Problems with the 2nd order acceleration

- The energy increase is second order of  $\beta$  and..
- ... the random velocities of clouds are relatively small:  $\beta \sim 10^{-4}$  !!!
- Some collisions result in energy losses! Only with the average one finds a net increase.
- Very little chance of a particle gaining significant energy!
- The theory does not predict the power law exponent

### 2.3.2.2.3 Fermi 1st Order Acceleration.

Let's imagine a shock moving through a plasma. In the reference system of the *unshocked* plasma the shock front approaches with speed  $\vec{u}_1$  while the *shocked* plasma (left behind) moves at a slower velocity  $\vec{V}$  where  $|\vec{V}| < |\vec{u}_1|$ . If we now change to the reference system where the shock-front is at rest the gas *unshocked* now appears to approach speed  $-\vec{u}_1$  while the *shocked* plasma recedes with speed  $-\vec{u}_2 = (\vec{V} - \vec{u}_1)$ . A test cosmic ray particle crossing from any side of the shock, will always face an encounter with plasma approaching at speed  $|\vec{V}|$ , hence  $\beta$  now refers to this speed, the speed of the shocked (downstream) gas in the upstream reference system.

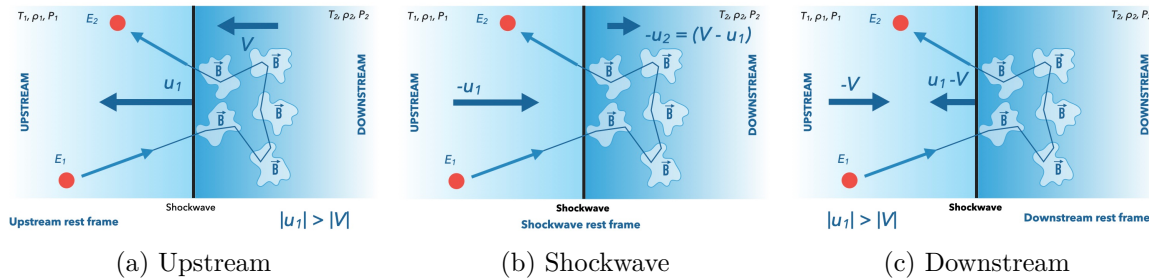


Figure 2.10: Fermi first order acceleration. Different reference systems.

- The outcome distribution of particles is not now 0, there is an asymmetry in the Fermi shock acceleration model, as particles in the upstream will re-enter the shock, only those going downstream can escape. Therefore the distribution follows the projection of a uniform flux on a plane:

$$\frac{dn}{d \cos \theta'_2} = 2 \cos \theta'_2 \quad \text{for } 0 \leq \cos \theta'_2 \leq 1$$

which gives:

$$\langle \cos \theta'_2 \rangle = \frac{\int \cos \theta'_2 \cdot \frac{dn}{d \cos \theta'_2} d \cos \theta'_2}{\int \frac{dn}{d \cos \theta'_2} d \cos \theta'_2} = \frac{2}{3}$$

- The incoming angle distribution is also the projection of an uniform flux on a plen but this time with  $-1 \leq \cos \theta_1 \leq 0$  and so  $\langle \cos \theta_1 \rangle = -2/3$

Particles entering the shockwave and exiting will have a gain of:

$$\xi = \frac{1 + \frac{4}{3}\beta + \frac{4}{9}\beta^2}{1 - \beta^2} - 1 \sim \frac{4}{3}\beta = \frac{4}{3} \frac{u_1 - u_2}{c}$$

#### 2.3.2.2.4 Escape Probability

The escape probability or loss rate of particles is given by the ratio of the incoming flux and the outgoing flux of particles.

- Incoming rate.** Let's assume that the diffusion of particles is so effective that close to the shockwave the distribution of particles is isotropic. In this case the rate of encounters for a plane shock is the projection of an isotropic flux onto the plane shock. Let's assume  $n$  to be the density of particles close to the shock, because it is isotropic it should follow:

$$dn = \frac{n}{4\pi} d\Omega$$

assuming the particles moving at relativistic speed, the velocity across the shock is  $c \cos \theta$  therefore the rate of encounters of particles upstream with the shock is given by:

$$R_{in} = \int dn c \cos \theta = \int_0^1 d \cos \theta \int_0^{2\pi} d\phi \frac{cn(E)}{4\pi} \cos \theta = \frac{cn(E)}{4}$$

where  $n(E)$  is the CR number density.

- Outgoing rate.** The outgoing rate is simply the number of particles escaping the system. In the shock rest frame, that's all particles not returning to the shockwave. In this reference system there is an outflow of cosmic-rays adverted downstream. Since particles are diffusing in all direction, the net outflow goes with the velocity of the downstream speed and is given simply by  $R_{out} = n(E)u_2$ ,

Therefore the escape probability is given by:

$$P_{esc} = \frac{R_{in}}{R_{out}} = \frac{4u_2}{c}$$

which for acceleration at shock gives:

$$\gamma = \frac{P_{esc}}{\xi} = \frac{3}{u_1/u_2 - 1}$$

So we get an estimate of the spectral index based on the relative velocities of the downstream and upstream gas in the shockwave.

### 2.3.2.3 Kinematic Relations at the Shock

In order to derive the exact value of the spectral index we need to obtain a relation between  $u_1$  and  $u_2$  using the kinematics of a shock wave. These equations are the conservation of mass, the Euler equation for momentum conservation and conservation of energy:

- **Conservation of mass:**

$$\partial_t \rho + \nabla \cdot (\rho \vec{u}) = 0$$

- **Conservation of momentum (Euler equation):**

$$\rho \frac{\partial \vec{u}}{\partial t} + \rho \vec{u} \cdot (\nabla \vec{u}) = \vec{F} - \nabla P$$

where  $\vec{F}$  is an external force, and  $\nabla P$  is a force due to a pressure gradient.

- **Conservation of energy:**

$$\frac{\partial}{\partial t} \left( \frac{\rho u^2}{2} + \rho U + \rho \Phi \right) + \nabla \cdot \left[ \rho \vec{u} \left( \frac{u^2}{2} + U + \frac{P}{\rho} + \Phi \right) \right] = 0$$

where this equation accounts for the kinetic, internal, and potential energy  $\Phi$ .

Let's assume a one-dimensional, steady shock in its rest frame (otherwise time derivatives must be taken into account).

Then the first equation becomes simply:

$$\frac{d}{dx}(\rho u) = 0$$

and the Euler equation simplifies to:

$$\frac{d}{dx}(P + \rho u^2) = 0$$

In the energy equation we assume  $\Phi = 0$ :

$$\frac{d}{dx} \left( \frac{\rho u^3}{2} + (\rho U + P)u \right) = 0$$

$$\frac{d}{dx} \left[ \rho u \left( \frac{u^2}{2} + U + \frac{P}{\rho} \right) \right] = 0$$

where  $U$  is the internal density per unit volume and we can write  $\rho U = \frac{P}{\Gamma - 1}$ , where  $\Gamma = c_p/c_v$  is the **adiabatic index** or heat capacity ratio.

### ! Conditions of discontinuity at the shockwave

Let's assume we are in the shock ref system. Applying these equations at the discontinuity of the shock we have the three conditions at the discontinuity of the shock:

$$\begin{aligned} \rho_1 u_1 &= \rho_2 u_2 \\ P_1 + \rho_1 u_1^2 &= P_2 + \rho_2 u_2^2 \\ \frac{\rho_1 u_1^2}{2} + \frac{\Gamma}{\Gamma - 1} P_1 &= \frac{\rho_2 u_2^2}{2} + \frac{\Gamma}{\Gamma - 1} P_2 \end{aligned}$$

For a gas with  $P = K\rho^\Gamma$  the speed of sound can be written as  $c_s = \sqrt{\Gamma P / \rho}$  or  $\rho c_s^2 = \Gamma P$ . From the second condition we can write:

$$P_1 + \rho_1 u_1^2 = \rho_1 u_1^2 \left( 1 + \frac{P_1}{\rho_1 u_1^2} \right) = \rho_1 u_1^2 \left( 1 + \frac{c_s^2}{\Gamma u_1^2} \right) = \rho_1 u_1^2 \left( 1 + \frac{1}{\mathcal{M}_1 \Gamma} \right)$$

For strong shocks  $\mathcal{M}_1 \gg 1$  then the pressure in the upstream is negligible  $P_1 \sim 0$

We can isolate  $\rho_2$  and  $P_2$  as:

$$\rho_2 = \frac{u_1}{u_2} \rho_1$$

$$P_2 = P_1 + \rho_1 u_1^2 - \rho_1 \frac{u_1}{u_2} u_2^2 = P_1 + \rho_1 u_1 (u_1 - u_2) \sim \rho_1 u_1 (u_1 - u_2)$$

Using these expression ot eliminate  $\rho_2$  and  $P_2$  from the third (enegy conservation) equation we have:

$$\frac{1}{2}u_1^2 = \frac{1}{2}u_2^2 + \frac{\Gamma}{\Gamma-1} \frac{P_2}{\rho_2} = \frac{1}{2}u_2^2 + \frac{\Gamma}{\Gamma-1} u_2(u_1 - u_2)$$

grouping by powers of  $u_2$ :

$$\left(\frac{\Gamma}{\Gamma-1} - \frac{1}{2}\right) u_2^2 - \frac{\Gamma}{\Gamma-1} u_2 u_1 + u_1^2 = 0$$

multiplying by  $2/u_1^2$ :

$$\left(\frac{\Gamma+1}{\Gamma-1}\right) t^2 - \frac{2\Gamma}{\Gamma-1} t + 1 = 0$$

where we defined  $t \equiv u_2/u_1$  this quadratic equation has the 2 solutions:

$$t = 1 \rightarrow u_1 = u_2$$

ie, no shock at all, and a second solution given by:

$$t = \frac{\Gamma-1}{\Gamma+1} \rightarrow \frac{u_2}{u_1} = \frac{\Gamma-1}{\Gamma+1}$$

for a monatomic gas with 3 degrees of freedom the ratio of specific heats is  $\Gamma = 1 + 1/f = \frac{5}{3}$ , so

$$\frac{u_2}{u_1} = \frac{1}{4}$$

No matter how strong a shock wave is, a mono-atomic gas can only be compressed by a factor of 4. The spectral index is then:

$$\gamma = \frac{P_{esc}}{\xi} = \frac{3}{u_1/u_2 - 1} = 1$$

If one keeps the factors of  $1/\mathcal{M}^2$  (to prove if you are brave):

$$\gamma \sim 1 + \frac{4}{\mathcal{M}^2} \sim 1.1$$

Which matches remarkably to what we derived to be the differential spectral index at the accelerator:

$$n(E) \propto E^{-(\gamma+1)} \sim E^{-2.1}$$

### 2.3.2.3.1 Maximum Energy

In an infinite planar shockwave, all particles upstream will encounter again the shockwave. However particles can advent downstream. In diffuse shock accelerations, particles will diffuse travelling a distance  $l_d$  upstream, until they are reached by the shock moving at speed  $u_1$  in the upstream reference system. Particles will cross when:

$$\begin{aligned} l_d &\simeq \sqrt{Dt_d} \\ l_d &= u_1 t_d \\ t_d &\approx \frac{D}{u_1^2} \end{aligned}$$

Assuming a diffusion that depends on energy in the form of  $D = D_0 E^\alpha$  we can get that the maximum energy corresponds to:

$$E_{max} \leq \left( \frac{u_1^2 t_d}{D_0} \right)^{\frac{1}{\alpha}}$$

where we can assume  $t_d$  to be the time during which the mechanism is working, ie the lifetime of the shockwave  $t_d \sim t_{age}$ . From the equation above we can conclude that the maximum energy:

- increases with time
- depends on: age, shock speed, magnetic field intensity and structure (through D)
- is not universal
- $D$  and therefore  $l_d$  increases with energy, and the each cycle energy increases, so the last cycle is the longest

We can rewrite the diffusion coefficient as:

$$D \sim \frac{l_d^2}{t_d} = l_d v$$

where  $v$  is the particle speed. A more detailed analysis gives  $D = \frac{1}{3} l_d v$  where the factor 3 comes from the 3 dimensions. In other words, the diffusion coefficient can be understood as the product of the particle velocity  $v \simeq c$  and its mean free path. At high energies, the mean free path between scatterings in the turbulent magnetic clouds can be approximated as  $l_d = r_L/r_0$ , where  $r_0$  is the size of the magnetic cloud and  $r_L$  the Larmor radius of the particle. Assuming that  $r_L \gg r_0$  we can re-write:

$$D = \frac{r_L c}{3} \sim \frac{1}{3} \frac{Ec}{ZeB}$$

Another way to see this, is to assume that mean diffusion path  $l_d$  cannot be smaller than the Larmor radius, since magnetic field irregularities in a smaller scale than the Larmor radius will be transparent. This is the regime of the Bohm diffusion and it is possible in highly turbulent magnetic fields, something that theoreticians think is possible when CR excite magnetic turbulence at shocks while being accelerated. This is called magnetic field amplification.

In that case, the diffusion coefficient depends linearly with energy ( $\alpha = 1$ ) and the equation above can be rewritten as:

$$E_{max} \leq 3 \frac{u_1}{c} ZeB(u_1 t_{age})$$

where  $t_{age}$  is the time in which the accelerator is working. Note that the product  $(u_1 t_{age})$  is the radius of an expanding shell. Using some estimates on the time ( $t_{age} \sim 1000$  yrs as the typical SN shockwave) and  $B_{ISM} \sim 3\mu G$  we can rewrite the maximum energy for SN shockwaves as:

$$E_{max} \leq Z \times 3 \times 10^4 \text{ GeV}$$

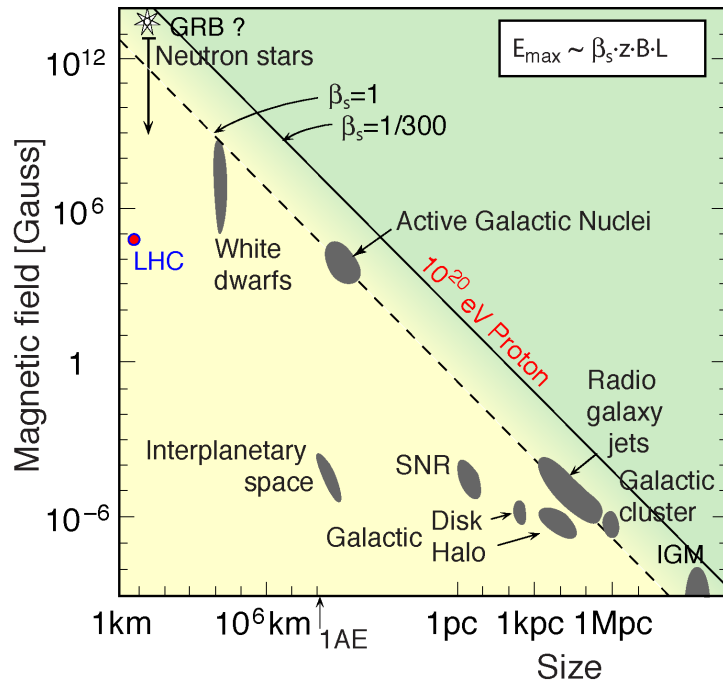
In other words, the shock-wave acceleration shown can accelerate CR **up to 100 Z TeV**, but not beyond this. Other acceleration mechanism are needed for the highest energy cosmic rays. We need very high magnetic fields (non-lineal acceleration mechanism). In these cases, even if this object cannot supply all the galactic cosmic rays the energy per particle may be orders of magnitude higher than those possible in shock acceleration by blast waves.

### Hillas Criteria

The equation of the maximum energy from shock acceleration can be rewritten as:

$$E_{max} \leq 10^{18} \text{ eV } Z \beta_s \left( \frac{R}{\text{kpc}} \right) \left( \frac{B}{\mu G} \right)$$

where  $\beta_s$  is the shock velocity,  $B$  the magnetic field strength, and  $R = u_1 t_{age}$  is the radius of the expanding shockwave, or in other words the size of the acceleration region. In 1984 Hillas arrived to a similar conclusion just by doing a back-of-an-envelope assumption that in order for it to accelerate CR particles to high energies in which he imposed that a condition where the size of the acceleration region must be at least twice the Larmor radius. The plot showing possible sources in the parameter space  $B$  vs  $R$  is usually referred as the Hillas' plot. For relativistic shockwaves ( $\beta_s \sim 1$ ) many sources are able to accelerate protons up to  $10^{20}$  eV, however for slower shockwaves ( $\beta_s \sim 1/300$ ) the number of source candidates is strongly reduced.



### 2.3.3 Sources of Galactic Cosmic Rays

#### 2.3.3.1 Supernova Remnants (SNRs)

**Supernova remnants (SNR)** remain the most likely candidates for CR acceleration up to at least  $10^{14}$  eV via the Fermi shock mechanism. Supernova explosions are very violent events which transfer a significant amount of energy in the ISM. We distinguish between the SN explosions –the actual events and the next few years) and Supernova remnants - what happens over the next few thousand years. Supernova explosion mechanism can be the carbon deflagration of white dwarfs (Type I) or the core collapse of massive stars (Type II) but the dynamical evolution of the supernova remnant (SNR) i.e., the expanding cloud of hot gas in the ISM is similar and can be divided in 3 phases depending on the relation between the ejected material,  $M_{ej}$  and the swept material  $M_{sw}$ :

- **Free Expansion Phase.**  $M_{ej} \gg M_{sw}$  The shock wave moves in the ISM gas at a highly supersonic speed. The speed is constant as there is no acceleration and so the shock radius scales as  $R_s(t) = v_e t$ . Behind the shockfront ISM gas starts to accumulate and a reverse shock starts to form. Sometimes we see first this reverse shock. At some point the

compressed ISM gas equals the ejected material, this marks the end of the free expansion phase. Given an initial density of ISM  $\rho_{ISM}$  we can define a swept material as:

$$M_{sw} = \frac{4\pi}{3}\pi R_{sw}^3 \rho_{ISM}$$

When the condition  $M_{sw} \simeq M_{ej}$  is reached, this marks the end of the free expansion phase and the swept radius can be defined as:

$$R_{sw} = \left( \frac{3M_{ej}}{4\pi\rho_{ISM}} \right)^{1/3}$$

This radius is reached at the defined swept time  $t_{sw} = R_{sw}/v_{sh}$  which is about 200-300 years.

- **Sedov-Taylor Phase.** Once the reverse shock reaches the nucleus, the interior of the SNR gets very hot that energy losses due to radiation are not possible (all atoms are ionized). The cooling of the gas is only due to the expansion, that's why this phase is the adiabatic phase. This is therefore a pressure-driven phase. Taking the pressure into account we can use the following formula:

$$\frac{d}{dt}(mv) = F$$

$$\frac{d}{dt} \left( \frac{4\pi}{3} R_{sh}^4 \rho_{ISM} \dot{R}_{sh} \right) = 4\pi R_{sh} P$$

The pressure and internal energy  $E$  of an ideal gas are related by:

$$P = (\gamma - 1) \frac{E}{V}$$

where  $V$  is the volume. Since this is an adiabatic expansion we can assume that the internal energy is equal to the explosion energy  $E = E_{SN}$ , and  $V = 4\pi R_{sh}^3/3$ . Assuming a mono-atomic gass with a adiabatic index  $\gamma = 5/3$  we obtain as pressure:

$$P = \frac{E_{SN}}{2\pi R_{sh}^3},$$

which inserting on the expression above we have:

$$\frac{d}{dt} \left( \frac{1}{3} R_{sh}^4 \rho_{ISM} \dot{R}_{sh} \right) = \frac{E_{SN}}{2\pi R_{sh}}$$

Solving for  $R_{sh}$  we obtained:

$$R_{sh}(t) = \left( \frac{25E_{SN}}{4\pi\rho_{ISM}} \right)^{1/5} t^{2/5}$$

$$v_{sh}(t) = \frac{2}{5} \left( \frac{25E_{SN}}{4\pi\rho_{ISM}} \right)^{1/5} t^{-3/5}.$$

As can be seen, the radius goes as  $R_{sh} \propto t^{2/5}$ . When temperature reaches the critical value of  $10^6$  K ionized atoms start to capture free electrons and can lose energy due to de-excitation. This is the end of the adiabatic phase. This phase can last 20,000 years.

- **Cooling or Snowplough phase** Due to the effective radiative cooling the thermal pressure decreases and the expansion slows down. More and more interstellar gas is accumulated until the swept-up mass is much larger than the ejected material. Finally the shell breaks up into clumps probably due to Rayleigh-Taylor instabilities. This phase lasts up to 500,000 years.

As we discussed, the  $E_{max}$  depends on how long the accelerator is active. Therefore an individual CR particle will gain the highest energy if it starts during the free expansion phase and stays with the shock front until and through the Sedov phase. There is a caveat, though, the  $E_{max}$  also depends on the magnetic field, and magnetic fields during the slow expansion of the Sedov phase are not strong enough to confine the CR particle. In this case, it seems the maximum CR energy may only be reached during the pre-Sedov expansion. This is the reason why young SNR are the main candidates to search for CR injection up to PeV energies.

### 2.3.3.2 Other Sources of Galactic Cosmic Rays

- **Neutron stars** Neutron stars, especially young fast-rotating pulsars and magnetars have extreme magnetic fields (up to  $10^{12}$  G in the case of magnetars) with complex structure that could accelerate CR up to the highest energies. These objects are far rarer than SNRs, however, only a dozen magnetars are known in the Milky Way, although many could exist in the local neighborhood.
- **Microquasars** are radio-intense X-ray binary stars with companion orbiting an accreting black hole. They are particularly interesting particle accelerators due to observation of VHE gamma ray emission and highly relativistic jets which could provide energy for UHECR

## 2.4 Extra-Galactic Cosmic Rays: The Knee and Beyond

### 2.4.1 The Knee

At energies of about  $5 \times 10^{15}$  eV a steepening in the spectrum from  $\gamma \sim 1.7 \rightarrow \gamma \sim 2$  known as the *knee* takes place. Already Peters in 1959 concluded that it could be due to:

- Consequence of the breakdown of an acceleration mechanism.

- Increased rate of escape from the galaxy at high energies.

```

elements = ("H", "He", "C", "N", "O", "Si", "Fe")
elements += ("1H-bar", "e-+e+", "AllParticles")

tabs = []
for energy_type in ("EKN", "ETOT"):
    for elem in elements:
        tab = crdb.query(
            elem,
            energy_type=energy_type,
            energy_convert_level=1,
        )
        if energy_type == "EKN":
            tab = convert_energy(tab, "EK")
        tabs.append(tab)
tab = np.concatenate(tabs).view(np.recarray)

with np.errstate(divide="ignore"):
    mask = (tab.err_sys[:, 0] > 0) & (tab.err_sta[:, 0] / tab.value < 0.5)
tab = tab[mask]

xlim = 1e4, 1e11

fig, ax = plt.subplots(1, 1, figsize=(6, 5))
for elem in elements:
    tab = tab[(xlim[0] < tab.e) & (tab.e < xlim[1])]
    ma = tab.quantity == elem
    if len(tab) == 0:
        continue
    color = "k" if elem == "AllParticles" else None
    t = tab[ma]
    if len(t) == 0:
        continue
    f = t.e**2.7
    sta = np.transpose(t.err_stab)
    color = "k" if elem == "AllParticles" else None
    ax.errorbar(t.e, t.value * f, sta*f, fmt=".", color=color, label=elem)

ax.loglog()
ax.set_ylabel(r"$E_k^{2.7} dJ/dE_k$ [GeV^{1.7}] / (m^2 s sr)]")
ax.set_xlabel(r"$E_k$ [GeV]")

```

```

ax.grid()
ax.legend(frameon=False, loc="lower center", ncol=2)

```

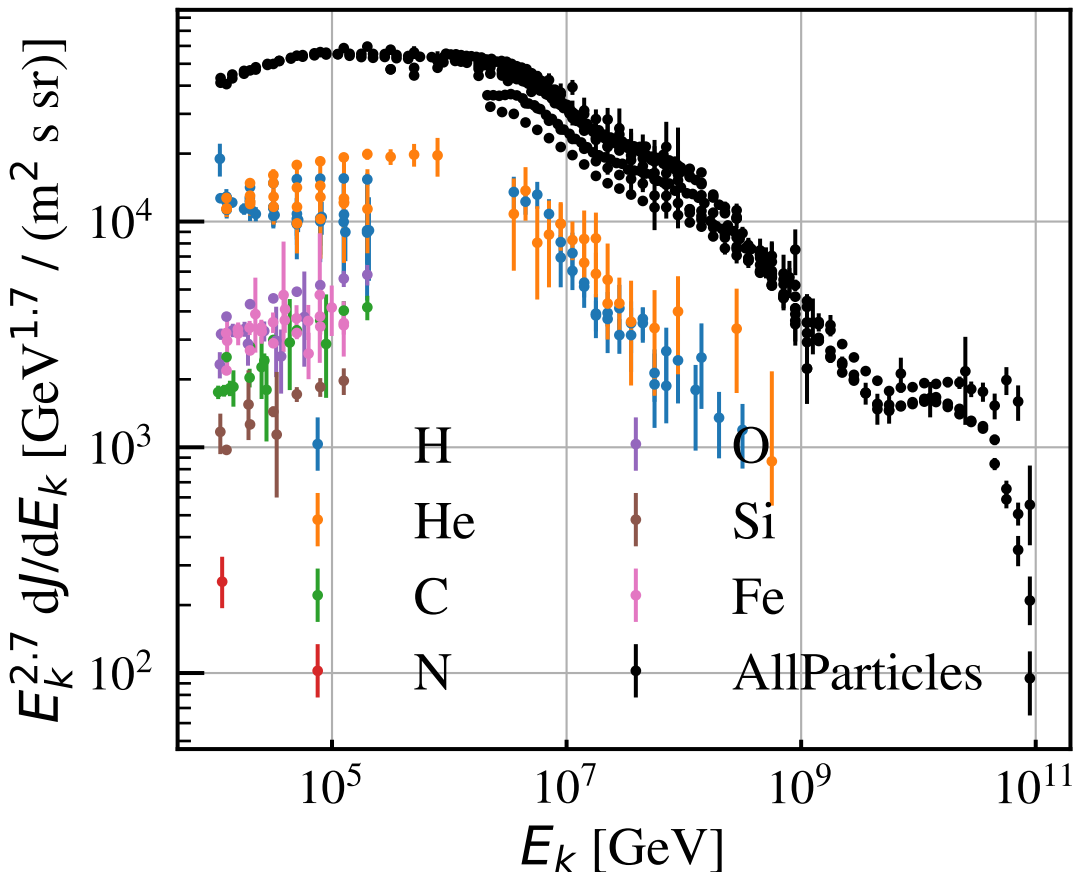
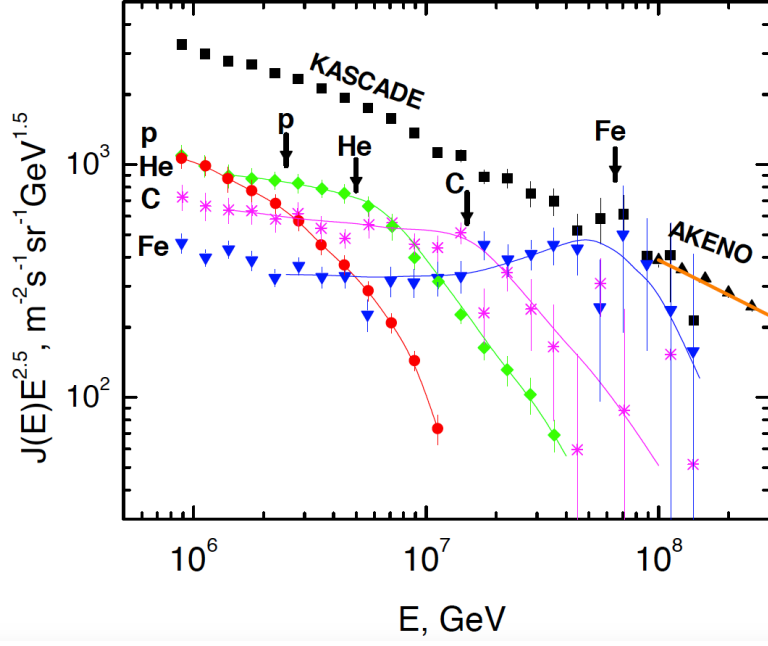


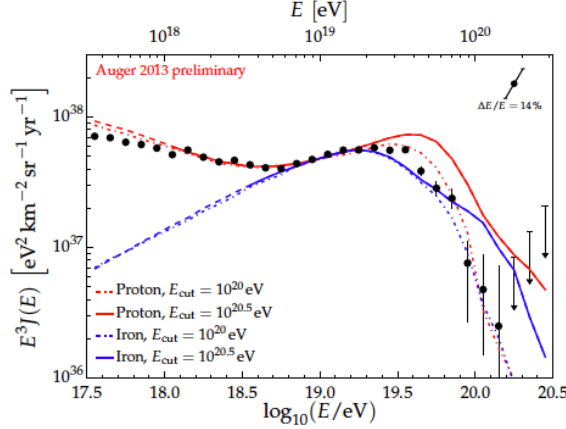
Figure 2.11: The Knee of the CR spectrum

A third explanation could be a change in CR interactions at  $\sqrt{s} \sim$  few TeV. The first two explanations produce a rigidity dependent *knee*, ie the position of the *knee* for different nuclei depends on  $Z$ , while the third explanation will depend on  $A$ . Experimentally the rigidity dependence is favored.



Experimentally at these energies we cannot observe cosmic-rays in a direct way. We need to start looking at their interactions with the atmosphere (see lecture 3 on air-shower physics). This imposes limitation on the precision of the cosmic ray composition. In particular different models of hadronic interactions have to be assumed.

#### 2.4.1.1 The Ankle and the End of the Spectrum

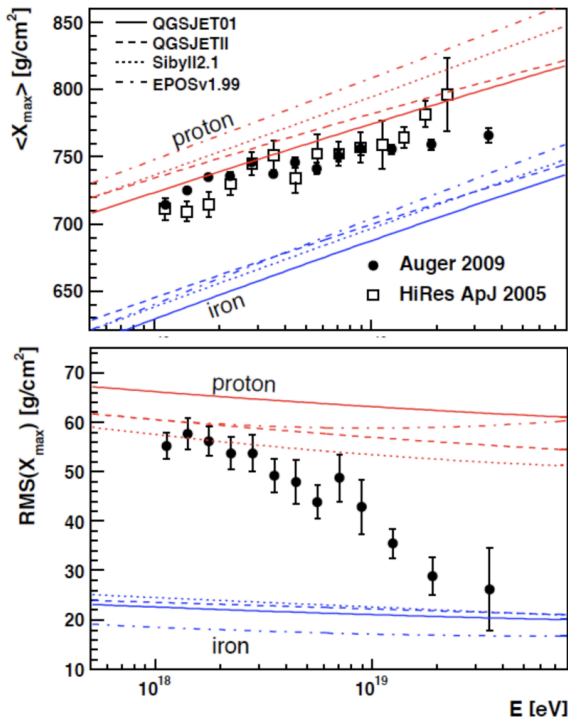


- A proton of energies  $10^{18}$  eV has a gyroradius of a kpc in a typical magnetic field which hints at an extra-Galactic origin for these energies.

- Greissen-Zatsepin and Kuz-min predicted that at energies of  $\sim 10^{19}$  eV will interact with the low energy photons of the CMB. This interaction leads to a suppression of flux above  $5 \times 10^{19}$  eV unless the sources are within a few tens of Mpc. This suppression is referred as GZK cutoff.

#### 2.4.1.2 High Energy Composition

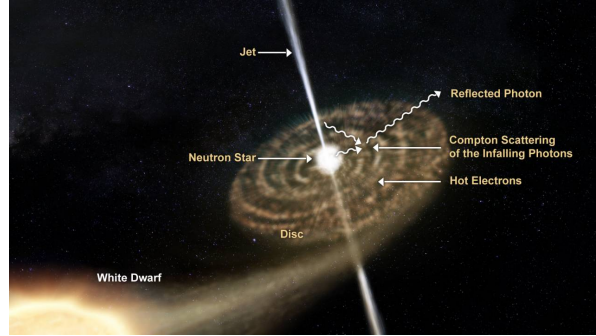
- Composition of the high energy CR spectrum involves only two archetypes: light nuclei (protons) and heavy nuclei (iron).
- The plots above show Auger / HiRes measurements near GZK cutoff, all favoring at least a mixed composition tending toward heavy at the higher energies.



#### 2.4.1.3 Sources of Extra Galactic Cosmic Rays

As we saw, CR in supernova remnants or blast waves can only accelerate CR **up to 100 Z TeV**. In order to explain CR beyond this energy, one has to invoke other processes such as Non-Linear Diffusion Acceleration, or extremely high magnetic fields (as suggested in Hillas plot).

Binary systems in which a compact object (black hole, neutrino star, pulsar) is permanently dragging material for an accompanying object (normal star or galaxy) and whirled into an accretion disk can generate enormous plasma motions with very strong electromagnetic fields. The image below shows an artistic representation of 4U 0614+091, a X-ray binary.



#### 2.4.1.4 Sources of UHECR: The Disk Dynamo

Black holes or neutrino stars will have matter accreting around them. Due to the gravitational pull matter will be ripped off in molecules, atoms, and ultimately elementary charge particles. The energy gain of infalling photons will correspond to the variation in the gravitational potential. If we equate the variation of gravitational potential to the kinetic energy of the accreting matter we have in the classical approach:

$$\frac{1}{2}m_p v^2 = \Delta E = - \int_{\infty}^R G \frac{m_p M}{r^2} = G \frac{m_p M}{R} \rightarrow v = \sqrt{\frac{2GM}{R}}$$

where  $M$ ,  $R$ , are the mass and radius of the central compact object.

- For a neutron star ( $M \approx 2 \times 10^{30}$  kg,  $R = 10$  km):  $\frac{\Delta E}{m_p} \sim 1.32 \times 10^{20}$  erg/g
- For a black hole ( $M \approx 10^8 M_{\odot}$ ,  $R = R_S = 2 \frac{GM}{c^2}$ ):  $\frac{\Delta E}{m_p} \sim 5 \times 10^{20}$  erg/g

The variable magnetic field of the neutron stars or black holes are perpendicular to the direction of the accretion disk generating a Lorentz force:

$$\vec{F} = e(\vec{v} \times \vec{B}) = e\vec{E}$$

So the energy obtained is

$$E = \int \vec{F} d\vec{s} = evB\Delta s$$

where  $\Delta s$  is the distance over which the force acts. Under plausible assumptions ( $v \sim c$ ,  $B = 10^6$  T,  $\Delta s = 10^5$  m) energies of  $3 \times 10^{19}$  eV are possible.

#### 2.4.1.5 Candidates of Extra Galactic Cosmic Rays Sources

The two main candidates for ExtraGalactic Cosmic Rays are:

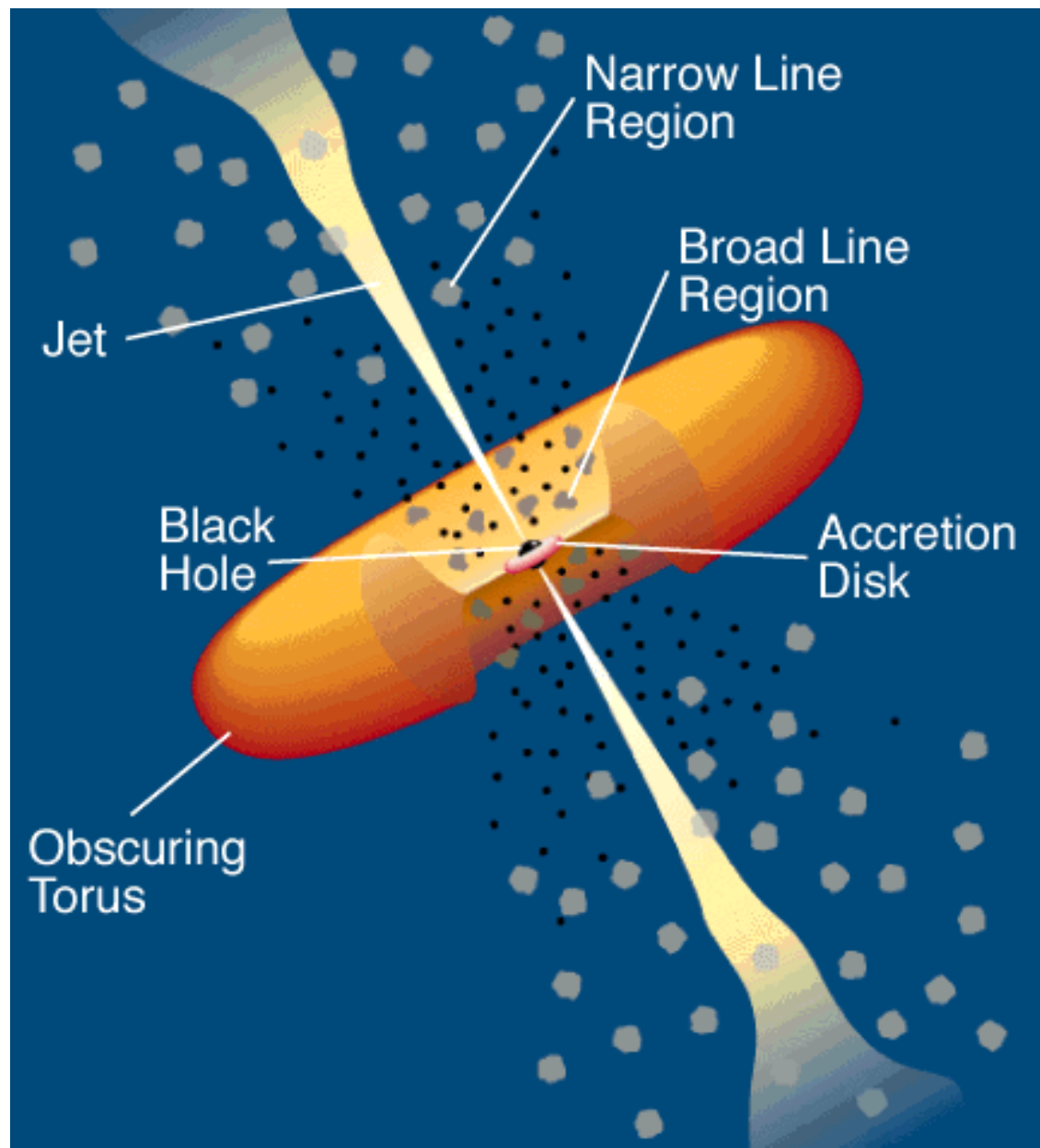
- Active Galactic Nuclei (AGN)
- Gamma Ray Bursts

##### 2.4.1.5.1 Active Galactic Nuclei (AGNs)

- Discovered in 1932 by K. Jansky looking for noise in transatlantic radio transmission for the Bell Telephone Labs. He found a persistent noise in the radio from the centre of the Galaxy too loud to be due to thermal black body radiation.
- 1953 Ginzburg & Shklovski suggested it was due to synchrotron radiation from highly relativistic electrons, confirmed with discovery of predicted polarization in M87 light.
- Sandage labeled 3C48 a quasar or quasi-stellar object (it appeared pointlike).
- In 1962 3C273 radio source position was found with precision of 1 arcsec, which allowed to find the optical counterpart at  $z = 0.158$  (not 1 star but a galaxy).
- In 1963 Hoyle and Fowler speculated that the tremendous emitted energy is due to the gravitational collapse of a very massive object.

##### i AGN Classification

- There are two broad classes: **Radio quiet** (90%) and **Radio Loud** (10%) depending on the presence of jets or not.
- The unified model of AGNs suggests that different AGNs are in fact the same object seen from different angles.



#### 2.4.1.5.2 Gamma-Ray Bursts

- GRBs are short bursts lasting a few seconds of  $\gamma$ -ray photons from 0.1 - 1 MeV.
- They were discovered in the 60s by the U.S. Vela satellites, which were built to detect gamma radiation pulses emitted by nuclear weapons tested in space as the US suspected

the URSS might carry on secret nuclear tests depiste the [Nuclear Test Ban Treaty](#).

- They have been hypothesized (given their occurrence) to have caused mass extinctions events (thousand times since life began), in particular they are associated with the [Ordovician–Silurian extinction](#).
- There is some observational evidence suggesting that progenitor of a GRB are stars undergoing a catastrophic energy release by the end of their lives → Hypernovas

The accepted phenomenological picture of GRBs is of an expanding relativistic wind *fireball* dissipating kinetic energy. The observed *afterglow* on some GRBs result from the collision of the expanding fireball and the surroundings.

In the fireball, the observed radiation is produced by synchrotron emission of shock accelerated electrons, similar to SNRs. Hence, it is likely that protons will be also shock accelerated.

The two conditions for GRBs sources of UHECR are:

1. The proton acceleration time must be smaller than the wind expansion time (burst duration).
2. The proton synchrotron loss time must exceed the acceleration time.

These two conditions lead to a constraint in the Lorentz boost factor for GRBs:

$$\gamma \geq 130 \left( \frac{E}{10^{20} \text{ eV}} \right)^{3/4} \left( \frac{0.01 \text{ s}}{\Delta t} \right)^{1/4}$$

which matches what we see from GRBs. However IceCube has [not seen any neutrino associated with GRBs](#) which puts in tension the idea that GRBs can be the only sources of UHECR.

## References

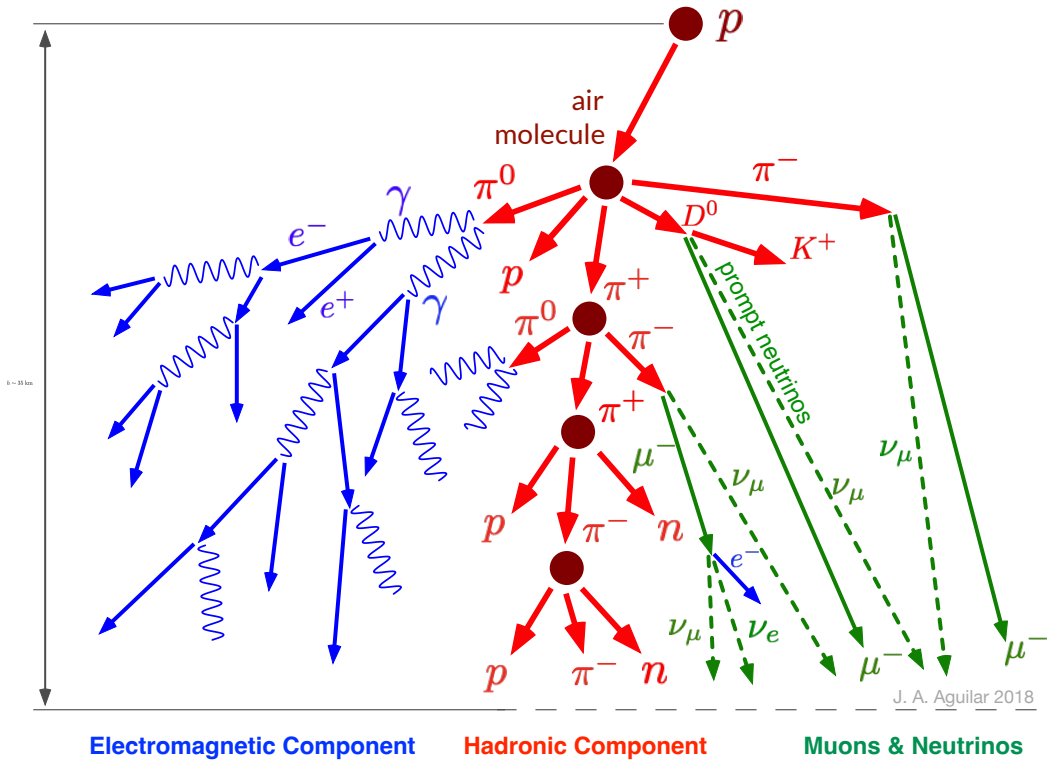
- Grupen, Claus. n.d. *Astro Particle Physics*.
- Kachelriess, M. 2008. “Lecture Notes on High Energy Cosmic Rays.” <https://arxiv.org/abs/0801.4376>.
- Kampert, Karl-Heinz, and Peter Tinyakov. 2014. “Cosmic Rays from the Ankle to the Cutoff.” *Comptes Rendus. Physique* 15 (4): 318–28. <https://doi.org/10.1016/j.crhy.2014.04.006>.
- Melia, Fulvio. 2009. *High-Energy Astrophysics*. Vol. 14. Princeton University Press. <http://www.jstor.org/stable/j.ctv21r3q4z>.
- Workman, R. L., and Others. 2022. “Review of Particle Physics.” *PTEP* 2022: 083C01. <https://doi.org/10.1093/ptep/ptac097>.

# 3 Cosmic Rays in the Atmosphere

## 3.1 Interactions of CR particles in the atmosphere

### 3.1.1 Introduction

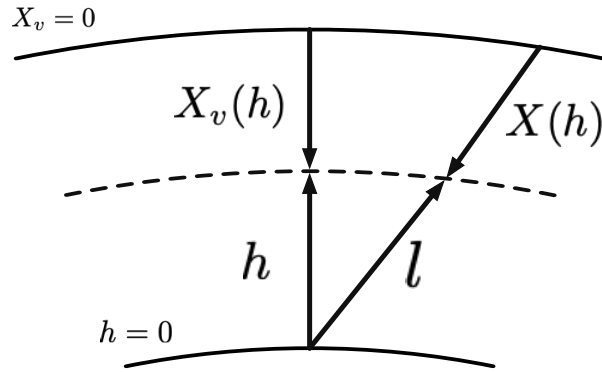
In this lesson we will see the different components of a cosmic air shower when cosmic rays interact with Earth's atmosphere. As seen in the figure below, we have 3 main components, the **electromagnetic component**, the **hadronic component** and muons and neutrinos which can be seen as the **muonic component**.



### 3.1.2 The Atmosphere

Before studying the interactions of cosmic rays in the atmosphere we need to setup a model that will describe our atmosphere. To study the cosmic rays interactions in the atmosphere it is useful to define a parameter that we will call the **vertical atmospheric depth** (sometimes also called column density) defined as the integral in altitude of the atmospheric density  $\rho$  above the observation level  $h$ :

$$X(h) = \int_h^\infty \rho(h') dh'$$



#### 3.1.2.1 The isothermal model of the Atmosphere

In an isothermal hydrostatic atmosphere a particular layer of gas at some altitude is static. That means that the downward (towards the planet) force of its weight, plus the downward force exerted by pressure in the layer above it, and the upward force exerted by pressure in the layer below, all sum to zero. Assuming a segment of area  $A$  and height  $dh$  we can write this equilibrium of forces as:

$$P \cdot A - (P + dP) \cdot A - (\rho Adh)g_0 = 0$$

$$dP = -g_0\rho(h)dh$$

Using the ideal gas law:

$$P = \frac{\rho RT}{M}$$

where  $R$  is the ideal gas constant,  $T$  is temperature,  $M$  is average molecular weight, and  $g_0$  is the gravitational acceleration at the planet's surface. We get

$$\frac{dP}{P} = -\frac{g_0 M}{RT} dh$$

assuming a constant and isothermal gas ( $\text{const } T$ ) we can integrate a pressure decreases exponentially with increasing height as:

$$P = P_0 e^{-\frac{g_0 M}{RT} h}$$

where we can define the **scale height** as:

$$h_0 = \frac{RT}{M g_0}$$

Since the temperature is assumed to be constant it follows that  $\rho$  also changes exponentially as  $\rho = \rho_0 e^{-h/h_0}$  and therefore the column density can be written as:

$$X = X_0 e^{-h/h_0}$$

where  $X_0$  is  $1030 \text{ g/cm}^2$  is the atmospheric depth at sea level,  $h = 0$ . In particular for the isothermal model we have that the relation between atmospheric depth (aka column density) and density is:

$$\rho(X) = \frac{X}{h_0}$$

### 3.1.2.1.1 The Scale Height

Using typical values ( $T = 273 \text{ K}$  and  $M = 29 \text{ g/mol}$ ) we get that  $h_0 \sim 8 \text{ km}$  which coincidentally is the approximate height of Mt. Everest.

In reality the temperature changes and hence the scale height decreases with increasing altitude until the tropopause.

This equations are valid for vertical particles, for zenith angles  $< 60^\circ$  (for which we can ignore the Earth's curvature) the formula is scaled with  $1/\cos \theta$  giving the *slant depth*

$$X_{\text{slant-depth}} = \frac{X}{\cos \theta}$$

### 3.1.3 Energy Losses in the Atmosphere

Charge particles when entering in the atmosphere will suffer different process of energy losses. We are going to review some of them

#### 3.1.3.1 Ionization Losses

The **ionization energy loss** of high energy charged particles with collision with atomic electrons is given by the Bethe-Block formula:

$$\left( \frac{dE}{dx} \right)_{ion} = - \left( \frac{4\pi N_0 z^2 e^4}{mv^2} \right) \left( \frac{Z}{A} \right) \left\{ \log \left[ \frac{2mv^2\gamma^2}{I} \right] - \beta^2 \right\}$$

where  $m$  is the mass of the electron,  $v$  and  $ze$  are the velocity and charge of the incoming particle,  $N_0$  is the Avogadro's number,  $Z$  and  $A$  are the atomic and mass numbers of the atom in the medium and  $x$  the path travelled, and  $I$  is the ionization potential of the medium is approximatively 10 Z eV.

- Since  $Z/A \sim \frac{1}{2}$  in most materials it depends little on the medium.
- It varies as  $1/v^2$  at low speed and independent of the incident particle mass.
- It reaches a minimum at about  $3Mc^2$  and it increases logarithmically until it reaches a plateau value.

#### 3.1.3.2 Radiation Losses

In addition to ionization losses, charge particles also undergo **bremsstrahlung** or braking radiation when travelling through a material given by:

$$\left( \frac{dE}{dx} \right)_{rad} = - \frac{E}{X_0}$$

where for electrons the **radiation length** is:

$$\frac{1}{X_0} = 4\alpha \left( \frac{Z}{A} \right) (Z + 1)^2 r_e^2 N_0 \log \left( \frac{183}{Z^{1/3}} \right)$$

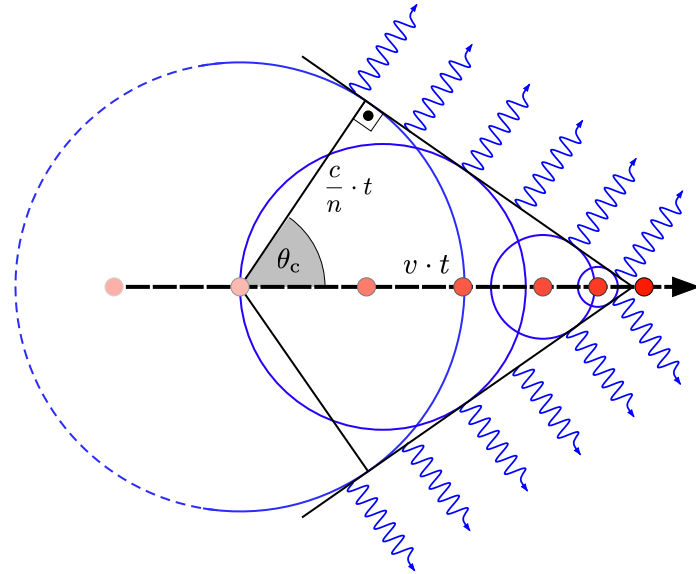
where  $r_e = e^2/4\pi m_e c^2$  is the classical electron radius and  $\alpha = \frac{1}{137}$  is the fine structure constant.

- Bremsstrahlung is proportional to  $\frac{1}{X_0} \propto r_e^2 \propto 1/m_e^2$ . The radiation length of a muon will be  $(m_\mu/m_e)^2$  times that for an electron.
- Bremsstrahlung is proportional to the energy.

The critical energy is the energy at  $(dE/dx)_{ion} = (dE/dx)_{rad}$ . Above this energy the radiation process dominates, below the ionization. For electrons this is roughly  $\epsilon_c \sim 600/Z$  MeV, and for the atmosphere this is  $\epsilon_e \sim 85$  MeV.

### 3.1.3.3 Cherenkov Radiation

When relativistic particles traverse a medium at a speed greater than the speed of light in that medium it can induce Cherenkov radiation.



Cherenkov light is emitted in the UV and blue region in a narrow cone with angle:

$$\cos \theta = \frac{ct/n}{\beta ct} = \frac{1}{\beta n}$$

so the threshold for production is  $\beta > \frac{1}{n}$ . Most of the components in the air shower will produce abundant Cherenkov light.

We will see more on Cherenkov radiation on the next lesson about  $\gamma$ -ray astronomy.

### 3.1.3.4 Pair production

If a photon from bremsstrahlung has enough energy  $E_\gamma > 2m_e$  it can produce a pair of electron positron. The cross-section rises quickly at the threshold of  $2m_e$  but in the high energy part it can be approximated to:

$$\sigma = \frac{7}{9} r_0^2 Z(Z+1) \log \left( \frac{183}{3\sqrt{Z}} \right)$$

The pair production cannot occur in vacuum, a photon disintegrated to the pair  $e^-e^+$  will have a null momentum in the CoM system, therefore a nucleus has to be present to absorb the momentum. As can be seen the radiation length  $X_0$  is very similar to the one from radiation losses. In fact we can write:

$$\frac{1}{X_{pair}} = \frac{7}{9} \frac{1}{X_0}$$

Which means that the **radiation lengths for braking radiation and pair production are comparable**.

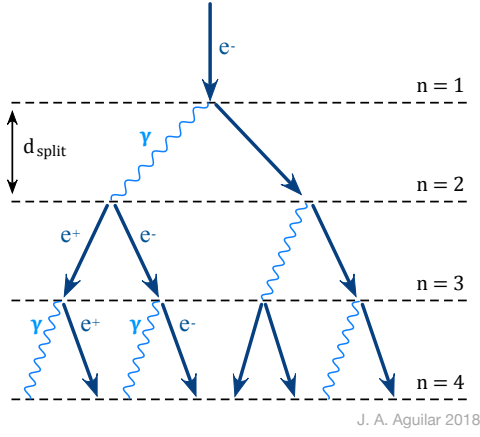
### 3.1.4 Electromagnetic Shower

When photons from radiation losses of electrons, have enough energy to produce pairs of positrons electrons, these can also produce photons which, in turn, can also produce pairs, etc, etc. This is called an **electromagnetic shower**.

#### 3.1.4.1 The Heitler Toy-Model

The Heitler toy model explains very well the development of an electromagnetic shower. As we saw, in the ultrarelativistic limit the radiation lengths for pair production and bremsstrahlung are comparable. We can define a distance  $d_{split} = X_0 \log 2$  where an electron will lose, on average, half of its energy.

An electron with initial energy  $E_0$  in a medium will generate a photon in a  $d_{split}$  length of energy  $E_0/2$ , in the next radiation length the photon can convert into  $e^+e^-$  each with energies  $E_0/4$ . After  $t$  steps the electrons, positrons will have energies of  $E(t) = E_0/2^t$ . This continues until the electrons, positrons fall below the critical energy of electrons,  $\epsilon_e$ , and ionization dominates. The process is illustrated in the figure below, where each step  $n$  corresponds to one  $d_{split}$  length.



J. A. Aguilar 2018

The Heitler model has the following properties:

- The shower has maximum at:

$$t_{max} = \frac{\log(E_0/\epsilon_e)}{\log 2}$$

- The maximum number of particles is:

$$N_{max} = 2^{t_{max}} = \frac{E_0}{\epsilon_e}$$

- The shower maximum will be at a depth  $X_{max}$ :

$$X_{max} = d_{split} \frac{\log(E_0/\epsilon_e)}{\log 2} = X_0 \log(E_0/\epsilon_e)$$

For air  $\epsilon_e = 85$  MeV and the **radiation length**  $X_0 = 36.7 \text{ g/cm}^2$ . Actual showers also spread laterally mostly due to Coulomb scattering. The lateral spread is a few times the so-called **Moliere unit** equal to  $21/\epsilon_e$  (MeV).

The  $X_{max}$  prediction of the Heitler model is in good agreement with Monte Carlo simulations. However, the electron to photon ratio of 2 is not in agreement given that the model predicts only one photon emitted by bremsstrahlung. Simulations show a ratio of 1/6 since in reality several photons are emitted and electrons lose energy much faster than photons do.

### 3.1.5 Hadronic Showers

Before modeling the baryon-induced showers or hadronic showers, we need to estimate the *nuclear mean free path* in the atmosphere. We can write the **standard mean free path** for  $\sigma_N^{air}$  nucleon-air cross section as:

$$l_N = \frac{1}{n\sigma_N^{air}}$$

where as we saw in the introduction  $n$  is the **number density** of targets, in our case air nuclei. This number density can be expresed as  $n = N_T/V$  where  $N_T$  is the total number of air nuclei in volume  $V$ .

The **density mean free path**, is defined as  $\lambda_N = \rho_{air}l_N$ , where  $\rho_{air} = n \cdot m_{air}$  where  $m_{air}$  is the mass of air nuclei, that can be written as  $m_{air} \sim Am_p$ . Puttin everything together we have that:

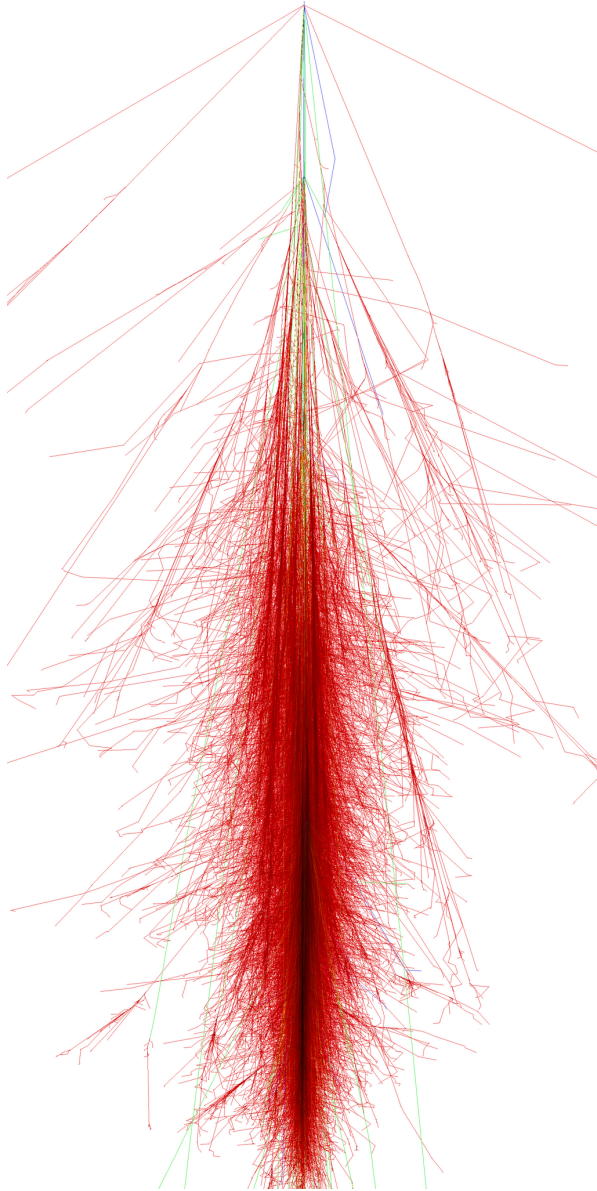
$$\lambda_N^{air} = \rho_{air}l_N = nAm_p \frac{1}{n\sigma_N^{air}} = \frac{Am_p}{\sigma_N^{air}}$$

For air  $A$  is average mean the mass number of air nuclei components (mainly nitrogen, oxygen) and we can assume it to be  $A \sim 14.5$  and  $\sigma_N^{air} \approx 300$  mb, which corresponds to  $\lambda_N^{air} \approx 80\text{g/cm}^2$ .

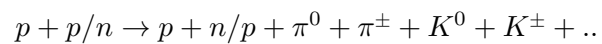
Note that this definition of the density mean free path is independent of the mass density of the medium, so if the density changes with altitude, like in the case of our atmosphere, the density mean free path is the same.

#### 3.1.5.1 The Heitler-Matthew Model

In the Heitler model can be adapted also for hadronic showers. This is what Matthew did. We can imagine a proton initiating the cascade instead of a photon/electron, in this case a hadronic air shower will develope:

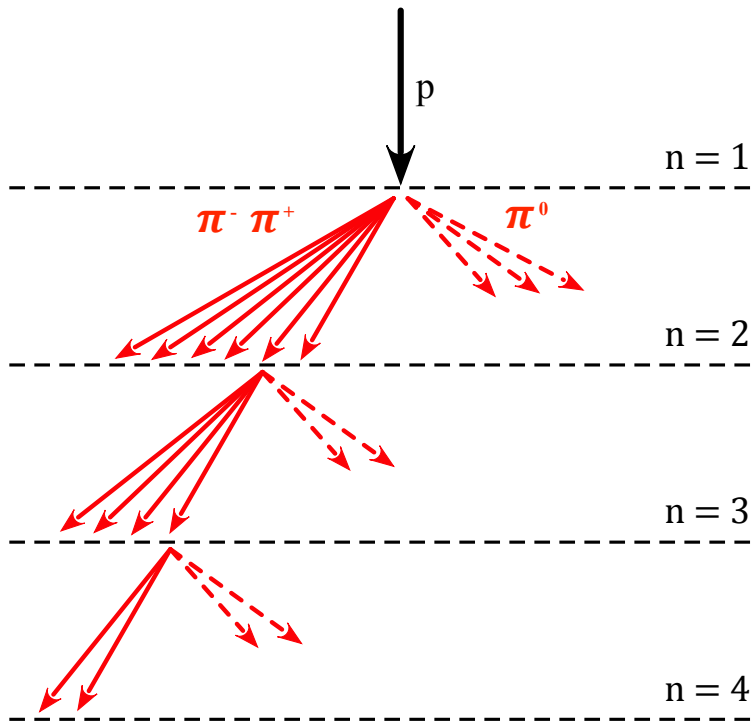


We can assume that the first interaction is defined by the proton mean free path  $\lambda_N^{air}$ . Defining the first interaction point where the proton will lose (on average) half of its energy this first interaction length is given as  $\lambda_N^{air} \log 2$  where for protons  $\lambda_N^{air} \approx 80\text{g/cm}$ . The following general interaction is expected:



We will focus only on pion production (same argument can be done for kaons). After the first

interaction we can use the simplified assumption that the hadronic interaction produces only  $3N_\pi$  pions. Of those  $2 N_\pi$  will be charged pions and  $N_\pi$  will be  $\pi^0$ .



J. A. Aguilar 2018

We also assume the energy is equally distributed among them, so  $2/3E_0$  will go to charge pions and  $1/3E_0$  will go to the neutral pions. The  $\pi^0$  has a very short decay time, so it will decay and produce an electromagnetic shower. Charge pions will continue generating hadronic shower in each  $d_{split} = \lambda_\pi^{air} \log 2$  with the mean free path of pions  $\lambda_\pi^{air} \sim 120\text{g/cm}^2$  until they reach the critical energy where pions decay is more probable than interactions  $\epsilon_\pi$ . On each step we assume that energy is equally divided among the  $3N_\pi$  pions. Therefore at each step  $t$  the energy of the pions is:

$$E_\pi = \frac{E_0}{(3N_\pi)^t}$$

The number of radiation lengths  $t$  to reach the critical energy ie  $E_\pi = \epsilon_\pi$ , and is given (as in the case of EM showers):

$$t_{max} = \frac{\log(E_0/\epsilon_\pi)}{\log(3N_\pi)}$$

Assuming that after that energy all charged pions (ie  $2N_\pi$ ) decay to muons, the number of muons is given by:

$$N_\mu = (2N_\pi)^{t_{max}}$$

introducing  $\beta = \log(2N_\pi)/\log(3N_\pi)$  we have:

$$N_\mu = (E_0/\epsilon_\pi)^\beta$$

This is also called the *multiplicity* and corresponds to the muon bundles as we will see later. For pions between 1 GeV and 10 TeV an appropriate number is  $N_\pi = 5$  and in that case  $\beta = 0.85$ . Therefore the number of muons doesn't grow linearly with the initial energy but a slower rate.

The definition of  $X_{max}$  is somehow less clear than in an EM shower. Hadronic showers are still dominated by electromagnetic processes, so we can assume that  $X_{max}$  depends dominantly on the first generation of  $\pi^0$  EM subshowers. For proton primaries, the first interaction will be given by the nucleon mean free path where in this first interaction the proton splits in  $3N_\pi$  particles, so  $p\pi^0$  with initial energy  $E_0/3N_\pi$  will initiate an EM shower. The depth of maximum is then obtained as the sum of the first proton interaction length and the shower maximum of the first EM sub-shower:

$$X_{max} = \lambda_N^{air} \log 2 + X_0 \log \left( \frac{E_0}{3N_\pi \epsilon_e} \right)$$

where again  $\epsilon_e$  is the critical energy of electrons. The expected values of this formula are low when compared to detailed simulations because it neglects the contributions of the next one or two generation of  $\pi^0$  production.

### **i** Superposition model for heavy nuclei air showers

We can extend the discussion to heavy nuclei by adopting the *Superposition model* in which a nucleus of mass  $A$  and energy  $E_0$  essentially generates  $A$  subshowers of energy  $E_0/A$ . In that case the muon multiplicity will be:

$$N_\mu = A \left( \frac{E_0}{A\epsilon_\pi} \right)^\beta \propto E_0^\beta A^{1-\beta}$$

therefore the muon multiplicity will depend on the CR composition. Likewise the shower

maximum is given by:

$$X_{max}^A(E_0) = X_{max}^p(E_0) - X_0 \log A$$

ie, for a given energy  $E_0$  the shower max depends on the mass of the CR primary and it is typically smaller than for protons (ie reach the maximum sooner in the atmosphere). For composition studies therefore it is necessary to measure  $X_{max}$  and the energy of the shower, which can be estimated from fluorescence techniques.

### 3.2 Muons and Neutrinos

The plot below shows the particle flux surviving after a certain altitude.

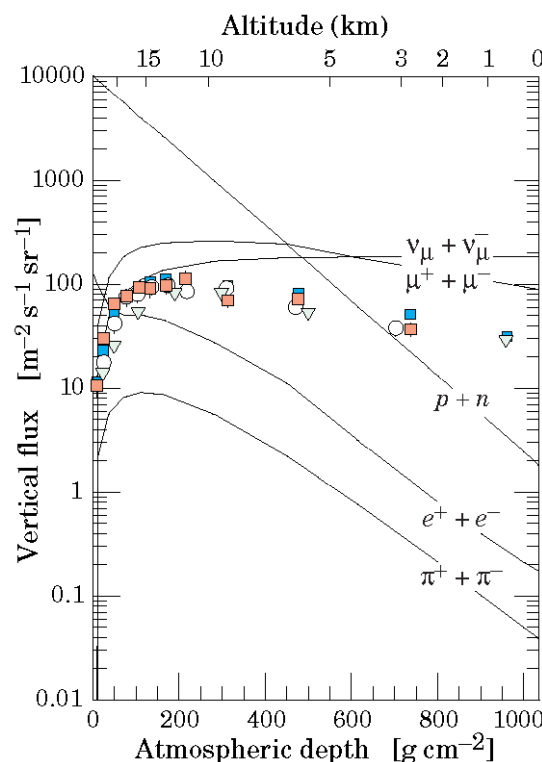


Figure 3.1: Source: Particle Data Group

We can extract different information from this plot:

- Primaries dominate up to 9 km, secondaries (electrons, pions) roughly follow the primary shape. Muons and neutrinos are continuously produced.

- Vertical fluxes for  $E > 1$  GeV. Points show the  $\mu^-$  measurements. Muons and neutrinos are produced in decays of mesons which are themselves produced by interactions of CR particles with air nuclei.
- They are the dominant flux at sea level and the only ones that can penetrate deep underground.

Electrons and nucleons fluxes above 1 GeV/c are about 0.2 and  $2 \text{ m}^{-2} \text{ s}^{-1} \text{ sr}^{-1}$  at sea level. Nucleons are the degraded remnants of the primary cosmic radiation. At sea level about 1/3 are neutrons.

### 3.2.1 Muons and Neutrinos Productions

The most important channels for muon and neutrino production are:

- Two body decays

$$\pi^\pm \rightarrow \mu^\pm + \nu_\mu(\bar{\nu}_\mu) \ (\sim 100\%)$$

$$K^\pm \rightarrow \mu^\pm + \nu_\mu(\bar{\nu}_\mu) \ (\sim 63.5\%)$$

- Three body decay

$$K_L \rightarrow \pi^\pm e^\pm \nu_e(\bar{\nu}_e) \ (\sim 38.7\%)$$

At lower energies, the muon decay is also important:

$$\mu^\pm \rightarrow e^\pm + \nu_e(\bar{\nu}_e) + \bar{\nu}_\mu(\nu_\mu)$$

For each of the 2-body decay channels, assuming the muon always decay the neutrino flavor ratio is:

$$:_{\text{e}} = \mathbf{2} : \mathbf{1}$$

**i** Mean free path for mesons,  $\pi, K$

Charged pions and Kaons can interact or decay. Both processes have a mean free path and one or the other will dominate depending on which mean free path is larger.

The **decay mean free path** of pions is given by  $l_\pi^d = \gamma c \tau_\pi$  where  $\gamma$  is the Lorentz factor of the pion. Multiplying for density we have the **density decay mean free path** as:

$$\lambda_\pi^d = \rho(X) \gamma c \tau_\pi$$

However the atmosphere density depends on the atmospheric depth as  $\rho(X) = X/h_0$ . In units of *slant depth*,  $X_{sd} = X/\cos \theta$  and expanding  $\gamma = E/m_\pi c^2$  we can rewrite the

density decay free path as:

$$\frac{1}{\lambda_\pi^d(E)} = \frac{m_\pi c^2 h_0}{E c \tau_\pi X_{sd} \cos \theta} = \frac{\epsilon_\pi}{E X_{sd} \cos \theta}$$

where  $E$ ,  $m_\pi$ ,  $\tau_\pi$  are the pion energy, mass and lifetime and we defined:

$$\epsilon_\pi = \frac{c \tau_\pi}{m_\pi c^2 h_0}$$

as a *critical energy*. The critical energy is such that the decay time equals the vertical atmospheric depth  $\lambda_\pi^d(\epsilon_\pi) = X_{sd} \cos \theta = X$ .

The **interaction mean free path** is the same as nucleon  $\lambda_\pi = A m_\pi / \sigma_\pi^{air}$  which as we saw is independent of  $X$ .

### **i** Critical energy for mesons, $\pi$ , $K$

Decay or interaction dominates depending on whether  $1/\lambda_\pi^d$  or  $1/\lambda_\pi$  is larger. This in turns depends on the ratio between the energy  $E$  and the critical energy  $\epsilon_\pi$ . For example, the value of the critical energy for pions is given by:

$$\epsilon_\pi = \frac{c \tau_\pi}{m_\pi c^2 h_0} \approx 115 \text{ GeV}$$

So we can distinguish two regimes.

- For  $E \gg \epsilon_\pi$  decay length is much larger than the atmospheric depth, so interaction dominates.
- For  $E \ll \epsilon_\pi$  decay dominates is much shorter than the atmospheric depth, so the pion will likely decay before interacting.

The same formulas can be derived for Kaons.

### 3.2.2 Muon Fluxes

The muon energy spectrum at sea level is a direct consequence of the meson source spectrum. Unlike electrons, muons will decay before reaching the ground in the GeV energy range. The muon decay length is given by:

$$d_\mu = \gamma \tau_\mu c$$

Where  $\tau_\mu$  is the muon lifetime of the order of  $2.2 \times 10^{-6}$  s. So for a muon of 1 GeV we have:

```

lifetime = 2.1969811e-6 # muon lifetime in seconds
import scipy.constants as cte
cspeed = cte.c
muon_mass = cte.value("muon mass energy equivalent in MeV") * 1e-3 # in GeV

energy = 1 # GeV

print(f"d = {(energy/muon_mass)*lifetime*cspeed*1e-3:.2f} km")

```

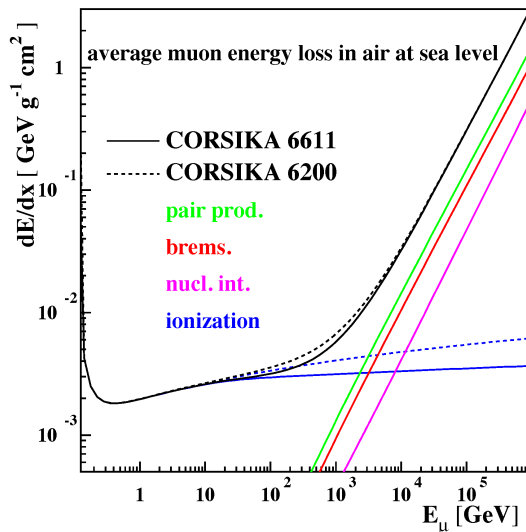
$d = 6.23 \text{ km}$

Compared to the typical atmospheric altitude of  $h \sim 15 \text{ km}$  it means that at those energies, muons will not reach the ground.

### 3.2.2.1 Energy regimes of muon fluxes

Three different regimes are distinguishable:

- $E_\mu \leq \epsilon_\mu$ , where  $\epsilon_\mu \sim 1 \text{ GeV}$ . This critical energy is when interaction probability and decay probability start to be comparable. Even more the muon energy losses become important. As we saw energy losses via ionization is almost constant, for muons is about  $\sim 2 \text{ MeV}/(\text{g/cm}^2)$  in air (and mostly independent on the material). However this is true only above energies of 1 GeV, below ionization losses increase drastically as can be seen in the figure below.



- $\epsilon_\mu \leq E_\mu \leq \epsilon_{\pi,K}$ , where  $\epsilon_\pi = 115$  GeV and  $\epsilon_K = 850$  GeV. In this range all mesons decay and muons spectrum follows the same of the parent spectrum of mesons and hence that of the primary CRs. The muon is almost independent of the zenith angle.
- $E_\mu \gg \epsilon_{\pi,K}$ , Mesons interaction length starts to be comparable to their decay length. This happens first for inclined showers and so the muon flux gets suppressed while it also starts to depend on the zenith angle (ie on the density of the atmosphere).

At even higher energies, above 1 TeV in air, muons will also start to lose energy via other radiative process (we will see that below when talking about muons underground).

### 3.2.2.2 Analytical approximation

An approximate extrapolation formula valid when muon decay is negligible ( $E_\mu > 100/\cos\theta$  GeV) and the curvature of the Earth can be neglected ( $\theta < 70^\circ$ ) is given by the Gaisser parametrization:

$$\frac{dN_\mu}{dE_\mu d\Omega} = \frac{0.14}{\text{cm}^2 \text{ s sr GeV}} \left( \frac{E_\mu}{\text{GeV}} \right)^{-2.7} [F_\pi(E_\mu, \theta) + F_K(E_\mu, \theta)]$$

where  $F_\pi$  and  $F_K$  represent the contributions from pions and kaons, respectively:

$$F_\pi(E_\mu, \theta) = \frac{1}{1 + \frac{1.1E_\mu \cos\theta}{115 \text{ GeV}}}$$

$$F_K(E_\mu, \theta) = \frac{0.054}{1 + \frac{1.1E_\mu \cos\theta}{850 \text{ GeV}}}$$

**Tutorial I: Plot the muon flux for two different angles**

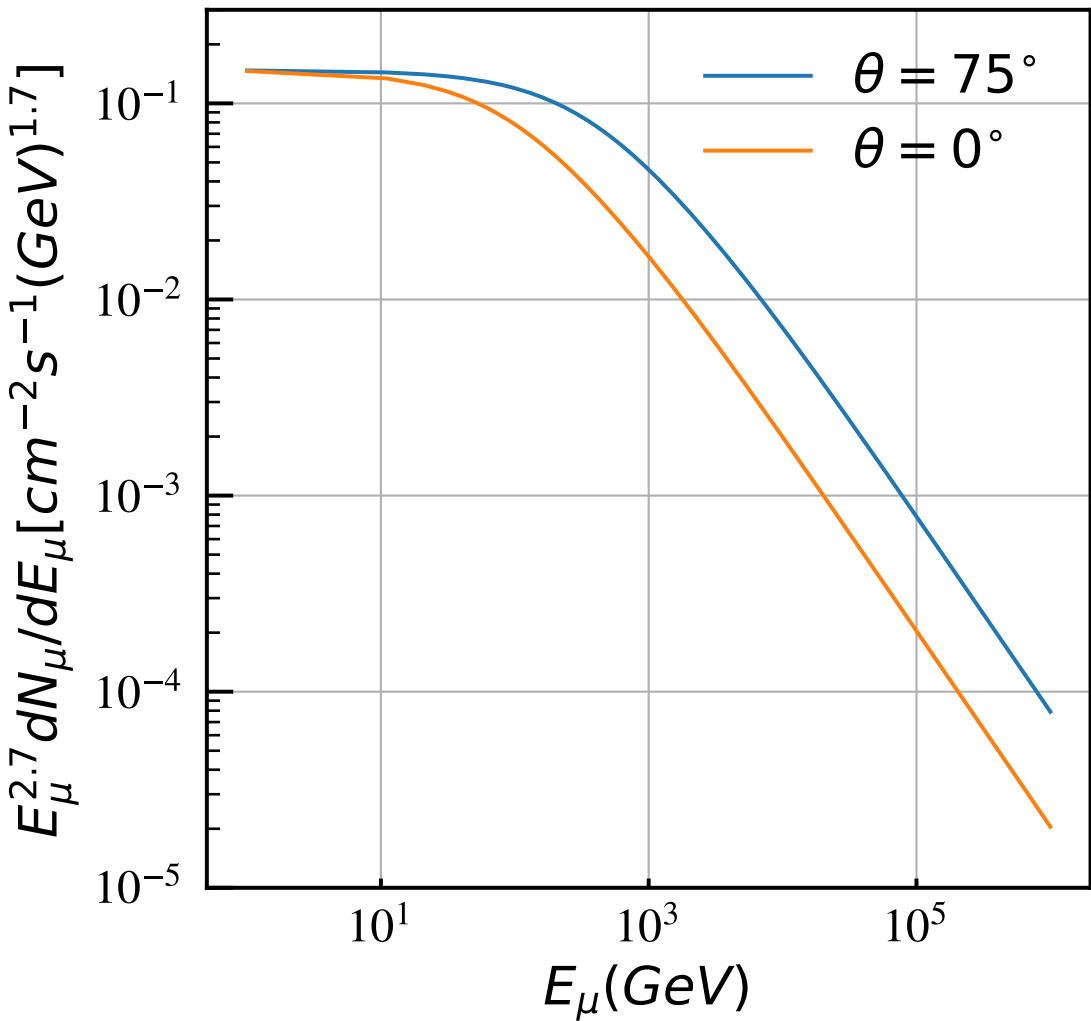
```

import matplotlib.pyplot as plt
import numpy as np
plt.rcParams['font.family'] = "STIXGeneral"
plt.rcParams.update({'axes.labelsize': 20})
plt.rcParams.update({'legend.fontsize': 20})
plt.rcParams.update({'figure.figsize': [8, 6]})
plt.rcParams['xtick.labelsize'] = 18
plt.rcParams['ytick.labelsize'] = 18
plt.rcParams['xtick.major.width'] = 1.5
plt.rcParams['xtick.minor.width'] = 1
plt.rcParams['xtick.major.pad'] = 8
plt.rcParams['xtick.direction'] = 'in'
plt.rcParams['ytick.major.size'] = 10
plt.rcParams['ytick.minor.size'] = 5
plt.rcParams['ytick.major.width'] = 1.5
plt.rcParams['ytick.minor.width'] = 1
plt.rcParams['ytick.major.pad'] = 8
plt.rcParams['ytick.direction'] = 'in'
plt.rcParams['legend.frameon'] = False
plt.rcParams['lines.linewidth'] = 1.5
plt.rcParams['axes.linewidth'] = 1.5

def muons(cangle, E):
    a = 1./(1.+ 1.1*E*cangle/115.)
    b = 0.054/(1.+ 1.1*E*cangle/850.)
    return 0.14 *E**-2.7 *(a + b)

fig = plt.figure(figsize=(6,6))
ax = plt.subplot(111)
ax.set_xscale("log")
ax.set_yscale("log")
ax.set_xlim(1e-5, 3e-1)
ax.set_xlabel(r"$E_\mu(\text{GeV})$")
ax.set_ylabel(r"$E_\mu^{\text{2.7}} dN_\mu/dE_\mu [\text{cm}^{-2}\text{s}^{-1} (\text{GeV})^{1.7}]$")
ax.grid()
E = np.arange(1e0, 1e6, 10)
ax.plot(E, E**2.7*muons(np.cos(75*np.pi/180.),E), label=r"$\theta = 75^\circ$")
ax.plot(E, E**2.7*muons(np.cos(0*np.pi/180.),E), label=r"$\theta = 0^\circ$")
plt.legend()
plt.show()

```



### 3.2.2.3 Measured muon flux

In reality below 10 GeV muon decay and energy loss become important and the Gaisser parametrization overestimates the muon flux as can be seen in the plot below:

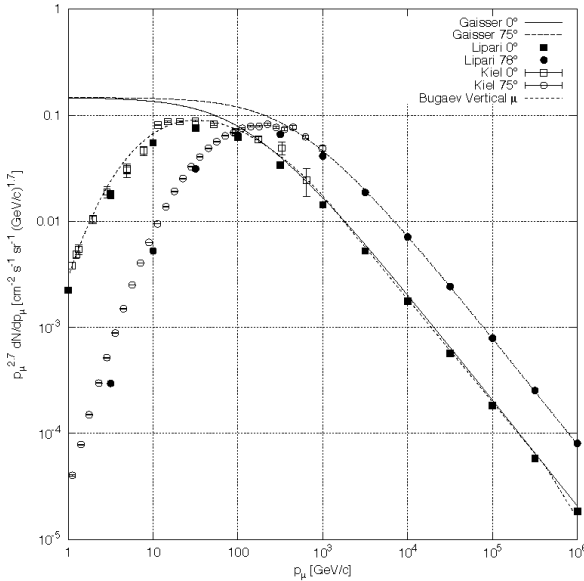


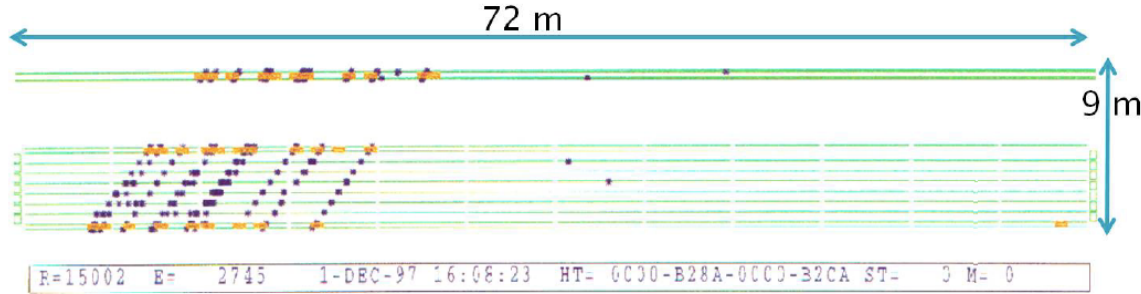
Figure 3.2: Source: Particle Data Group

As can be seen from the measured muon flux has the following characteristics:

- Muons are the most numerous charged particles at sea level
- The mean energy of muons at the ground is  $\sim 4$  GeV.
- The integral intensity of vertical muons above 1 GeV/c at sea level is  $\approx 70\text{m}^{-2}\text{s}^{-1}\text{sr}^{-1}$  or  $\approx 1\text{cm}^{-2}\text{min}^{-1}$ .

### 3.2.3 Muon Bundles

Sometimes muons also come in groups or **bundles** of parallel muons originated from the same primary CR. Muon bundles sometime look like a single high energy muon. The multiplicity (number of muons in the bundle) if can be measured is correlated with the mass of the original CR. The image below shows a muon-bundle event observed with the MACRO underground detector.



### 3.2.3.1 Charge Ratio

The muon charge ratio reflects the excess of  $\pi^+$  over  $\pi^-$  and  $K^+$  over  $K^-$  and the fact that there are more protons than neutrons in the primary spectrum.

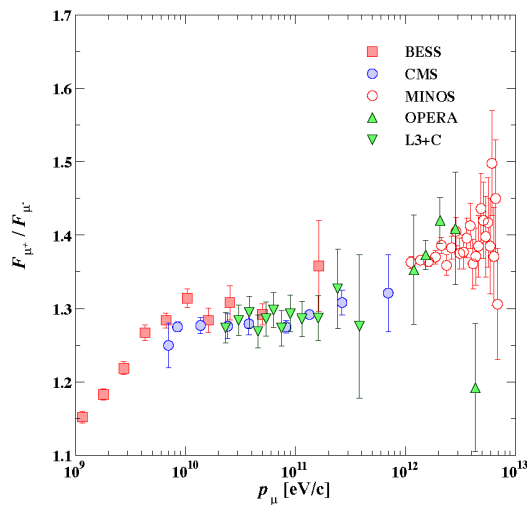


Figure 3.3: Source: Allkofer et. al. Phys. Lett. B36, 425 (1971). Jokisch et. al. Phys. Rev. D19, 1368 (1979)

The increase with energy of the ratio is due to an increasing importance of kaons coming from the process  $p + N \rightarrow + K^- + \dots$

Assuming the following reactions for the production of  $\pi^+$  and  $\pi^-$ :

$$p + N \rightarrow p' + N' + k\pi^+ + k\pi^- + r\pi^0$$

$$p + N \rightarrow n + N' + (k+1)\pi^+ + k\pi^- + r\pi^0$$

where  $k$  and  $r$  are the multiplicity of the particle species. Assuming same cross sections we obtain:

$$R = \frac{N(\pi^+)}{N(\pi^-)} = \frac{2k+1}{2k} = 1 + \frac{1}{2k}$$

for low energies  $k = 2$  and  $R \sim 1.25$

### 3.2.4 Neutrinos Fluxes

- Neutrinos are the most abundant CR product at sea level, yet they have only recently (compared to other particles) measured due to their extremely low cross-section.
- The process giving neutrino fluxes are the same as for the muons (we saw already) plus the muon decay. Taking into account the decay of pions, kaons and muons gives to a flavor ratio of:  $\nu_\mu : \nu_e = 2 : 1$  and  $\nu_e/\bar{\nu}_e \sim \mu^+/\mu^-$
- At few GeV ( $> \epsilon_\mu$ ) muons will not decay and  $\nu_e$  will be suppressed as the main source of  $\nu_e$  is the muon decay.

**Tutorial II: Plot the  $\nu_\mu$  and  $\nu_e$  atmospheric flux using the package DaemonFlux  
@Yanez:2023lsy**

```

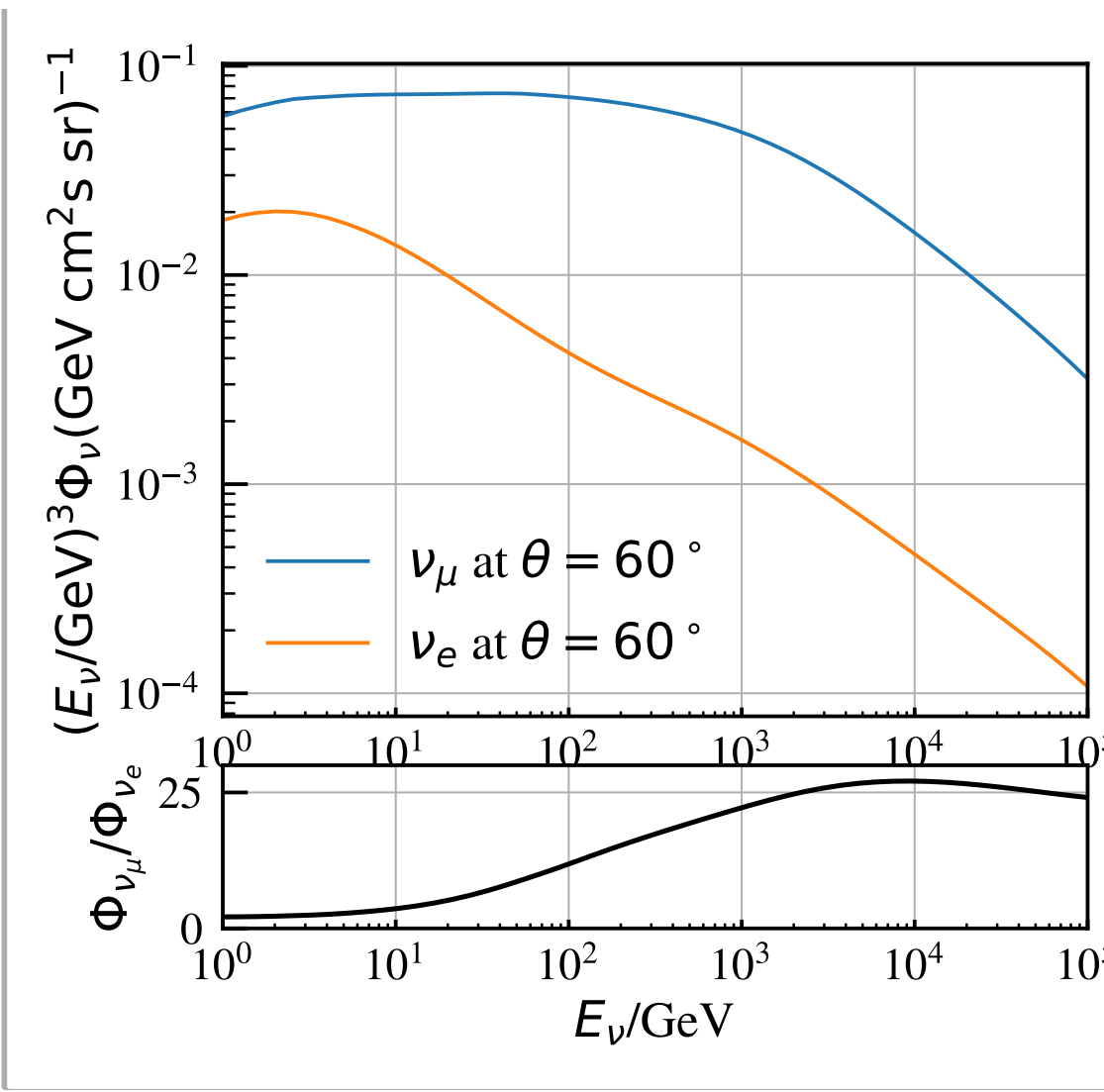
from daemonflux import Flux
fl = Flux(location='generic', use_calibration=True, debug=1)
egrid = np.logspace(0,5)

# Start with a square Figure.
fig = plt.figure(figsize=(6, 6))
gs = fig.add_gridspec(2, 1,
                      left=0.1, right=0.9, bottom=0.1, top=0.9,
                      height_ratios = (4, 1), wspace=0.05, hspace=0.12)
# Create the Axes.
ax_1 = fig.add_subplot(gs[0])
ax_2 = fig.add_subplot(gs[1], sharex=ax)

ax_1.plot(egrid, fl.flux(egrid, "60", "numuflux")+fl.flux(egrid, "60", "antineumu"), label=r"$\Phi_{\nu_\mu} + \Phi_{\bar{\nu}_\mu}$ at $\theta = 60^\circ$")
ax_1.plot(egrid, fl.flux(egrid, "60", "nueflux"), label=r"$\Phi_{\nu_e}$ at $\theta = 60^\circ$")
ax_1.legend()
ax_1.loglog()
ax_1.grid()
ax_2.plot(egrid, fl.flux(egrid, "60", "numuflux")/fl.flux(egrid, "60", "nueflux"), label=r"$\Phi_{\nu_\mu}/\Phi_{\nu_e}$ at $\theta = 60^\circ$")
ax_2.grid()
ax_2.set_xscale("log")
ax_2.set_yscale("log")
ax_2.set_xlim(1, 1e5)
ax_1.set_xlim(1, 1e5)
ax_2.set_xlabel(r"$E_{\nu}/\text{GeV}$")
ax_1.set_ylabel(r"$\Phi_{\nu_\mu} (\text{GeV})^3$ / $\Phi_{\nu_e}$")
ax_2.set_ylabel(r"$\Phi_{\nu_\mu}/\Phi_{\nu_e}$")

Text(0, 0.5, '$\Phi_{\nu_\mu}/\Phi_{\nu_e}$')

```



**i Note**

In astrophysical sources the ration 2:1 persists. Why pions don't decay in to electrons?

### 3.2.5 Fluxes and Kinematics

As mentioned neutrinos and muons are strongly correlated. However due the two-body kinematics, the energy spectra of the  $\nu$ 's and  $\mu$ 's from mesons decay are different. For example, the energy of the muon in CoM is given by:

$$E_\mu^* = (m_\pi^2 + m_\mu^2)/2m_\pi = 109.8 \text{ MeV}$$

and for the neutrino:

$$E_\nu^* = (m_\pi^2 - m_\mu^2)/2m_\pi = 29.8 \text{ MeV}$$

In the laboratory system, the energies are boosted by the Lorentz factor  $\gamma = E_\pi/m_\pi$ , but as can be seen muon carry a much larger fraction of energy than neutrinos. For energies about  $1 \text{ TeV} < E_\nu < 10^3 \text{ TeV}$ , the angle averaged atmospheric  $\nu_\mu + \bar{\nu}_\mu$  can be approximated by a power law spectrum:

$$\frac{dN_{\nu_\mu + \bar{\nu}_\mu}}{dE_\nu} = 7.8 \times 10^{-11} \left( \frac{E_\nu}{1 \text{ TeV}} \right)^{-3.6} \text{ cm}^2 \text{ s}^{-1} \text{ sr}^{-1} \text{ GeV}^{-1}$$

### 3.2.5.1 Fluxes as Function of Zenith

Another difference with respect to the muon fluxes is their dependency with respect to the zenith angle. Since atmospheric muons are not absorbed by the Earth, their spectrum spans to the whole sky. The following plot shows the calculated neutrino flux at 1,300 m depth with energies  $E_\nu = 10 \text{ GeV}$ .

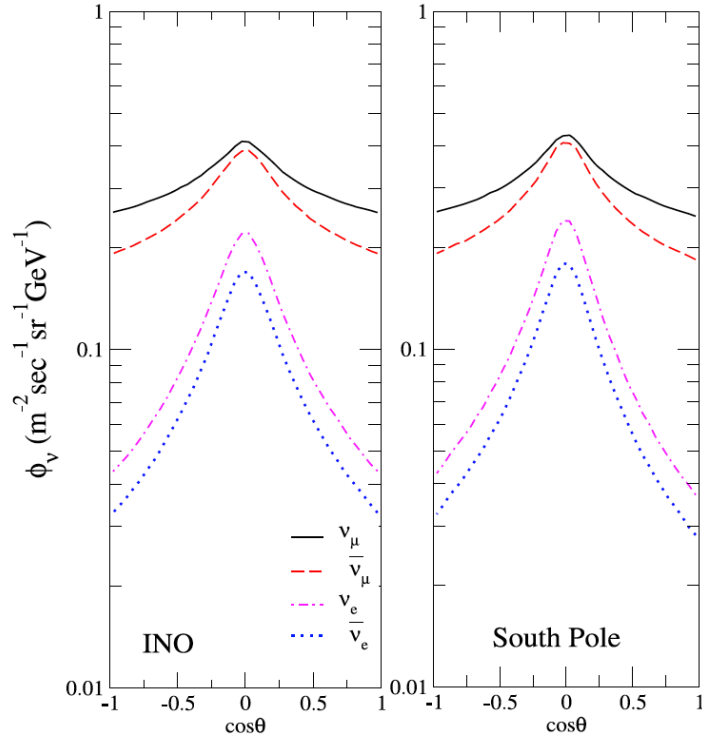


Figure 3.4: Source: [arXiv:1210.5154](https://arxiv.org/abs/1210.5154)

The peak at the horizon in the atmospheric neutrino flux is due to the so-called *secant theta effect*. This effect occurs because pions and kaons that are produced nearly skimming the Earth have more flight time in less dense atmosphere, so they have more chance to decay than interact.

### 3.2.6 Prompt Fluxes

Apart from kaons and pions, charmed mesons will also be produced in the atmosphere. Charm particles have lifetimes so short ( $10^{-12}$ s) they almost always decay before interacting. Muons and neutrinos from charm decay are called *prompt* muons/neutrinos. They have the following peculiarities:

- The energy spectrum follows the one of the primary cosmic rays ie that of  $\sim E^{-2.7}$ .
- Since there is no competition between decay and interaction of the charm particle, the *prompt* flux is fully **isotropic**.
- Since neutrinos are produced in 3-body decays they produced the same amount of  $\nu_\mu$  and  $\nu_e$ .

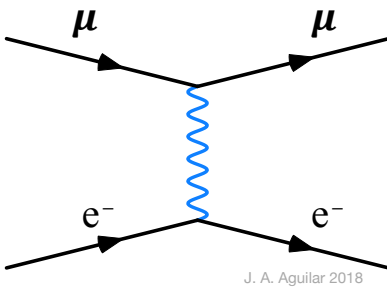
It is important to note that the prompt fluxes have not been observed yet.

## 3.3 Particles Underground

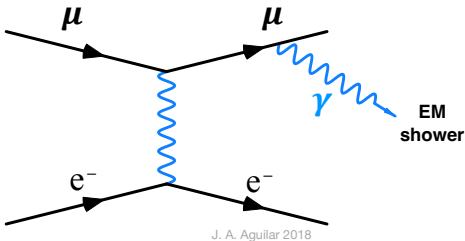
### 3.3.1 Muon Interactions

When muon reaches the ground the will experience the following interactions when travelling through matter with a higher density than air. The will losse energy mostly through the following processes:

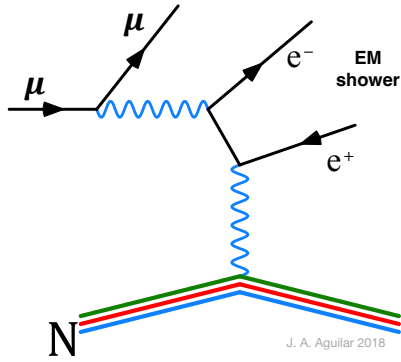
- **Ionization.** The continuous energy loss of muons passing through a medium as it ionize the material along the path. We saw however that ionization is mostly independent of the material, as most of them have values of  $Z/A \sim 0.5$ .



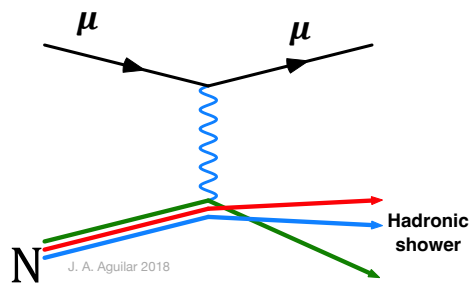
- **Bremsstrahlung.** Also called braking radiation. In the electric field of a nucleus or atomic electrons, muons can radiate high energy photons. If the photon has energy enough it can initiate an electromagnetic shower.



- **Pair production.** A muon can radiate a virtual photon which, again in the electric field of a nucleus, can convert into a real  $e^+e^-$  pair. As in the case of bremsstrahlung, the pair production will initiate an electromagnetic shower.

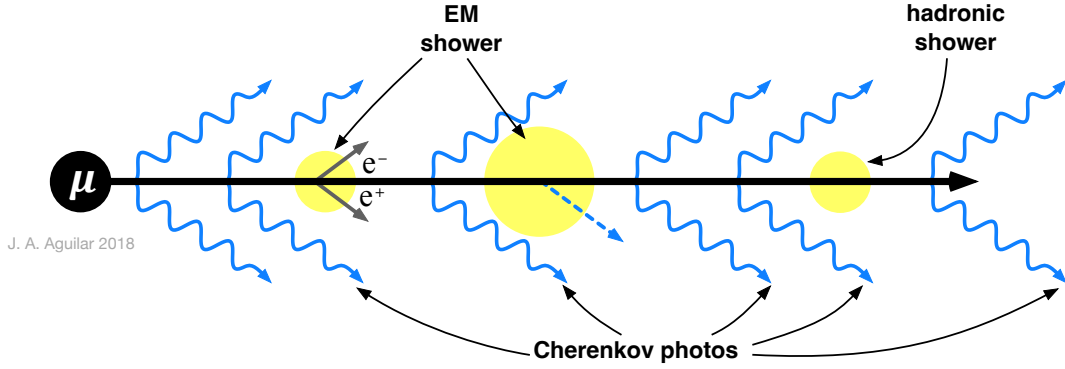


- **Photonuclear interactions.** A muon can radiate a virtual photon which directly interacts with a nucleus in the muon propagation medium. The interaction is either electromagnetic or following the fluctuation of the photon into a quark-antiquark pair (i.e. a virtual vector meson). This interaction will generate an hadronic shower.



### 3.3.2 Muon Energy losses

The energy losses due to ionization are continuous while in radiation processes the energy is lost in bursts along the muon path. When a muon is travelling through a dielectric medium like ice or water, it will emit cherenkov photons as wells, but due to the stochastics energy losses electromagnetic and hadronic showers are generated along the muon track. The following figure illustrates this process:



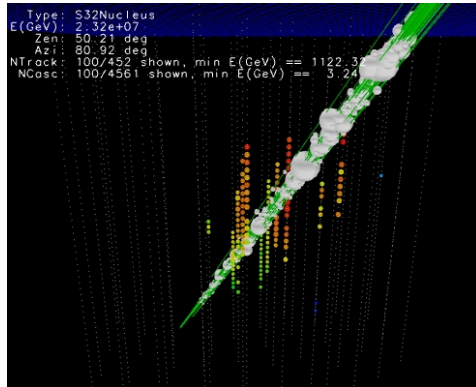
It is worth noting that photonuclear interactions are subdominant when compared to bremsstrahlung and pair-production, so most of the showers will be electromagnetic showers. The equation that describes the energy loss for muons at high energy can be simplified to:

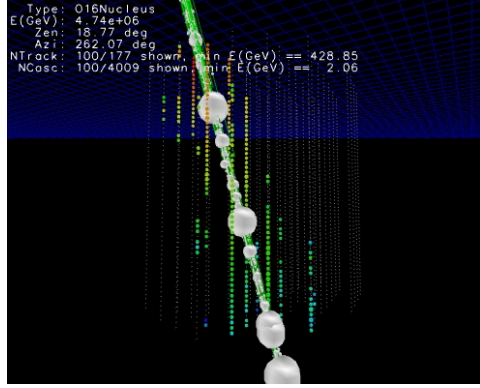
$$\frac{dE_\mu}{dX} = -\alpha - \beta E_\mu$$

where  $X$  is the thickness of the material (in g/cm<sup>2</sup>),  $\alpha$  is the energy loss due to ionization and  $\beta = \beta_{br} + \beta_{pair} + \beta_{ph}$  are the three discrete energy loss processes: bremsstrahlung, electron-positron production and electromagnetic interaction with the nuclei. Thickness is also given sometimes in units of meters water equivalent (1 m.w.e. = 10<sup>2</sup> g/cm<sup>2</sup>). Due to the energy dependency of the radiative processes, higher energy muons will have more stochastic energy losses than lower energy muons.

The **critical energy** is when both losses are equal, ie  $\epsilon_\mu = \alpha/\beta$ . Typical values are  $\alpha \approx 2 \text{ MeV g}^{-1} \text{ cm}^2$  and  $\beta \approx 4 \times 10^{-6} \text{ g}^{-1} \text{ cm}^2$ , so  $\epsilon_\mu \approx 500 \text{ GeV}$ .

The following plots show simulated muon bundles in [IceCube](#). The stochastic energy losses are particularly clear in the right figure.





### 3.3.3 Muon Range

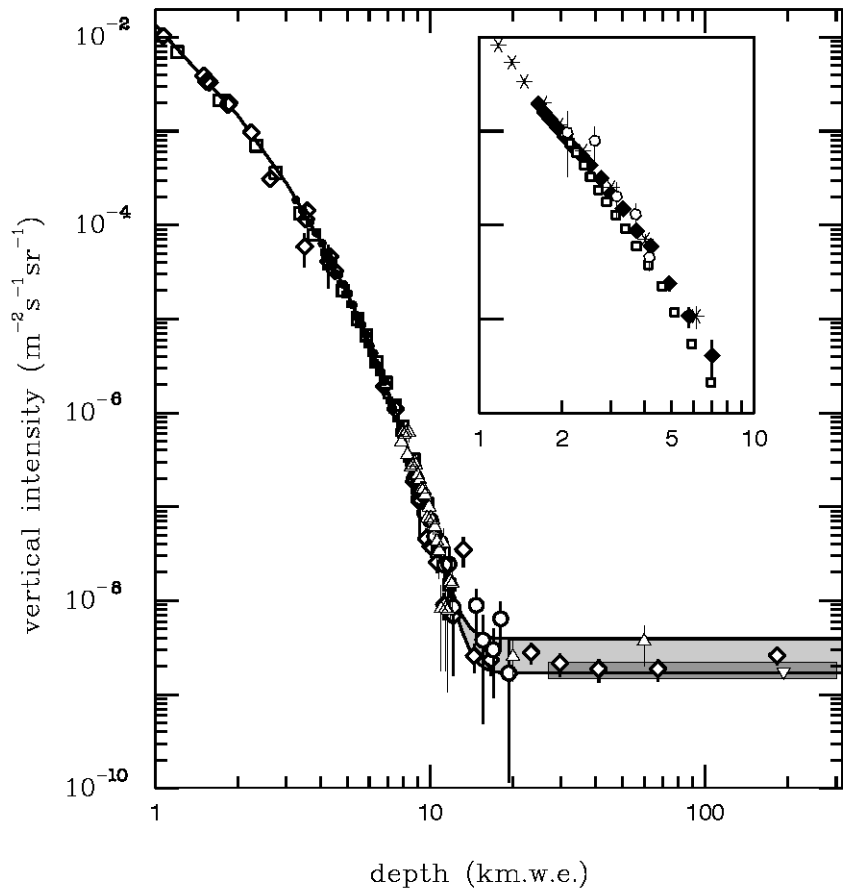
By solving the energy loss equation we can estimate the range  $R$  for a muon  $E_\mu$ , ie the underground depth this muon will reach until its energy is 0 (in reality the muon when reaching low energies will decay):

$$R(E_\mu) = \frac{1}{\beta} \log \left( 1 + \frac{E_\mu}{\epsilon_\mu} \right)$$

Assuming the muon spectrum at sea level can be approximated to a power law  $I_\mu(> E_\mu) = AE_\mu^{-\gamma}$  and using the relationship between range and energy we can write the *depth-intensity relation* (DIR):

$$I_\mu(> E_\mu, R) = A \left[ \frac{\alpha}{\beta} (e^{\beta R} - 1) \right]^{-\gamma}$$

The plot below shows the depth-intensity muons for vertical directions. The grey-area are neutrino-induced muons (horizontal, up-wards)

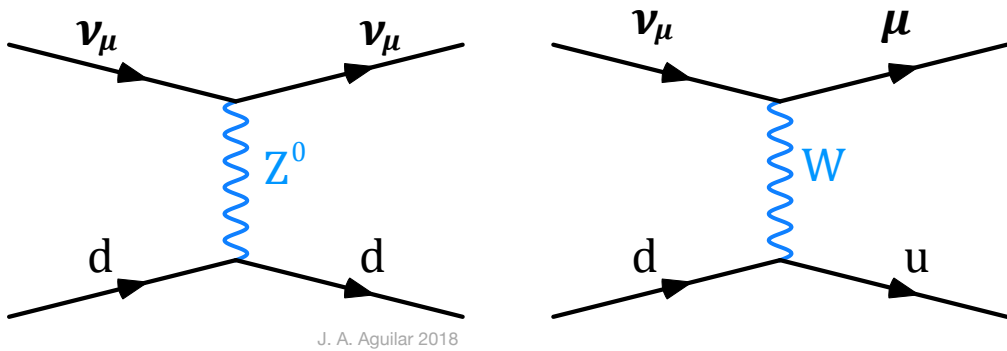


### 3.3.4 Neutrino Interactions

#### 3.3.4.1 Weak interaction

Neutrinos feel only the weak force thus interactions with matter mediated by  $W$  and  $Z$  bosons with cross-sections typical of weak processes. Feynman diagrams factor along two lines:

- Neutral current (NC) interactions - exchange of  $Z$
- Charged current (CC) interaction - exchange of  $W^\pm$



Neutrinos will scatter from electrons as well as nuclear matter.

- For energies  $E_\nu < 1\text{GeV}$  neutrinos interact with hadrons via **elastic or quasielastic scattering**.
- For energies  $E_\nu \gg 1\text{GeV}$  neutrinos do not scatter on hadrons as a compound of quarks, they start to *see* and interact directly with the quarks, this is the so-called **Deep Inelastic Scattering**.

### 3.3.5 Neutrino cross-sections at GeV energies

The anti-neutrino cross-section at GeV energies is a factor  $\sim 2$  lower (naively should be 3, but the factor 2 comes from the structure function of the nucleus) than the neutrino cross-section due to the helicity.

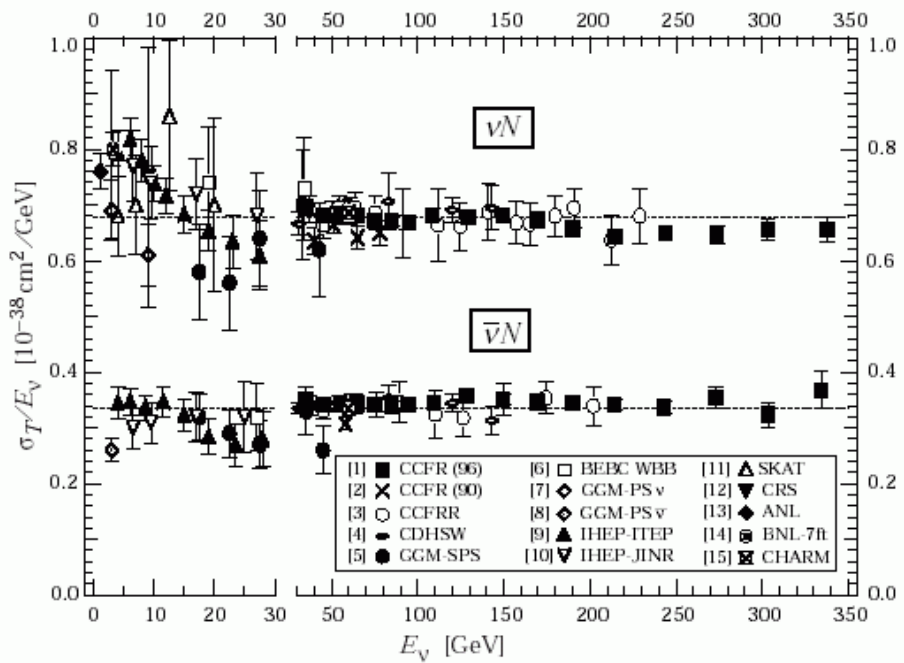


**Figure 30.10:**  $\sigma_T/E_\nu$ , for the muon neutrino and anti-neutrino charged-current total cross section as a function of neutrino energy. The error bars include both statistical and systematic errors. The straight lines are the averaged values over all energies as measured by the experiments in Refs. [1–4]:  $= 0.677 \pm 0.014$  ( $0.334 \pm 0.008$ )  $\times 10^{-38}$  cm $^2$ /GeV. Note the change in the energy scale at 30 GeV. (Courtesy W. Seligman and M.H. Shaevitz, Columbia University, 2001.)

At  $E_\nu \gg 1\text{GeV}$  the total DIS cross-section (ie, assuming CC and NC together) can be approximated to:

$$\begin{aligned}\sigma_{\nu p} &\simeq 0.69 \times 10^{-38} \left( \frac{E_\nu}{1\text{ GeV}} \right) \text{ cm}^2 \\ \sigma_{\bar{\nu} p} &\simeq 0.35 \times 10^{-38} \left( \frac{E_\nu}{1\text{ GeV}} \right) \text{ cm}^2\end{aligned}$$

Sometimes the cross-section is expressed as  $\nu + N$  where  $N$  is the nucleon definition as:

$$N = \frac{n+p}{2}$$

**i** Earth is transparent to GeV neutrinos

We are going to calculate the mean free path of neutrinos of energies of  $\sim \text{GeV}$ . Note that mean free path can be expressed as:

$$l = \frac{1}{n_N \sigma_{\nu N}}$$

where  $n_N$  is the number density of *nucleons* and not atoms. As we saw in lecture 2 we can re-express the number density as:

$$n_N = \frac{N_A}{\mathcal{M}} \rho$$

where  $\mathcal{M}$  is the molar mass of one mole of nucleons and  $\rho$  is the mass density of the medium. However, by definition a mol of nucleons has a mass of 1 g (Remember that a mol of  $^{12}C$  atoms has a mass of 12 g). So, we can rewrite as  $n_N = N_A \rho$ . Below there is another way to estimate the mean free path:

```
from astropy import constants as ct
from astropy import units as u
#Earth mass
print (ct.M_earth)

#Neutron/proton mass
print (ct.m_n)

#Earth radius
print (ct.R_earth)

#number of nucleons
N = ct.M_earth/ct.m_n

#Earth volume
Ve = 4/3*np.pi*ct.R_earth**3

#Nucleon density
Nd = N/Ve

#Cross section
s = 1e-38 * u.cm**2
#Mean free path:
L = 1/(s * Nd.to(1/u.cm**3))

print (f"The mean free path is: {L.to(u.km):.2f}")

Name      = Earth mass
Value    = 5.972167867791379e+24
Uncertainty = 1.3422009501651213e+20
Unit     = kg
Reference = IAU 2015 Resolution B 3 + CODATA 2018
```

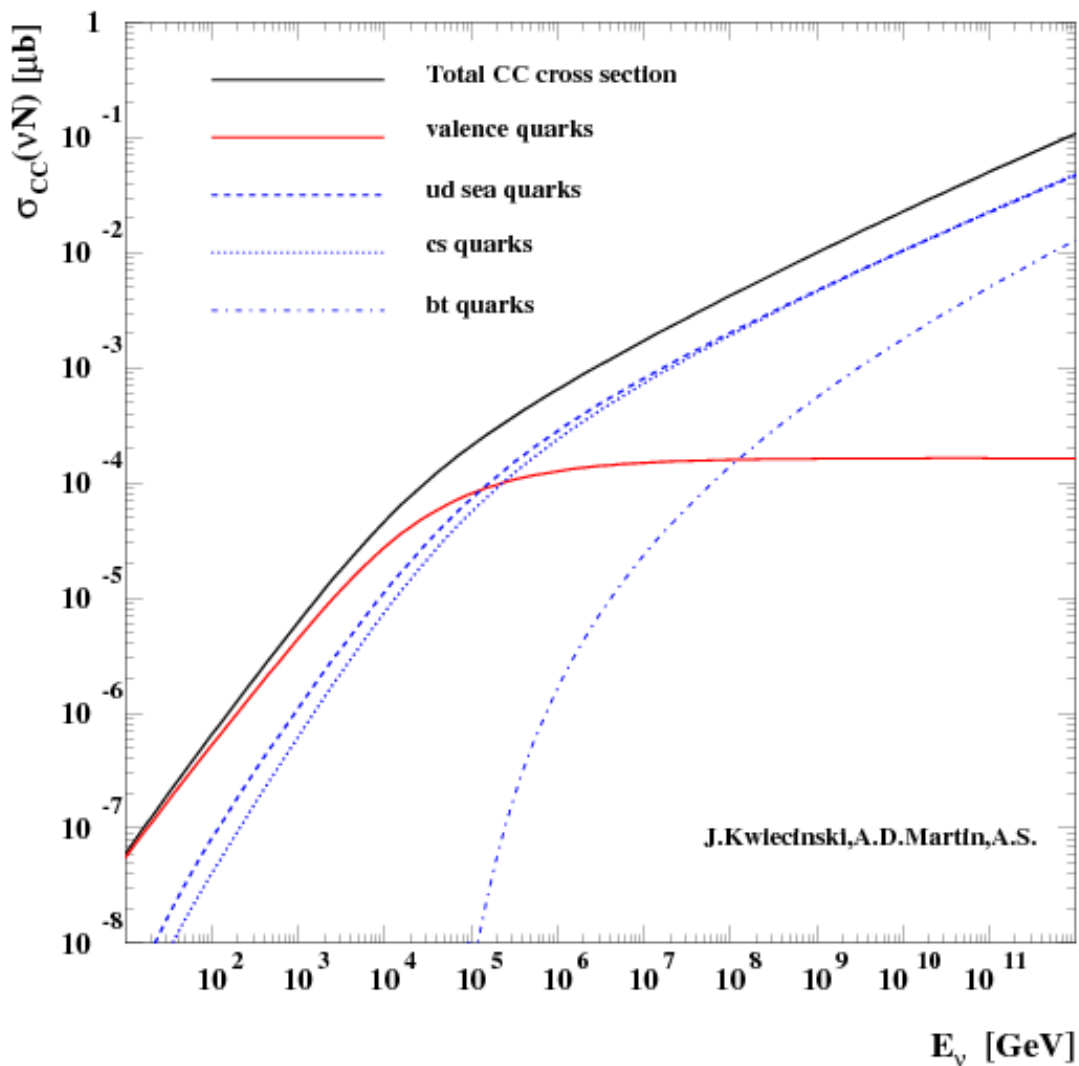
```

Name      = Neutron mass
Value     = 1.67492749804e-27
Uncertainty = 9.5e-37
Unit      = kg
Reference = CODATA 2018
Name      = Nominal Earth equatorial radius
Value     = 6378100.0
Uncertainty = 0.0
Unit      = m
Reference = IAU 2015 Resolution B 3
The mean free path is: 304808158.92 km

```

### 3.3.6 Neutrino cross-sections at TeV energies

- At low energies the valence quark parton distribution dominates and both the neutrino NC and CC cross-section grows linear with energy since the transfer momemtum is  $q^2 \ll M_{W,Z}$  and so the propagator term is  $\sim 1/M_{W,Z}^2$
- Above  $10^4$  GeV where the gauge-boson propagator restricts the momentum transfer to values near  $M_{W,Z}$  ( $\sim 1/(q^2 - M_{W,Z}^2)$ ) and damps the cross-section increase.



### 3.3.7 High energy Cross-Sections

The following shows the neutrino cross section:

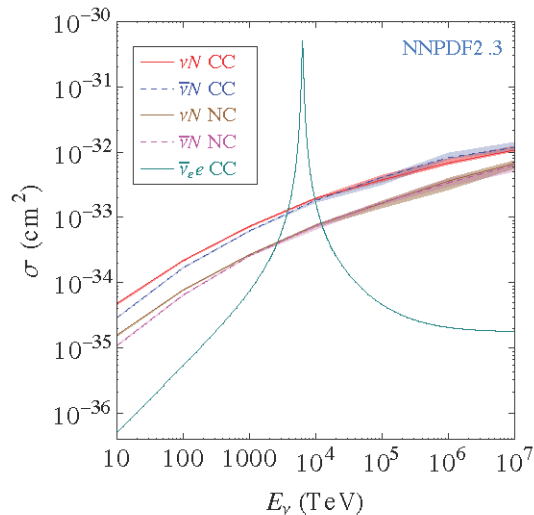


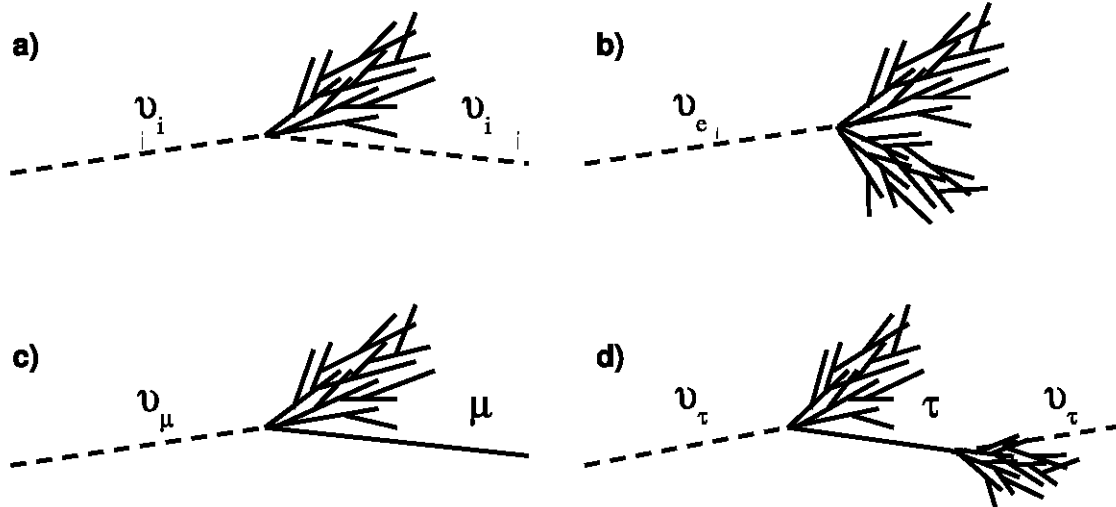
Figure 3.5: Calculated neutrino cross sections taken from [arXiv:1309.1764](https://arxiv.org/abs/1309.1764)

- At high energies the asymmetry between neutrinos and antineutrinos is lost due to the interaction with *sea quarks* ( $q\bar{q}$ )
- Neutrinos interact mostly with hadrons (quarks) instead of electrons due to their larger target mass. However at  $E_\nu \approx 6.3$  PeV the Glashow resonance appears:  $\hbar\nu_e + e \rightarrow W$  making the cross-section higher than the one with hadrons.

**i** Earth is opaque to PeV neutrinos

- At about 100 TeV the mean free path for neutrino-nucleus scattering is about  $10^{10}$  c.m.w.e. which is about the matter thickness along the Earth diameter.
- This means that UHE neutrino observatories (like IceCube) the flux of neutrinos coming from the nadir is strongly suppressed.
- There is only one exception. A very high energy beam of  $\nu_\tau$  at one side of the Earth  $E \gg 1$  PeV can end up at the other side as lower energy  $\nu_\tau, \nu_e, \nu_\mu$  through the **tau regeneration** effect:  $\nu_\tau \rightarrow \tau \rightarrow \nu_\tau$

### 3.3.8 Neutrino signatures in a neutrino detector



- b) In CC  $\nu_e$  interactions an hadronic and EM shower initiated by the  $e$  is produced. About 20% of the energy goes in the hadronic shower and 80% to the lepton and therefore to the EM shower.
- d) In CC  $\nu_\tau$  d) interaction again an hadronic and EM shower are produced as the  $\tau$  decays almost immediately to pions or other charge leptons. In the decay another  $\nu_\tau$  is produced **tau regeneration effect**. At very high energies the two showers can be separated giving a *double bang* signature or a *lollipop* if the first shower happens outside the detector.
- c) In CC  $\nu_\mu$  the muon only undergoes radiation losses (not ionization) and hence the track of the muon can be reconstructed.
- a) In NC only an hadronic shower is visible.

### 3.3.9 Event rate in an underground experiment.

An estimate of the detection rate of neutrino events is equivalent to calculate the rate of a neutrino-induced muon/cascades flux:

$$R(E_{vis}, \theta) = \int_{E_{vis}} P_{\nu \rightarrow l}(E_\nu, E_{vis}) P_{shadow}(\theta, E_\nu) \frac{dN_\nu}{dE_\nu} dE_\nu$$

where:

- $P_{\nu \rightarrow l}(E_\nu, E_{vis})$  is the probability that a neutrino interacts with an nucleus to produce a  $\mu$  or an EM or hadronic cascade with a minimum energy  $E_{vis}$  visible in the detector.
- $P_{shadow}(\theta, E_\nu)$ . Probability of neutrino with zenith angle  $\theta$  and energy  $E_\nu$  of being absorbed by Earth.
- $dN_\nu/dE_\nu$ . Neutrino flux at the surface.

**Interaction probability:**  $P_{\nu \rightarrow l}$

The probability of a neutrino to produce a lepton or shower visible in the detector can be written as:

$$P_{\nu \rightarrow l} = N_A \int_{E_{min}}^{E_\nu} dE_l \frac{d\sigma}{dE_l} r_l(E_l, E_{vis})$$

where  $r_l$  is the detection range of the produced lepton/cascade with energy  $E_l$  ending with the minimal energy  $E_{vis}$ , and  $d\sigma/dE_l$  is the neutrino cross-section to produce a lepton/cascade with energy  $E_l$ .

At high energy the event rate is dominated by neutrino-induced muons due to the long range of the high energy muons.

**Earth Shadow:**  $P_{shadow}$

The mean free path of neutrinos can be expressed as  $\lambda = (N_A \sigma_{tot})^{-1}$ . The shadow fact then can be expressed as:

$$P_{shadow} = e^{-N_A \sigma_{tot} X(\theta)}$$

Where  $X(\theta)$  is the column depth travelled by the neutrino through the Earth with a zenith angle  $\theta$ .

See **Exercises 2** for an evaluation of the event rate in an underground detector.

### 3.3.10 Neutrino Oscillations

Neutrinos are generated in flavor eigenstate however propagation is done in mass eigenstate, since each planar wave has a different frequency given their different masses, the neutrino detected (also in flavor eigenstate) will have a different interference pattern than the one generated given rise to neutrino flavor oscillations.

- As a result of these changes in relative phases, neutrinos oscillate from one flavor to another as they travel. Low-energy neutrinos oscillate in a shorter distance than high-energy neutrinos.
- A curious aspect of quantum physics is that only the **probability of the flavor of neutrino changes as it travels**.
- The neutrino *only becomes a definite flavor when it interacts* in a detector - by finding whether an electron, muon, tau is created.

### 3.3.11 The PMNS Matrix

The Pontecorvo-Maki-Nakagawa-Sakata matrix is the one that relates the mass eigenstates with the flavor eigenstates:

$$\begin{pmatrix} \nu_e \\ \nu_\mu \\ \nu_\tau \end{pmatrix} = U_{PMNS} \begin{pmatrix} \nu_1 \\ \nu_2 \\ \nu_3 \end{pmatrix}$$

with:

$$\begin{aligned} U_{PMNS} &= \begin{pmatrix} c_{12}c_{13} & s_{12}c_{13} & s_{13}e^{-i\delta} \\ -s_{12}c_{23} - c_{12}s_{23}s_{13}e^{i\delta} & c_{12}c_{23} - s_{12}s_{23}s_{13}e^{i\delta} & s_{23}c_{13} \\ s_{12}s_{23} - c_{12}c_{23}s_{13}e^{i\delta} & -c_{12}s_{23} - s_{12}c_{23}s_{13}e^{i\delta} & c_{23}c_{13} \end{pmatrix} \\ &= \begin{pmatrix} 1 & 0 & 0 \\ 0 & c_{23} & s_{23} \\ 0 & -s_{23} & c_{23} \end{pmatrix} \begin{pmatrix} c_{13} & 0 & s_{13}e^{-i\delta} \\ 0 & 1 & 0 \\ -s_{13}e^{i\delta} & 0 & c_{13} \end{pmatrix} \begin{pmatrix} c_{12} & s_{12} & 0 \\ -s_{12} & c_{12} & 0 \\ 0 & 0 & 1 \end{pmatrix} \end{aligned}$$

where  $s_{ij} = \sin \theta_{ij}$ ,  $c_{ij} = \cos \theta_{ij}$ . The term  $\delta$  is a CP violation term, if  $s_{13} = 0$  we won't be able to measure  $\delta$  as it always multiplies  $s_{13}$

### 3.3.12 The 2-flavor mixing case

Let's assume 2 flavor eigenstates identified as rotations of 2 mass eigenstates:

$$\begin{pmatrix} \nu_e \\ \nu_\mu \end{pmatrix} = \begin{pmatrix} \cos \theta & \sin \theta \\ -\sin \theta & \cos \theta \end{pmatrix} \begin{pmatrix} \nu_1 \\ \nu_2 \end{pmatrix}.$$

The angle  $\theta$  is called the mixing angle.

The mass eigenstates evolve as plane waves with fixed momentum  $p$ :

$$|\nu_i(t, x)\rangle = e^{-i(E_i t - p_i x)} |\nu_i(0, 0)\rangle$$

Let's imagine we start at  $(x, t) = (0, 0)$  with a pure beam of  $\nu_e$ :

$$\begin{pmatrix} 1 \\ 0 \end{pmatrix} = \begin{pmatrix} \cos \theta & \sin \theta \\ -\sin \theta & \cos \theta \end{pmatrix} \begin{pmatrix} \nu_1(0, 0) \\ \nu_2(0, 0) \end{pmatrix}.$$

$$|\nu_1(0, 0)\rangle = \cos \theta$$

$$|\nu_2(0, 0)\rangle = \sin \theta$$

and as they evolved:

$$|\nu_1(t, x)\rangle = \cos \theta e^{-i(E_1 t - p_1 x)}$$

$$|\nu_2(t, x)\rangle = \sin \theta e^{-i(E_2 t - p_2 x)}$$

So after a while the wave form of the  $\nu_\alpha$  is given by:

$$|\nu_e(t, x)\rangle = \cos^2 \theta e^{-i(E_1 t - p_1 x)} + \sin^2 \theta e^{-i(E_2 t - p_2 x)} = A_e$$

$$|\nu_\mu(t, x)\rangle = -\sin \theta \cos \theta e^{-i(E_1 t - p_1 x)} + \cos \theta \sin \theta e^{-i(E_2 t - p_2 x)} = A_\mu$$

### 3.3.12.1 Example of survival probability for the 2-flavor mixing

$$\begin{aligned} P(\nu_e \rightarrow \nu_\mu) &= |\langle \nu_\mu(t, x) | \nu_e(0, 0) \rangle|^2 = |\cos \theta \sin \theta (e^{i(E_2 t - p_2 x)} - e^{i(E_1 t - p_1 x)})|^2 \\ &= \cos^2 \theta \sin^2 \theta |e^{i(E_2 t - p_2 x)} - e^{i(E_1 t - p_1 x)}|^2 \end{aligned}$$

using  $e^{\pm ix} = \cos x \pm i \sin x$

$$\begin{aligned} P(\nu_e \rightarrow \nu_\mu) &= 2 \cos^2 \theta \sin^2 \theta (1 - \cos(E_2 t - p_2 x - E_1 t - p_1 x)) \\ &= \sin^2 2\theta \sin^2 \left( \frac{(E_2 - E_1)t - (p_2 - p_1)x}{2} \right) \\ &= \sin^2 2\theta \sin^2 \left( \frac{\Delta m_{12}^2 L}{4E} \right) \end{aligned}$$

using  $p_i = \sqrt{E_i^2 - m_i^2} \sim E_i(1 - \frac{m_i^2}{E_i^2})$ , and in natural units  $t = x = L$  we can write the phase difference as:

$$(E_2 - E_1)t - (p_2 - p_1)x = \left(\frac{m_1^2}{2E_1} - \frac{m_2^2}{2E_2}\right)L = \frac{\Delta m_{12}^2 L}{2E}$$

And the survival probability is:

$$P(\nu_e \rightarrow \nu_e) = 1 - P(\nu_e \rightarrow \nu_\mu) = 1 - \sin^2 2\theta \sin^2 \left( \frac{\Delta m_{12}^2 L}{4E} \right)$$

Replacing  $\hbar$  and  $c$  the expression can be written as:

$$P(\nu_e \rightarrow \nu_e) = 1 - \sin^2 2\theta \sin^2 \left[ 1.27 \left( \frac{\Delta m_{12}^2}{\text{eV}^2} \right) \frac{L/\text{km}}{E/\text{GeV}} \right]$$

We assumed that the mass eigenstates are created with the same energy or momentum and so  $E_i = E_j$ . This assumption is not necessary and it comes from the fact we use the plane wave approximation. Using the correct formalism of wave packets the result is the same.

### Tutorial III: Plot the survival probability of $\nu_e \rightarrow \nu_e$

```
import astropy.units as u

L = 180 # km

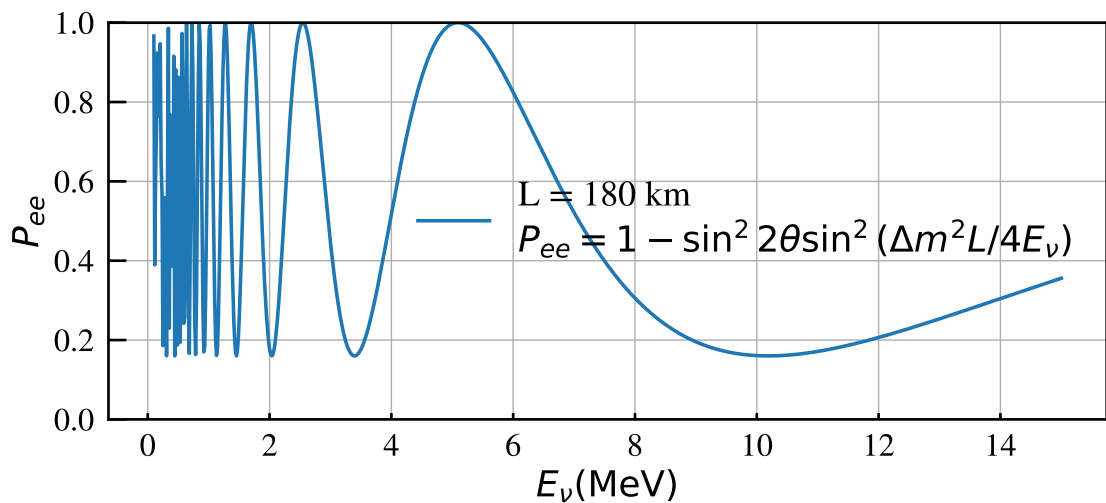
delta_m_sun = 7.0e-5 # eV^2
sin_square_theta_12 = 0.84 #maximum mixing

def prob_survival(E, L):
    return 1 - sin_square_theta_12 * np.sin(1.27*delta_m_sun * L / E)**2

fig, ax = plt.subplots(figsize=(10,4))
ax.set_ylimits(0,1)
ax.set_xlabel(r"$E_\nu (\text{MeV})$")
ax.set_ylabel("$P_{ee}$")

E = np.linspace(0.1, 15, 1000) #in MeV

ax.plot(E, prob_survival(E*1e-3,L), lw=2,
        label="L = %i km\n%L+r\"$P_{ee}" = 1 -\sin^2 2\theta\sin^2(\Delta m^2 L/4E_\nu)$")
plt.legend(loc="best")
ax.grid()
plt.show()
```



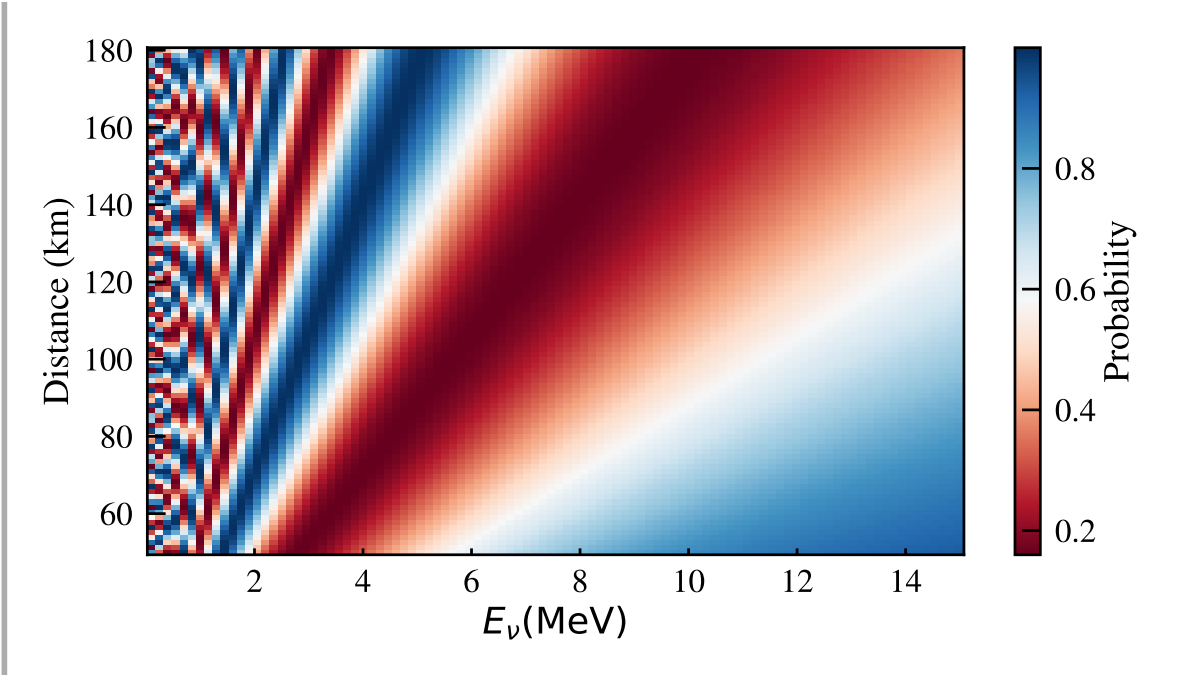
Eventually at low enough E / long baselines, neutrino beam becomes fully mixed and energy resolution and source extent conspire to produce 50/50 beam.

```

y, x = np.meshgrid(np.linspace(50,180,100), np.linspace(0.1, 15, 100) )
z = prob_survival(x*1e-3,y)
fig = plt.figure(figsize=(10,5))
ax = plt.subplot(111)
img = ax.pcolormesh(x, y, z, cmap = 'RdBu', shading='auto')

cax = fig.colorbar(img)
ax.set_ylabel("Distance (km)")
ax.set_xlabel(r"$E_{\nu}$ (MeV)")
cax.set_label("Probability")

```



### 3.3.13 General case

Taking greek letters of the flavor eingenstates and latin letter the mass eingenstates we can write:

$$|\nu_\alpha(x, t)\rangle = \sum_{k=1,2,3} U_{\alpha k} |\nu_k(x, t)\rangle = \sum_{k=1,2,3} U_{\alpha k} e^{-i\Phi_k} |\nu_k(0, 0)\rangle$$

inverting the mixing matrix we have:

$$|\nu_k(0, 0)\rangle = \sum_{\gamma} U_{\gamma k}^* |\nu_{\gamma}(0, 0)\rangle$$

putting it in the equation above:

$$|\nu_\alpha(x, t)\rangle = \sum_{k=1,2,3} U_{\alpha k} e^{-i\Phi_k} \sum_{\gamma} U_{\gamma k}^* |\nu_{\gamma}(0, 0)\rangle$$

If we want to evaluate the probability of finding a neutrino  $\beta$  when we had  $\alpha$  is the transition amplitude is given by:

$$\begin{aligned}
\mathcal{A}(\nu_\alpha(0,0) \rightarrow \nu_\beta(x,t)) &= \langle \nu_\beta(x,t) | \nu_\alpha(0,0) \rangle \\
&= \sum_\gamma \sum_k U_{\gamma k} e^{i\Phi_k} U_{\beta k}^* \langle \nu_\gamma(0,0) | \nu_\alpha(0,0) \rangle \\
&= \sum_k U_{\alpha k} e^{i\Phi_k} U_{\beta k}^*
\end{aligned}$$

where we used the fact that flavor eigenstates are orthogonal and hence  $\langle \nu_\gamma(0,0) | \nu_\alpha(0,0) \rangle = \delta_{\gamma,\alpha}$ .

The oscillation probability is then:

$$\begin{aligned}
P(\nu_\alpha \rightarrow \nu_\beta) &= |\mathcal{A}(\nu_\alpha(0,0) \rightarrow \nu_\beta(x,t))|^2 = \left| \sum_k U_{\alpha i} e^{i\Phi_i} U_{\beta i}^* \right|^2 \\
&= \sum_i U_{\alpha i} e^{i\Phi_i} U_{\beta i}^* \sum_j U_{\alpha j}^* e^{-i\Phi_j} U_{\beta j} \\
&= \sum_j \sum_i U_{\alpha i} U_{\beta i}^* U_{\alpha j}^* U_{\beta j} e^{-i(\Phi_j - \Phi_i)}
\end{aligned}$$

where  $\Phi_i = E_i t - p_i x$  and so:

$$\Phi_i - \Phi_j = (E_i - E_j)t - (p_i - p_j)x$$

using  $p_i = \sqrt{E_i^2 - m_i^2} \sim E_i(1 - \frac{m_i^2}{E_i^2})$  we can write the phase difference as:

$$\Phi_i - \Phi_j = (\frac{m_i^2}{2E_i} - \frac{m_j^2}{2E_j})L = \frac{\Delta m_{ij}^2 L}{2E}$$

where we used the fact that at relativistic speeds  $t = x = L$  and a dodgy approximation where we assumed that the mass eigenstates are created with the same energy or momentum and so  $E_i = E_j$ . This assumption is not necessary, but we find that whatever assumption is made you get the same result. The fact that we have to make such an approximation comes from the way that we are modelling the mass eigenstates as plane waves. If we were to do the analysis assuming that the mass states were wavepackets instead we would not need the equal momentum (equal energy) assumption and would still get the same answer.

With this we can rewrite the oscillation probability as:

$$\begin{aligned}
P(\nu_\alpha \rightarrow \nu_\beta) &= \delta_{\alpha\beta} - 4 \sum_{i>j} \text{Re}(U_{\alpha i}^* U_{\beta i} U_{\alpha j} U_{\beta j}^*) \sin^2(\frac{\Delta m_{ij}^2 L}{4E}) \\
&\quad + 2 \sum_{i>j} \text{Im}(U_{\alpha i}^* U_{\beta i} U_{\alpha j} U_{\beta j}^*) \sin(\frac{\Delta m_{ij}^2 L}{2E}),
\end{aligned}$$

For  $\delta = 0$  the last term is 0.

### 3.3.14 About symmetries.

- Consequences of CPT invariance:

$$P(\nu_\alpha \rightarrow \nu_\beta) = P(\bar{\nu}_\beta \rightarrow \bar{\nu}_\alpha)$$

- Conditions of CP invariance:

$$P(\nu_\alpha \rightarrow \nu_\beta) = P(\bar{\nu}_\alpha \rightarrow \bar{\nu}_\beta)$$

- Condition os T invariance:

$$P(\nu_\alpha \rightarrow \nu_\beta) = P(\nu_\beta \rightarrow \nu_\alpha) \text{ and } P(\bar{\nu}_\alpha \rightarrow \bar{\nu}_\beta) = P(\bar{\nu}_\beta \rightarrow \bar{\nu}_\alpha)$$

Only if  $U$  is not real we can have CP violation effects ie:

$$P(\nu_\alpha \rightarrow \nu_\beta) - P(\bar{\nu}_\alpha \rightarrow \bar{\nu}_\beta) = 4 \sum_{i>j} \text{Im}(U_{\alpha i}^* U_{\beta i} U_{\alpha j} U_{\beta j}^*) \sin\left(\frac{\Delta m_{ij}^2 L}{2E}\right)$$

### 3.3.15 Mass hierarchy

But this means that neutrinos oscillations can be described in terms of 6 parameters:  $\theta_{12}$ ,  $\theta_{13}$  and  $\theta_{23}$  plus 2 mass-squared differences,  $\Delta m_{12}^2$  and  $\Delta m_{32}^2$  and one CP violating phase  $\delta_{CP}$ . Although we can measured the mass-squared differences in neutrino oscillation experiments, we cannot know the absolute scales nor the mass hierarchy.

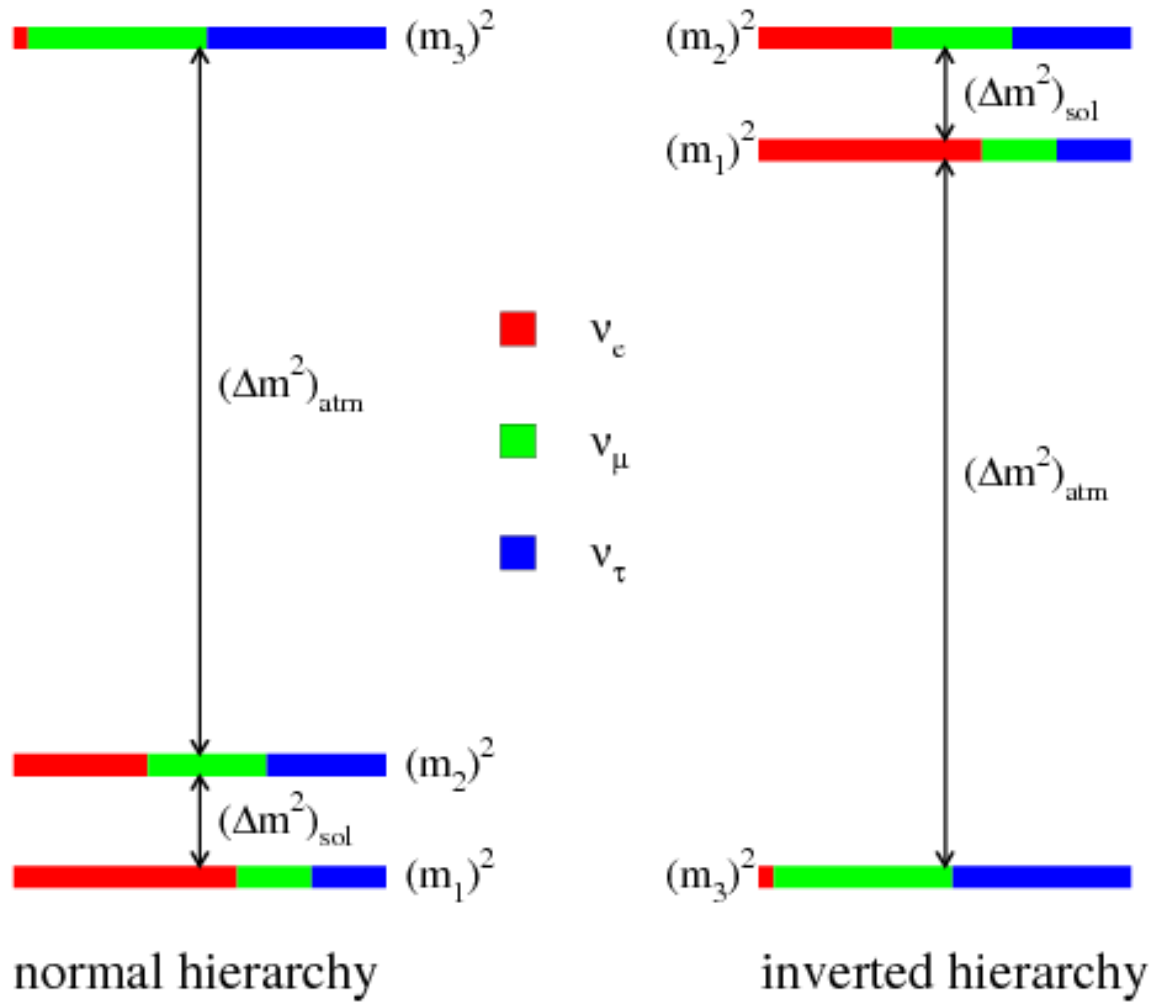


Figure 3.6: Source: [arXiv:1205.2671](https://arxiv.org/abs/1205.2671)

Where  $\Delta m_{12}^2 = \Delta m_{Sol}^2$  and  $\Delta m_{31(2)}^2 = \Delta m_{atm}^2$ . Sometimes  $\Delta m_{atm}^2$  is defined as:

$$\Delta m_{atm}^2 = \left| m_3^2 - \frac{(m_1^2 + m_2^2)}{2} \right|$$

#### Measurements Status Assuming  $\Delta m_{21}^2 \ll \Delta m_{31}^2 \sim \Delta m_{32}^2$  and small  $\theta_{13}$  different detectors can prove different sectors of the oscillation parameters:

- **Atmospheric and Long Baseline Accelerators:**

$$\begin{pmatrix} 1 & 0 & 0 \\ 0 & c_{23} & s_{23} \\ 0 & -s_{23} & c_{23} \end{pmatrix}$$

If  $\Delta m_{21}^2 L/E \ll 1$  this experiments are sensitive to the oscillation  $P(\nu_\mu \rightarrow \nu_\tau) \simeq \sin^2 2\theta_{23} \sin^2 \frac{\Delta m_{31}^2}{3E} L$

- **Short Baseline Reactors:**

$$\begin{pmatrix} c_{13} & 0 & s_{13}e^{-i\delta} \\ 0 & 1 & 0 \\ -s_{13}e^{i\delta} & 0 & c_{13} \end{pmatrix}$$

If  $\Delta m_{21}^2 L/E \ll 1$  this experiments are sensitive to the oscillation

$$P(\nu_e \rightarrow \nu_e) \simeq 1 - \sin^2 2\theta_{13} \sin^2 \frac{\Delta m_{31}^2}{3E} L$$

- **Solar and Long Baseline:**

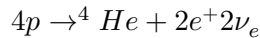
$$\begin{pmatrix} c_{12} & s_{12} & 0 \\ -s_{12} & c_{12} & 0 \\ 0 & 0 & 1 \end{pmatrix}$$

If  $\Delta m_{31}^2 L/E \gg 1$  this experiments are sensitive to the oscillation

$$P(\nu_e \rightarrow \nu_e) \simeq 1 - \sin^2 2\theta_{12} \sin^2 \frac{\Delta m_{12}^2}{3E} L$$

### 3.3.16 Solar Neutrinos

Neutrinos from the Sun are produced by some of the fusion reactions in the *pp* chain or the CNO cycle. The combined effect is:



From the beginning of the solar-neutrino observation a deficit of the electron neutrino predicted by the Standard Solar Model was observed: *the solar-neutrino problem*

In 1999 SNO in Canada started taking data. This experiment was able to detect  $\nu_e$  by CC interactions and  $\nu_x$  by NC interaction solving the mystery of the solar-neutrino problem. It is now understood as a neutrino flavor oscillation. The results of SNO together with KamLAND

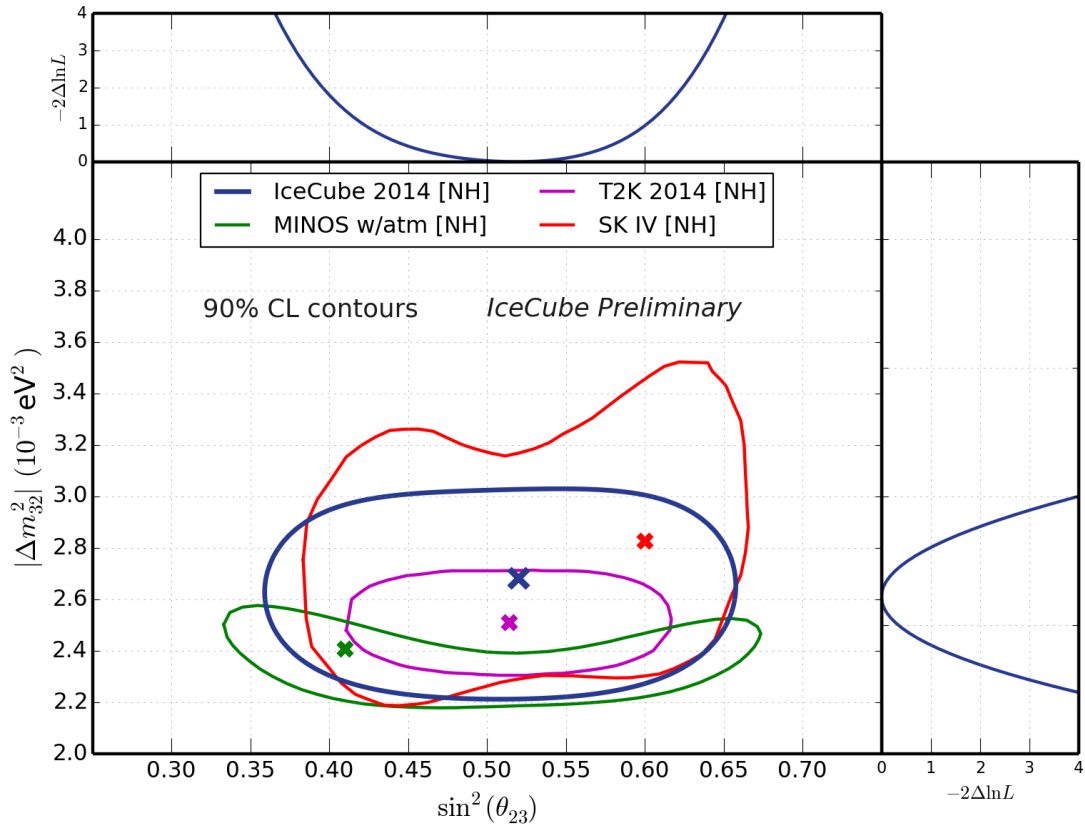
(a long baseline neutrino detector) confirmed the Large Mixing Angle solution (LMA) of the solar sector:

$$\sin^2 \theta_{12} \simeq 0.30$$

$$\Delta m_{12}^2 \equiv \Delta m_\odot^2 \simeq 8 \times 10^{-5} \text{ eV}^2$$

### 3.3.17 Atmospheric Neutrinos

First evidence of atmospheric neutrino oscillations came from Super-Kamiokande experiment in 1998. By scanning in zenith angle, is like changing the  $L$ .



If atmospheric mixing is non-maximal, it remains to determine in which “octant” the mixing angle  $\theta_{23}$  lies. For a  $\theta_{23}$  in the first octant ( $< 45^\circ$ ) the mass eigenstate  $\nu_3$  is **tau heavy**, i.e., the tau neutrino fraction is larger than the muon neutrino fraction. Conversely, for a  $\theta_{23}$  in the second octant ( $> 45^\circ$ ) the state  $\nu_3$  is **muon heavy**.

### 3.3.18 Reactor Neutrinos

- Double Chooz:  $\sin^2 2\theta_{13} = 0.109 \pm 0.030 \pm 0.025 \neq 0$  at  $2.9\sigma$
- Daya Bay:  $\sin^2 2\theta_{13} = 0.089 \pm 0.010 \pm 0.005 \neq 0$  at  $7.7\sigma$
- RENO:  $\sin^2 2\theta_{13} = 0.113 \pm 0.013 \pm 0.019 \neq 0$  at  $4.9\sigma$

### 3.3.19 Neutrino oscillations in matter.

The  $U_{PMNS}$  matrix must be modified to account for the fact that electron neutrinos have an extra interaction not present for  $\nu_\mu$  and  $\nu_\tau$  when travelling through matter. Elastic scattering of  $\nu_e$  on electron can occur via exchange of a charged  $W$ -boson as well as by exchange of the neutral  $Z$ -boson adding a term  $V_e = G_F \sqrt{2} N_e$  in the mass differences for electrons.

Without entering in the maths, what happens here is that a resonance effect occurs, ie, even if the mixing angle is small in vacuum it can get amplified in matter. This resonance can be expressed as a condition on the electron density  $N_e$  which is appropriate for systems such as stellar interiors (Sun or supernovae too) where provided the core density is high enough, there is always a region in the neutrinos' path exiting the star where it passes through resonance.

This is known as the **MSW effect** for the theorists who discovered it - Mikheyev, Smirnov, and Wolfenstein.

### 3.3.20 Tutorial III: Calculate the probabilities of $\nu_e \rightarrow \nu_x$ as function of L/E

```
def PMNS_Factory(t12, t13, t23, d):  
    s12 = np.sin(t12)  
    c12 = np.cos(t12)  
    s23 = np.sin(t23)  
    c23 = np.cos(t23)  
    s13 = np.sin(t13)  
    c13 = np.cos(t13)  
    cp = np.exp(1j*d)  
    return np.array([[c12*c13, s12*c13, s13*np.conj(cp)],  
                   [-s12*c23 - c12*s23*s13*cp, c12*c23 - s12*s23*s13*cp, s23*c13],  
                   [s12*s23 - c12*s23*s13*cp, -c12*s23 - s12*c23*s13*cp, c23*c13]])  
  
def posc(a, b, U, dm2, LEratio):  
    """  
    Gives the oscillation probability for nu(a) -> nu(b)  
    for PMNS matrix U, and L in km and E in GeV, and dm2 in eV^2  
    """  
    s = 0
```

```

for j in range(2):
    for i in range(j+1, 3):
        arg = 5.068*dm2[i+j-1]*LEratio
        mxe = np.conj(U[a, i])*U[b, i]*U[a, j]*np.conj(U[b, j])
        s += -4*mxe.real*np.sin(0.25*arg)**2 + 2*mxe.imag*np.sin(0.50*arg)
    if a == b: s += 1.0
return s

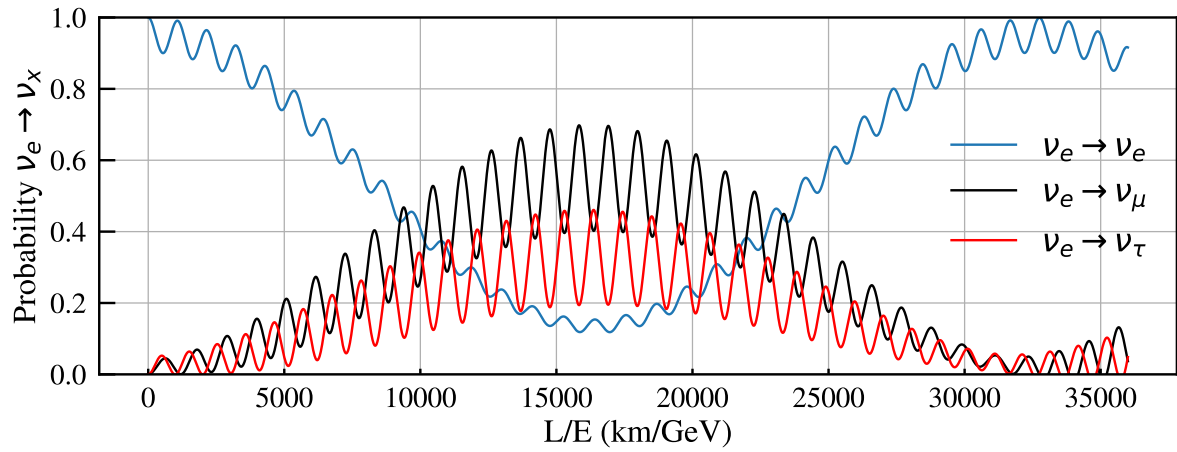
t12 = np.arcsin(0.312**0.5)
t13 = np.arcsin(0.0251**0.5) #Controlls the size of the small wiggles.
#t13 = np.arcsin(0.0)
t23 = np.arcsin(0.42**0.5)

dm2 = [ 7.58E-05, 2.27E-03, 2.35E-03]
delta = 0

U = PMNS_Factory(t12, t13, t23, delta)

LE = np.linspace(0, 36000, 3600)
Pe = posc(0, 0, U, dm2, LE)
Pm = posc(0, 1, U, dm2, LE)
Pt = posc(0, 2, U, dm2, LE)
fig, ax = plt.subplots(figsize=(12,4))
ax.plot(LE, Pe, '-', label=r'$\nu_e \rightarrow \nu_e$')
ax.plot(LE, Pm, 'k', label=r'$\nu_e \rightarrow \nu_\mu$')
ax.plot(LE, Pt, 'r', label=r'$\nu_e \rightarrow \nu_\tau$')
ax.set_xlabel("L/E (km/GeV)")
ax.set_ylabel(r"Probability $\nu_e \rightarrow \nu_x$")
ax.set_yscale(0,1)
ax.grid()
plt.legend(loc="best")
plt.show()

```



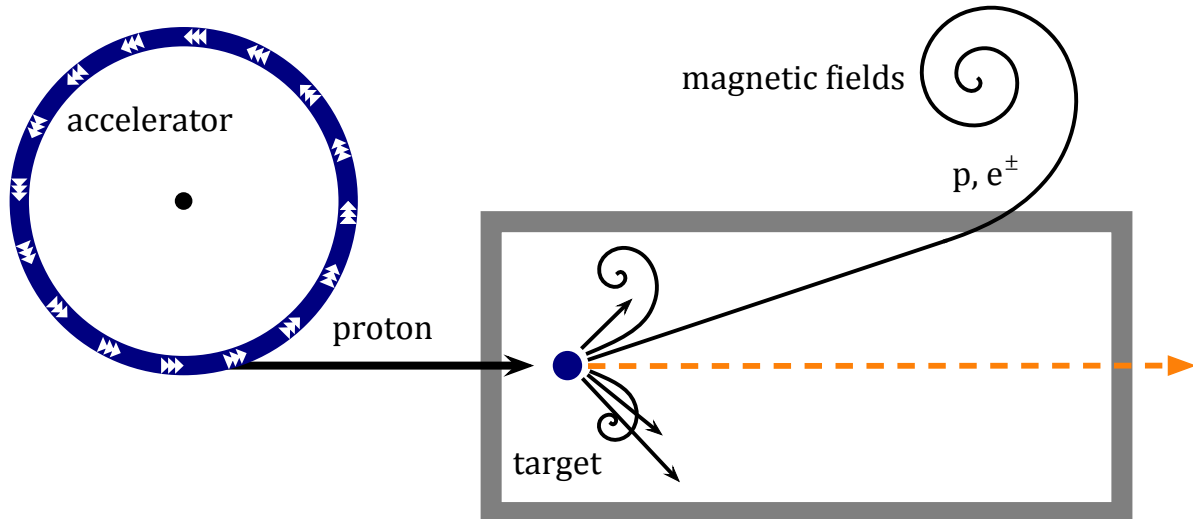
### 3.4 What else?

- Pressure and temperature effects in the muon and neutrino fluxes.
- Sterile neutrinos, are there more than 3 neutrinos? What does cosmology tell us, what do experiments tell us? (LSND and reactor anomalies)

# 4 Multimessenger Astronomy

## 4.1 The Beam Dump

Cosmic ray accelerated are typically surrounded by a radiation field and matter eventually interacting and producing secondary particles. The picture is similar to that of beam dumps in particle accelerators at Earth, where a beam of particles is aimed at a specific target. Among the secondary particles produced we have gamma-rays and neutrinos both of them will point to the accelerators.



A cosmic-ray source it is said to be opaque or **optically thick** if photons and protons cannot escape from the source without lossing all or most of their energy. Alternatively a transparent source it is said to be **optically thin**. A source that is very optically thick won't be visible in any messenger except neutrinos. We call those source *hidden sources*.

## 4.2 Gamma-ray Astronomy

As we saw, the origin of CR remains a mystery due to the deflection of CRs in their travel. Only CR astronomy at  $10^{19}$  eV will be possible if the composition of these UHECR are protons, but even in this case the GZK limits the horizon.

Gamma-ray astronomy provides an fundamental tool to observe the Universe using neutral deep penetrating gamma-ray particles. Originally the distinction between gamma-rays and X-rays was due to the nuclear production mechanism. X-rays are the product of transition of electrons in the atomic shell, while gamma-rays are produced in the atomic nucleus. This distinction also leads to a classification in energy. X-rays are typically below 100 keV. Photons with  $E > 100$  keV are called gamma-rays.

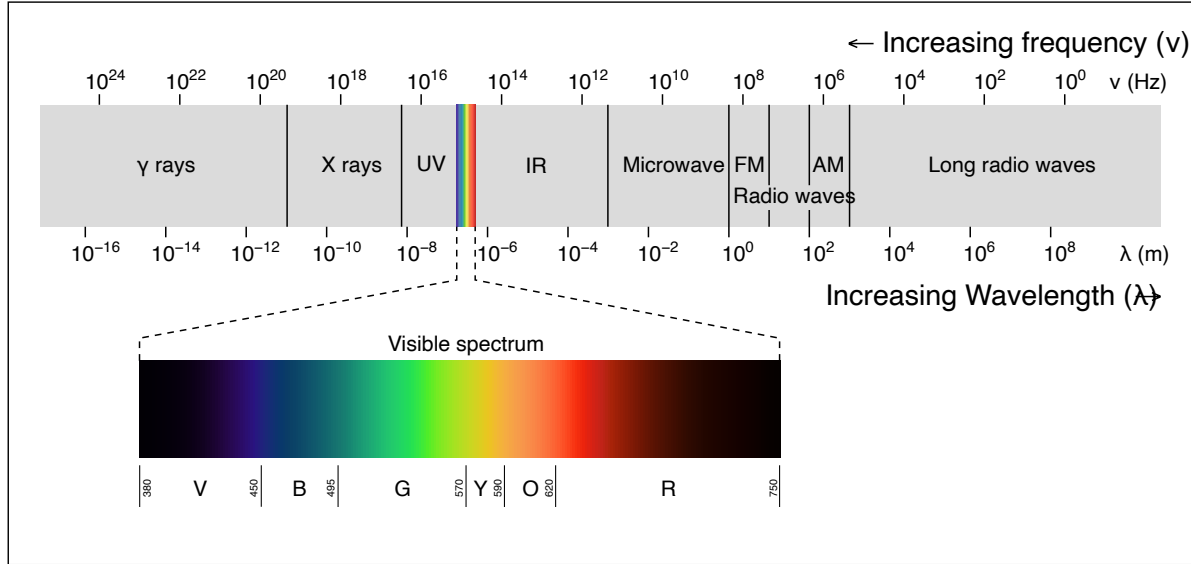


Figure 4.1: Source: Wikipedia

#### 4.2.1 Spectral Energy Distribution

In gamma-ray astronomy is usual to study an object emission by its spectral energy distribution (SED). The SED on an object is its energy emitted plotted against some measure of the photon - frequency or wavelength. The reason astronomers do this is to see how much energy is produced by the object as a function of frequency or wavelength. The SED is typically characterized by  $\nu F_\nu$ , and it is measured in units of  $\text{ergs cm}^{-2} \text{ s}^{-1}$ , ie. it indicates the rate of energy emitted per surface. The function  $F_\nu$  is the flux density which indicates the rate of energy emitted per surface and also per frequency, so it is expressed as  $\text{ergs cm}^{-2} \text{ s}^{-1} \text{ Hz}^{-1}$ . All of this doesn't need to be confused with the spectrum! which is what we are being using to characterize CRs. In CR physics spectrum in the rate of particles per unit energy and surface and it is measured on  $\text{GeV}^{-1} \text{ cm}^{-2} \text{ s}^{-1}$ . The spectrum multiply by energy, gives you the rate of particles per unit surface. Multiplying again by energy give use the energy rate per unit surface. Therefore we have the relation:

$$\nu F_\nu = E^2 \frac{dN}{dE}$$

## 4.2.2 Gamma-ray production mechanism

Sources of CR can also produce gamma-rays by different mechanisms roughly divided in two main categories:

### 4.2.2.1 Leptonic models:

In this models only leptons (mostly electrons) will produce gamma-ray emission. The mechanism mostly: \* **Synchrotron radiation.** \* **Inverse Compton Scattering.**

### 4.2.2.2 Hadronic model:

In hadronic models, gamma-rays are produced as a result of acceleration to high energies of protons or other hadrons. The mechanism of gamma-ray production in hadronic models are mainly: \*  $\pi^0$  decay. \* **Proton synchrotron radiation.**

Another categories for gamma-ray production can some exotic models like dark matter annihilation, or matter-antimatter annihilation and nuclear transformation.

## 4.2.3 Leptonic models

### 4.2.3.1 Synchrotron radiation

Synchrotron radiation is extremely important for astrophysics as it was realized by Shklovskii in 1957 when studing the non-thermal emission of the Crab remnant. In order to understand better the synchrotron radiation we will have to dig in a bit in electromagnetism. We already saw that a charge particle of charge  $q$ , for example an electron, moving with velocity  $v$  in a magnetic field  $\vec{B}$  feels an external force:

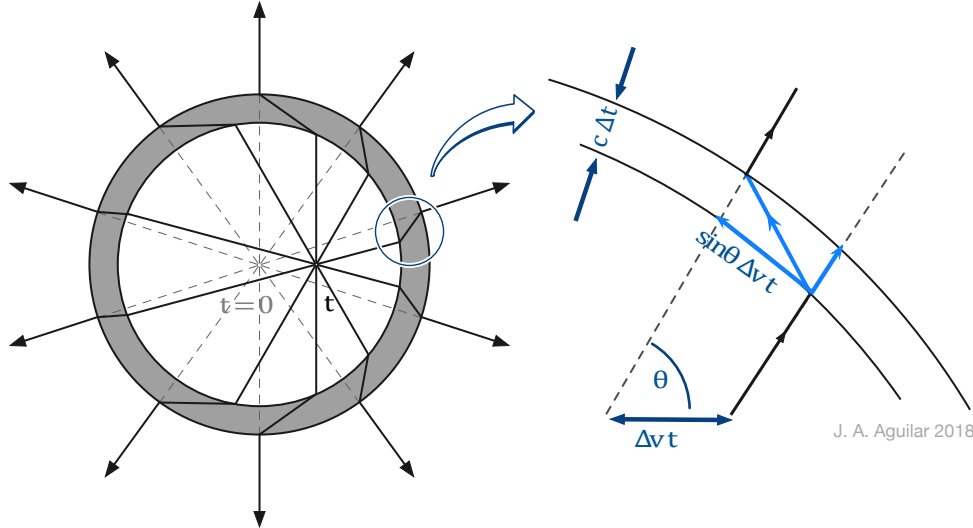
$$\vec{F} = \frac{q}{c}(\vec{v} \times \vec{B})$$

Now, because of the force on the particle is perpendicular to the motion, the magnetic field cannot do work on the particle, and so its speed does not change, i.e.  $|v| = \text{constant}$ , but there is an acceleration since the direction will change. On the other hand an accelerated electrical charge radiates electromagnetic waves! which... will slow down the particle...

The reason of this apparent inconsistency comes from the fact that we treat the electric field lines as the purely Coulombic action-at-a-distance. In reality we have to take into account that as a particle moves, the electric field lines need to *re-arrange* and this re-arrangement cannot happen at a speed faster than the speed of light.

Here are going to derive the radiation emission for a particle with an acceleration and we are going to do it by messing around with the Coulomb fields. For a more formal argument derived from Maxwell equations you can see the book of Longair.

Let's assume that the particle is at rest at the moment  $t = 0$ . The electric field lines clearly point away from the origin. At that moment the particle accelerates which brings the velocity of the particle to  $\Delta v$  in a time  $\Delta t$ , after that the particle continues with uniform velocity.



After a certain time, the particle will be in the position  $t\Delta v$ . In a sphere located far way (with a radius larger than  $ct$ ), the electric field lines are still those of the stationary particle, since they field lines cannot “know” yet that the particle has moved, so the point radially towards the origin at  $t = 0$ . Inside a sphere of radius  $c(t - \Delta t)$ , the electric field lines are already those from the electron that moves at a constant velocity.

The perturbation of the electric field lines needs to propagate radially, this *kink* is nothing more than a radiation! From simple geometry relations we can get that:

$$\frac{E_\theta}{E_r} = \frac{\Delta v t \sin \theta}{c \Delta t} = \frac{r \sin \theta}{c^2} \frac{\Delta v}{\Delta t}$$

where  $r = ct$ , and  $E_r$  is simply the Coulomb field  $E_r = q/4\pi\epsilon_0 r^2$  or in [gaussian units](#) since the kink is really small and the eletric field along the kink remains the same  $E_r = q/r^2$  and therefore the transverse component becomes:

$$E_\theta = \frac{qa \sin \theta}{c^2 r}$$

where we used the fact that  $\Delta v/\Delta t$  is just the acceleration  $a$ . An interesting fact appears here,  $E_\theta$  depends on  $r^{-1}$  and not  $r^{-2}$  so for larger  $r$ ,  $E_\theta$  is going to dominate over  $E_r$ . Accompanying

this transverse electric field there will be a magnetic field, which is a property of an electromagnetic wave. In other words, an electromagnetic pulse is generated by the accelerated charge particle. Since this is an electromagnetic radiation there is an energy flow per unit area, per second and the direction is given by the Poynting vector (with  $|E| = |B|$  as in electromagnetic wave):

$$\vec{S} = \frac{c}{4\pi}(\vec{E} \times \vec{B})$$

Which points in the radial direction. In this case can be reduced to:

$$|S| \equiv \frac{dE}{dt dA} = \frac{c}{4\pi} E_\theta^2 \vec{n}$$

Which is the energy flow per unit area per second. The unit area  $dA$  can be rewritten in terms of the solid angle as  $dA = r^2 d\Omega$ , and so the rate of energy loss through the area subtended by the solid angle  $d\Omega$  at distance  $r$  is given by:

$$\left( \frac{dE}{dt d\Omega} \right)_{rad} = \frac{q^2 a^2 \sin^2 \theta}{4\pi c^3}$$

Notice that this energy loss rate follows a *dipole* pattern  $dP/d\Omega \propto \sin^2 \theta$  and that  $\theta$  is defined along the acceleration line. If we now integrate over all solid angles we obtain that the emitted power is given by:

$$P \equiv - \left( \frac{dE}{dt} \right)_{rad} = \frac{2q^2 a^2}{3c^3}$$

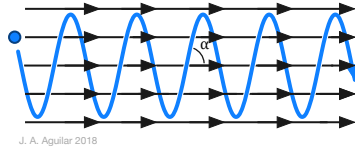
Which is call the *Larmor's formula*. Note that this is valid for any form of acceleration  $a$ .

In the relativistic case this formula can be rewritten as:

$$P = \frac{2q^2}{3c^3} \gamma^4 [\gamma^2 a_\parallel^2 + a_\perp^2]$$

#### 4.2.4 Single-electron in uniform magnetic field

In an uniform magnetic field, a high energy charged particle, for example an electron, moves in spiral path at a constant *pitch angle*,  $\alpha$ .



Its velocity along the field lines is constant  $v_{\parallel} = v \cos \alpha = \text{const.}$ , but its circular component  $v_{\perp} = v \sin \alpha$ . Let's first attack the non-relativistic case.

##### 4.2.4.1 Non relativistic case: Cyclotron radiation

From Newton's law and the Lorentz force we have that:

$$m_e a_{\perp} = m_e \frac{v_{\perp}^2}{r_{gyr}} = \frac{ev_{\perp}B}{c}$$

where  $r_{gyr}$  is the gyroradius which can be written as:

$$r_{gyr} = \frac{v_{\perp}}{\omega_{gyr}} = \frac{v \sin \alpha}{\omega_{gyr}}$$

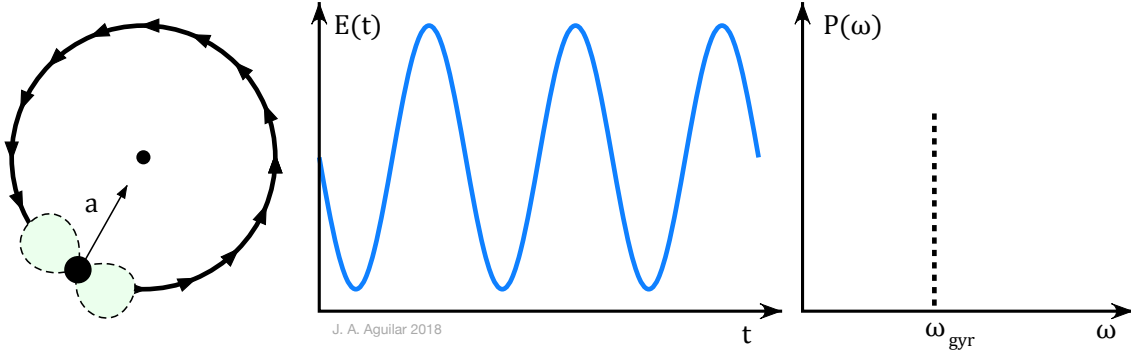
where we can define the gyrofrequency as:

$$\omega_{gyr} \equiv \frac{eB}{m_e c}$$

Therefore according to the Larmor's equation of power emitted we can write:

$$P = \frac{2e^2}{3c^3} \omega_{gyr}^2 v^2 \sin^2 \alpha$$

Note the Larmor formula does not tell us frequency spectrum, but if a particle is moving in a circular motion, then from an observer far way, the "aparent" motion will be sinusoidal as illustrated in the figure below.



In particular since the power  $P$  depends on  $|v^2|$  for a distance in the  $x - y$  plane, power will vary as  $\sin^2(\omega_{gyr}t)$  and so the electric field line will change as  $E(t) \propto \sin(\omega_{gyr}t)$ . The radiated emission will appear as *monochromatic* with an angular frequency given precisely by the particle circular frequency  $\omega_{gyr}$ . This is known as the *cyclotron* radiation. In this case the dipole emission pattern is turning around with the particle and an observer in the laboratory frame will see the same frequency. As a consequence also the radiation is independent of the viewing angle.

#### 4.2.4.2 Relativistic case: Synchrotron radiation.

Things are slightly different when we consider the relativistic case where electrons move at  $\beta \rightarrow 1$ . Using again Newton's law with the Lorentz force we have:

$$\gamma m_e \frac{dv_\perp}{dt} = \frac{ev_\perp B}{c}$$

where we can obtain the perpendicular acceleration as:

$$a_\perp = \frac{ev \sin \alpha}{\gamma m_e c}$$

where now the electron's relativistic angular gyroradius frequency is given by:

$$\omega_{gyr}^{rel} \equiv \frac{eB}{\gamma m_e c}$$

which is exactly related to the classical angular frequency as  $\omega_{gyr}/\gamma$ . According to the relativistic Larmor's formula above we have that:

$$P = \frac{2e^2}{3c^3} \gamma^4 \left( \frac{ev \sin \alpha}{\gamma m_e c} \right)^2$$

We can re-arrange this formula by assuming ultra-relativistic electrons  $\beta \rightarrow 1$  and that we have an average number of electrons with different pitch angles and so  $\langle \sin^2 \alpha \rangle = 2/3$ . We are going also to use the definition of the Thomson cross-section:

$$\sigma_T \equiv \frac{8\pi}{3} r_0^2$$

where  $r_0$  is the electron classic radius defined (in gaussian units) as:

$$r_0 = \frac{e^2}{m_e c^2}$$

with that we can write the power loss as:

$$P = \frac{4}{3} \sigma_T c U_B \gamma^2$$

where  $U_B = B^2/8\pi$  is the magnetic field energy density. The power depends on the electron mass via the Thomson cross-section and the  $\gamma$ . In total it gives  $P \propto m_e^{-4}$  for the electrons. That's why for protons the synchrotron radiation is not as important as it is for electrons. The mean free-path for electrons given their losses due to synchrotron is (for typical astrophysical values):

$$l_{syn} = \left( \frac{1}{E} \frac{dE}{dt} \right)^{-1} \sim 100 \text{ pc}$$

That's the reason why electrons are not the main component of CR since they cannot travel long distances. If we want now to derive the power emitted per frequency, things get also a bit more complicated. One first thing to take into account is that in the relativistic regime the power radiated will be distorted. From Lorentz transformations we can derive that an angle  $\Psi$  in the particle rest frame will be seen in laboratory frame as:

$$\sin \Psi = \frac{\sin \Psi'}{\gamma(1 + \beta \cos \Psi')}$$

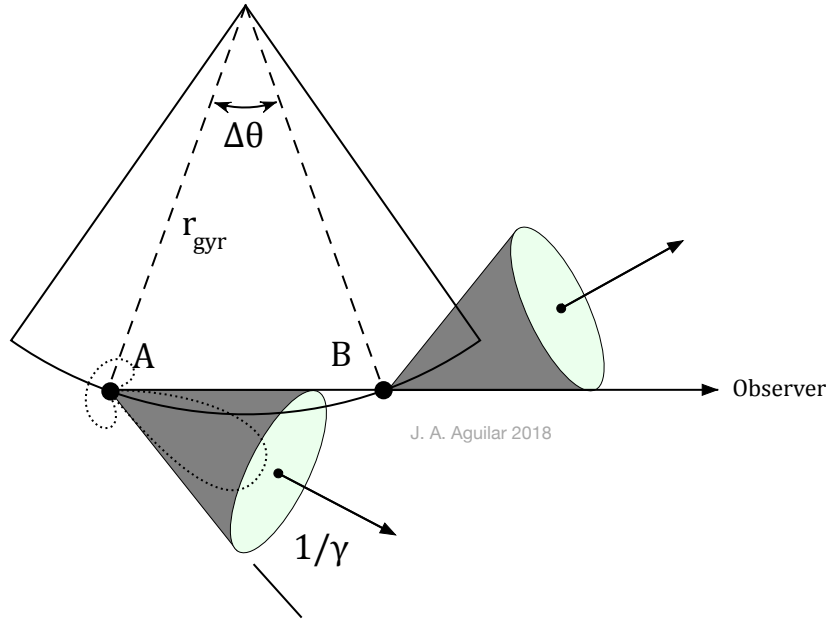
(we saw this in the Exercises 1). For small angles we have that

$$\sin \Psi \sim \Psi \sim \frac{1}{\gamma}$$

i.e., while the power is radiated nearly isotropically (dipole) in the particle's instantaneous rest frame, most of it will be *beamed* into a narrow cone of angle  $\sim 1/\gamma$  in the laboratory frame.

Note that I'm referring to an *instantaneous* rest frame, what does it even mean? Well it means that I in the particle rest frame, where the velocity of the particle is 0, the acceleration on the other hand is not 0, so eventually the particle will move. Ie, there is no particle rest frame, but there is an instantaneous rest frame.

This beaming in the lab reference frame has an impact on how the viewer sees the electric field variation. It is no longer a sinusoidal, instead the emission is pulsed every time the cone sweeps around the line of sight of an observer as illustrated below:



Since each cone beaming has a half amplitude of  $1/\gamma$  the radiation from an observer is visible during a  $\Delta\theta \sim 2/\gamma$ . During this angular distance the particle travels from A to B at an angular frequency given by  $\omega_{gyr}^{rel}$  which means that  $\Delta t_{AB}$  is given by:

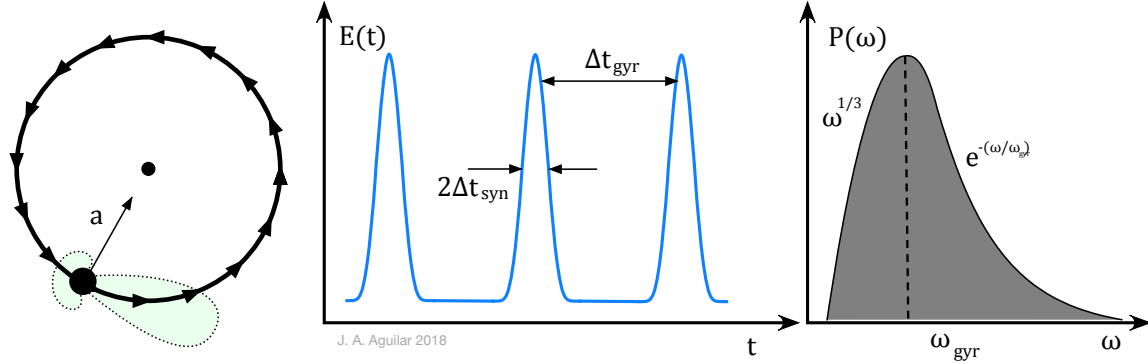
$$\Delta t_{AB} = \frac{\Delta\theta}{\omega_{gyr}^{rel}} = \frac{2}{\gamma\omega_{gyr}^{rel}}$$

Given the relativistic speed of the the electron, the frequency of the radiation is no longer a sinusoidal. When a photon is emitted at the point B the photon emitted in A has already travelled a distance  $c\Delta t_{AB}$ . Therefore the time interval between photons is given by:

$$\Delta t_{sync} = \frac{c\Delta t_{AB} - v_\perp \Delta t_{AB}}{c} \approx \Delta t_{AB}(1 - \beta) \approx \Delta t_{AB} \frac{1 - \beta^2}{1 + \beta}$$

$$\Delta t_{sync} \approx \frac{\Delta t_{AB}}{2\gamma^2} = \frac{1}{\gamma^3 \omega_{gyr}^{rel}} = \frac{1}{\gamma^2 \omega_{gyr}}$$

So synchrotron radiation is a very spiky series of widely spaced narrow pulses of time  $2\Delta t_{sync}$ , and adjacent spikes are separated in frequency  $\Delta t_{gyr} = 1/\nu_{gyr}^{rel} = \gamma/\nu_{gyr}$ . The emission from an observer is illustrated below:



The power spectrum (ie power as function of frequency) illustrated in the plot on the right is no longer a monochromatic sinusoidal signal, but the Fourier transform of this time series of pulses. Taking of all the Fourier components into account results in the following expression for one electron (the formal derivation can be found for example in *Classical Electrodynamics* by J. D. Jackson):

$$P(\nu)d\nu = \frac{\sqrt{3}e^3 B \sin \alpha}{m_e c^2} \frac{\nu}{\nu_c} \int_{\nu/\nu_c}^{\infty} K_{5/3}(\psi) d\psi$$

where  $K_{5/2}$  is the Bessel function of order 5/2, and we expressed the power spectrum in terms of the frequency  $\nu = \nu_{gyr} = \omega_{gyr}/2\pi$  and where we defined the critical frequency as:

$$\nu_c \equiv \frac{3}{2}\gamma^2 \nu_{gyr} \sin \alpha$$

which is the frequency at which the power spectrum will peak. In general terms we can describe the shape of the synchrotron power spectrum of a single electron has a logarithmic slope at low frequencies as  $P \propto \nu^{1/3}$ , a broad peak near the critical frequency  $\nu_c$ , and a sharp fall off at higher frequencies.

#### 4.2.4.3 Spectrum for several electrons for optically thin sources

If a synchrotron source containing any arbitrary distribution of electron energies is optically thin ( $\tau \ll 1$ ), then its spectrum is the superposition of the spectra from individual electrons and its flux density cannot rise faster than  $\nu^{1/3}$  at any frequency  $\nu$ . The energy distribution of cosmic-ray electrons in most synchrotron sources is roughly a power law:

$$n(E)dE \propto E^{-\delta}dE$$

We make the very simple and crude approximation that each electron radiates all of its power at a single critical frequency:

$$\nu_c \simeq \gamma^2 \nu_{gyr}$$

We can assume that the luminosity or total power emitted per unit volume per unit frequency,  $L(\nu)d\nu$  is given by the power emitted for each individual electron times the number of electrons:

$$L(\nu)d\nu = Pn(E)dE = - \left( \frac{dE}{dt} \right) n(E)dE$$

where

$$E = \gamma m_e c^2 \simeq \left( \frac{\nu}{\nu_{gyr}} \right)^{1/2} m_e c^2$$

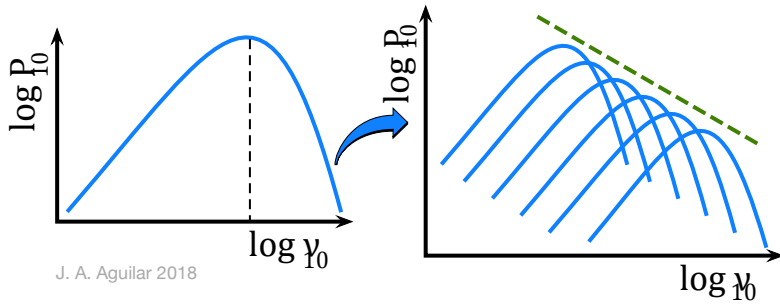
and so

$$\frac{dE}{d\nu} \simeq \frac{m_e c^2 \nu^{-1/2}}{2 \nu_{gyr}^{1/2}}$$

putting all together gives:

$$L_\nu \propto B^{(\delta+1)/2} \nu^{(1-\delta)/2}$$

That is, the synchrotron spectrum of a power-law energy distribution is itself a power law. This idea is represented in the figure below:



For example in our Galaxy we expect the electron population to have a spectral index of  $\delta \sim 2.4$ , and so the synchrotron radiation should have an spectral index of  $\sim 0.7$ .

#### 4.2.4.4 Power spectrum for several electrons for optically thick sources

The argument of a power law synchrotron spectrum as a power-low with spectral index  $\alpha = (1 - \delta)/2$  it's true as long as no absorption of photons by the emitting region happens. At low frequencies however synchrotron suffers from self-absorption, in which a photon interacts with a charge in a magnetic field. This also happens in *optically thick* sources. Therefore at low frequencies its emission is absorbed and re-emitted as blackbody radiation. The derivation of the synchrotron self-absorption is complicated so we are going to give only an heuristic approach. The problem with the re-emission of low frequencies as a black-body radiation is that a power-law distribution does not have a characteristic temperature. We can however assume that each electrons emits energy at a given frequency (given that the synchrotron emission of individual electrons is highly peak at a given frequency):

$$\nu_c \equiv \frac{3}{2} \gamma^2 \nu_{gyr} \sin \alpha$$

in order to calculate an *effective temperature* we can use that for an ultrarelativistic gas we have the relation:

$$E_e = 3kT_e(\nu)$$

where  $E_e = \gamma m_e c^2$ , since  $\gamma \propto \nu^{1/2}$  we have that:

$$T_e(\nu) \propto \nu^{1/2}$$

The black-body radiation or Rayleigh-Jeans is proportional to  $\nu^2$  but given the extra dependency of  $T_e(\nu)$  it is changed as:

$$L(\nu) \propto T(\nu) \nu^2 B^{-1/2} \sim \nu^{1/2} \nu^2 B^{-1/2} \sim \nu^{5/2} B^{-1/2}$$

A thing to note is that this part of the spectrum is independent of the orginal electron power-law spectral index.

#### 4.2.5 Tutorial I. Working with SED

We are going to plot some SED using a python module called [naima](#). This package allows for the calculation of non-thermal radiation from relativistic particle populations.

```
%matplotlib inline
import numpy as np
import matplotlib.pyplot as plt

%config InlineBackend.figure_format = 'svg'
import naima
import astropy.units as u

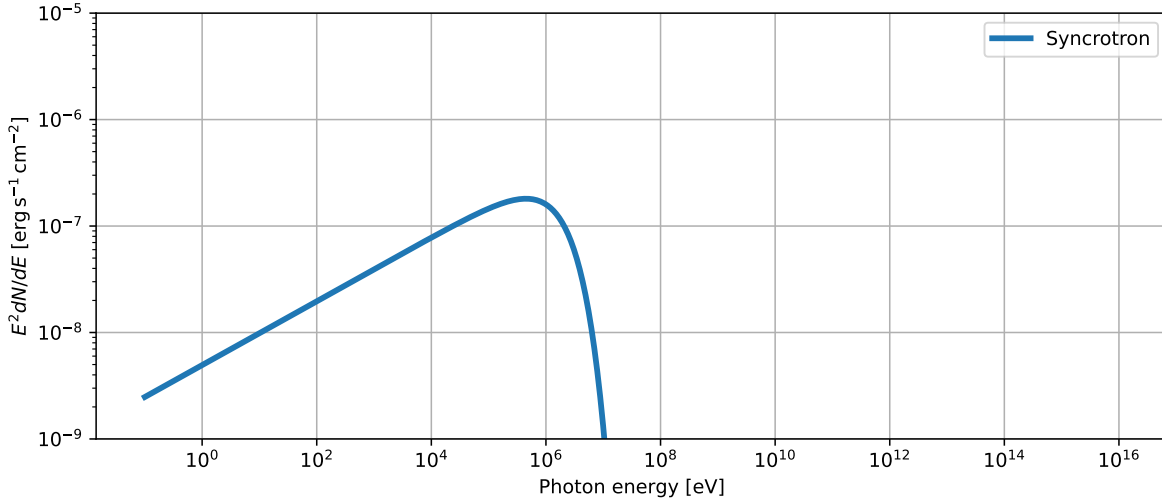
# First we are going to define a population of electrons with a PowerLaw model
e_pl = naima.models.PowerLaw(1e35*u.Unit('1/eV'), 1*u.TeV, 2.4)

#Now the equivlent synchrotron radiation for a magnetic field of 100 uG
syn = naima.models.Synchrotron(e_pl, B=100*u.uG)

spectrum_energy = np.logspace(-1,16,1000)*u.eV
sed_syn = syn.sed(spectrum_energy, distance=1.5*u.kpc)

fig = plt.figure(figsize=(10,4))
ax = plt.subplot(111)
ax.loglog(spectrum_energy,sed_syn,lw=3,label='Syncrotron')

ax.set_yscale('log')
ax.set_xscale('log')
ax.set_xlim(1e-9, 1e-5)
ax.set_xlabel('Photon energy [{}]\n'.format(spectrum_energy.unit.to_string('latex_inline')) + 
              spectrum_energy.unit.to_string('latex_inline')))
ax.set_ylabel('E^2 dN/dE [{}]\n'.format(sed_syn.unit.to_string('latex_inline')) + 
              sed_syn.unit.to_string('latex_inline')))
ax.grid()
ax.legend(loc='upper right')
plt.show()
```



#### 4.2.6 Inverse Compton scattering.

Compton discovered that photons can transfer part of their energy to electrons in a collision. In astrophysics the inverse Compton effect electrons accelerated to high energy collide with photons from the blackbody radiation (thermal photons) or starlight photons and transfer energy to them.

In astrophysics the inverse compton scattering is very important as a fast electrons that produce the synchrotron component can hit a low-energy photon and transfer a large fraction of its energy to the photon. For low energy photons, the scattering is elastic, and this regime is called the classical *Thomson regime*. However, for high energy photons where  $E_\gamma \gg m_e c^2$  the scattering is not elastic and the energy of the scattered photons changes. This regime is called the *Klein-Nishina*. The cross-section for this *inelastic* scattering is given by:

$$\frac{d\sigma_{KN}}{d\Omega} = \frac{r_e^2}{2} \frac{E_{\gamma,out}^2}{E_{\gamma,in}^2} \left( \frac{E_{\gamma,out}}{E_{\gamma,in}} + \frac{E_{\gamma,in}}{E_{\gamma,out}} - \sin^2 \theta \right)$$

In the low energy regime  $E_{\gamma,in} = E_{\gamma,out}$  and the cross-section approaches that of the Thomson scattering.

##### 4.2.6.1 Maximum energy of inverse Compton

Let's assume the lab reference system,  $O$ , and the electrons rest frame system  $O'$ . The energy of the photon is then given by:

$$E'_{\gamma,in} = \gamma E_{\gamma,in} (1 + \beta \cos \theta)$$

where  $\gamma$  and  $\beta$  refer obviously to the electron. Since in the electron's rest frame the scattering happens at low-energy we can assume that the scattering is described by the elastic Thomson regime, ie, the photon is scattered with the same energy in the electron's rest frame. Going back to the lab frame we have then:

$$E_{\gamma,out} = \gamma E'_{\gamma,out} (1 + \beta \cos \theta')$$

but  $E'_{\gamma,in} = E'_{\gamma,out}$ . The maximum energy transfer will be that of a head-on collision in which the electron  $\cos \theta = \cos \theta' = 1$  is bounced backwards we have that:

$$\nu_{max} = \nu_0 \gamma^2 (1 + \beta)^2 \simeq 4\nu_0 \gamma^2$$

As electrons are moving in an isotropic photon field they will see mostly head on collisions. So the energy spectrum of scattered photons peak close to the maximum frequency. This relation is very important for astrophysics, because it tells us a relation between the energy of electrons and the spectrum of photons. We know there are electrons with  $\gamma \sim 100 - 1000$  and therefore the resulting photon emission is of very high energy. For example assuming electrons with  $\gamma \approx 1000$  we have:

Waveband	Frequency (Hz) $\nu_0$	Scattered Frequency (Hz)
Radio	$10^9$	$10^{15} = \text{UV}$
Far-infrared	$3 \times 10^{12}$	$3 \times 10^{18} = \text{X-rays}$
Optical	$4 \times 10^{14}$	$4 \times 10^{21} = \gamma\text{-rays}$

The hand-waving argument  $\nu \sim \nu_0 \gamma^2$  has also implication on the spectrum of photons. If electrons follow a power-law in the form of:

$$dn(E) \propto E^{-p} dE$$

we can derive the spectrum of scattered photons which will follow a power-law as:

$$I(\nu) \propto \nu^{-\frac{p-1}{2}}$$

because electrons lose energy by a factor  $\gamma^2$  and the frequency of photons is  $\nu \approx \nu_0 \gamma^2$

### Note

In some cases the synchrotron spectrum can interact with the same electron population that generated them via IC, scenario is called *Synchrotron Self Compton* (SSC). When external photons are present IC does not need the synchrotron field. Such process is referred as *External Inverse Compton*

#### 4.2.7 Tutorial II Working with SED

We are going now to calculate the IC spectrum using the CMB as the radiation field:

```
from astropy.constants import c

IC = naima.models.InverseCompton(e_pl, seed_photon_fields=['CMB'])

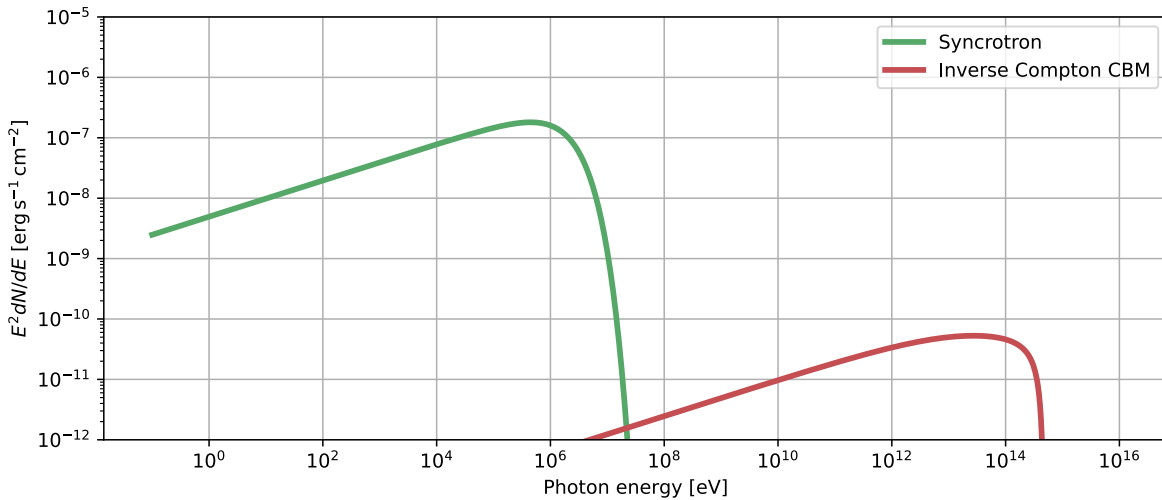
sed_ic_cbm = IC.sed(spectrum_energy, distance=1.5*u.kpc, seed="CMB")

fig2 = plt.figure(figsize=(10,4))
ax = plt.subplot(111)
ax.loglog(spectrum_energy,sed_syn,lw=3,label='Syncrotron',c=naima.plot.color_cycle[1])

ax.loglog(spectrum_energy,sed_ic_cbm,lw=3,
           label='Inverse Compton CBM', c=naima.plot.color_cycle[2])

ax.set_yscale('log')
ax.set_xlabel('Photon energy [{0}]\n{1}'.format(
    spectrum_energy.unit.to_string('latex_inline'),
    sed_syn.unit.to_string('latex_inline')))
ax.set_ylabel('$E^2 dN/dE$ [{0}]'.format(
    sed_syn.unit.to_string('latex_inline')))

ax.grid()
ax.legend(loc='upper right')
plt.show()
```



#### 4.2.7.1 Case of study: Active Galactic Nuclei

As we saw, blazars are a particular classification of AGNs with their relativistic plasma jet oriented close to the line of sight. Because blazars have their jets pointing towards, the full emission comes from a relatively small region (the width of the jets) and so these objects can exhibit rapid variability (due to the smaller causally connected regions). The typical SED for AGNs is characterized by a synchrotron component extending from radio to X-ray frequencies, and a second component peaking at gamma-ray frequencies due to either inverse-Compton radiation (or from hadronic processes). The plot below shows the spectral energy distribution of nearby ( $z = 0.044$ ) blazar 1ES 2344+514 during a flaring and a quiet state.

#### 4.2.7.2 Lightcurves and flares

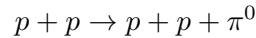
In addition to the SED one could measure the light-curve or number of photons (or energy density) as a function of time. This is usually done to illustrate the variability of the source. For AGNs it is possible to make the lightcurve for different energy ranges, and therefore addressing different emission mechanism.

Sometimes it is possible to observe a *flare* in high energy photon range but with no activity detected in soft/hard X-ray. These are called **orphan flare**. This is interesting since in the SSC scenarios the X-rays (due to synchrotron) and TeV gamma-rays (due IC scattering) must be correlated. An orphan flare is therefore an indication that SSC scenario might be excluded, while the EC is still possible. As we will see also an hadronic scenario in which TeV photons come from  $\pi^0$  is still possible.

## 4.2.8 Hadronic models

### 4.2.8.1 Pion decay

Accelerated protons in the source can produce charged and neutral pions via proton-proton interaction. In this context a CR proton with energy  $E_p$  and momentum  $p_p$  interacts with the ISM at rest in the process:



There is a threshold for this production given by the invariant:

$$s = E_{CoM}^2 = (E_p + m_p)^2 - p_p^2 = (2m_p^2 + m_{\pi^0}^2)^2$$

As we saw in lesson 2, the available energy to produce particles can be derived as:

$$\epsilon = E_{CoM} - 2m_p$$

The energy threshold to produce a pion at rest is then:

$$E_{p,th} = \frac{m_{\pi^0}^2 + 4m_p m_{\pi^0} + 2m_p^2}{2m_p} = \frac{m_{\pi^0}^2}{2m_p} + 2m_{\pi^0} + m_p$$

```
mp = 938.28 #MeV
mpion = 134.976 #MeV
print(f"Kinetic energy threshold for pion production {(mpion**2/(2*mp) + 2*mpion):.1f} MeV")
```

Kinetic energy threshold for pion production 279.7 MeV

The pions are produced with the same power law as the parent proton. Neutral pions decay rapidly ( $\tau = 8.4 \times 10^{-17}$  ns, compared to 26 ns of charged pions) into two photons. In the CoM each photon from the pion decay has an energy of  $E_\gamma^* = m_{\pi^0}/2 \approx 70$  MeV as we saw for the 2-body decay. In order to calculate the energy in the lab system we need to make a Lorentz transformation:

$$E_\gamma = \gamma(E_\gamma^* + \beta_\pi p_\gamma^* \cos \theta^*)$$

where (\*) denotes the CoM. Since pion is an isoscalar the decay is isotropic the limits are determined by  $\cos \theta^* = \pm 1$ . These limits are:

$$\frac{m_{\pi^0}}{2} \sqrt{\frac{1-\beta}{1+\beta}} \leq E_\gamma \leq \frac{m_{\pi^0}}{2} \sqrt{\frac{1+\beta}{1-\beta}}$$

where  $\beta$  is the velocity of the parent pion and we used  $p^* = E^*$  for photons.

#### 4.2.8.2 Pion bump

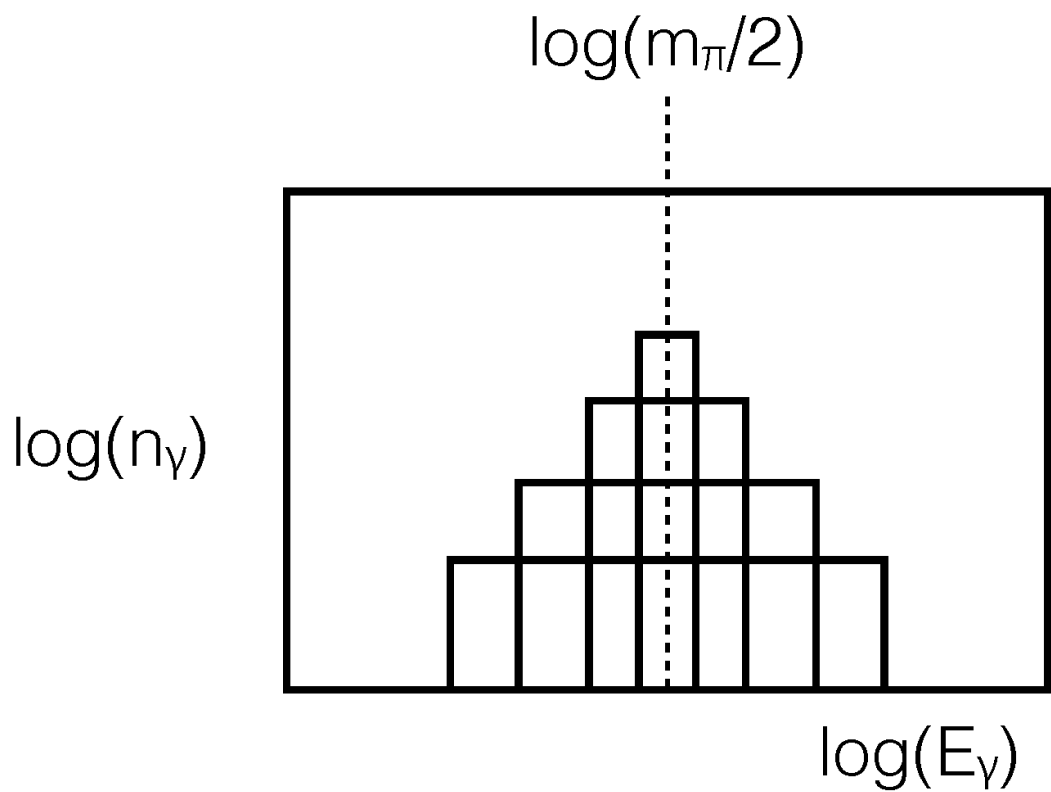
But what is the distribution of photons? Since the decay is isotropic in the CoM:

$$dN = \frac{1}{4\pi} d\Omega = \frac{1}{2} d \cos \theta^*$$

Using the lorentz transformation from CoM system and the lab system we can express:  
 $d \cos \theta^* = dE_\gamma / (\gamma \beta_\pi p_\gamma^*) = 2dE / (\gamma \beta_\pi m_{\pi^0})$  and thus:

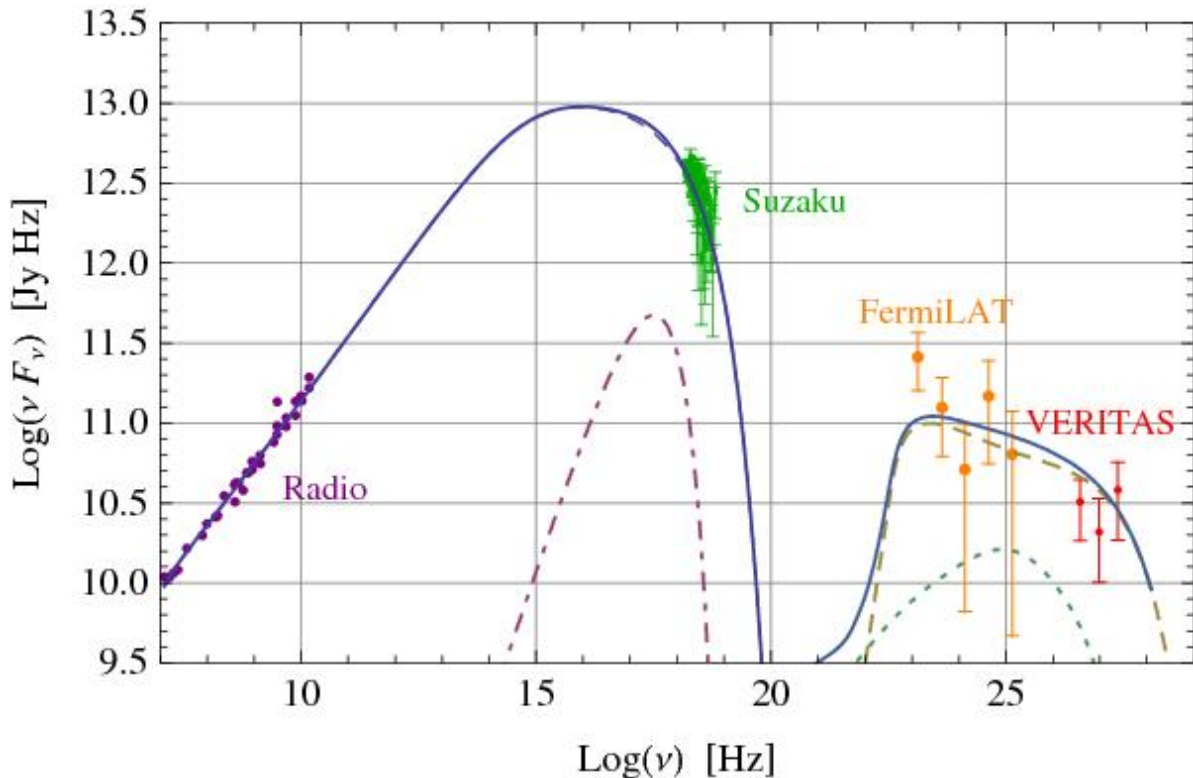
$$dN = \frac{dE}{\gamma \beta_\pi m_{\pi^0}}$$

Then the distribution of photons  $dN/dE = \text{const.}$  ie is constant on a box from  $E_{min}$  to  $E_{max}$  when plotted as  $\log(E_\gamma)$ . If many pions are decaying, the distribution of photons will be superposition of boxes around  $m_{\pi^0}$ . This is the so-called *pion bump*.



#### 4.2.9 Pion bump in SNR with Molecular Cloud

In 2013 Fermi (a gamma-ray satellite) confirmed the pion-bump in two old SNRs with Molecular Cloud.



So did we find the sources of Galactic Cosmic Rays? No. The steep gamma-ray spectrum at high energies suggests that the acceleration is not very active any more (as expected from old SNRs) and hence, even though there might be some particle acceleration these are not the sources of Galactic Cosmic Rays.

#### 4.2.10 Galactic gamma-ray diffuse emission

Diffuse gamma-ray emission is that not associated with a particular source. Fermi-LAT observed gamma-ray counts in the energy range from 200 MeV to 100 GeV. The signal is dominated by the diffuse Galactic emission, which is strongest in the plane of our Galaxy and toward the Galactic center but present all over the sky. The following shows the diffuse gamma-ray emission from 200 MeV to 100 GeV.

The gamma-ray diffuse emission are produced primarily the  $\pi^0$  produced by interactions of cosmic rays protons with the ISM. The Inverse Compton scattering on star light is less important as well as bremsstrahlung (braking radiation). In the plot below the models are split into the three basic emission components:

- $\pi^0$ -decay (red, long-dashed)
- IC (green, dashed),

- and bremsstrahlung (cyan, dash-dotted).

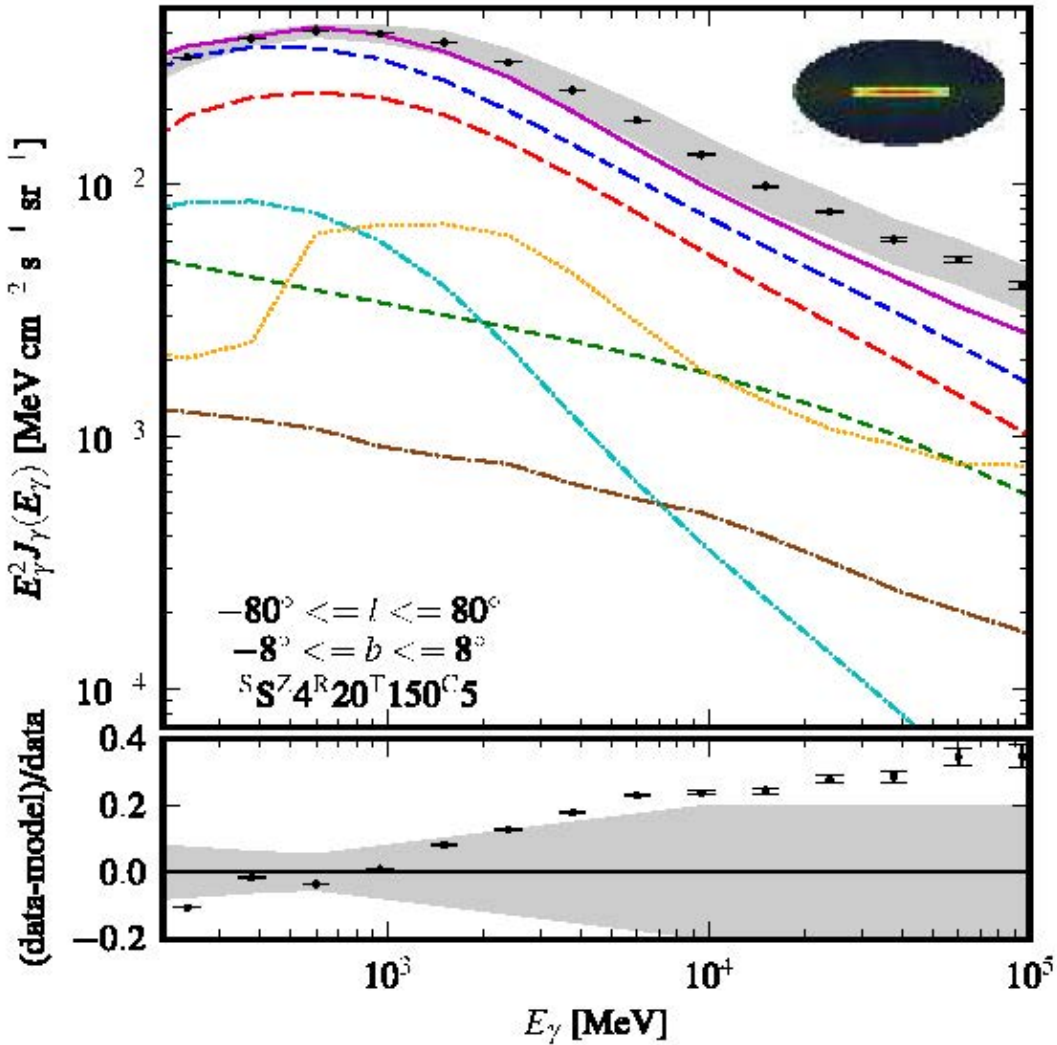


Figure 4.2: Source: Taken from [arXiv:1202.4039](https://arxiv.org/abs/1202.4039)

#### 4.2.11 Extragalactic Background Light

As we saw, VHE gamma-rays ( $E_\gamma = 30$  GeV) have a limited horizon due to their interaction with the CMB and the [Extragalactic Background Light \(EBL\)](#). The EBL is difficult to measure directly due to strong foregrounds from our solar system and the Galaxy. The TeV signal of distant AGNs are (partially) absorbed at the highest energies by the EBL. The absorption is

energy dependent and increases with distance. Observations of very far distant AGNs can be used to put constraints on the amount of EBL. However it is difficult to distinguish between an intrinsic softening of blazar spectra and a softening caused by the interaction with low energy EBL photons. The plot below shows the gamma-ray horizon and measurements from some Imaging Atmospheric Cherenkov Telescopes (IACTs) up to  $z=0.536$ .

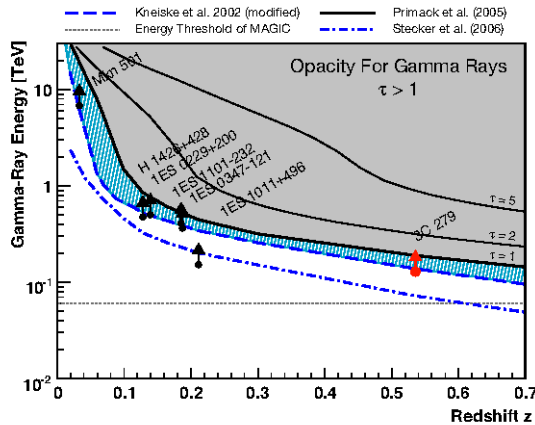


Figure 4.3: Source: Taken from arXiv:0904.0774v2

#### 4.2.12 Gamma-ray Detection

##### 4.2.12.1 The atmosphere

The Earth's atmosphere is opaque to photons with energy above 10 eV, meaning that to observe gamma-rays directly we need to place the detector above the atmosphere. A turning point in gamma-ray astronomy was the launch of the first satellite-borne telescope, SAS-2, in 1972.

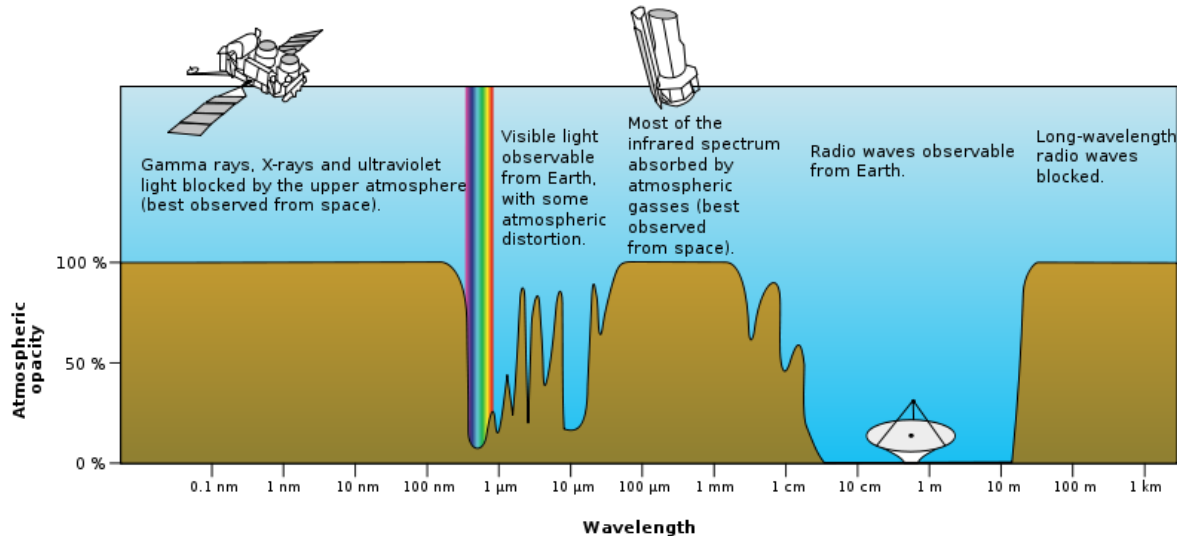
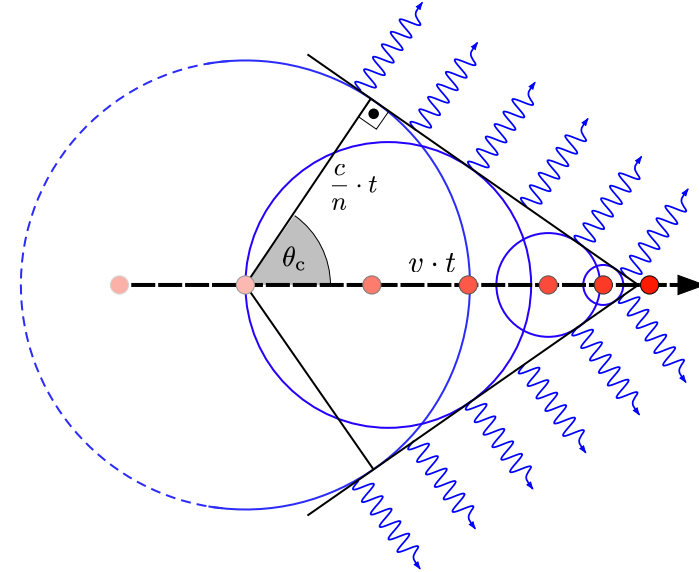


Figure 4.4: Source: scienceofdoom.wordpress.com

The major limitation of satellite experiments is their low area which limits their use to  $\leq 100$  GeV. At 100 GeV is when electromagnetic showers from the initial photon can be detected in ground-based telescopes.

#### 4.2.13 Cherenkov emission

When relativistic particles traverse a medium at a speed greater than the speed of light in that medium it can induce Cherenkov radiation. Cherenkov light is emitted in the UV and blue region in a narrow cone with angle:



$$\cos \theta = \frac{ct/n}{\beta ct} = \frac{1}{\beta n}$$

In the relativistic limit  $\beta \sim 1$  we can write:

$$\sin \theta = \sqrt{1 - \frac{1}{n^2}} = \sqrt{\frac{n^2 - 1}{n^2}} = \sqrt{\frac{(n-1)(n+1)}{n^2}} \approx \sqrt{2(n-1)}$$

In the atmosphere the spectral index depends on the altitude (same as density and pressure):

$$n = 1 + \epsilon_0 e^{-h/h_0}$$

where  $\epsilon_0 \simeq 2.8 \times 10^{-4}$  at sea level.

#### 4.2.14 Tutorial II: Plot of the Cherenkov angle as function of the spectral index.

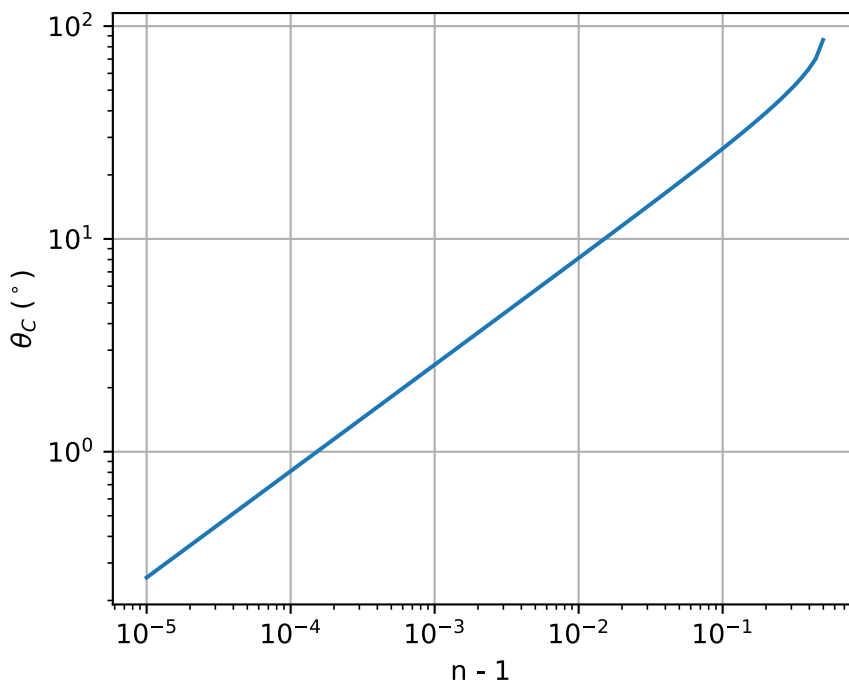
```
diffn = np.logspace(-5, 0, 100) #n - 1 from 0.0001 to 1
fig, ax = plt.subplots(figsize=(5,4))

#lets remove the values that will give errors in the arcsin:
diffn = diffn[np.where(np.sqrt(2*diffn) <= 1.)]
```

```

#In the relativistic limit
ax.plot(diffn, np.degrees(np.arcsin(np.sqrt(2*diffn))))
ax.set_yscale("log")
ax.set_xscale("log")
ax.set_xlabel("n - 1 ")
ax.set_ylabel(r"$\theta_C$ ($^\circ$)")
ax.grid()
plt.show()
thetaw = np.degrees(np.arcsin(np.sqrt(2*(1.33 -1))))
print(r"Cherenkov angle in water: $\theta_C = %.2f^\circ" %thetaw)
#For the atmosphere n = 1.0003
thetaatm = np.degrees(np.arcsin(np.sqrt(2*(1.0003 -1))))
print(r"Cherenkov angle in the atmosphere: $\theta_C = %.2f^\circ" %thetaatm)

```



Cherenkov angle in water:  $\theta_C = 54.33^\circ$   
 Cherenkov angle in the atmosphere:  $\theta_C = 1.40^\circ$

#### 4.2.15 Number of photons

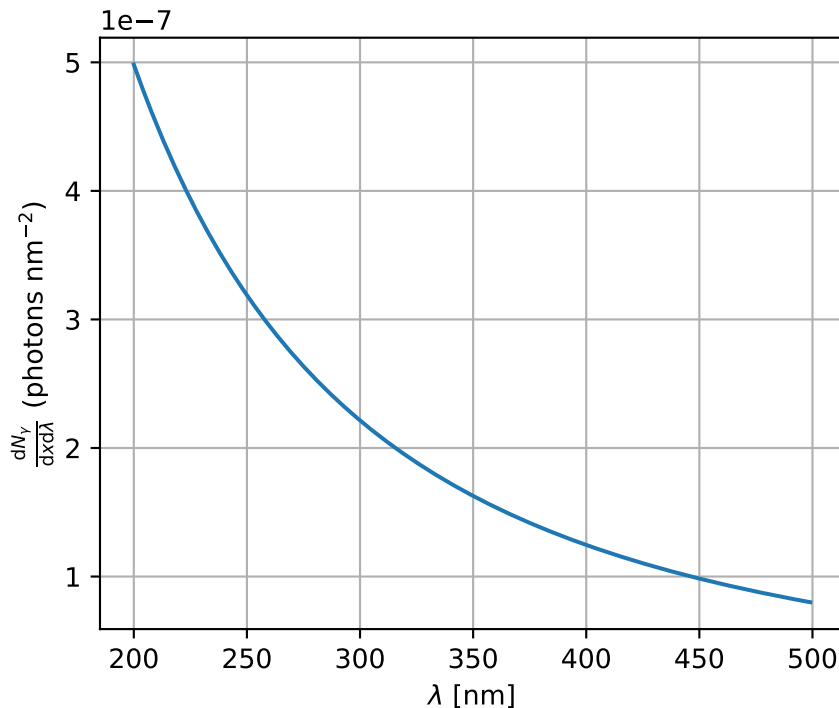
The number of photons from Cherenkov radiation follows the *Frank-Tamn* formula:

$$\frac{dN}{dx} = 2\pi\alpha z^2 \int_{\lambda_1}^{\lambda_2} \sin^2 \theta \frac{d\lambda}{\lambda^2}$$

For relativistic particles,  $\beta \sim 1$  in water  $n = 1.33$  the Cherenkov spectrum is:

```
import scipy.constants as cte
alpha = cte.alpha #fine structure constant

fig, ax = plt.subplots(figsize=(5,4))
wl = np.arange(200, 500, 1)
n = 1.33
ax.plot(wl, 2 * np.pi * alpha * ( 1- 1/n**2)/wl**2)
ax.set_xlabel(r"\lambda [nm]")
ax.set_ylabel(r"\frac{dN_\gamma}{dx\lambda} (\text{photons nm}^{-2}\text{s}^{-1})")
ax.grid()
plt.show()
```



#### 4.2.16 Atmospheric extinction.

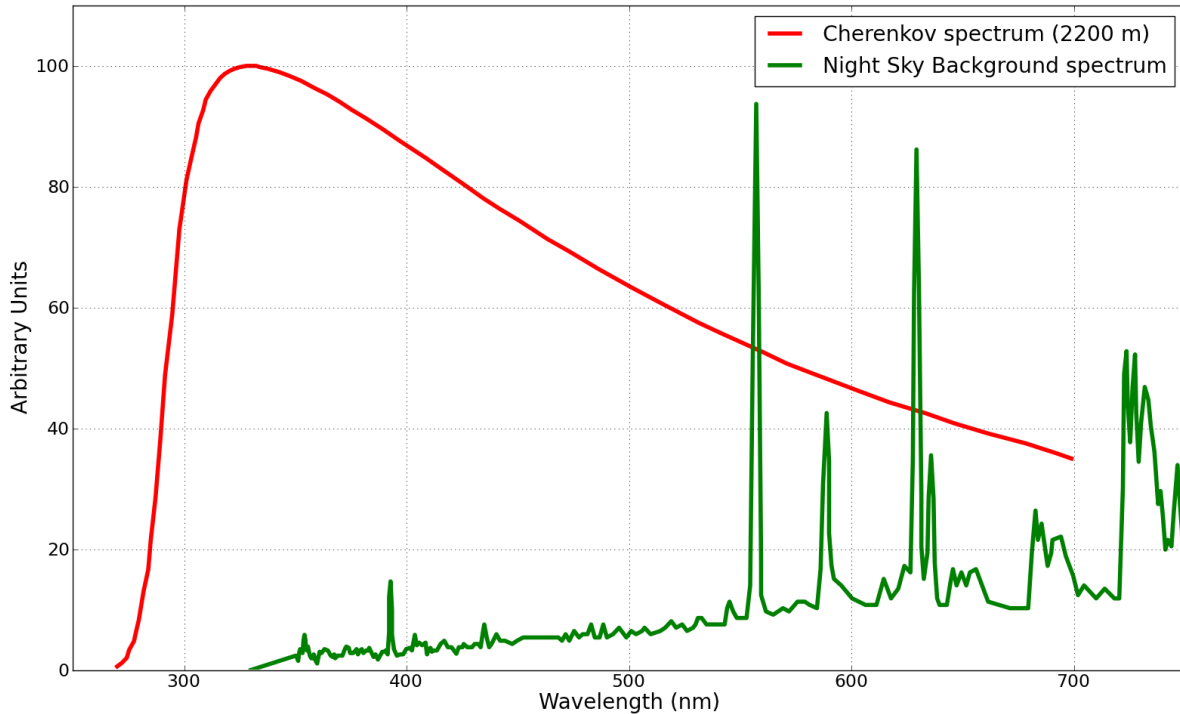
Once in the atmosphere, the Cherenkov light can suffer absorption and scattering due to several processes:

- Rayleigh scattering:

$$I = I_0 \frac{8\pi^4 \alpha^2}{\lambda^4 R^2} (1 - \cos^2 \theta)$$

where  $R$  is the distance to the particle and  $\theta$  the scattering angle.

- Absortion by ozone, above 20 km.
- Aerosol, dust. Independent of  $\lambda$ .



This processes change the Cherenkov spectrum dependending on the altitude. In ice on the other hand, there is no UV absorption and the Cherenkov spectrum keeps the  $1/\lambda^2$  tendency.

## 4.3 Gamma-rays, Cosmic-Rays and Neutrinos

### 4.3.1 Introduction

Both gamma-rays and neutrinos are produced as secondary products of Cosmic-Rays interactions. The dominant channels are:

$$p\gamma \rightarrow \Delta^+ \rightarrow \begin{cases} p\pi^0 & (2/3) \\ n\pi^+ & (1/3) \end{cases}$$

$$pp \rightarrow \begin{cases} pp\pi^0 & (2/3) \\ nn\pi^+ & (1/3) \end{cases}$$

The same processes occur with neutrons instead of protons leading to  $\pi^-$  production. The resulting neutrons can decay or interact. One assumption is that escaping neutrons decay as  $n \rightarrow p + e^- + \nu_e$  producing the observed CRs. This is called the **magnetic confinement models** in which the protons are trapped in the magnetic fields and only neutrons escape. The **Waxman-Bachall models** on the other hand assume that some protons escape, and therefore the observed flux of cosmic rays is a lower-limit on the total number of accelerated protons. In both scenarios the charged and neutral pions will decay as:

$$\begin{aligned} \pi^+ &\rightarrow \mu^+ \nu_\mu \rightarrow e^+ \nu_e \bar{\nu}_\mu \nu_\mu \\ \pi^- &\rightarrow \mu^- \bar{\nu}_\mu \rightarrow e^- \bar{\nu}_e \nu_\mu \bar{\nu}_\mu \\ \pi^0 &\rightarrow \gamma\gamma \end{aligned}$$

Clearly the productions of neutrinos, cosmic-rays and  $\gamma$ -rays are closely related.

### 4.3.2 p-p interactions

For environments where radiation density is low (too few photons)  $pp$  interactions dominate over  $p\gamma$  interactions. The cross section of  $pp$  interactions is almost energy independent  $\sigma_{pp} \sim 4 \times 10^{-26} \text{ cm}^2$  (See [Kelner et al.](#)). The cross section of this process has a threshold given by:

$$E_{th} = m_p + m_\pi(m_\pi + 4m_p)/2m_p \sim 1.2 \text{ GeV}$$

Therefore most of accelerated protons can interact in the source if there is enough material and the spectra of secondary particles closely follows that of the parent proton spectrum assuming the meson *cooling time* (we usually call *cooling* to any process of energy loss due to radiation) and interaction length are larger than decay time/length (in other words, if the meson decays before loosing energy or interacts).

- If the proton spectrum is **softer** than  $dN_p/dE \sim E^{-2}$ , most of the electromagnetic and neutrino power is in the energy band of 1 GeV. Gamma-ray emission is dominated by the  $\pi^0$  decay.
- If the proton spectrum is **harder** than  $dN_p/dE \sim E^{-2}$ , most of the energy output from proton interactions is at high energy. In this case the main contribution in gamma-ray comes from IC from secondary  $e^-e^+$  pairs produced in  $\pi^\pm$  decays.

### 4.3.3 p-gamma interactions

The cross-section of this process has a higher energy threshold than  $pp$  interactions given by:

$$E_{th} = \frac{m_p m_\pi + m_\pi^2}{\epsilon_{ph}} \simeq 7 \times 10^{16} \left[ \frac{\epsilon_{ph}}{1 \text{ eV}} \right]^{-1}$$

where  $\epsilon_{ph}$  is the target photon energy. Because this threshold only the highest energy protons can efficiently interact with the soft-photon fields. This process is the one typically considered for UHECR and extragalactic sources such as AGNs and Gamma-ray Bursts.

### 4.3.4 The Waxman-Bahcall neutrino flux

The neutrino flux from an optical thin (ie transparent for nucleon-meson interactions) source is usually referred as the [Waxman-Bahcall flux](#).

To derive it let's assume only the extragalactic CR contribution. The energy density is, as we calculated in Lecture 3 given by:

$$\rho_{CR} = \int E n(E) dE = 4\pi \int_{E_{min}}^{E_{max}} \frac{E}{c} I(E) dE \sim 3 \times 10^{-19} \text{ ergs cm}^{-3}$$

where assume the extreme energies of the accelerator to be  $E_{max}/E_{min} \sim 10^3$ . If the source is optically thin for  $p\gamma$  and  $pp$  interactions then the energy flux of neutrinos cannot be greater than that of cosmic-rays (this can only happen in an optically thick source where cosmic-rays do not escape but only neutrinos do). To estimate a bound then we can therefore assume that the same energy density of cosmic rays ends up in neutrinos and electromagnetic energy:

$$\int E_\nu I_\nu(E_\nu) dE_\nu = c \frac{\rho_{CR}}{4\pi}$$

Assuming that the neutrino follows a power law of spectrum with an differential spectral index of 2 and a maximum  $E_{max} = 10^8$  GeV the produced neutrino flux is:

$$E_\nu^2 I_\nu(E_\nu) \sim 5 \times 10^{-8} \text{ GeV cm}^{-2} \text{ s}^{-1} \text{ sr}^{-1}$$

The Waxman-Bahcall flux is sometimes referred as a bound, in part because more energy is transfer to the neutron than the charged pion (roughly a factor 4 times more) and so:

$$E_{\nu_\mu}^2 I_{\nu_\mu}(E_{\nu_\mu}) \sim 1 - 5 \times 10^{-8} \text{ GeV cm}^{-2} \text{ s}^{-1} \text{ sr}^{-1}$$

The value derived above does not account for several things:

- There are more CR than observed at Earth due to the GZK-effect. It also ignores the evolution of the sources as red-shift → **increase the neutrino flux**.
- In  $p\gamma$  muon neutrinos (and antineutrinos) from the pion decay  $\pi^+ \rightarrow \mu^+ \nu_\mu \rightarrow e^+ \nu_e \bar{\nu}_\mu \nu_\mu$  only receive 1/2 of the energy of the charged pion (assuming each lepton carries the same energy) → **decrease the neutrino flux**.

In practice these corrections compensate. The other uncertainty is from where to chose  $E_{min}$  ie the transition to Galactic sources. In general we can construct a more generic relation between the CR and neutrino flux of the form of:

$$\begin{aligned} \rho_{CR}(E_{min}) &= n_{\nu/p} \rho_\nu(E_{min}) = n_{\nu/p} \int_{E_{min}} n_\nu(E_\nu) E_\nu dE_\nu \\ n_{\nu/p} 4\pi \int_{E_{min}} \frac{I_\nu(E_\nu)}{c} E_\nu dE_\nu &= 4\pi \int_{E_{min}} \frac{I_p(E_p)}{c} E_p dE_p \end{aligned}$$

where  $n_{\nu/p}$  refers to the number of neutrinos per proton interaction. Ignoring the integrals we get the relation:

$$E_\nu I_\nu(E_\nu) \sim n_{\nu/p} E_p I_p(E_p)$$

Using that the energy of the neutrinos will be a fraction  $\langle x_{p \rightarrow \nu} \rangle$  of the proton energy we can rewrite it as:

$$I_\nu(E_\nu) \sim n_{\nu/p} \frac{1}{\langle x_{p \rightarrow \nu} \rangle} I_p(E_p)$$

### 4.3.5 The neutrino and gamma connection

#### 4.3.5.1 Extragalactic p-gamma: Energy fraction

Due to isospin the  $\Delta^+$  decays more often to  $p$  than  $n$ .

$$p\gamma \rightarrow \Delta^+ \rightarrow \begin{cases} p\pi^0 & (2/3) \\ n\pi^+ & (1/3) \end{cases}$$

In both cases, the fraction of energy that goes to the pions is  $\langle x_{p \rightarrow \pi} \rangle \sim 0.20$ . Assuming the pion decays:

$$\pi^0 \rightarrow \gamma\gamma, \text{ and } \pi^+ \rightarrow \mu^+\nu_\mu \rightarrow e^+\nu_e \bar{\nu}_\mu \nu_\mu$$

We have that: 1.  $\gamma$ 's take 1/2 of the neutral pion energy. 2. Leptons take 1/4 of the charge pion energy.

And so:

$$\begin{aligned} \langle x_{p \rightarrow \nu} \rangle &= \frac{1}{4} \langle x_{p \rightarrow \pi} \rangle = \frac{1}{20} \\ \langle x_{p \rightarrow \gamma} \rangle &= \frac{1}{2} \langle x_{p \rightarrow \pi} \rangle = \frac{1}{10} \end{aligned}$$

#### 4.3.5.2 Extragalactic p-gamma: Number of particles

If we consider only  $\nu_\mu$  we have 2  $\nu_\mu$  per pion decay, as well as 2  $\gamma$ 's per pion decay. So the spectra can be related as:

$$\begin{aligned} I_{\nu_\mu}(E_{\nu_\mu}) &= 2 \times \frac{1}{3} \frac{1}{\langle x_{p \rightarrow \nu} \rangle} I_p(E_p) \\ I_\gamma(E_\gamma) &= 2 \times \frac{2}{3} \frac{1}{\langle x_{p \rightarrow \gamma} \rangle} I_p(E_p) \end{aligned}$$

Let's assume a proton spectrum  $I_p(E_p) \propto E_p^{-2}$  and so  $I_p(E_p) \propto E_{\nu_\mu}^{-2} \langle x_{p \rightarrow \nu} \rangle^2$

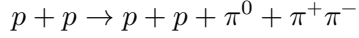
$$\begin{aligned} I_{\nu_\mu}(E_{\nu_\mu}) &\propto 2 \times \frac{1}{3} \langle x_{p \rightarrow \nu} \rangle E_{\nu_\mu}^{-2} \rightarrow 2 \times \frac{1}{3} \times \frac{1}{20} E_{\nu_\mu}^{-2} \\ I_\gamma(E_\gamma) &\propto 2 \times \frac{2}{3} \langle x_{p \rightarrow \gamma} \rangle E_\gamma^{-2} \rightarrow 2 \times \frac{2}{3} \times \frac{1}{10} E_\gamma^{-2} \end{aligned}$$

So:

$$I_{\nu_\mu}(E_{\nu_\mu}) \sim \frac{1}{4} I_\gamma(E_\gamma)$$

#### 4.3.5.3 Galactic $p p$

In a matter dominated environment such as Galactic SN shocks CRs interact with the H in the Galactic disk via  $p p$  interactions. As we saw these interactions have a lower threshold than  $p\gamma$ . Let's consider the reaction:



where we assume that pions are produced with the same probability (1/3). Doing the same calculation as before we get that:

$$\begin{aligned} I_{\nu_\mu}(E_{\nu_\mu}) &\propto 2 \times \frac{1}{3} \langle x_{p \rightarrow \nu} \rangle E_{\nu_\mu}^{-2} \rightarrow 2 \times \frac{2}{3} \times \frac{1}{20} E_{\nu_\mu}^{-2} \\ I_\gamma(E_\gamma) &\propto 2 \times \frac{2}{3} \langle x_{p \rightarrow \gamma} \rangle E_\gamma^{-2} \rightarrow 2 \times \frac{1}{3} \times \frac{1}{10} E_\gamma^{-2} \end{aligned}$$

#### 4.3.5.4 Astrophysical Neutrino Oscillations

In the discussion above we focused on muon neutrinos, however we ignored the fact that neutrino oscillate. We saw that the probability of neutrino flavor for  $\delta = 0$  can be written as:

$$\begin{aligned} P(\nu_\alpha \rightarrow \nu_\beta) &= \sum_j \sum_i U_{\alpha i} U_{\beta i}^* U_{\alpha j}^* U_{\beta j} e^{-i \frac{\Delta m_{ij}^2 L}{2E}} \\ &= \delta_{\alpha\beta} - 4 \sum_{i>j} \text{Re}(U_{\alpha i}^* U_{\beta i} U_{\alpha j} U_{\beta j}^*) \sin^2\left(\frac{\Delta m_{ij}^2 L}{4E}\right) \end{aligned}$$

For a non-monochromatic neutrino beam, the probability has to be averaged over the spectrum. The sin term will be averaged to 0.5 for large distances  $L$ . And thus the probability does not depend on time and can be written as a matrix:

$$P(\nu_\alpha \rightarrow \nu_\beta) = \sum_j |U_{\alpha j}|^2 |U_{\beta j}|^2$$

#### 4.3.6 Tutorial II: Calculation of astrophysical neutrino oscillations

```

import numpy as np
import scipy as sp

def PMNS_Factory(t12, t13, t23, d):
    s12 = np.sin(t12)
    c12 = np.cos(t12)
    s23 = np.sin(t23)
    c23 = np.cos(t23)
    s13 = np.sin(t13)
    c13 = np.cos(t13)
    cp = np.exp(1j*d)
    return np.array([[c12*c13, s12*c13, s13*np.conj(cp)],
                    [-s12*c23 - c12*s23*s13*cp, c12*c23 - s12*s23*s13*cp, s23*c13],
                    [s12*s23 - c12*s23*s13*cp, -c12*s23 - s12*c23*s13*cp, c23*c13]])

##Probability of flavor change when L->inf
def Prob(a, b, U):
    """
    Gives the oscillation probability for nu(a) -> nu(b)
    for PMNS matrix U, and L in km and E in GeV
    """
    s = 0
    for i in range(3):
        s += (np.conj(U[a,i])*U[b,i]*U[a,i]*np.conj(U[b,i])).real
    return s

def ProbMatrix(U):
    return np.array([[Prob(0, 0, U), Prob(0, 1, U), Prob(0, 2, U)],
                    [Prob(1, 0, U), Prob(1, 1, U), Prob(1, 2, U)],
                    [Prob(2, 0, U), Prob(2, 1, U), Prob(2, 2, U)]])

t12 = np.arcsin(0.306**0.5)
t13 = np.arcsin(0.0251**0.5)
t23 = np.arcsin(0.42**0.5)
U = PMNS_Factory(t12, t13, t23, 0)

```

The probability of a neutrino flavor factor of  $(\nu_e^{source}, \nu_\mu^{source}, \nu_\tau^{source})$  to change into a flavor vector  $(\nu_e^{Earth}, \nu_\mu^{Earth}, \nu_\tau^{Earth})$  is given by:

$$(\nu_e^{Earth} \nu_\mu^{Earth} \nu_\tau^{Earth}) = P_{\alpha\beta} (\nu_e^{Source} \nu_\mu^{Source} \nu_\tau^{Source})$$

Assuming at the source the flavor ratio is (1:2:0) we have that:

```
Prob(0, 0, U) + Prob(1, 0, U) + Prob(2, 0, U)
```

1.005381376348095

```
source = np.array([1, 1, 1])
P = ProbMatrix(U)
Earth = np.dot(P, source)
print (Earth)
```

[1.00538138 1.00204305 1.00854641]

Thus, almost equal number of electron, muon and tau astrophysical neutrinos are expected to be observed at Earth due to oscillations. More info at [arXiv:hep-ph/0005104](https://arxiv.org/abs/hep-ph/0005104)

#### 4.3.7 Gamma-ray neutrino relation

After oscillations the neutrino and gamma-rays relations are given by:

$$\frac{dN_\nu}{dE_\nu} = \frac{1}{2} \frac{dN_\gamma}{dE_\gamma} \text{ for } p + p$$

$$\frac{dN_\nu}{dE_\nu} = \frac{1}{8} \frac{dN_\gamma}{dE_\gamma} \text{ for } p + \gamma$$

Assuming an  $E^{-2}$  spectrum.

### **4.3.8 Neutrino Astronomy**

#### **4.3.9 Diffuse flux of Astrophysical Neutrinos**

The first detection of high-energy neutrinos of cosmic origin in 2013 by the IceCube Neutrino Observatory opened a new window to the non-thermal processes in our universe. The first strong evidence for a cosmic neutrino component came from a search using data from May 2010 to April 2012 [35], where two shower-like events from interactions within the detector with energies above 1 PeV were discovered. A follow-up search for events starting in the detector with more than 30 TeV deposited energy that utilized the same dataset identified 25 additional high-energy events. The spectrum and zenith angle distribution of the events was incompatible with the hypothesis of an atmospheric origin at  $> 4\sigma$ . IceCube has since collected independent evidence for an astrophysical neutrino signal by analyzing different event signatures.

##### **4.3.9.1 Starting Events**

Neutrino interactions are identified in IceCube by searching for an interaction vertex within the instrumented volume. This search is sensitive to both shower-like and track-like events. Since the main background for this search is comprised of muons from CR air showers, the rejection strategy is to identify Cherenkov photons from a track entering the detector. For that, the outer parts of the instrumented volume are assigned to a “veto” region. An event is rejected if a certain number of Cherenkov photons are found in this veto region at earlier times than the photons produced at the interaction vertex. The energy threshold for this analysis is about  $E_\nu \sim 30$  TeV.

##### **4.3.9.2 Through-going muons**

Muons produced in CC neutrino interactions far outside the detector can still reach the instrumented volume to produce track-like events. Even at 1 TeV a muon can penetrate several kilometers of ice before it stops and decays. This allows observation of high-energy neutrino interactions from a much larger volume than the instrumented one, thereby substantially increasing the effective area of the detector.

##### **4.3.9.3 The spectral fit**

The results of a combined analysis fits the neutrino flux to a power-law between 27 TeV and 2 PeV consistent with an unbroken power law with a best-fit spectral index of  $-2.49 \pm 0.08$  given by:

$$E^2 \Phi(E) = 2.06^{+0.35}_{-0.26} \times 10^{-8} \left( \frac{E}{100 \text{ TeV}} \right)^{-0.46 \pm 0.12} \text{ GeV s}^{-1} \text{ sr}^{-1} \text{ cm}^{-2}.$$

However using only the high energy through-going muons (above 200 TeV) yields a preferred spectral index of  $-2.13 \pm 0.13$

#### 4.3.10 The Search for Point Sources

In the case where the cosmic neutrino flux is dominated by bright individual sources, they should be detectable as a local excess of events on the sky with respect to the atmospheric neutrino and diffuse cosmic neutrino background. The sensitivity of a search for such features depends crucially on the precision by which the direction of the neutrinos can be reconstructed from the data, i.e. on the detector angular resolution. No indication for a neutrino point source has been found in the IceCube data so far. The null result of a point-source of neutrinos, can be transformed into an flux upper limit at a given confidence level. This upper limits represents the neutrino flux that we can be certain to exclude, since IceCube did not see a point source.

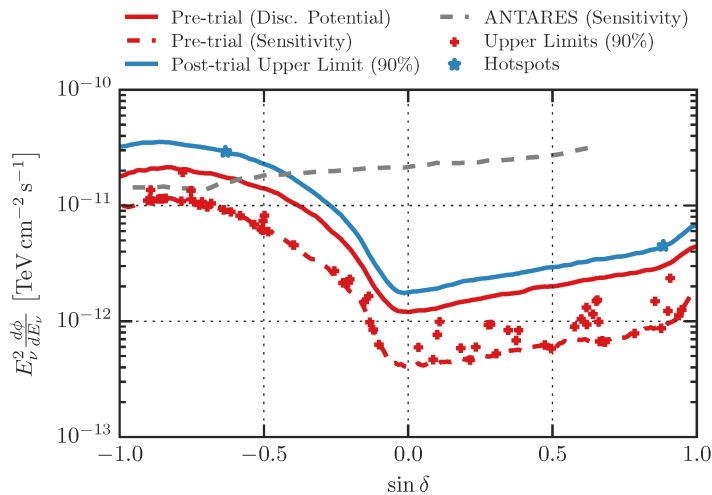
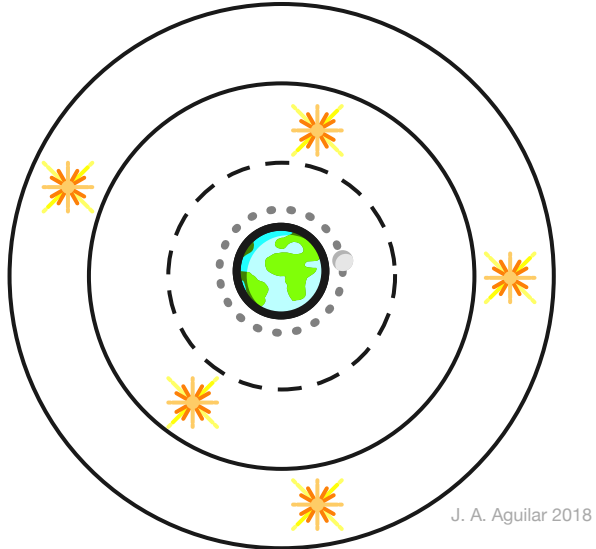


Figure 4.5: Source: IceCube

#### 4.3.11 The Olbers' Paradox

Altough the most famous formulation of the problem comes from Henrich Olbers (1826), probably it was Kepler in 1610 the first to note that the most obvious observation, the night sky is dark, has very important consequences.



The idea is quite simple, suppose there is a source population with typical luminosity  $L$  in ergs/s and a number density of  $n$ , then the total power emitted per unit area will be:

$$F = \int L n \frac{dV}{4\pi^2} = \frac{1}{4\pi} \int L n d\Omega dr$$

Integrating over all distances we can obtain the energy per steradian per second, and assuming the luminosity is independent of distance as well as number density we have that:

$$\frac{dF}{d\Omega} = \frac{1}{4\pi} L n \int_0^\infty dr \rightarrow \infty$$

The sky should be bright! The solution of this puzzle is the fact the Universe is dynamic and time dependent! In other words, if the Universe is expanding the radiation from increasingly distant sources is increasingly less. Also stars seems to have had a cosmological evolution, for example, there are more quasars per unit volume at  $z \sim 2$  than now.

Although the Olbers' paradox is no more a paradox, it represents the *problem* that arises with neutrino astronomy. Since the extragalactic space is completely transparent for neutrinos, the flux of neutrinos that might arrive at Earth will have a significant contribution from very distant and faint sources. Let's assume now a source population with typical neutrino luminosity  $L\nu(E)$  and with a number density population given by:

$$n(z) = n_0(1+z)^m$$

where  $n_0$  is the *local density* of the source population, (ie the population close to our epoch  $z = 0$ ). The parameter  $m$  describes the source cosmological evolution (ie, when sources to appear in the history of the Universe, and how they evolved). Typical values are  $m = 3$  for star-formation-like evolution and  $m = 0$  for no evolution.

Since the Universe expands and sources move with the *Hubble flow* we are going to use the comoving line of sight distance, defined as (see Lecture 2):

$$D_c(z) = \int_t^{t_0} c dt = \frac{c}{H_0} \int_0^z \frac{dz'}{E(z')}$$

where we introduced the function:

$$E(z) \equiv \sqrt{\Omega_M(1+z)^4 + \Omega_r(1+z)^5 + \Omega_k(1+z)^3 + \Omega_\Lambda(1+z)}$$

revisiting the formula of the energy rate of neutrinos per steroradian we have:

$$\frac{dF_\nu}{d\Omega} = \frac{1}{4\pi} \frac{c}{H_0} \int_0^\infty \frac{L_\nu(E_\nu)n_0(1+z)^m}{E(z)} dz$$

The expresion above needs an extra correction. We assumed that energy emitted by the source will be the same at the arrival, however energy will be red-shifted according to  $E_\nu(1+z)$  so the formula it's technically:

$$\frac{dF_\nu}{d\Omega} = \frac{1}{4\pi} \frac{c}{H_0} \int_0^\infty \frac{L_\nu(E_\nu(1+z))n_0(1+z)^m}{E(z)} dz$$

Assuming the luminosity follows a power law with,  $L_\nu \propto E^{-\gamma}$ , we can rewrite the expression as:

$$\frac{dF_\nu}{d\Omega} = \xi \frac{c}{H_0} \frac{L_\nu(E_\nu)n_0}{4\pi}$$

where the unit-less parameter  $\xi$  is the integral that contains information on the expansion and cosmological evolution of the sources and the spectral index of the sources defined as:

$$\xi = \int_0^\infty \frac{(1+z)^{(m-\gamma)} dz}{E(z)}$$

Assuming an spectral index of 2, and expressing it as function of the scale factor knowing that:

$$\frac{dz}{1+z} = -\frac{da}{a} \rightarrow dz = -\frac{da}{a^2}$$

and that  $z = \infty \rightarrow a = 0$ ,  $z = 0 \rightarrow a = 1$ , we can rewrite the integral as:

$$\xi = \int_0^1 \frac{a^{-m} da}{E(a)}$$

Where it will depend on the cosmic evolution of the sources. Typical star forming rate evolution (SFR) has an evolution of  $m = 3.4$  in our local universe  $z < 1$  and  $m = -0.3$  for  $1 < z < 4$  and  $m = -3.5$  elsewhere.

#### 4.3.12 Tutorial III: Calculate the value of $\xi$

We are going to calculate the value of the parameter  $\xi$  for different cosmological evolution of the sources. The SFR evolution is given by the following broken power law formula:

```
def rho(z):
    if z < 1.:
        return (1. + z)**3.4
    elif z >= 1. and z <= 4.:
        return (1+1.)**3.4 * ((1.+z)/(1.+1.))**-0.3
    else:
        return (1.+1.)**3.4*((1.+4.)/(1.+1.))**-0.3*((1.+z)/(1.+4.))**-3.5

ax = plt.subplot(111)

z = np.linspace(0, 7, 1000)
vrho = np.vectorize(rho)

ax.plot(z, vrho(z))
ax.set_xlabel("z")
ax.set_ylabel("$n_{\text{SFR}}(z)/n_0$")
ax.grid()

from astropy.cosmology import Planck13 as cosmo
from scipy import integrate

def xi(z):
    return cosmo.H0.value/cosmo.H(z).value * rho(z) * (1 + z)**(-2)
```

```

integral = integrate.quad(lambda z: xi(z), 0., np.inf)[0]

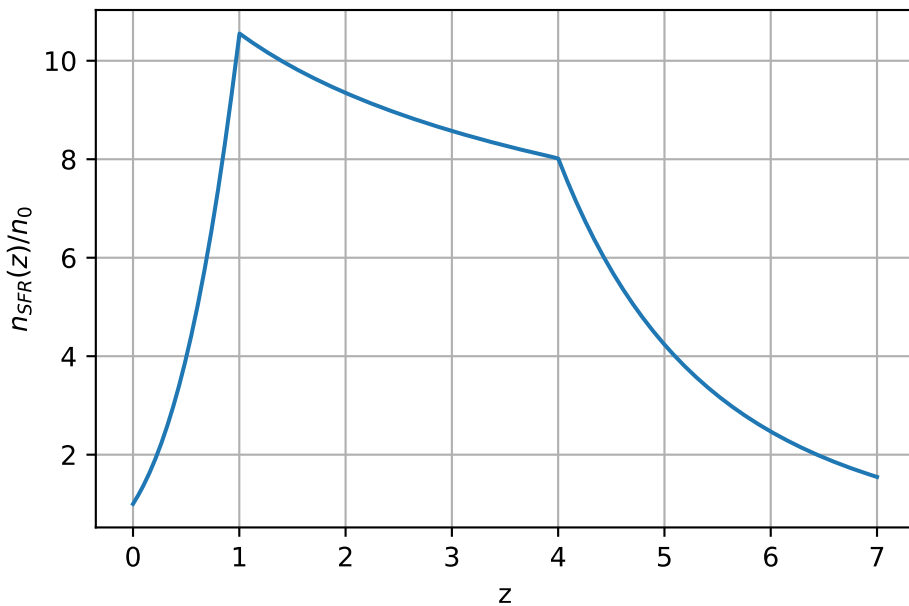
print(r"\xi$ = %.2f for an evolution of SFR" %(integral))

integral = integrate.quad(lambda z: cosmo.H0.value/cosmo.H(z).value * (1 + z)**(-2), 0., 2)

print(r"\xi$ = %.2f for no cosmological evolution up to redshift z < 2" %(integral))

```

$\xi = 2.39$  for an evolution of SFR  
 $\xi = 0.48$  for no cosmological evolution up to redshift  $z < 2$



Therefore the parameter  $\xi$  varies between  $0.5 \sim 3$ . We can equate this total neutrino flux per steroradian to the flux observed by IceCube (assuming a spectral index of 2):

$$\xi \frac{c}{H_0} \frac{L_\nu(E_\nu)n_0}{4\pi} = E^2 \Phi_\nu \sim 2.06 \times 10^{-8} \frac{\text{GeV}}{\text{cm}^2 \text{s} \text{sr}}$$

```

#I'm going to use units to avoid stupid mistakes
import astropy.units as u
from astropy import constants as const
from IPython.display import display, Markdown

xi = 0.48

```

```

icecube_flux = 2.06e-8 * u.GeV/u.cm**2/u.s/u.sr

Ln = icecube_flux * cosmo.H0.to(1/u.s)/const.c.to(u.Mpc/u.s) * 4 * np.pi * u.sr * xi
Ln = Ln.to(u.erg/u.Mpc**3/u.yr)

display(Markdown(r"$n_0 L_\nu \sim \text{icecube\_flux} \cdot \text{cosmo.H0} \cdot \text{const.c} \cdot \text{xi} \cdot 4 \cdot \pi \cdot \text{u.sr} \cdot \text{Ln}$"))

```

$$n_0 L_\nu \sim 1.4 \times 10^{43} \frac{\text{erg}}{\text{yr Mpc}^3}$$

ie, it reaches the value of:

$$n_0 L_\nu \sim 10^{43} \frac{\text{erg}}{\text{Mpc}^3 \text{yr}}$$

note that this is almost independent of the value of  $\xi$ . We can represent this relation in a diagram now called Kowalski's plot:

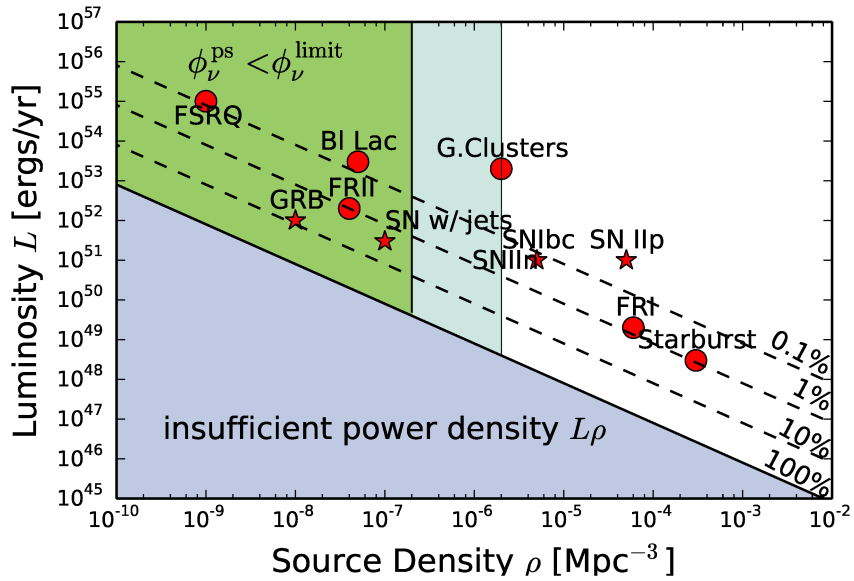


Figure 4.6: Source: Taken from [arxiv:1411.4385](https://arxiv.org/abs/1411.4385)

Constrains can also be obtained from the point-source limits. The argument is as follows, if the source population that is responsible of the diffuse astrophysical flux observed in IceCube, is rate (has a low density) then the closest of these sources should have provided a signal in the point-source analysis. Let's assume that  $d$  is the distance to the nearest source for a source population with local density  $n_0$  so:

$$n_0 \frac{4}{3} \pi d^3 = 1$$

since there is 1 source in an sphere of radius  $d$ . We can estimate the closest distance to a source of this population as:

$$d = \left( \frac{1}{\frac{4}{3} \pi n_0} \right)^{1/3} \propto n_0^{-1/3}$$

and thus the estimated neutrino flux for this single point-source is:

$$E^2 \Phi_{\nu}^{ps} = \frac{L_{\nu}}{4\pi d^2} \sim L_{\nu} n_0^{2/3}$$

A typical value of the neutrino point-source upper limits can be obtained for the Northern sky as:

$$E^2 \Phi_{\nu}^{u.l.} \leq 2 \times 10^{-9} \text{ GeV cm}^{-2} \text{s}^{-1}$$

so we have the 2 constrains together:

$$n_0^{-1/3} \leq \frac{\Phi_{\nu}^{u.l.}}{10^{43} \frac{\text{erg}}{\text{Mpc}^3 \text{yr}}}$$

which leads to the following condition on the local density of sources from the point-source upper limits:

```
flux_upperlimit = 2e-9 * u.GeV/u.cm**2 / u.s

n0 = np.power(flux_upperlimit/Ln, -3)
n0 = n0.to(u.Mpc**-3)

display(Markdown(r"$n_0 \geq {}$".format(n0.value, n0.unit.to_string("latex_inline"))))
```

$$n_0 \geq 2.8 \times 10^{-6} \text{ Mpc}^{-3}$$

#### **4.3.12.1 References**

- High energy neutrinos in the context of multimessenger astrophysics. J. Becker [arXiv:0710.1557v2](https://arxiv.org/abs/0710.1557v2)
- Cosmic Neutrinos from the Sources of Galactic and Extragalactic Cosmic Rays. F. Halzen [arxiv:0611915](https://arxiv.org/abs/0611915)

# 5 Dark Matter

## 5.1 Existance of Dark Matter

There are several hints or proves of the existance of additional matter not visible.

### 5.1.1.1 The mass-to-light ratios

The sun has a ratio of  $\frac{M_\odot}{\mathcal{L}_\odot} \sim 1$  Our milky way  $M_{MW}/\mathcal{L}_{MW} \sim 10$ . Galaxy cluster  $M_{cluster}/\mathcal{L}_{cluster} \sim 500$

#### 5.1.1.1 The virial theorem

Apart from the mass-to-light ratios another evidence of missing mass came from two different ways of estimating the mass of galaxie clusters. For that let's review what is the virial theorem:

In a system made of particles (like galaxies) with momemtum the scalar  $G$  is defined by the equation:

$$G = \sum_{k=1}^N \vec{p}_k \cdot \vec{r}_k$$

where  $\vec{p}_k$  is the momemtum of the  $k$  particule and  $\vec{r}_k$  its possition. The average of the time derivative of  $G$  is 0 in bound systems, ie, in systems that are holding together forever, like galaxies in galaxy cluster bound by gravity. The virial theorem states that in systems where  $G$  is constant, ( $\langle dG/dt \rangle_\tau = 0$ ), then:

$$\langle T \rangle = -\frac{1}{2} \sum_{k=1}^N \langle \vec{F}_k \cdot \vec{r}_k \rangle$$

Zwicky was the first to use the virial theorem to infer the existence of unseen matter while examining the Coma galaxy cluster in 1933. In a common case the potential of a system can be described:

$$V(r_{kj}) = \alpha r_{kj}^n$$

where the total potential energy is:

$$V_{TOT} = \sum_{k=1}^N \sum_{j>k} V(r_{kj})$$

and so the virial theorem can be rewritten as:

$$\langle T \rangle = -\frac{1}{2} \sum_{k=1}^N \langle \vec{F}_k \cdot \vec{r}_k \rangle = \frac{1}{2} \sum_{k=1}^N \sum_{j>k} \frac{dV}{dr} r_{kj} = \frac{1}{2} \sum_{k=1}^N \sum_{j>k} n \alpha r_{kj}^{n-1} r_{kj}$$

$$2\langle T \rangle = n \langle V_{TOT} \rangle$$

in the particular case of gravitational systems we have that  $n = -1$ . Ie, by measuring the kinetic energy of the system, we can infer the total gravitational potential and hence the mass:

$$\langle V_{TOT} \rangle = -G_N \frac{M_{TOT}^2}{\langle r \rangle}$$

while the total kinetic energy can be written as

$$\langle T \rangle = \frac{1}{2} M_{TOT} \langle v^2 \rangle$$

so we can extract the total mass as:

$$M_{TOT} \simeq \frac{\langle r \rangle \langle v^2 \rangle}{G_N} \gg \sum m_{galaxies}$$

which for the Coma cluster turned out to be much more than the mass estimated just by simply counting the galaxies in the cluster.

### 5.1.1.2 About Zwicky

Fritz Zwicky was a prolific scientist and made important contributions in many areas of astronomy but he is rather unknown. He coined the term dark matter, supernova and predicted the existence of neutron stars (2 years after the discovery of the neutron)... He also proposed an alternative cosmology explaining the red-shift as tired light.

He also believed in re-arranging the planets in the solar system using rockets to make them habitable.

## 5.1.2 2. The rotational curves of Galaxies

In Kelperian systems, like our solar system, where most of the mass is at the center one can infer the centripital force of a mass orbiting the system as:

$$\frac{mv^2}{r} = G \frac{mM}{r^2}$$

where  $M$  is the inner mass. In this case the velocity of the orbiting masses  $m$  is expected to follow  $v \propto 1/\sqrt{r}$ . In the case of spiral galaxies, where the total mass is at the center, the velocity of external objects (like our Sun), was expected to follow the same trend, however it was obsevered that most of the spiral galaxies had rotational velocities of  $v \sim \text{cte}$ . It can be deducted that there is matter density (a halo) that should follow  $\rho \propto r^{-2}$  in order to explain the constant mass.

Vera Rubin measured the rotation curves of large number of galaxies up to 110 kpc. They all showed the similar behavoir proving that this was an universal feature.

### 5.1.2.1 About Vera

More info on Vera Rubin can be found on [wikipedia](#).

## 5.1.3 3. Gravitational lensing

In general relativity, the presence of matter (energy density) can curve spacetime, and the path of a light ray will be deflected as a result. This process is called gravitational lensing and in many cases can be described in analogy to the deflection of light by (e.g. glass) lenses in optics.

The angle of deviation from gravitational lensing is given by:

$$\alpha = \frac{4GM}{c^2 b}$$

where  $b$  is the impact parameter or the closest distance.

The analysis of the distance in this figure gives the relation:

$$D_{LS} \sin \frac{\alpha}{2} = \frac{1}{2}(D_s \sin \theta_1 - D_s \sin \theta_s)$$

making small angle approximations gives:

$$\alpha D_{LS} = D_s(\theta_1 - \theta_s)$$

therefore

$$\theta_s = \theta_1 - \frac{4GM}{c^2} \frac{D_{LS}}{D_s D_L} \frac{1}{\theta_1}$$

in the particular case of a colinearity between the source and the lens, ie  $\theta_s = 0$ , we have:

$$\theta_1 \equiv \theta_E = \left( \frac{4GM}{c^2} \frac{D_{LS}}{D_s D_L} \right)^{1/2}$$

which is known as the Einstein ring

#### 5.1.4 4. Cosmic Microwave Background

As we show the microwave background radiation can be decomposed just like sound from a musical instrument can be broken into harmonics. From the features of its *power spectrum*, i.e. the amount of radiation associated to each frequency, astrophysicists can calculate the quantity of dark matter contained in the Universe. As we saw in Lecture 2, the current cosmological model  $\Lambda$ CDM, has the following components for matter and dark energy:

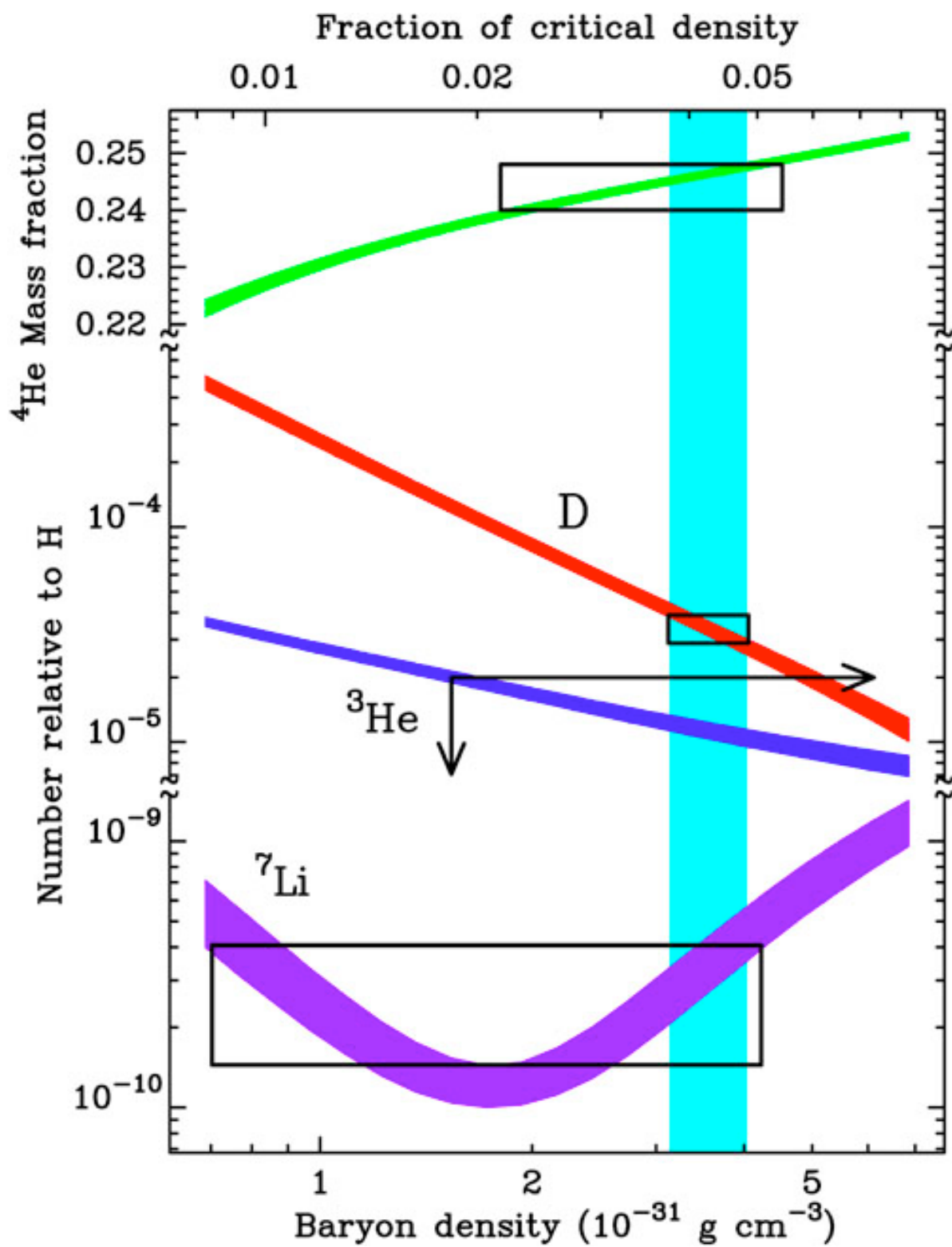
$$\Omega_\Lambda \simeq 0.70, \quad \Omega_m \simeq 0.30$$

### **5.1.5 5. Big Bang nucleosynthesis (BBN)**

It is known that the elements observed in the Universe were created in either of two ways:

- Light elements (deuterium, helium, and lithium) were produced in the first few minutes of the Big Bang
- Heavier elements than helium are thought to have an stellar origin and be formed much later in the history of the Universe.

Roughly three minutes after the Big Bang itself, the temperature of the Universe who was at roughly  $10^{32}$  K cooled down to approximately  $10^9$  Kelvin when nucleosynthesis, or the production of light elements, could take place. The prediction of light elements as function of the baryon density can be seen in this plot:



As can be seen the predictions depend strongly on the baryon density (ie neutrons and protons) at the time of the nucleosynthesis. In particular they depend on the relative abundance of baryons relative to radiation, the baryon-to-photon ratio. Since the photon energy density is well known from the CMB, the observations of primordial abundances of the isotopes of hydrogen, helium and lithium provide a strong constraint on the baryon density. The estimate of baryon density is then  $\Omega_b h^2 \simeq 0.02$

## 5.2 Dark matter?

In January 1860 the French mathematician Urbain Le Verrier announces the discovery of a new planet that he named Vulcan between Mercury and the Sun (following his earlier successful prediction of Neptune in 1856) explaining the precession of Mercury. During years, amateur astronomers claimed to have seen the planet. However we know now the precession is explained by Einsteins gravity.

Today, the search continues for these so-called vulcanoid asteroids. None have been found yet and searches have ruled out asteroids larger than about 6 km. Neither SOHO nor STEREO have detected a planet inside the orbit of Mercury so far.

### 5.2.1 Modified Newtonian Dynamics (MoND)

What if the mass discrepancy can be solved without “adding” matter. In 1983 Mordehai Milgrom proposed that a modified newtonian dynamics could explain the dynamics of galaxies in the small acceleration regime. In MOND, violation of Newton’s Laws occurs at extremely small accelerations, characteristic of galaxies yet far below anything typically encountered in the Solar System or on Earth.

### 5.2.2 The Bullet Cluster

It is usually quoted as the “irrefutable proof of CDM” it consists on two colliding galaxy clusters. At a statistical significance of  $8\sigma$ , it was found that the spatial offset of the center of the total mass from the center of the baryonic mass peaks cannot be explained with an alteration of the gravitational force law alone

[Here](#) is an interesting post from theorist Sabine Hossenfelder about recent papers on the Bullet Cluster and its implication on the Dark Matter nature of the mass discrepancy:

## 5.3 Dark Matter Candidates

### 5.3.1 Introduction

Assuming that Dark Matter exists, there are some conditions this matter must satisfy. It must:

- stable at least for the life time of the Universe.
- not interacting electromagnetically (it is dark).
- Can interact weakly
- it must have a density of  $\Omega_{DM} \sim 0.2$  since:

$$\Omega_{matter} = \Omega_{baryon} + \Omega_{\nu HDM} + \Omega_{CDM} \simeq 0.05 + 0.01 + 0.24 = 0.30$$

### 5.3.2 The Boltzmann equation

Imagine that dark matter is a non-interacting, non-relativistic particle with number density given  $n_\chi \propto a^{-3}$ . As the universe expands the density is diluting according to:

$$\frac{dn_\chi}{dt} = -3Hn_\chi$$

Since  $H = da/dt$ . Now let's imagine that dark matter is in thermal equilibrium with the standard model, we are talking here about “chemical” equilibrium in which particles interact and convert among each other while keeping the *total number of particles*. Ie, in this case it will mean that dark matter particles annihilate to SM ( $\chi\chi \rightarrow f\bar{f}$ ) and SM particles produce dark matter particles ( $f\bar{f} \rightarrow \chi\chi$ ). Dark matter annihilation happens at the rate that depends on the square of dark matter number density (because we need 2 DM particles) and the thermally average annihilation cross-section, so we can add this term in the equation above  $n_\chi^2 \langle \sigma_A v_\chi \rangle$ . On the contrary, the conversion of SM particles to DM can be produced as a rate of  $-n_{SM}^2 \langle \sigma_{A,inv} v_\chi \rangle$ . At equilibrium, both processes must compensate so we can write:

$$n_{\chi,eq}^2 \langle \sigma_A v_\chi \rangle = n_{SM}^2 \langle \sigma_{A,inv} v_\chi \rangle$$

which leads us to the Boltzmann equation written as:

$$\frac{dn_\chi}{dt} = -3Hn_\chi - \langle \sigma_A v_\chi \rangle (n_\chi^2 - n_{\chi,eq}^2)$$

### 5.3.3 Thermal freeze-out and the WIMP ‘miracle’

From the boltzman equation is easy to see what would happen in an Universe with no expansion,  $H = 0$ . It is clear that if  $n_\chi^2 > n_{\chi,eq}^2$  annihilation will dominate until the number of  $\chi$  particles drops to its equilibrium value. If the universe is expanding, but the expansion is slow, we still can ignore the term  $-3Hn_\chi$  but temperature will change and it will change the number density in equilibrium. For cold dark matter, like not relativistic wimps with mass  $M_\chi \gg T$ , this follow the equilibrium density function from the Boltzmann relation:

$$n_{\chi,eq}(T) = \left( \frac{M_\chi T}{2\pi} \right)^{3/2} \exp \left( \frac{-M_\chi}{T} \right)$$

In other words, the number density of dark matter drops as the temperture goes down and Universe expands. (Hot dark matter on the other hand will be  $n_\chi^{HDM}(T) \sim T^3$ ) What happens is that annihilation processes like  $\chi\chi \rightarrow f\bar{f}$  happen easily, but because  $\chi$  is heavy, inverse annihilation processes like  $f\bar{f} \rightarrow \chi\chi$  happen only very rarely (with photons on the tail of the momentum distribution).

At some point the expansion of the Universe becomes important and we no longer can ignore the term  $-3Hn_\chi$ . As  $n_\chi$  becomes smaller, the expansion rate becomes more important than the annihilation term that depends on  $n_\chi^2$ . Dark matter particles are separated away from each other and they cannot annihilate. This is the freeze-out of dark matter. At that moment the number density of dark matter becomes estable in a solution called the freeze-out abundance.

In a radiation dominated Universe the expansion of the Universe is given by:

$$H(T) \propto \frac{T^2}{M_{Pl}}$$

where  $M_{Pl}$  is the plank mass. So according to the Boltzman equation, in an expanding Universe the moment of the freeze-out is given by the condition:

$$n_\chi(T_{fo})\langle\sigma_A v_\chi\rangle = 3H(T_{fo})$$

where we can assume that  $n_\chi = n_{\chi,eq}$ . After the freeze-out, the number density changes scales with  $a(t)^{-3}$  but also  $T$  scales with  $a(t)^{-1}$  so the number density of dark matter particles today can be written as:

$$n_\chi(T_0) \sim n_\chi(T_{fo}) \left( \frac{T_0}{T_{fo}} \right)^3 \sim \left( \frac{T_0}{T_{fo}} \right)^3 \times \frac{T_{fo}^2/M_{Pl}}{\langle\sigma_A v_\chi\rangle}$$

The mass density is then,  $\rho_\chi = M_\chi n_\chi$  and dividing by the critical energy gives:

$$\Omega_\chi = \frac{\rho_\chi}{\rho_c} \sim \frac{10^{-25}}{\langle \sigma_A v_\chi \rangle} \text{cm}^3 \text{s}^{-1}$$

Finding the right relic density of dark matter is the same as finding the right value of  $\langle \sigma_A v_\chi \rangle$ . As it happens this values turns out to be in the same range expected for the weak interactions. This is called the WIMP miracle...

### 5.3.4 Direct detection

The differential rate per unit detector mass is given by:

$$\frac{dR}{dE_R} = \frac{n_\chi}{m_N} \left\langle v \frac{d\sigma}{dE_R} \right\rangle$$

As can be seen the rate depends on the dark matter density since  $n_\chi = \rho_\chi / m_\chi$ , the velocity of DM,  $v$  and their differential cross-section.

The recoil energy can be measured by this three different techniques:

- Phonon/Thermal: vibration (seen as rise in T) in a crystal due to the recoiled of the nucleus impacted by the WIMP.
- Ionization: an electron is pushed away from its nucleus. A magnetic field drives the electron to a charge detector
- Scintillation: an electron absorbs energy in the interaction. A short time after, it de-excites and emits a photon.

### 5.3.5 Indirect detection

The flux of particles observed in a indirect detector using  $\gamma$ -rays or neutrinos can be deducted from this formula:

$$\frac{d\Phi_x}{dE_x} = \frac{1}{4\pi} \frac{\langle \sigma_A v \rangle}{2m_\chi^2} \frac{dN_x}{dE_x} \int_0^{\Delta\Omega} d\Omega \int_{l.o.s} \rho_\chi^2(r(s, \Psi, \theta)) ds$$

where  $x = \gamma$ -rays,  $\nu$ . The J-Factor is the integral of the density square (we need two dark matter particles to annihilate) along the line of sight. There are many halo models in the market. Simulations favor that the DM collapse give “cuspy” profiles, i.e. more peaked (good for enhancing the signal). Observations of rotation curves of galaxies favor “cored” profiles, i.e. constant density cores Substructure not well resolved below  $\sim 10^5 M_\odot$ , which may have an important effect due to the  $\rho^2$  dependency of signal Effect of baryons is still unclear:

- steepening through adiabatic contraction
- flattening through star bursts

### 5.3.6 Targets for indirect detection

**Dwarf Galaxies:** \* clean (low star formation) \* largest mass-to-light ratio \* boost factors irrelevant \* about 25 known dwarf satellites of MW \* best limits for  $\langle \sigma_A v \rangle$ : already at natural scale for small masses ( $\sim 10$  GeV) with Fermi-LAT

**Galaxy Cluster:** \* Largest gravitationally bound objects in the Universe \* Dark matter dominated \* Substructure is quite uncertain \* Boost factors could be very large, making them competitive with dwarf galaxies in the most optimistic cases \* Astrophysical background could be important (AGNs, CR interacting with hadronic material...)

**Isotropic emission:** \* Spectrum: power law from 200 MeV to 100 GeV with  $\gamma = 2.4$ ) \* Mainly due to extragalactic unresolved sources: starburst and normal galaxies, galaxy clusters, shocks by the assembly or large scale structures \* Detection of DM difficult, but upper bounds can be set assuming contributions from these populations, able to discard the PAMELA excess DM interpretation

#### Galactic Center:

- Brightest source of DM by two orders of magnitude
- Large astrophysical background
- For GeV searches also interaction of CRs with molecular material in the inner Galaxy
- Searches focused slightly off the most inner GC
- More effect of the DM profile, since it is closer

**Sun and Earth** \* Only visible in neutrinos. \* Low or nonexistent background \* Less effects on the Halo model profiles \* Dark Matter is accumulated as an effect of the capturing of dark matter, these searches can prove the  $\sigma_{\chi N}$

#### Absorption in the Sun

The mean free path of neutrinos in the Sun is given by:

$$\lambda = \frac{A_H}{N_A \rho \sigma} = \frac{1 \text{ mol}}{6.023 \times 10^{23} \text{ mol/gr} \cdot 1.6 \times 10^5 \text{ gr/cm}^3 \cdot 0.686 \times 10^{-38} \text{ cm}^2/\text{GeV} \cdot 5000 \text{ GeV}} = 3.0 \times 10^5 \text{ cm} \ll 7 \times 10^{10} \text{ cm}$$

### 5.3.7 Capturing of DM in local celestial bodies

Dark Matter in the Sun or Earth is accumulated by scattering processes of DM followed by gravitational capture of DM. It is not the relic density that we can find for instance at the Center of the Galaxy or other astrophysical places like Dwarf Galaxies, etc. Let's assume  $N$  to be the number of DM particles in a celestial body. The equation that govern the evolution of this density can be described as:

$$\frac{dN}{dt} = C_c - C_A N^2 - C_E N$$

The various elements of this equation are:

- $C_E$  is the “evaporation” of dark matter, it is the escape of DM due to their thermal velocity being equivalent to the escape velocity of the celestial body. The Sun’s escape velocity is  $v_{esc} \simeq 1156$  km/s. Assuming DM particles sink into the core of the Sun and gain the thermal velocity the typical velocity is:

$$v_\chi \simeq c \left( \frac{1\text{keV}}{m_\chi} \right)^{1/2} \geq v_{esc}^\odot \rightarrow m_\chi \leq 0.1\text{GeV}$$

only for very low masses the evaporation term is important.

- $C_A$  is the annihilation term which depends on the factor  $\langle \sigma_A v \rangle$  and an effective volume.
- $C_c$  is the capture term and it depends on the DM-nucleon cross-sections  $\sigma_{\chi-N}$ . For capture in the Earth the main contribution comes from the spin-independent cross-section which is quadratically proportional to  $A^2$  of the elements in Earth. It is also proportional to the DM flux, ie (for the Sun):

$$C_c \sim \frac{\rho_\chi}{m_\chi} v_\chi \left( \frac{M_\odot}{m_N} \right) \sigma_{\chi-N}$$

By solving the equation above (ignoring the evaporation term) we can express the total annihilation rate  $\Gamma_A$  is expressed as:

$$\Gamma_A = \frac{1}{2} C_A N^2 = \frac{C_c}{2} \left[ \tanh(\sqrt{C_c C_A} t) \right]^2$$

where  $t$  is the lifetime of the celestial body. It is clear from this equation that equilibrium is reached when:

$$t_{eq} \equiv \frac{1}{\sqrt{C_c C_A}}$$

For the Earth, this equilibrium time is of the order of  $10^{11}$  years if the spin-independent WIMP-proton cross-section is  $\hat{\{SI\}}_{-p} 10^{-43} cm^2$  which is longer than the age of the solar system  $t_{Earth} \sim 4.5$  Gyr. In the Sun however, most models predict  $t_{eq} \ll t_\odot$  and therefore we can assume that equilibrium is reached in the Sun.

## 5.4 Bibliography

- PDG review on Dark Matter [pdg.lbl.gov/2016/reviews/rpp2016-rev-dark-matter.pdf](http://pdg.lbl.gov/2016/reviews/rpp2016-rev-dark-matter.pdf)
- Particle Dark Matter: Observation, Models and Searches. Gianfranco Bertone. DOI: [10.1017/CBO9780511770739](https://doi.org/10.1017/CBO9780511770739)
- Some reviews in the arxiv:
  - <https://arxiv.org/abs/hep-ph/0404175>
  - <https://arxiv.org/abs/hep-ph/9506380>

## References

- Grupen, Claus. n.d. *Astro Particle Physics*.
- Kachelriess, M. 2008. “Lecture Notes on High Energy Cosmic Rays.” <https://arxiv.org/abs/0801.4376>.
- Kampert, Karl-Heinz, and Peter Tinyakov. 2014. “Cosmic Rays from the Ankle to the Cutoff.” *Comptes Rendus. Physique* 15 (4): 318–28. <https://doi.org/10.1016/j.crhy.2014.04.006>.
- Melia, Fulvio. 2009. *High-Energy Astrophysics*. Vol. 14. Princeton University Press. <http://www.jstor.org/stable/j.ctv21r3q4z>.
- Workman, R. L., and Others. 2022. “Review of Particle Physics.” *PTEP* 2022: 083C01. <https://doi.org/10.1093/ptep/ptac097>.